

IN THE SUPREME COURT OF NEVADA

MOTOR COACH INDUSTRIES, INC.,

Appellant,

vs.

KEON KHIABANI; ARIA KHIABANI,
minors, by and through their guardian MARIE-
CLAUDE RIGAUD; SIAMAK BARIN, as
executor of the ESTATE OF KAYVAN
KHIABANI, M.D. (decedent); THE ESTATE
OF KAYVAN KHIABANI, M.D. (decedent);
SIAMAK BARIN, as executor of the ESTATE
OF KATAYOUN BARIN, DDS (decedent);
and the ESTATE OF KATAYOUN BARIN,
DDS (decedent),

Respondents.

Electronically Filed
Apr 24 2020 10:37 a.m.
Elizabeth A. Brown
Clerk of Supreme Court

APPEAL

**From the Eighth Judicial District Court, Clark County
The Honorable Adriana Escobar, District Judge
District Court Case No. A-17-755977-C**

RESPONDENTS' APPENDIX - VOLUME 1 - PAGES 1-120

WILL KEMP, ESQ. (#1205)

ERIC M. PEPPERMAN, ESQ. (#11679)

Kemp Jones, LLP

3800 Howard Hughes Parkway, 17th Fl.

Las Vegas, Nevada 89169

Email: emp@kempjones.com

PETER S. CHRISTIANSEN, ESQ. (#5254)

KENDELEE L. WORKS, ESQ. (#9611)

Christiansen Law Offices

810 S. Casino Center Blvd., Suite 104

Las Vegas, Nevada 89101

ATTORNEYS FOR RESPONDENTS

CHRONOLOGICAL TABLE OF CONTENTS TO APPENDIX

Tab	Document	Date	Vol.	Pages
1	Plaintiffs' Trial Exhibit No. 126 (MCI Engineering Test Report – Wind Tunnel – August, 1993)	02/23/18	1	0001-0098
2	Plaintiffs' Trial Exhibit No. 221 (Photo – RR 2)	02/26/18	1	0099
3	Plaintiffs' Trial Exhibit No. 222 (Photo – RR 3)	02/26/18	1	0100
4	Plaintiffs' Trial Exhibit No. 223 (Photo – RR 4)	02/26/18	1	0101
5	Plaintiffs' Trial Exhibit No. 224 (Photo – RR 5)	02/26/18	1	0102
6	Plaintiffs' Trial Exhibit No. 139 (1981 – Aerodynamic Effects to a Bicycle Caused by a Passing Vehicle – Y. Kato)	03/09/18	1	0103-0109
7	Plaintiffs' Proposed Verdict Form	03/21/18	1	0110-0113
8	Order - Eighth Judicial District Court, Case No. A-17-755977-C	05/23/18	1	0114-0120

ALPHABETICAL TABLE OF CONTENTS TO APPENDIX

Tab	Document	Date	Vol.	Pages
8	Order - Eighth Judicial District Court, Case No. A-17-755977-C	05/23/18	1	0114-0120
7	Plaintiffs' Proposed Verdict Form	03/21/18	1	0110-0113
1	Plaintiffs' Trial Exhibit No. 126 (MCI Engineering Test Report – Wind Tunnel – August, 1993)	02/23/18	1	0001-0098
6	Plaintiffs' Trial Exhibit No. 139 (1981 – Aerodynamic Effects to a Bicycle Caused by a Passing Vehicle – Y. Kato)	03/09/18	1	0103-0109
2	Plaintiffs' Trial Exhibit No. 221 (Photo – RR 2)	02/26/18	1	0099
3	Plaintiffs' Trial Exhibit No. 222 (Photo – RR 3)	02/26/18	1	0100
4	Plaintiffs' Trial Exhibit No. 223 (Photo – RR 4)	02/26/18	1	0101
5	Plaintiffs' Trial Exhibit No. 224 (Photo – RR 5)	02/26/18	1	0102

MOTOR COACH INDUSTRIES ENGINEERING TEST REPORT

TEST NO.: 93-0026

DATE: AUGUST, 1993

DESCRIPTION:

A WIND TUNNEL INVESTIGATION OF THE AERODYNAMIC
CHARACTERISTICS OF BUSES

REPORT BY: INSTITUTE FOR AEROSPACE RESEARCH

SECTION NO.: -

PART/ASSY NO.: -

COACH UNIT NO.: -

REF: -
-
-
-

COMMENTS: -
-
-

APPENDIX 1: RUN LOG

RUN	TYPE	FRONT	REAR	TRIP	HATCH	RAIL	MIRROR	MISC	C _D (90)	PHOTO
13	YAW	SMOOTH CJ3	STANDARD CJ3	NO	NONE	NONE	NONE	NONE	0.376	P1
14	Re									
16	YAW				STD	STD			0.377	P2
18	Re	STANDARD CJ3								P3
19	YAW								0.584	
21	Re	MERCEDES								P4
22	YAW								0.620	
25	Re	PROPOSAL 1								P5
26	YAW								0.363	
28	Re	PROPOSAL 2								P6
29	YAW								0.436	
31	Re	PREVOST								P7
32	YAW								0.404	
34	Re	SETRA								P8
35	YAW								0.625	
37	YAW	STANDARD CJ3					CJ3 FWD		0.596	P9
39	Re	PROPOSAL 2		YES			NONE			P10
40	YAW								0.365	
42	YAW						CJ3 FWD		0.394	P11
44	YAW						CJ3 AFT		0.405	P12

right Appendix

RUN	TYPE	FRONT	REAR	TRIP	HATCH	RAIL	MIRROR	MISC	C _D (90)	PHOTO
46	YAW	PROPOSAL 2	STANDARD CJ3	YES	STD	STD	SETRA		0.434	P13
48	YAW						PREVOST		0.422	P14
50	Re		BEVELLED				NONE			P15
51	YAW								0.299	
53	YAW						CJ3 FWD		0.339	P11
55	YAW						CJ3, RIGHT FWD, LEFT AFT		0.349	P16
57	YAW							SKIRTS	0.330	P17
58	YAW							AIR DAM	0.393	P18
59	YAW							TIRE FAIRING	0.353	P19
60	YAW							VORTEX GEN.	0.354	P20
61	YAW					MOD		NONE	0.351	P21
63	YAW	PREVOST	STANDARD CJ3	YES	STD	STD	PREVOST		0.447	P22
65	YAW	PREVOST					NONE		0.418	P23
66	Re									
68	Re	PROPOSAL 1								P24
69	YAW								0.367	
71	Re	SMOOTH CJ3								P25
72	YAW	0.380								

Pages 93 Total

Fig. _____
Diag. _____

**REPORT
RAPPORT**

**APPLIED AERODYNAMICS
LABORATORY
LABORATOIRE
D'AÉRODYNAMIQUE APPLIQUÉE**

Date August 1993

Lab. Order _____
Comm. Lab. 5602

File _____
Dossier _____

For Motor Coach Industries
Pour _____

Reference MCI P.O.#M151843
Référence _____

LTR-AA- 9

A WIND TUNNEL INVESTIGATION OF THE
AERODYNAMIC CHARACTERISTICS OF BUSES
FOR MOTOR COACH INDUSTRIES

Submitted by Dr. L. Elias
Présenté par _____
Laboratory Head/Chef de laboratoire

Author R.R. Cooper
Auteur _____

Approved Dr. G.F. Marsters
Approuvé _____
Director General/Le directeur général

THIS REPORT MAY NOT BE PUBLISHED WHOLLY OR
IN PART WITHOUT THE WRITTEN CONSENT OF THE
INSTITUTE FOR AEROSPACE RESEARCH

CE RAPPORT NE DOIT PAS ÊTRE REPRODUIT, NI EN
ENTIER NI EN PARTIE, SANS UNE AUTORISATION
ÉCRITE DE L'INSTITUT DE RECHERCHE AÉROSPATIALE

Copy No _____
Copie Nr. _____

TABLE OF CONTENTS

Page #

ABSTRACT

1.0 INTRODUCTION	1
2.0 WIND TUNNEL SIMULATION	1
2.1 Reynolds Number Effects	2
2.2 Extrapolation to Full Scale - The Aerodynamic Coefficient	2
2.3 Effects of the Natural Wind	3
3.0 EFFECTS OF AERODYNAMICS ON PERFORMANCE	5
3.1 Fuel Consumption	5
3.2 Cross-wind Handling	8
4.0 TEST PROGRAM	10
4.1 Model Installation	10
4.2 Model Configurations	10
4.3 Definition of the Measurement Coordinate Systems	11
4.4 Test Procedure	11
5.0 RESULTS	12
6.0 DISCUSSION AND INTERPRETATION OF RESULTS	12
6.1 Reynolds Number Effects	12
6.2 Front-End Shape Effects	13
6.3 Rear-End Shape Effects	14
6.4 Mirrors	14
6.5 Miscellaneous Modifications	15
6.6 The Best Combination	16
6.7 Flow Visualization	17
7.0 CONCLUSIONS	18
8.0 NOTATION	18
9.0 REFERENCES	19

FIGURES

APPENDIX 1: RUN LOG

APPENDIX 2: PHOTOGRAPHIC LOG

APPENDIX 3: DATA TABULATION

APPENDIX 4: DATA PLOTS

ABSTRACT

A wind tunnel test was performed to evaluate the aerodynamic drag of seven front-end shapes and 2 rear-end shapes for an intercity bus for Motor Coach Industries . The front-end shapes represented the current production bus - the CJ3, three competing buses, and three new designs. The rear-end shapes represented the current production bus and a new design. The wind tunnel measurements demonstrated that the best combination, consisting of the new rear plus the Proposal 1 front, produced a reduction in wind-averaged drag coefficient of 41.5% compared to the standard CJ3 configuration. This drag reduction is equivalent to a fuel saving of 8.75 litres for each 100 km travelled at a steady speed of 90 km/h and 14.63 litres for each 100 km travelled at 120 km/h. The new configuration had a lower drag coefficient than the three competitors.

RESUMÉ

Un essai en soufflerie a été réalisé pour évaluer la traînée aérodynamique de sept formes d'avant et de deux formes d'arrière d'autocar pour Motor Coach Industries. Les formes de l'avant étaient celles d'un modèle de série (le CJ3), de trois modèles concurrents et de trois nouveaux modèles. Les formes de l'arrière étaient celles du modèle de série et d'un nouveau modèle. Les mesures ont permis de constater que la meilleure combinaison, soit le nouveau modèle d'arrière avec le projet d'avant n° 1, produisait une réduction de 41,5% du coefficient de traînée pondéré en fonction du vent par rapport à la configuration CJ3. Cette réduction représente une économie de carburant de 8,75 litres pour 100 kilomètres parcourus à une vitesse stabilisée de 90 km/h et de 14,63 litres pour 100 kilomètres parcourus à une vitesse stabilisée de 120 km/h. Le coefficient de traînée de la nouvelle configuration était plus faible que celui des trois modèles concurrents.

1.0 INTRODUCTION

Aerodynamic forces and moments have an important influence on the operation of a high-speed, intercity bus. Aerodynamic drag absorbs a significant proportion of the engine power required at speed, thus affecting fuel consumption and passing acceleration. The aerodynamic side force, rolling moment, and yawing moment are important to handling because they provide a disturbance that deflects a bus from its path in the presence of side winds or passing vehicles.

A wind tunnel investigation was performed in the 2m x 3m wind tunnel of the Applied Aerodynamics Laboratory of the National Research Council to evaluate the influence of these parameters for a new bus designed by Motor Coach Industries, Winnipeg, Manitoba. The wind tunnel program was conducted with a 1:10 scale model of the bus and the purposes of the wind tunnel tests were:

- 1) to investigate alternative front-end and rear-end designs to determine which provided the lowest aerodynamic drag,
- 2) to determine the effect of mirrors and other detail modifications on the best front and rear combination from (1),
- 3) to compare the aerodynamic performance of the best combination with several competitive buses,
- 4) to estimate the fuel savings provided by the new design, relative to the current production bus and to the competition.

2.0 WIND TUNNEL SIMULATION

The wind tunnel simulation provides an approximation of the environment encountered by a bus moving along a road [1]¹. In the wind tunnel, Figure 1, air is blown over a model mounted above a fixed groundboard that is specially-designed to simulate the effects of the road surface over which the real bus moves. The accuracy of the wind tunnel measurements will be functions of several parameters, the most important of which are the test Reynolds number, the level of model detail, and the effectiveness of the ground simulation. The level of model detail and the fixed ground plane will produce small errors in the absolute values of the measured aerodynamic forces. For example, the smooth model surfaces and fixed groundboard will cause the model drag measurements to be lower than for the full-scale bus. However, the differences in aerodynamic forces between any two configurations will not be influenced by these factors. Thus, the wind tunnel will be an accurate predictor of the changes between configurations and, therefore, provides a powerful tool for the aerodynamic optimization of a new bus design. The measured aerodynamic changes can be used to provide accurate estimates of the performance changes produced by any shape modification.

Many small details like side window framing, break lines in the body surface, wheel rotation, and heat exchanger airflows were not included in the model because past experience has shown that their effects were small and did not affect the aerodynamic differences measured

¹ Numbers in square parentheses indicate references to be found following the main body of the text.

between major configurations. Previous wind tunnel tests have demonstrated that the measured aerodynamic changes correlate well with road measurements for commercial road vehicles [2]. In summary, the wind tunnel's main strength comes from its ability to predict the differences or increments between the various test configurations. Thus, even though a model might have simplified surface detailing, accurate drag differences between configurations will be obtained, and the wind tunnel will permit the reliable selection of the best aerodynamic configuration. In fact, the wind tunnel can provide much more accurate measurements of small aerodynamic changes than is possible from road tests.

The data measured in the wind tunnel need to be extrapolated to full scale. This requires a method of converting the measured forces and moments from model scale to full scale - done through the concept of the aerodynamic coefficient - and a mechanism for incorporating a realistic interpretation of the wind environment in which a road vehicle operates - provided by the wind-averaged drag coefficient. These items, as well as the effects of Reynolds number, will be discussed in the following sections.

2.1 Reynolds Number Effects

The Reynolds number is the aerodynamic similarity parameter, defined as

$$Re = 1.9 \times 10^4 V_r w \quad (1)$$

where V_r = resultant airspeed due to combined wind and vehicle motion, equal to the wind tunnel test speed, km/h.
 w = characteristic length, chosen as the maximum legal width, 2.59 m full scale, 0.259 m. model scale.

Ideally, the Reynolds number should have the same value in the wind tunnel test as for the bus on the road to guarantee that the two flow fields are identical. This is not possible with a 1:10-scale model because the required test speed is approaching a speed where supersonic effects become significant. Fortunately, it turns out that the Reynolds number must only be high enough to guarantee that the boundary layers on the front face of the model becomes turbulent before reaching the front edges, requiring a Reynolds number of only 1.0×10^6 to 2.0×10^6 [3], compared to the full-scale value of 5.0×10^6 at 100 km/h. The present tests were run near the maximum speed of the wind tunnel, providing a test Reynolds number of 1.4×10^6 , 28% of full scale at 100 km/h. This is sufficiently high for the majority of the tests, although flow tripping may be required for some of the smaller edge radii [3] to ensure full-scale behaviour.

2.2 Extrapolation to Full Scale - The Aerodynamic Coefficient

The measurements of aerodynamic force and moment made on the bus can be converted to a dimensionless form that are independent of model size and test speed, and are only a function of model shape and Reynolds number. This is done by dividing the measured forces and moments by reference forces and moments that are related to the test airspeed and to the model size. Taking drag as an example, if the drag force is divided by a reference force formed as a product of the

test airstream pressure, the reference dynamic pressure, and a model reference area, commonly chosen to be the frontal area at zero yaw angle, then the drag coefficient is defined as

$$C_D = \left[\frac{D}{qA} \right] = \left[\frac{D}{3.858 \times 10^{-2} \rho V_r^2 A} \right] \quad (2)$$

where D = aerodynamic drag force, N.
 $(3.858 \times 10^{-2} \rho V_r^2)$ = dynamic pressure, Pascals
 ρ = air density, 1.226 kg/m³ at S.T.P.
 A = reference frontal area, 8.358 m² full scale, 0.08358 m² model scale

Equation (2) has units of N/N., and so possess no dimensions. The full-scale drag value can be calculated from the same relationship, at any full-scale airspeed, by substitution of that airspeed, the full-scale frontal area, and the measured, model-scale drag coefficient into the inverted equation.

The moments are non-dimensionalized in a similar fashion, except that a reference moment is required in these cases. This moment is based on the reference force defined above, times an arbitrary moment arm that is commonly chosen to be the vehicle wheelbase, which is taken here as the distance between the front axle and the drive axle. Using yawing moment as an example, the yawing moment coefficient is defined as

$$C_N = \left[\frac{N}{qAb} \right] = \left[\frac{N}{3.858 \times 10^{-2} \rho V_r^2 Ab} \right] \quad (3)$$

where N = aerodynamic yawing moment, N-m.
 b = reference length, chosen as wheelbase, 7.225 m. full scale, 0.7225 m. model scale.

The other two force coefficients - lift and side force - and the other two moment coefficients - pitch and roll - are defined in exactly the same way.

2.3 Effects of the Natural Wind

The Earth's surface winds blow with random magnitude and direction relative to the direction of motion of a bus, causing random, time-varying changes in the resultant velocity vector at the bus. The main effect of the wind, from the perspective of the wind tunnel flow simulation, is to produce a non-zero yaw angle at the bus. This angle can be simulated in the wind tunnel by rotating the model about a vertical axis, relative to the direction of the approaching airstream. The resultant velocity vector produced by a combination of wind and bus motion is shown in the vector diagram of Figure 2, and its direction and magnitude can be calculated from

$$\psi = \tan^{-1} \left\{ \frac{[(V_w/V_b)\sin\phi]}{[1 + (V_w/V_b)\cos\phi]} \right\} \text{ deg.} \quad (4)$$

and

$$V_r = V_b \left\{ 1 + (V_w/V_b)^2 + 2(V_w/V_b)\cos\phi \right\}^{1/2} \text{ km/h,} \quad (5)$$

where

- ψ = wind-induced yaw angle, deg.
- ϕ = wind direction relative to the direction of bus motion, deg.
- V_w = wind speed, km/h.
- V_b = bus road speed, km/h.
- V_r = resultant airspeed, km/h.

An example of the effect of the natural wind on the yaw angles encountered by a vehicle operating at constant speed is presented in Figure 3. This graph shows the probability of exceeding a given yaw angle at a road speed of 90 km/h and it can be seen that the yaw angle induced by the wind is at or below 9° for 90% of the time. A higher road speed reduces the angle range while a lower road speed increases it.

The random variation of the resultant velocity vector means that no single yaw angle represents the average drag of a bus on the road and that the resultant airspeed is almost never equal to the road speed. The typical drag level on the road consists of a weighted average over the yaw curve, where the weighting must reflect the probabilistic effects of the wind. The concept of the "wind-averaged" drag coefficient, $\bar{C}_D(V_b)$, has been developed to quantify these wind effects, as defined in the SAE Recommended Practice for the Wind Tunnel Testing of Trucks and Buses [4], and as discussed in [5]. The wind-averaged drag coefficient is defined as

$$\bar{C}_D(V_b) = \frac{1}{2\pi} \int_0^{2\pi} C_D(\psi) [V_r/V_b]^2 d\phi = \frac{1}{2\pi} \int_0^{2\pi} C_D(\psi) [1 + (V_w/V_b)^2 + 2(V_w/V_b)\cos\phi] d\phi \quad (6)$$

The wind-averaged drag coefficient is obtained by averaging the drag coefficient curve over the range of yaw angles produced by the national annual average mean hourly wind at bus mid-height of 11 km/h, assumed to blow equally probably from all directions, weighted by the ratio of the resultant speed to the road speed, $(V_r/V_b)^2$, to convert to the road speed of the bus as the reference speed. The use of this single wind speed and the equally-probable directional assumption are well supported by meteorological data averaged at 32 sites across Canada. In this fashion, each drag-coefficient-versus-yaw-angle curve is reduced to a single, weighted, average, drag coefficient for every road speed, V_b , greatly facilitating data comparisons and providing a more meaningful number for the estimation of global fuel usage. The wind-averaged drag coefficient also simplifies the computation of bus fuel consumption or speed performance since the road speed is now the reference speed, rather than the varying, resultant airspeed, whose effects are now included in the drag coefficient. The wind-averaged drag coefficient represents the average performance of many buses operated over the entire country for a long period of time. The average drag coefficients for specific regions and specific seasons would differ from this value.

As the road speed varies, the yaw angles produced by the mean wind will change. At low bus speeds, V_r will be increasingly larger than V_b (equation 2) and the maximum yaw angle (equation 1) will increase also. Both of these trends will increase $\bar{C}_D(V_b)$ as V_b decreases. The change in $\bar{C}_D(V_b)$ with road speed can be conveniently related to the value at 90 km/h, a common maximum legal speed, by

$$\bar{C}_D(V_b) = \bar{C}_D(90) [90/V_b]^{0.22} \quad (7)$$

This equation is a fit of the wind-averaged drag coefficient between 70 km/h and 120 km/h and slightly under-predicts the wind-averaged drag coefficient below 70 km/h. The wind-averaged drag coefficient is now based on the road speed, V_b , and the wind-averaged aerodynamic drag is given by

$$\bar{D}(V_b) = 3.858 \times 10^{-2} \rho V_b^2 (\bar{C}_D(V_b) A) \quad (8)$$

The variation of the wind-averaged drag and of wind-averaged drag coefficient with changing bus road speed are emphasized by explicitly indicating their functional dependence on V_b .

3.0 EFFECTS OF AERODYNAMICS ON PERFORMANCE

Aerodynamic forces and moments can affect several aspects of the performance of a bus. Aerodynamic drag is a major component of the total resistance which must be overcome by the engine. Thus, it will have an effect on fuel consumption and on high-speed acceleration. As previously mentioned, the aerodynamic side force and yawing moment produced by the action of the natural wind or adjacent vehicles, and to a lesser extent the associated aerodynamic rolling moment, can deflect the bus from its intended path. The aerodynamic lift and pitching moment cause a change to the vertical reaction forces at the wheels, typically reducing the load on the front wheels and increasing the load on the rear wheels. These latter effects are so small for a bus, compared to passenger and cargo weight changes, that their effects can be ignored. The other items will be discussed in the following sections.

3.1 Fuel Consumption

The fuel consumed by the engine is directly proportional to the total tractive effort required to propel the bus at a given speed. The total resistance that the engine must overcome at a constant speed is composed of the following major elements:

- rolling resistance due to tires and wheel bearings,
- drive line losses in transmitting engine power from the flywheel to the drive wheels,
- grade resistance due to climbing or descending hills,
- cornering resistance due to increased tire rolling resistance in corners,

- parasitic losses due to pumps and fans,
- aerodynamic drag due to an interaction between the moving bus and the windy atmosphere.

At speeds above 90 km/h, the aerodynamic drag becomes the largest component of propulsive power. For example, at a constant speed of 90 km/h on a flat, straight road, it is estimated by equation (15) that 40% of the fuel is consumed by aerodynamic drag, 30% by rolling resistance and 30% by accessories for the standard MCI CJ3 bus (Fig. 5). At 120 km/h, the aerodynamic component of fuel usage increases to 52% of the fuel consumed. Even if the terrain is curved and hilly, the aerodynamic drag will consume the same amount of fuel as on a flat road at the same average speed although, because of the additional fuel required for corners and hill climbing, the percentage of the total will be reduced. The aerodynamic drag on a bus is primarily due to retarding pressure forces - positive on the front end and negative on the rear end. Smaller additional contributions are made by skin friction and parasitic losses due to exposed running gear, miscellaneous protruding frames, and underbody roughness.

The power at the drive wheels required to propel the bus at a road speed of V_b km/h can be written as

$$P(V_b) = \left[\frac{D_t(V_b) V_b}{3600} \right] \text{ kw.} \quad (9)$$

and the corresponding engine power is

$$P_g(V_b) = \left[\frac{D_t(V_b) V_b}{3600 \eta} \right] + P_o \text{ kw.} \quad (10)$$

where η = transmission efficiency factor, assumed to be 0.85 for a single drive axle
 P_o = power used by the accessories, kw.
 $D_t(V_b)$ = total resistance to motion, aerodynamic drag plus rolling resistance, N.
 $= [\bar{D}(V_b) + R]$

The rolling resistance, R , can be represented by

$$R = (a_1 + a_2 V_b) M \text{ N.} \quad (11)$$

where V_b = road speed, km/h.
 M = bus mass, kg.
 a_1 = rolling resistance coefficients

Typical values for the two rolling resistance constants for radial truck or bus tires are

$$a_1 = 5.3 \times 10^{-2} \text{ N/kg.} \quad \text{and} \quad a_2 = 4.0 \times 10^{-4} \text{ N-hr/kg-km.} \quad (12)$$

The accessory power requirements are difficult to determine. Part of the accessory load will be variable, even at constant rpm, due to fluctuating demands for electrical power and air conditioning. Other components of this load, such as power to the cooling fan, will be rpm dependent. A single linear dependence of accessory power requirements versus road speed was assumed as an approximation to the accessory power demand. While the assumed power function will probably under-predict the accessory power requirements at low speeds, in the intermediate gears, it should provide a reasonable full-load estimate at higher speeds in top gear, where aerodynamic effects are dominant. The following function was assumed for the accessory power requirements as a function of engine power level and road speed

$$P_a = P_o [7.70 \times 10^{-3} + 1.50 \times 10^{-3} V_b] \quad \text{kw,} \quad (13)$$

where P_o = engine power rating, kw.

Substitution of equations (2), (7), (11), and (13) in equation (10) gives the total engine power as

$$\begin{aligned} \bar{P}_e(V_b) = & \left[\frac{(5.30 \times 10^{-2} + 4.00 \times 10^{-4} V_b) M V_b}{3600 \eta} \right] + \left[\frac{3.858 \times 10^{-2} \rho V_b^3 (\bar{C}_D(V_b) \cdot A)}{3600 \eta} \right] \\ & + [P_o (7.70 \times 10^{-3} + 1.50 \times 10^{-3} V_b)] \end{aligned} \quad (14)$$

Note that the wind-averaged drag coefficient is used in the aerodynamic drag equation in place of the regular drag coefficient, so necessitating the use of the road speed, V_b , in the calculation, instead of the resultant airspeed. The three major terms in equation (14) are plotted in Figure 4 for the standard CJ3 configuration. The wind-averaged drag coefficient used was the speed-dependent wind-averaged drag coefficient, equation (8). The drag coefficient at 90 km/h was 0.732, the frontal area was 8.36 m², the assumed bus mass was 16500 kg, the engine power was 300 kw, and the transmission efficiency was 0.85. The fuel consumed at a given power level is obtained by using the specific fuel consumption of the engine. A useful average value, characteristic of turbo-charged diesel engines, is $SFC = 0.275$ g/kw-h (0.045 imp. gal/hp-h or 0.38 lb/hp-h). The fuel consumed per 100 kilometres is given by

$$\mu = \left[\frac{100 \cdot SFC \cdot P_e}{V_b} \right] = 27.5 \left[\frac{P_e}{V_b} \right] \quad \text{g/100-km.} \quad (15)$$

Combining equations (14) and (15), the wind-averaged bus fuel consumption, $\bar{\mu}(V_b)$, can be expressed in terms of vehicle size, mass, road speed, and wind-averaged drag coefficient by

$$\begin{aligned} \bar{\mu}(V_b) = & \left[\frac{(1.46 + 1.10 \times 10^{-2} V_b) M}{3600 \eta} \right] + \left[\frac{1.061 \rho V_b^2 (\bar{C}_D(V_b) \cdot A)}{3600 \eta} \right] \\ & + \left[P_o \cdot \left(\frac{2.12 \times 10^{-1}}{V_b} + 4.13 \times 10^{-2} \right) \right] \quad \ell/100\text{-km}. \end{aligned} \quad (16)$$

Inverting the fuel usage calculated from equation (16) and dividing by 100 will give the fuel consumption in km/ℓ. Equation (16) shows that the fuel consumed by aerodynamic drag varies directly with the frontal area, the drag coefficient and with the square of speed. The latter variation is the reason for the importance of aerodynamic effects at higher speeds. The primary aerodynamic parameter is the product of drag coefficient and frontal area, $\bar{C}_D(V_b) \cdot A$, often termed the drag-area. The fuel consumed by rolling friction is only a weak function of speed, being approximately proportional to $V_b^{1/4}$. The three terms of equation (16) are plotted in Figure 5 and the relative importance of the fuel consumed to overcome aerodynamic drag at high speed is evident. The change in fuel consumption due to a change in aerodynamic drag is given by

$$\Delta \mu(V_b) = 2.947 \times 10^{-4} \rho V_b^2 (\Delta \bar{C}_D(V_b) \cdot A) / \eta \quad \ell/100\text{-km}. \quad (17)$$

where $\Delta \bar{C}_D = \bar{C}_D(\text{reference}) - \bar{C}_D(\text{modified})$ is the difference in wind-averaged drag coefficient between the original and the modified configurations. This equation will be used frequently to compute fuel savings in the discussions that follow.

3.2 Cross-wind Handling

The deflection of the bus from its path under the influence of side winds cannot be computed simply from aerodynamic force and moment measurements alone, but must be obtained from a dynamic analysis of the bus and its driver. However, it is possible to make a few general statements about the static directional stability of the bus as a guide to assessing the qualitative effects of changes in the lateral aerodynamic forces and moments. The lateral aerodynamic quantities that affect cross-wind handling are comprised of the side force, the yawing moment, and the rolling moment, and are defined in the sketch of Figure 6.

The side force and the yawing moment have the strongest effect on the lateral deviation of the bus from its path when acted on by a side wind, with the yawing moment being the most important parameter. The rolling moment is a second-order parameter through the influence of roll angle on roll-induced steering - a function of the suspension design.

The side force and the yawing moment both act to deflect the bus away from the direction of the incident wind and are, as a consequence, statically destabilizing (weathercock unstable). If the driver takes no corrective action, the bus would leave the road. The side force and the yawing moment are coupled, since the side force, acting at some point along the length of the bus termed the yaw centre of pressure, can be considered to have produced the yawing moment.

Similarly, the side force and the rolling moment are coupled, except that the roll centre of pressure is measured vertically from the co-ordinate reference centre at ground level.

The side force variation with yaw angle is nearly the same for most bus configurations while the yawing moment varies more with bus shape. Effectively, the yaw centre of pressure moves forward or rearward along the length of the bus as the front and rear shapes are changed. A bluff body, like a square-edged rectangular block, has a yaw centre of pressure at the mid-length point of the body. A streamlined shape, like an aerofoil, has the yaw centre of pressure at a point one-quarter of the aerofoil length aft of the leading edge. A bus, being well streamlined at the front end, may have its centre of pressure even farther forward. As a bus becomes more streamlined and develops lower aerodynamic drag, so its centre of pressure moves forward, and the bus becomes less weathercock stable. Simply put, it blows around more in the wind. Again, without a complete dynamic analysis, it is impossible to quantify the degradation in cross-wind handling. However, there is an anecdotal measure of this effect available.

It was reported by MCI engineering staff that a few drivers have commented that the MCI CJ3 bus is better handling in a cross wind than the Prevost H3-40. It appears that only some drivers have noticed this handling difference, and they say that it is not large. Thus the aerodynamic differences between these configurations, both of which were tested in this program, define the boundary of a just-perceptible threshold in yawing moment change or, equivalently, yaw centre of pressure movement. The centre of pressure location for a small range of yaw angles near zero yaw can be obtained from the ratio of the slope of the yawing moment coefficient curve divided by the slope of the side force coefficient curve. Analytically, this is expressed as

$$(x_{cp}/b) = \left[\frac{dC_N/d\psi}{dC_S/d\psi} \right] \quad (18)$$

where x_{cp} = location of the centre of pressure ahead of the chosen moment centre at the mid-wheelbase point, m.
 b = reference length, 7.225 m.full scale, 0.7225 m. model scale
 $dC_N/d\psi$ = slope of the yawing moment coefficient versus yaw angle curve for the yaw range between $\pm 3^\circ$, deg^{-1}
 $dC_S/d\psi$ = slope of the side force coefficient versus yaw angle curve for the yaw range between $\pm 3^\circ$, deg^{-1}

The locations of the yaw centres of pressure for the two configurations just mentioned, measured forward from the mid-wheelbase point, were found to be

CONFIGURATION	(x_{cp})
MCI (#37)	2.06 m.
Prevost (#63)	2.29 m.

Thus a forward, destabilizing movement of the centre of pressure of about 0.23 m. is just detectable by some drivers and several times this change might be acceptable.

4.0 TEST PROGRAM

The primary purpose of the wind tunnel test program was to select the front and rear end shapes from the new proposals that gave the lowest aerodynamic drag, while a secondary purpose was the comparison of the best of the new proposals with the current MCI bus and with buses from competing manufacturers. At the same time, the remaining aerodynamic forces and moments were measured so that their effects on stability and cross-wind handling could be assessed. Both smoke and a surface oil film were used to visualize the flow over and on the surface of the best combination. The test program is summarized in the Run Log of Appendix 1.

4.1 Model Installation

A 1:10 scale model of the bus chassis was mounted on the standard NRC vehicle ground plane, Figure 1. The model accurately duplicated the external geometry of the bus. The seven front-end shapes, one of the two rear-end shapes, and the body side and roof panels were numerically milled from mahogany. The second rear end was manufactured using stereolithography. The body components were attached to chassis and running gear manufactured from aluminum. The model included such details as fenders, wheels and wheel wells, drip rails, escape hatches, and mirrors. No internal flows, air intakes, underbody roughness, engine bay openings, or window frames were reproduced. The former were excluded because of the difficulty of representing cooling flows adequately at model scale and because their effects would be the same for each configuration, and the latter because the frames were so shallow as to be unimportant and the other openings were too complex and, once again, would cause no relative difference between configurations. The external surfaces of the model were smooth and leak-free, representing flush windows, doors, and seals. The front and rear faces of the bus could be readily removed to permit the testing of alternate components.

The bus was connected to the six-component, mechanical balance of the wind tunnel by pins extending from the standard model-mounting plate, through the groundboard cover plate, into the front and rear tire contact patches. This provided an aerodynamic-interference-free mounting. The six balance outputs were averaged digitally over a 10 second period at repetition rates of 20 samples per second per channel to form stable averages with an overall measuring accuracy of $\pm 0.5\%$.

4.2 Model Configurations

The two prototype front-end shapes had been designed to provide good aerodynamics through a combination of windshield slope, face curvature, and edge rounding, within the bounds of aesthetic, engineering, and operational requirements. The other five front ends included the current MCI CJ3 production bus and three competitors designs. One alternate rear-end shape to the standard was tested, based on the optimal-design information presented in [3]. The effect of additional components such as drip rails, escape hatches, and mirror shape and location were also investigated. The bus model was designed to permit the rapid evaluation of alternate front-end and rear-end designs through the use of removable components. The model chassis, the seven front ends, and the two rear ends that were tested are shown in the drawings of Figure 7 and the photographs of Figure 1. A complete set of photographs of all of the model configurations

tested is presented in Appendix 2.

The front-end shapes consisted of the following:

1) Standard CJ3	The standard CJ3 front including all window moulding details.
2) Smooth CJ3	A modified CJ3 front with larger edge radii and flush glass.
3) Proposal 1	A new design with flush glass.
4) Proposal 2	A new design with flush glass.
5) Prevost H3-40	Competitor.
6) Mercedes 0404	Competitor.
7) Setra S315	Competitor.

The rear-end shapes consisted of the following:

1) Standard CJ3	Top and sides parallel to the top and sides of the main bus with 204 mm rear-edge radii.
2) Bevelled Rear	Roof and sides of the body bevelled at an angle of 15° to the main panels over the last 1m of the body with rear-edge radii of 51 mm.

4.3 Definition of the Measurement Coordinate System

Six components of aerodynamic force and moment were measured simultaneously. The measurements in this report are presented in a body-fixed co-ordinate system that is defined in Figure 6. These measured forces and moments were reduced to coefficient form as defined in the Notation, Section 8.0, and as discussed in Section 2.2.

4.4 Test Procedure

Each configuration was tested over a range of eight yaw angles from -3° to +12° in the following sequence: -3.0°, -1.5°, 0.0°, 1.5°, 3.0°, 6.0°, 9.0°, 12.0°. The yaw angles were set by rotating the model in the wind tunnel sequentially through the required set of angles, under computer control, and pausing at each angle sufficiently long to acquire the necessary measurements. The yaw tests were performed at a wind speed of 302 km/h (84 m/sec). At this speed, the model Reynolds numbers were 0.34 and 0.26 of those of the full-scale bus at 90 km/h and 115 km/h, respectively. Additional tests were also made over a range of Reynolds numbers at 0° yaw angle to investigate the Reynolds number sensitivity of the drag. Some tests were also run with strips of grit upstream of the rounded front edges to ensure that the boundary layers on the front face had gone through transition before the flow reached the edges.

5.0 RESULTS

The following presentations, discussions and interpretations of results focus primarily on aerodynamic drag, although the location of the yaw centre of pressure for important configurations will be presented to allow an assessment of cross-wind handling changes. A total of 37 runs were performed during the wind tunnel test. A detailed summary of these runs is given in Appendix 1. In addition, this Appendix summarizes the wind-averaged drag coefficients at a road speed of 90 km/h. Appendix 3 contains a complete tabulation of the wind tunnel data and Appendix 4 presents plots of all the aerodynamic coefficients.

6.0 DISCUSSION AND INTERPRETATION OF RESULTS

This Section presents the major findings of the investigation and summarizes these in terms of the measured changes in wind-averaged drag coefficients, in terms of the expected changes in fuel consumption that would result, and in terms of the changes in cross-wind sensitivity that accompany the drag changes. The changes in fuel consumption were computed only at 90 km/h and 120 km/h.

The best combination of front and rear components was selected from the three new front-end and two rear-end designs. This combination was compared in detail to the standard MCI 102 CJ3 bus and to the three competitors from the point of view of fuel usage.

6.1 Reynolds Number Effects

After the first set of measurements were made with the seven front ends, an examination of the data showed an apparent anomaly in the yaw data for the Proposal 2 front end at yaw angles greater than $+3^\circ$, where the drag was observed to increase more rapidly than would be expected. This was judged to be a result of leading-edge flow separation due to insufficiently high Reynolds number for this configuration. No other configuration showed this effect. It was decided to trip the flow on this and the three other smooth, front-end configurations - Proposal 1, Smooth CJ3, and Prevost H3-40 - to make sure that such effects were eliminated. Fine, #40-grit particles were sprinkled sparsely on 0.5-cm wide strips of glue painted on each front face, just upstream of the front edges, to encourage early boundary layer transition. A typical application is shown in photograph P???. A comparison of the variation of drag coefficient with Reynolds number at 0° yaw angle of the four, smooth-edged configurations is presented in Figure 8, with and without the trip strips.

Generally, the absence of a trip results in high drag coefficients at low Reynolds numbers, followed by a rapid drop in drag coefficient above some threshold Reynolds number that varies from model to model. This drop results from the natural transition of the boundary layer on the front face of each model from laminar to turbulent, so reducing the occurrence of flow separation from the front edges. The presence of the grit strips ensures that the flow is turbulent, causing the drag drop at much lower Reynolds numbers. The end result is a flow field on the model that is more typical of the full scale bus at its higher operating Reynolds number.

The effect of the flow trips on the yaw behaviour of these four configurations at the test Reynolds number of 1.4×10^6 is summarized in Figure 9. The measurements with and without grit on the Smooth CJ3 front and the Proposal 1 front are identical. The presence of the trip lowers the drag on the Prevost front slightly at yaw angles $\leq 6^\circ$ and smooths the drag curve at higher yaw angles. The flow trip had the greatest effect on the Proposal 2 front configuration substantially lowered its drag coefficients for yaw angles above 3° .

The remainder of the measurements on these four configurations were made with the trips present because they were felt to better represent full scale.

6.2 Front-End Shape Effects

The first set of measurements were made to select the best new front-end shape from the new proposals. All the front ends were tested without mirrors and with the standard CJ3 rear end. Figure 10 summarizes the drag results for the new front-end shapes. It shows that all three of the new shapes are nearly identical to each other and are better than the current MCI CJ3 front. The Proposal 2 shape was chosen by the attending MCI engineers as the best shape because of its good aerodynamic performance, its ease of manufacture compared to Proposal 1, and because of its styling. Figure 11 compares the standard MCI front end and the Proposal 2 shape with shapes used by the competition. Both the Setra and the Mercedes front ends have higher drag than the standard MCI shape and much higher drag than the Prevost or the MCI Proposal 2 shapes. The MCI Proposal 2 shape has slightly lower drag than the Prevost shape for $\psi \leq 3^\circ$ and increasingly lower drag at higher yaw angles. Table 6.1 summarizes the wind-averaged drag coefficients, the fuel consumption changes, and centre-of-pressure locations for these seven geometries. Figure 12 compares the side force and the yawing moment coefficients. The higher-drag front ends usually have the lower yawing moments and, consequently, smaller magnitudes for the yaw centre of pressure locations, as also seen in Table 6.1.

TABLE 6.1: FRONT-END SHAPE EFFECTS WITH CJ3 REAR

CONFIGURATION	90 km/h			120 km/h			$x_{cp}^\#$
	\bar{C}_D	$\Delta \bar{C}_D$	$\Delta \bar{\mu}^*$	\bar{C}_D	$\Delta \bar{C}_D$	$\Delta \bar{\mu}^*$	
STD CJ3, #19	0.584			0.558			1.95
SMOOTH CJ3, #72	0.380	0.204	5.87	0.370	0.188	9.62	2.29
PROPOSAL 1, #69	0.367	0.217	6.25	0.360	0.198	10.13	2.40
PROPOSAL 2, #40	0.365	0.219	6.30	0.357	0.201	10.29	2.25
PREVOST, #65	0.418	0.166	4.78	0.386	0.172	8.8	2.06
SETRA, #35	0.625	-0.041	-1.18	0.601	-0.043	-2.20	1.98
MERCEDES, #22	0.620	-0.036	-1.04	0.598	-0.040	-2.05	1.62

* change in fuel consumption, $\mathcal{L}/100\text{-km.}$, positive represents a fuel saving.

distance in m. forward of the mid-wheelbase point.

6.3 Rear-End Shape Effects

The alternate rear end utilized the optimum rear body bevel angle of 15° and bevel length of 1.0 m full scale, as specified in [3]. This geometry has the potential to reduce the base drag by 40% to 60%, based on the data presented in [3], with the level of reduction being dependant on the shape of the forward part of the bus. This rear shape is compared to the standard, CJ3 rear shape, both with and without the standard, CJ3 mirrors in Figure 13. The effects of mirrors will be discussed in more detail in the following Section. The new rear shape reduces the drag and moves x_{cp} forward in both cases. The wind-averaged drag coefficients, fuel consumption changes, and centre-of-pressure locations are presented in Table 6.2.

TABLE 6.2: EFFECT OF BEVELLED REAR WITH PROPOSAL 2 FRONT

CONFIGURATION	90 km/h			120 km/h			$x_{cp}^{\#}$
	\bar{C}_D	$\Delta \bar{C}_D$	$\Delta \bar{\mu}^*$	\bar{C}_D	$\Delta \bar{C}_D$	$\Delta \bar{\mu}^*$	
CJ3 REAR, NO MIR, #40	0.365			0.357			2.25
BEV REAR, NO MIR, #51	0.299	0.066	1.90	0.295	0.062	3.17	2.78
CJ3 REAR, CJ3 MIR, #42	0.394			0.385			2.28
BEV REAR, CJ3 MIR, #53	0.339	0.055	1.58	0.331	0.054	2.76	2.80

* change in fuel consumption, $\ell/100\text{-km.}$, positive represents a fuel saving.

distance in m. forward of the mid-wheelbase point.

6.4 Mirrors

The effects of mirror shape and position were investigated for the Proposal 2 front with the CJ3 rear. Three sets of mirrors were fabricated - the current MCI design, the Prevost design, and the Setra design. The Setra and Prevost mirrors were mounted in one position only, photographs P13 and P14, while the MCI mirrors were mounted with three alternate positions. These positions were forward, aft, and asymmetrical, as shown in photographs P11, P12, and P16. The asymmetrical configuration is more representative of real operation, where the left-hand mirror was set more aft than the right-hand mirror, which was set in the forward position. The effect of mirror position and type can be seen in Figure 14. The addition of any mirror is seen to increase the drag, with the Setra mirrors causing the largest increase. The standard MCI mirrors produced higher drag in the aft position than in the forward position. This may be explained by the fact that the planes of the mirrors in the forward positions were nearly parallel to the flow around the front, side edges, whereas they were more nearly perpendicular to the flow in the aft position. The drag coefficients for the asymmetrical positions were between the values for the other two positions. The Prevost mirrors provided slightly lower drag than the MCI mirrors for $\psi \leq 3^\circ$ but much higher drag above this angle. Apparently, the Prevost mirrors caused flow separation over at least part of the downwind side of the bus. The results of the mirror variations are summarized in Table 6.3.

TABLE 6.3: MIRROR EFFECTS WITH PROPOSAL 2 FRONT AND CJ3 REAR

CONFIGURATION	90 km/h			120 km/h		
	\bar{C}_D	$\Delta\bar{C}_D$	$\Delta\bar{\mu}^*$	\bar{C}_D	$\Delta\bar{C}_D$	$\Delta\bar{\mu}^*$
NO MIRRORS, #40	0.365			0.357		
MCI MIRRORS FWD, #42	0.394	-0.029	-0.83	0.385	-0.028	-2.20
MCI MIRRORS AFT, #44	0.405	-0.040	-1.15	0.398	-0.041	-3.07
MCI ASSYM. MIRRORS*	0.415	-0.050	-1.44	0.403	-0.046	-2.35
SETRA MIRRORS, #46	0.434	-0.069	-1.99	0.425	-0.068	-4.35
PREVOST MIRRORS, #48	0.422	-0.057	-1.64	0.397	-0.040	-1.84

* change in fuel consumption, $\ell/100\text{-km.}$, positive represents a fuel saving.

* estimated as #40+ (#55-#51).

6.5 Miscellaneous Modifications

A series of small modifications were made to investigate the following:

- wheel skirts closing the sides of the wheel wells, P17; Run # 57
- a front air dam below and behind the bumper, P18; Run # 58
- tire fairings to shield the tires from the oncoming flow, P19; Run # 59
- rear side vortex generators, P20; Run # 60
- a modified drip rail, P21; Run # 61

Most of these modifications had only small effects on the drag. Of them, only the wheel skirts produced a drag reduction while the remainder produced no change or a drag increase. The results of these tests are summarized in Table 6.4.

TABLE 6.4: MISCELLANEOUS SMALL MODIFICATIONS TO THE PROPOSAL 2 FRONT WITH BEVELLED REAR AND ASYMMETRICAL MIRRORS

CONFIGURATION	90 km/h			120 km/h		
	\bar{C}_D	$\Delta\bar{C}_D$	$\Delta\bar{\mu}^*$	\bar{C}_D	$\Delta\bar{C}_D$	$\Delta\bar{\mu}^*$
STANDARD, #55	0.349			0.341		
WHEEL FAIRINGS, #57	0.330	0.019	0.55	0.324	0.017	0.31
AIR DAM, #58	0.393	-0.044	-1.27	0.380	-0.038	-1.94
TIRE FAIRINGS, #59	0.353	-0.004	-0.23	0.349	-0.008	-0.41
VORTEX GENERATORS, #60	0.354	-0.005	-0.14	0.346	-0.005	-0.31

* change in fuel consumption, $\ell/100\text{-km.}$, positive represents a fuel saving.

6.6 The Best Combination

A comparison can now be made between the best new configuration, the Proposal 2 front with the bevelled rear, the current production MCI CJ3 bus, the Prevost H3-40 bus, the Mercedes 0404 bus, and the Setra S315 bus. These configurations were composed of the following elements:

New MCI	-	Proposal 2 front, bevelled rear, asymmetrical mirrors
MCI CJ3	-	CJ3 front, CJ3 rear, asymmetrical mirrors (estimate)
Prevost H3-40	-	Prevost front, CJ3 rear, Prevost mirrors
Mercedes 0404	-	Mercedes front, CJ3 rear, Prevost mirrors (estimate)
Setra S315	-	Setra front, CJ3 rear, Setra mirrors (estimate)

Estimates were used for the drag of most of the mirror geometries because not all of the front-end configurations were tested with the required mirrors or mirror locations. In each case where an estimate was made, the additional drag increment due to the mirror change, based on the mirror measurements made with the Proposal 2 front, were added to account for these mirrors on the other bus shapes. Table 6.5 summarizes the differences in drag and fuel consumption between these configurations, using the Proposal 2 configuration as the reference. The drag increments added to account for the incorrect mirror geometries are summarized in the table. Thus, the wind-averaged drag coefficients quoted are those for the run indicated, plus the additional mirror drag increment, $\Delta \bar{C}_{D_{mir}}$.

TABLE 6.5: COMPARISON OF FULLY-EQUIPPED BUSES

CONFIGURATION	90 km/h				120 km/h				$x_{cp}^{\#}$
	$\Delta \bar{C}_{D_{mir}}$	\bar{C}_D^*	$\Delta \bar{C}_D$	$\Delta \bar{\mu}^*$	$\Delta \bar{C}_{D_{mir}}$	\bar{C}_D	$\Delta \bar{C}_D^*$	$\Delta \bar{\mu}^*$	
NEW MCI, #55		0.349				0.341			2.81
MCI CJ3, #37	0.010	0.606	-0.257	-7.40	0.010	0.581	-0.240	-12.28	2.06
PREVOST, #63		0.447	-0.098	-2.82		0.415	-0.074	-3.79	2.29
MERCEDES, #22	0.029	0.649	-0.300	-8.64	0.029	0.627	-0.286	-14.63	1.62
SETRA, #35	0.069	0.694	-0.345	-9.93	0.068	0.669	-0.328	-16.78	1.98

* equal to the wind-averaged drag coefficient for the run number stated plus the mirror drag increment $\Delta \bar{C}_{D_{mir}}$.

* change in fuel consumption, $l/100\text{-km.}$, positive represents a fuel saving.

distance in m. forward of the mid-wheelbase point.

The drag coefficient curves for these configurations are compared in Figure 15 and the side force and yawing moment coefficient curves are presented in Figure 16. Once again, estimated mirror drag coefficients have been added to the configurations noted above. The key for Figure 15 summarizes the measurements that were combined to produce the curves plotted.

Figure 17 compares the fuel consumption of the new design with those of the other four main configurations, as functions of road speed, for identical masses of 16,500 kg, identical drive-line losses of 15%, and identical frontal areas of 8.36 m². The new bus is seen to provide a large reduction in fuel consumption compared to the standard MCI CJ3 bus and the two European buses, and a substantial advantage over the Prevost bus. The current MCI CJ3 is inferior to the Prevost H3-40. The improvement of the new configuration over the MCI CJ3 results from both front and rear shape improvements while the advantage over the Prevost bus comes primarily from the rear-end shape. The new MCI configuration would have a yaw centre of pressure location that is 0.52 m ahead of that for the Prevost bus.

6.7 Flow Visualization

The flow over the best combination was observed, or visualized, using two techniques. First, smoke was used to obtain a gross overview of the external flow field and, second, a fine pigment suspended in an oil mixture was painted on the surface of the bus to show the details of the surface flow. Both flow visualization techniques were performed at zero yaw angle only.

The smoke flow photographs of Figure 18 show a few important details of the flow. Figures 18a, 18b, and 18c clearly indicate that the gross flow follows the contour of the bus, both up over the front top edges and down over the rear bevel. Figure 18d shows the wake of a mirror extending along the side of the bus.

The surface-oil-flow photographs of Figure 19 contain more detail than do the smoke flow photographs. Figure 19a shows the stagnation point on the front face of the bus. The flow streamline that strikes the bus at this point comes to a complete stop, providing the point of highest positive pressure on the front face. The remaining streamlines turn and diverge from this point. While the smoke showed that the flow around the front edges was attached, the oil flow shows that there is a very small separation region, or bubble, at the downstream edges of the top and side corners. Here, the flow separates and immediately re-attaches, producing a small separated cavity parallel to these corners, as indicated by the accumulations of oil. The small separation causes little or no drag increase although it indicates that the edge radius should be increased for a greater margin from separation - an observation that is consistent with the Reynolds number sensitivity observed for this configuration.

The influence of the mirror can be seen over the full length of the side of the bus in Figures 19b and 19c. The two lines above and below the mirror on the bus body indicate separation lines feeding a pair of vortices induced by the mirror. These vortices contribute to the drag increase caused by the mirrors and could be a source of aerodynamic noise. The mirror on the driver's side, in the aft position, showed an almost identical flow pattern.

Figure 19d shows the rear-end flow. The flow is attached on the bevelled top and side panels and is separated over the bluff base. It appears that a horizontal, trapped vortex sits on the upper third of the base, in the region that is covered with the oil mixture. It is fed by the flow over the roof and along the upper sides of the body. The strength of this vortex flow may tend to keep this region scoured clear of dirt. The remaining, lower, separated flow region is fed by the underbody flow and by the side flows coming over and out of the rear wheel wells. It should be the dirtier region because it is fed by the most dirt-laden flow from the wheels and because the larger, more diffuse vortex contains lower-speed flows.

7.0 CONCLUSIONS

A wind tunnel test was performed to select the best aerodynamic configuration for a new bus - Proposal 2 with a bevelled rear end - from a set of proposed designs, and to compare this configuration to the current production MCI CJ3 and to three competitors - the Prevost H3-40, the Mercedes 0404, and the Setra S315. The new design had lower aerodynamic drag than the other buses, resulting in lower predicted power consumptions and lower fuel consumptions. The reduced fuel consumption has an obvious and strong impact on the direct operating cost of the bus while the lower required power level should result in reduced noise, increased drive line reliability, better passing acceleration, and greater drive tire life. An indication of the superior performance of the new bus is given in the following table.

PERFORMANCE COMPARISON AT 120 km/h

BUS	\bar{C}_D	TOTAL POWER, kw	FUEL CONSUMPTION $\ell/100\text{-km.}$
New MCI	0.349	197.8	45.3
MCI CJ3	0.606	252.8	57.9
Prevost H3-40	0.447	214.8	49.2
Mercedes 0404	0.649	260.9	59.8
Setra S315	0.694	271.4	62.2

This design is a good compromise between low drag, as shown by these tests, and ease of manufacture, according to the attending MCI engineers. It would be possible to design a lower-drag front end for this new configuration, one that might have a wind-averaged drag coefficient below 0.30, but it may require a significant change to the driving position and mirrors, as well as being a more difficult and expensive geometry to manufacture.

8.0 NOTATION

- a_i rolling resistance coefficients, equation (12)
- b reference width for moment coefficients, wheelbase, 7.225 m. full scale, 0.7225 m. model scale
- C_D drag coefficient, $D/(1/2\rho V^2 A)$
- $\bar{C}_D(V_b)$ wind averaged drag coefficient based on *bus road speed*, $\bar{C}_D(V_b) = \bar{D}/(1/2\rho V_b^2 A)$
- C_L drag coefficient, $L/(1/2\rho V^2 A)$
- C_M drag coefficient, $M/(1/2\rho V^2 A b)$
- C_N drag coefficient, $N/(1/2\rho V^2 A b)$
- C_R drag coefficient, $R/(1/2\rho V^2 A b)$
- C_S drag coefficient, $S/(1/2\rho V^2 A)$
- D aerodynamic drag force, N.

$\overline{D}(V_b)$	wind-averaged drag, includes the effects of the 11 km/h annual hourly mean wind speed blowing with equal probability from all directions, N.
D_t	total resistance to the forward motion of a bus due to aerodynamic drag, rolling resistance of tires, and wheel bearing losses, N.
$dC_N/d\psi$	slope of the yawing moment coefficient versus yaw angle curve, deg^{-1}
$dC_S/d\psi$	slope of the side force coefficient versus yaw angle curve, deg^{-1}
M	bus mass, kg.
$P(V_b)$	power required at the rear wheels for propulsion of the bus at speed V_b , kw.
P_a	accessory power consumption, kw.
P_e	engine power, P_a/η , kw.
$\overline{P}_e(b)$	wind-averaged engine power, kw.
P_o	engine power rating, kw.
R	rolling resistance of tires and wheel bearings, N.
V_b	bus road speed, km/h.
V_r	resultant air speed due to wind and bus motion, equivalent to wind tunnel test speed, equation (5), km/h.
V_w	speed of the natural wind, km/h.
w	reference length for Reynolds number, maximum legal vehicle width, 2.56 m.
x_{cp}	centre of pressure of the side force vector relative to the mid-wheelbase origin of coordinates, equation (18), m.
ρ	air density, 1.226 kg/m^3 at S.T.P.
ψ	yaw angle, the angle between the direction of the resultant wind and the direction of bus motion, equation (4), deg.
ϕ	direction of the natural wind relative to the direction of bus motion
η	transmission efficiency
μ	bus fuel consumption, $\ell/100\text{-km}$.
$\overline{\mu}(V_b)$	wind-averaged bus fuel consumption, equation (16), $\ell/100\text{-km}$.

9.0 REFERENCES

1. Cooper, K. R., The Wind Tunnel Simulation of Surface Vehicles.
2. Cooper, K. R., The Effect of Aerodynamics on the Performance and Fuel Consumption of Trucks and Buses.
3. Cooper, K. R., The Effect of Front-Edge Rounding and Rear-Edge Shaping on the Aerodynamics of Bluff Vehicles in Ground Effect.
4. The Wind Tunnel Testing of Buses and Trucks.
5. Cooper, K. R., The Wind Tunnel Testing of Eight Commercially-Available Aerodynamic Drag Reducing Devices.

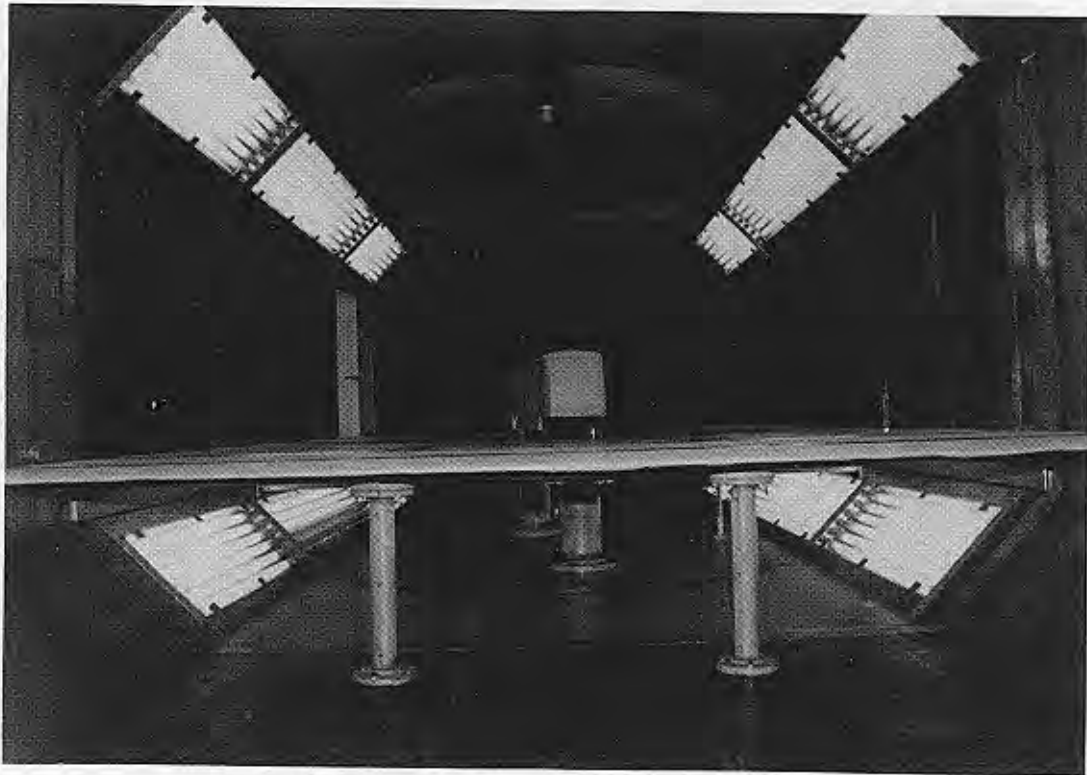


FIG. 1a: SMOOTH CJ3 MODEL ON GROUNDBOARD LOOKING DOWNSTREAM

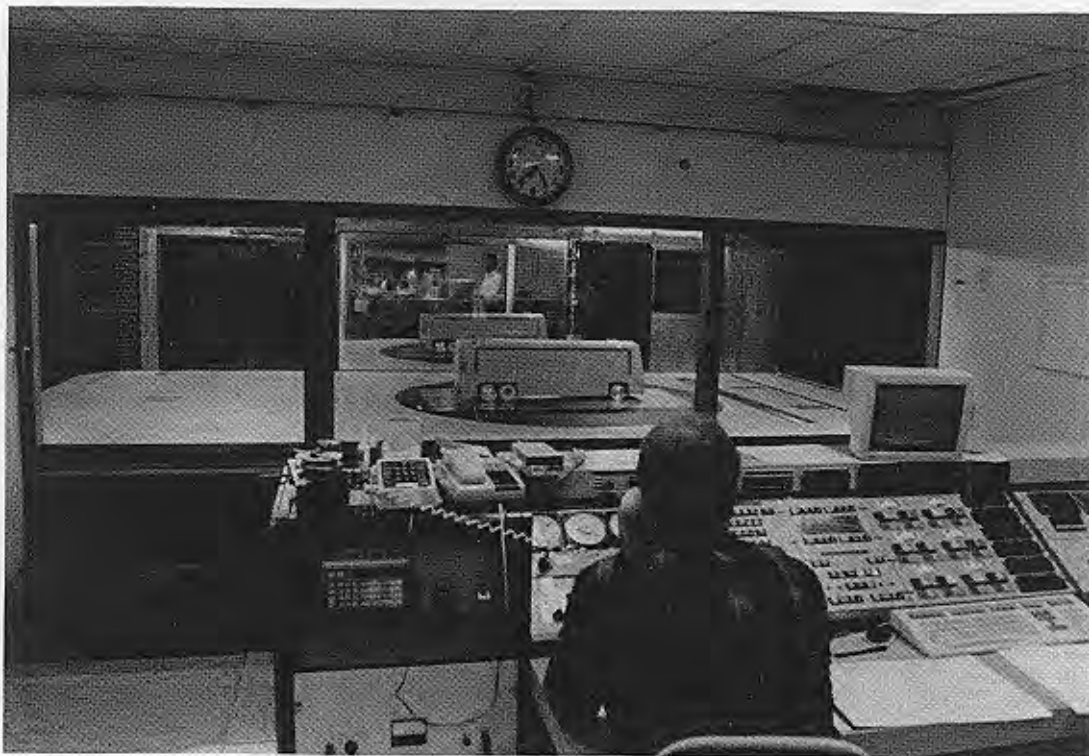


FIG. 1b: TEST SECTION AND CONTROL ROOM VIEWED FROM BEHIND OPERATOR

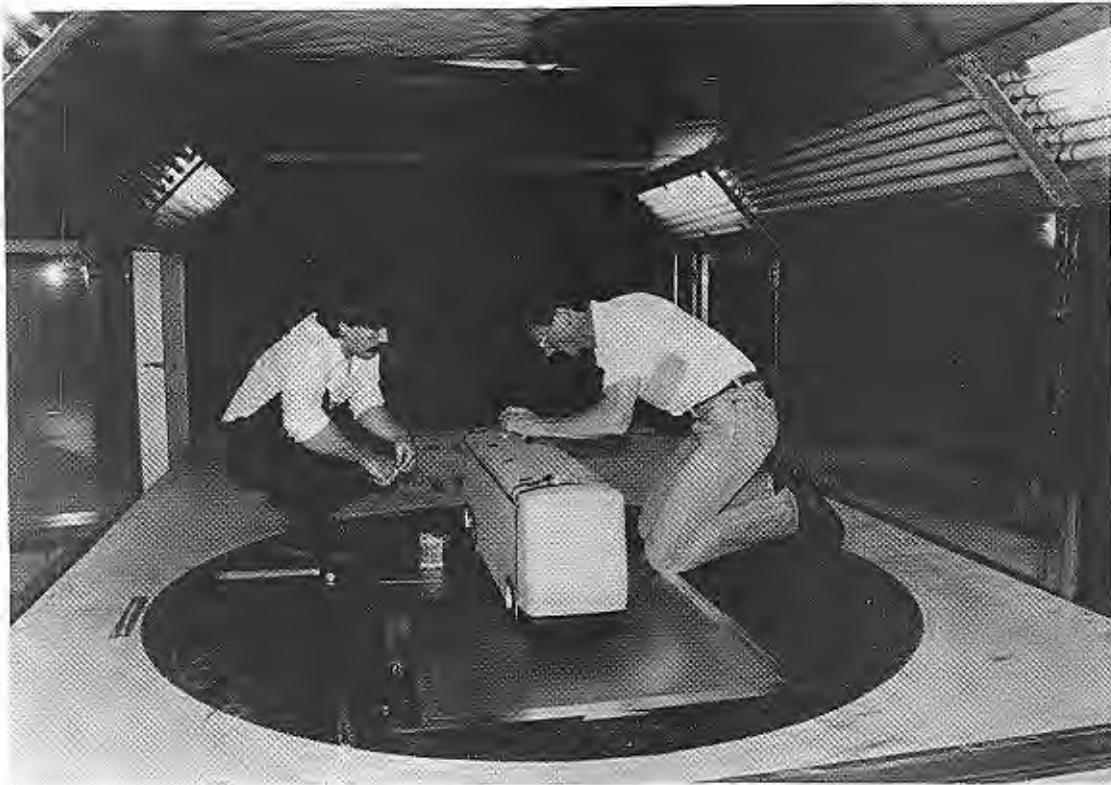


FIG. 1c: FITTING HATCHES, SMOOTH CJ3



FIG. 1d: MODEL WITH ALTERNATE FRONT AND REAR COMPONENTS

(from left to right - Standard CJ3, Setra S315, Prevost H3-40, Mercedes 0404, Smooth CJ3, Proposal 1, Bevelled Rear, Proposal 2 - note suction slot just upstream of the turntable)



FIG. 2: RESULTANT VELOCITY VECTOR DIAGRAM

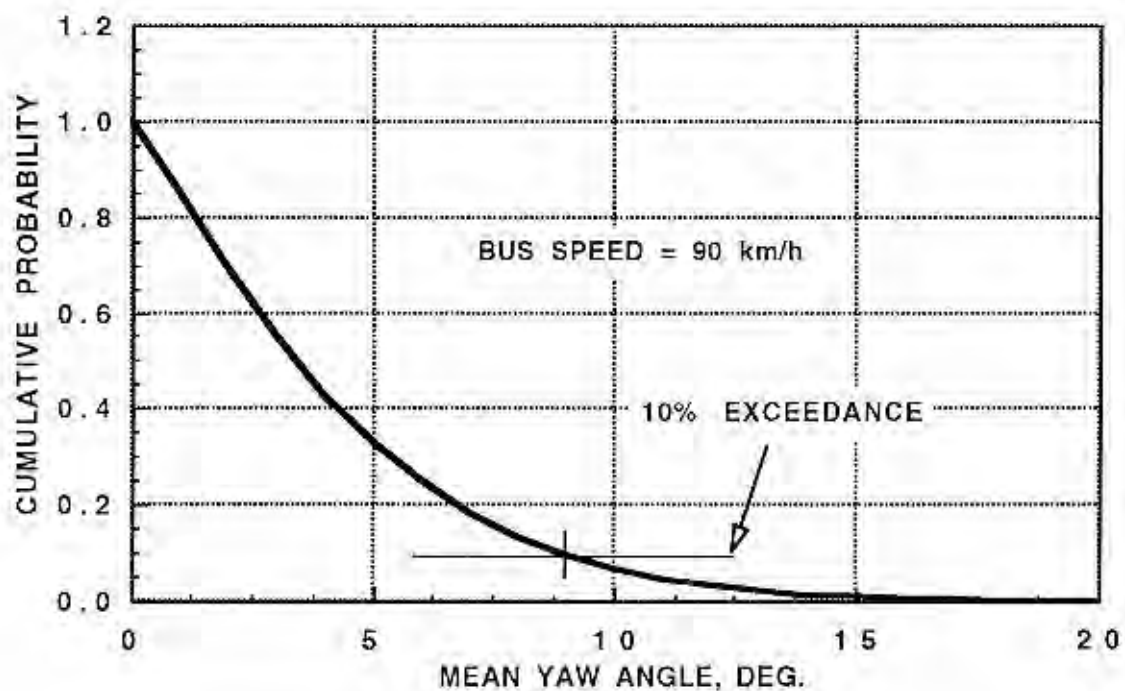


FIG. 3: PROBABILITY OF EXCEEDING A GIVEN YAW ANGLE
AT A BUS SPEED OF 90 km/h

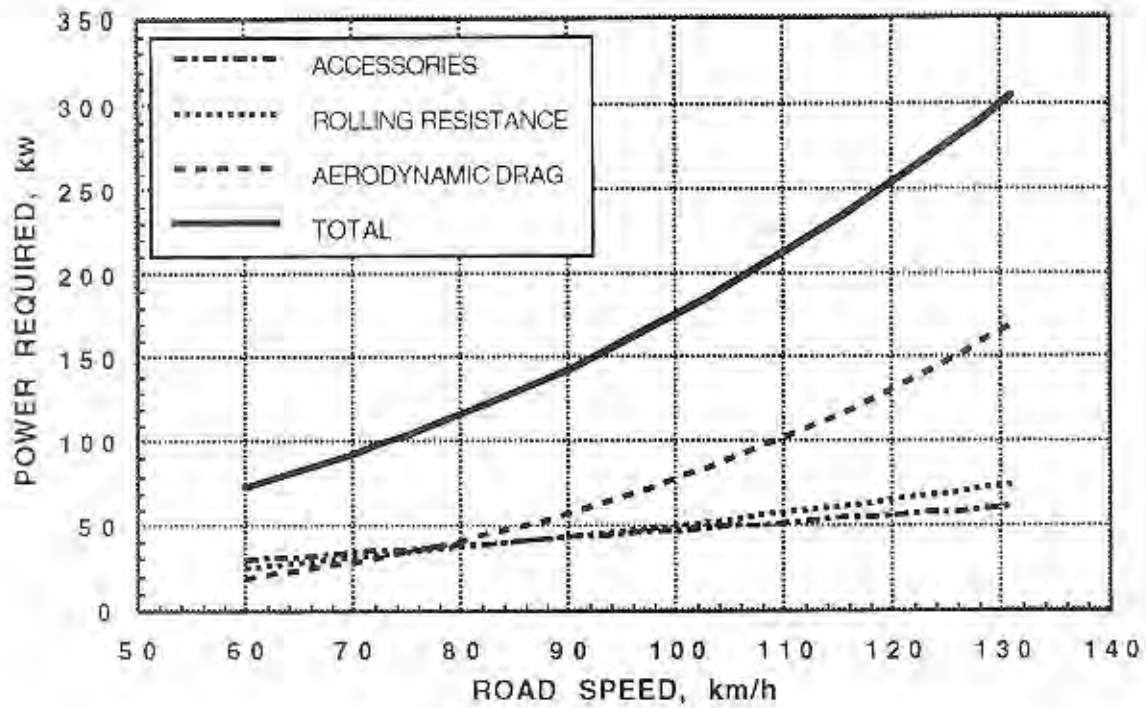


FIG. 4: POWER COMPONENTS FOR THE STANDARD CJ3

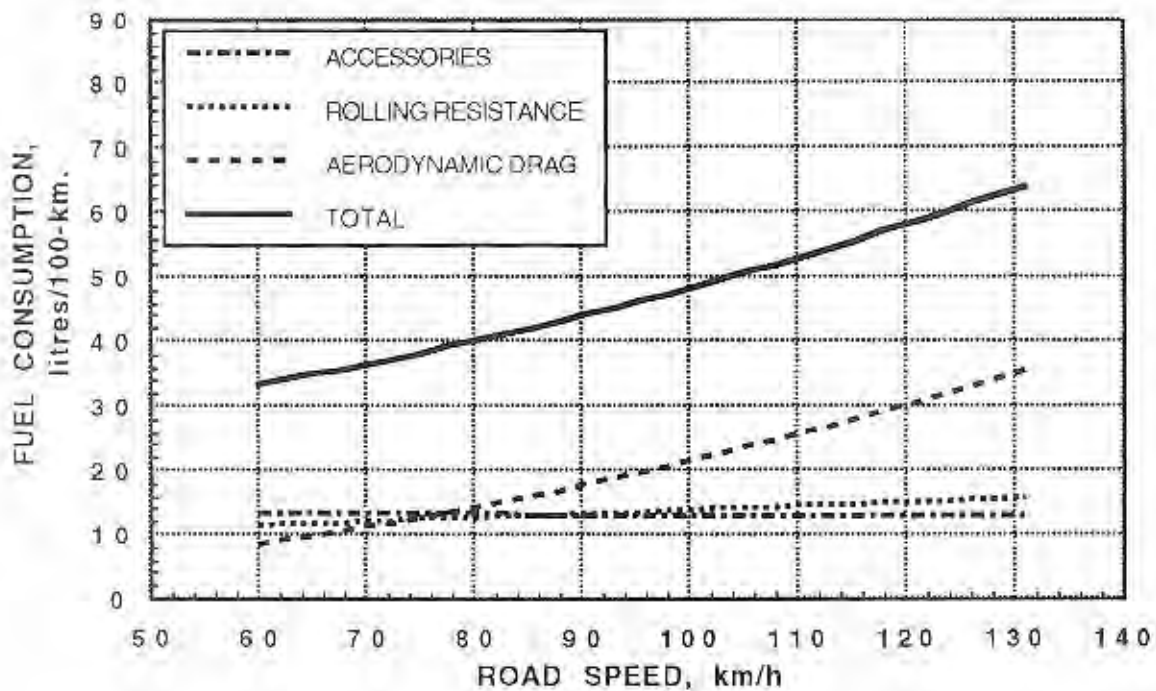


FIG. 5: COMPONENTS OF FUEL CONSUMPTION FOR THE STANDARD CJ3

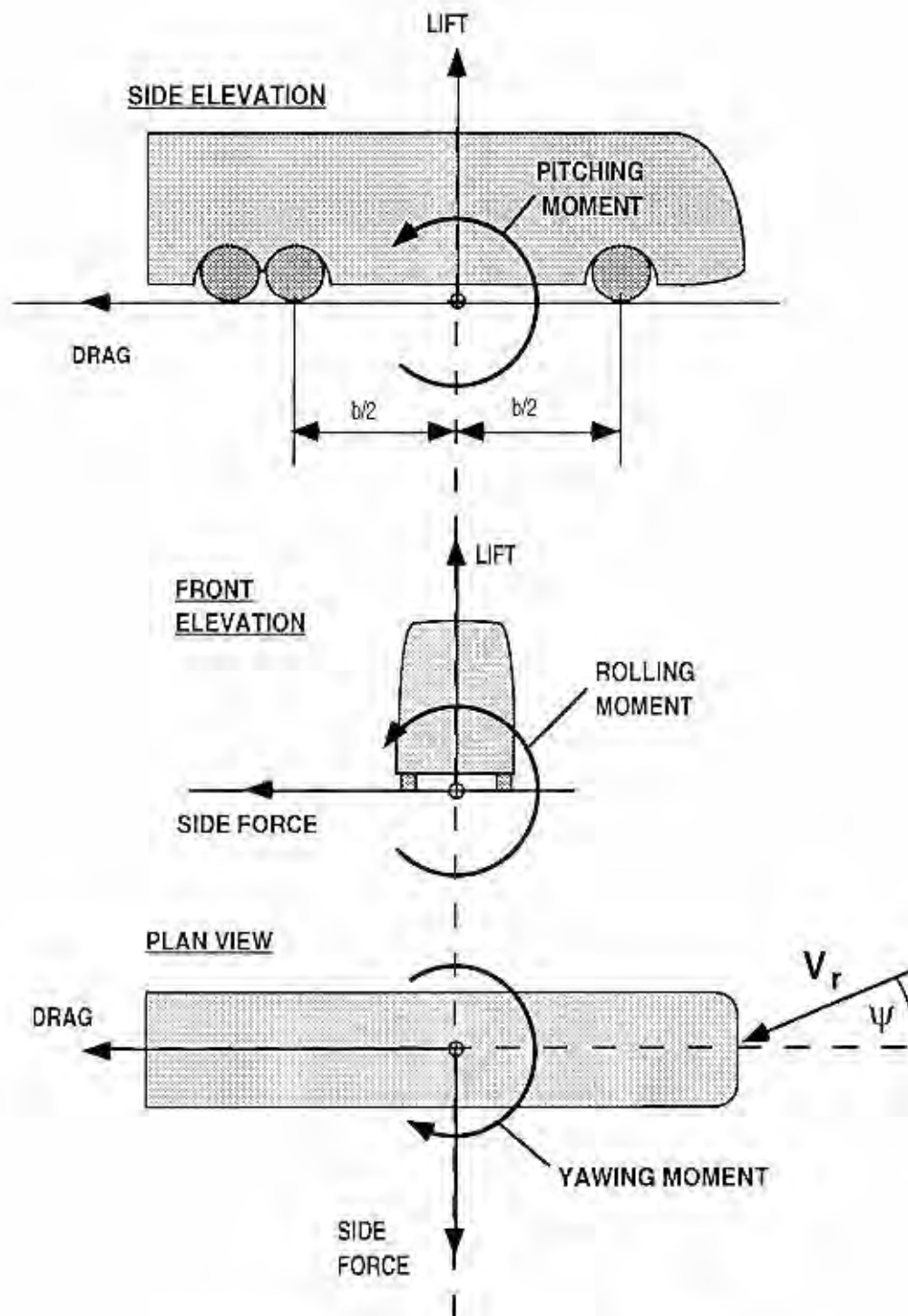
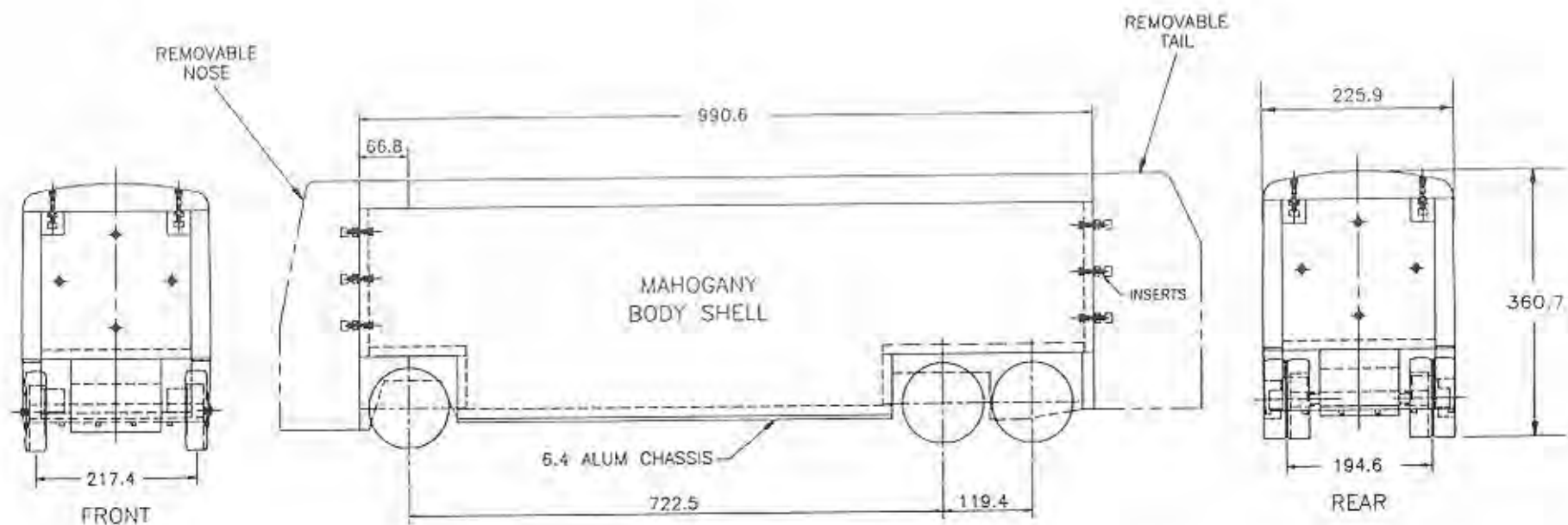


FIG. 6: MEASUREMENT CO-ORDINATE SYSTEM



• ALL DIMENSIONS IN mm

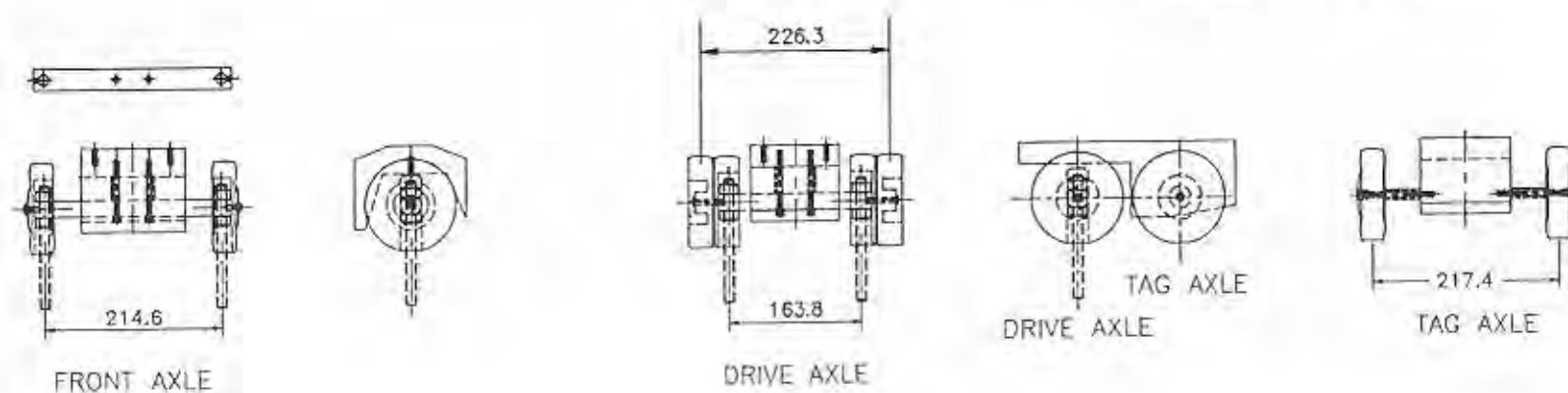
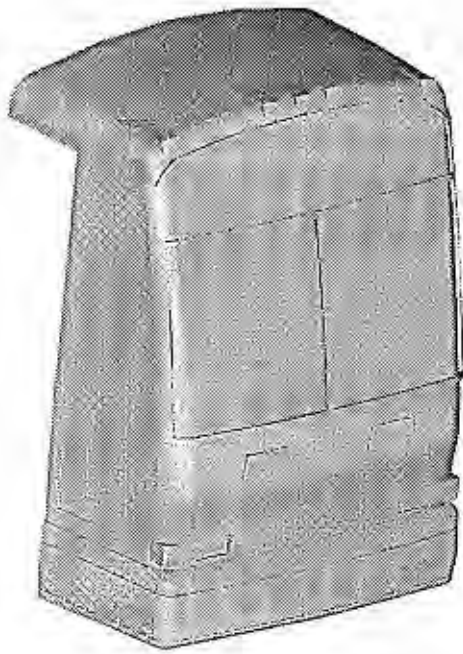
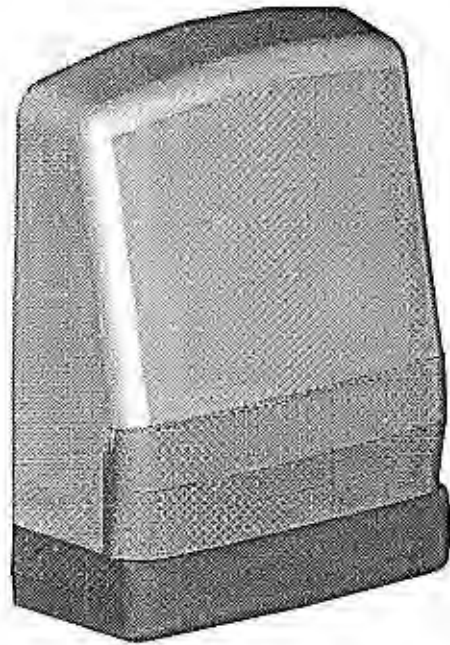


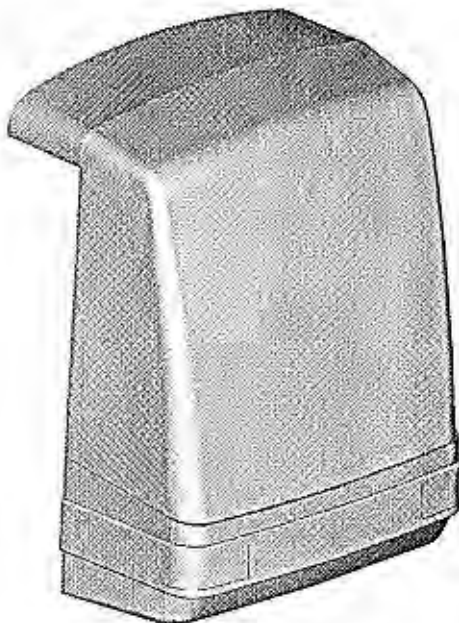
FIG. 7a: CHASSIS DETAILS



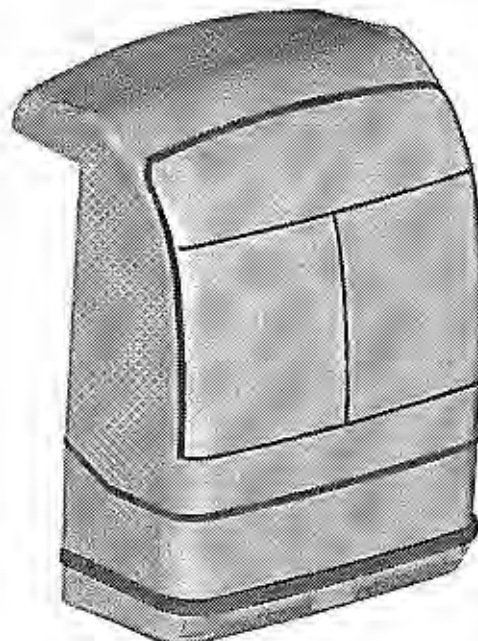
Standard MCI CJ3



Smooth MCI CJ3

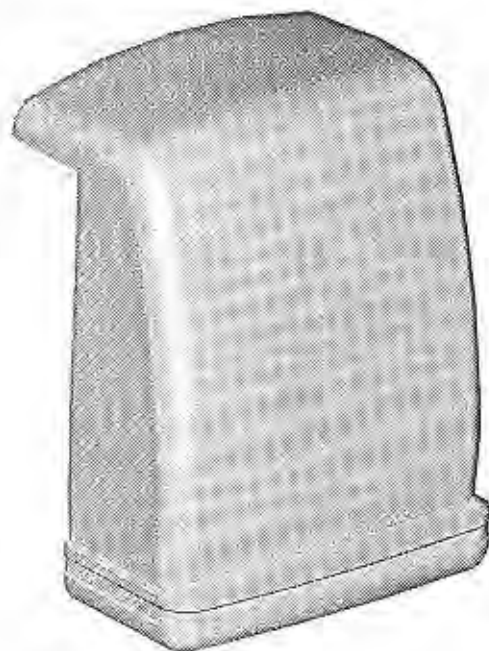


MCI Proposal 2

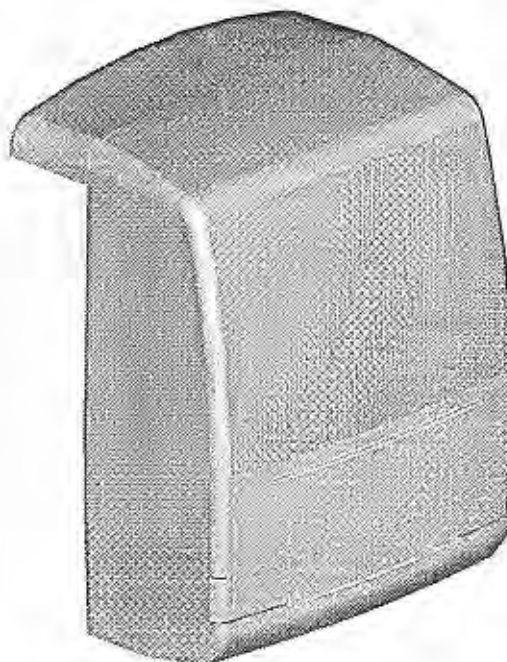


MCI Proposal 1

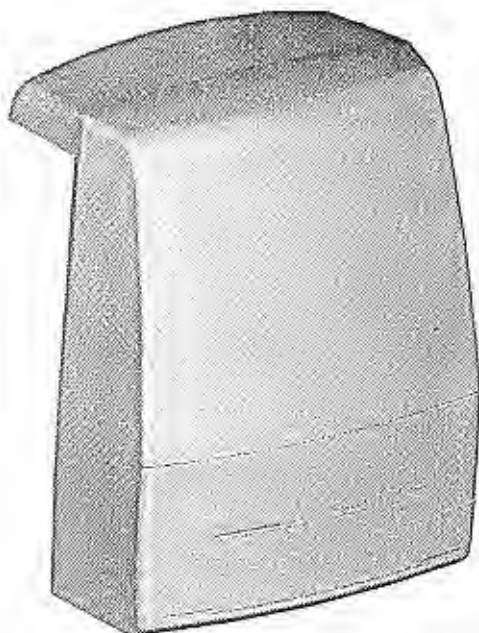
FIG. 7b: MCI FRONT-END CONFIGURATIONS



Prevost H3-40

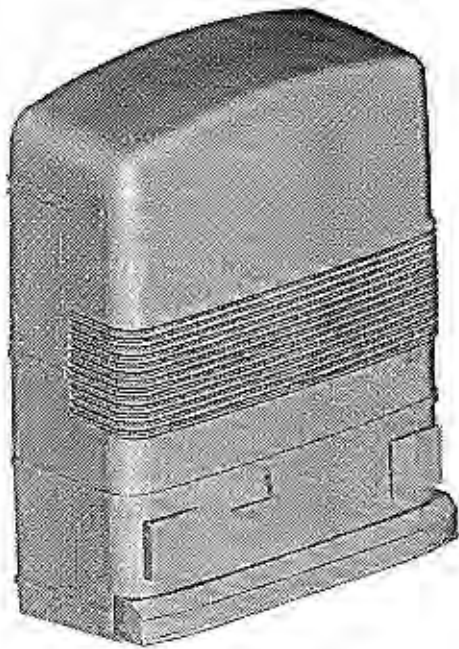


Mercedes 0404

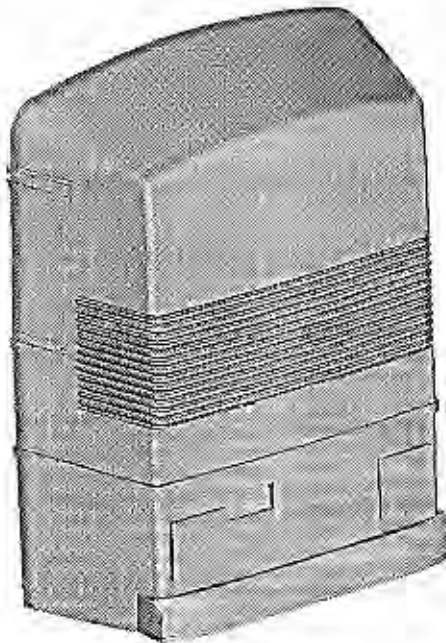


Setra S315

FIG. 7c: COMPETITORS' CONFIGURATIONS



Standard MCI CJ3



15° Beveled

FIG. 7d: REAR-END CONFIGURATIONS

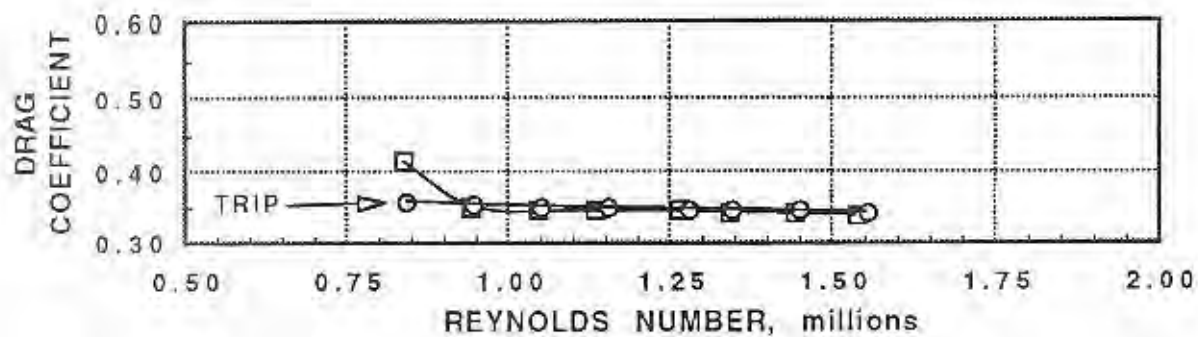


FIG. 8a: REYNOLDS NUMBER AND FLOW TRIP EFFECTS - PROPOSAL 1 FRONT

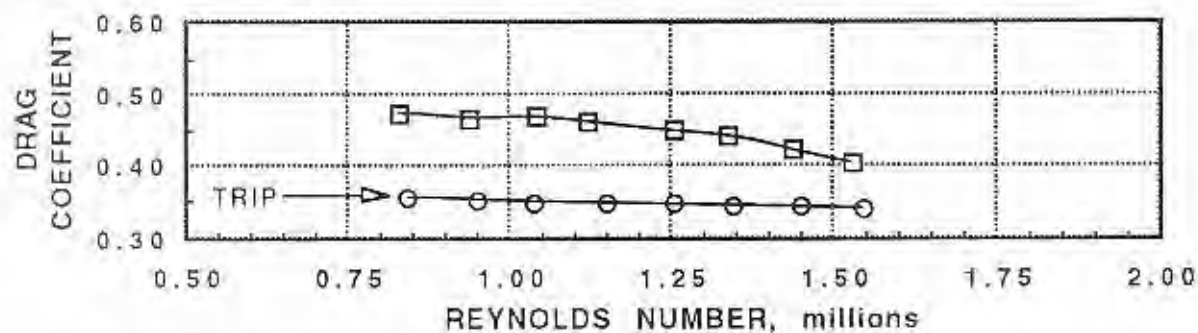


FIG. 8b: REYNOLDS NUMBER AND FLOW TRIP EFFECTS - PROPOSAL 2 FRONT

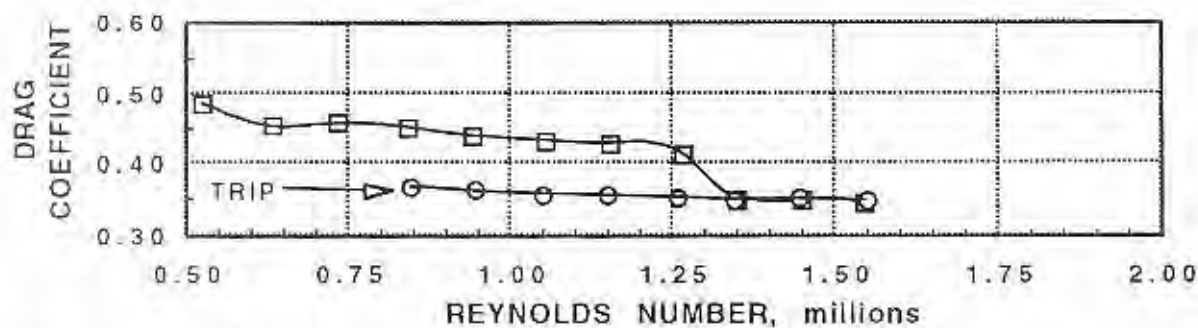


FIG. 8c: REYNOLDS NUMBER AND FLOW TRIP EFFECTS - SMOOTH C3 FRONT

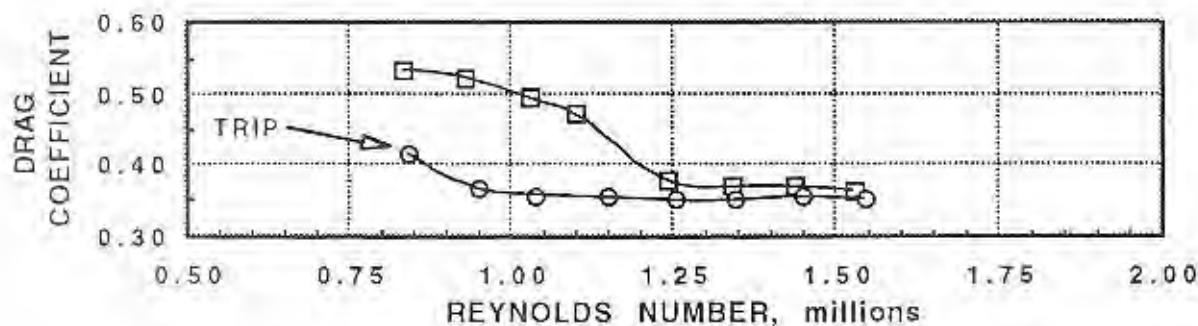


FIG. 8d: REYNOLDS NUMBER AND FLOW TRIP EFFECTS - PREVOST FRONT

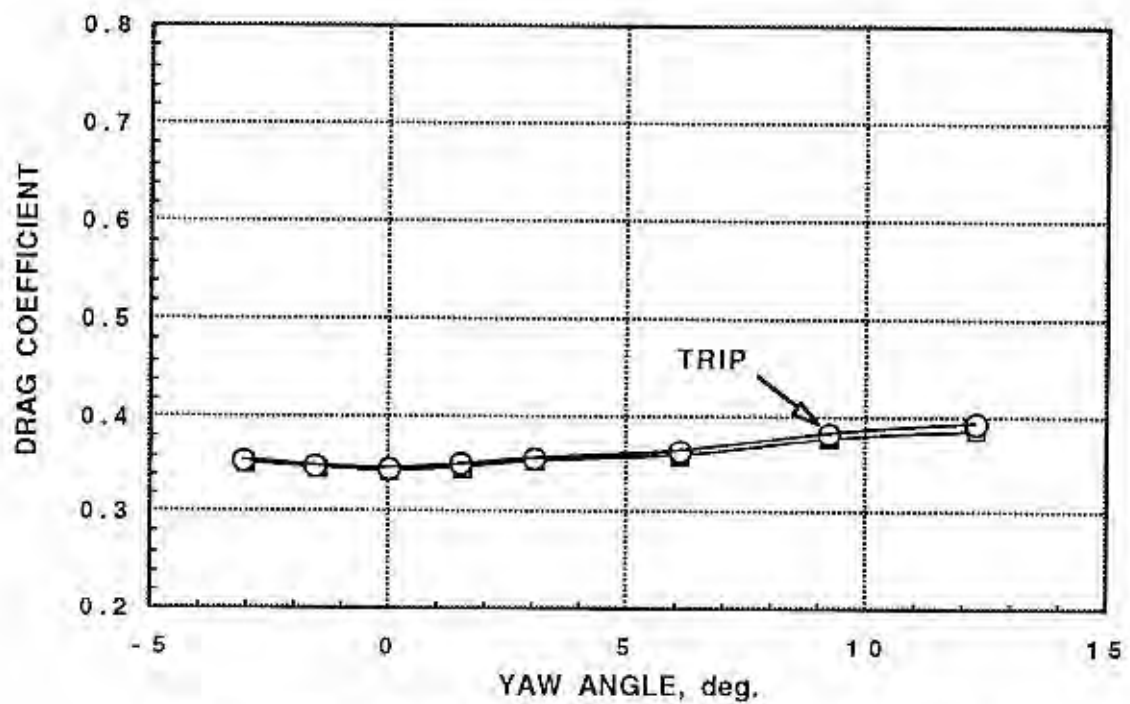


FIG. 9a: EFFECT OF FLOW TRIP - PROPOSAL 1 FRONT

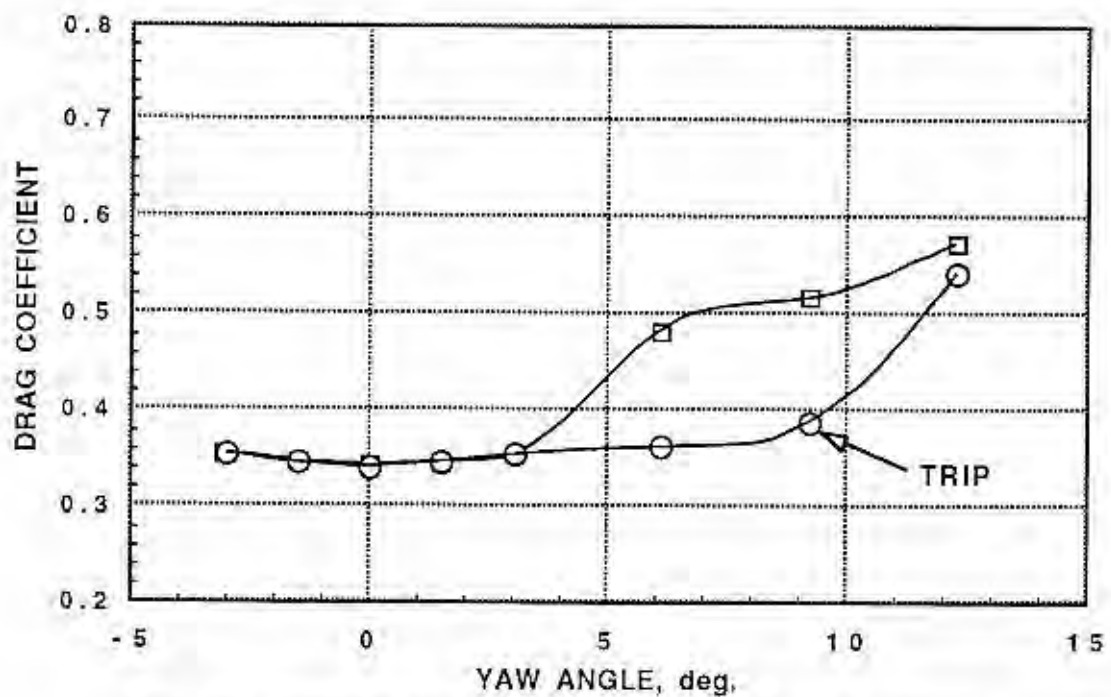


FIG. 9b: EFFECT OF FLOW TRIP - PROPOSAL 2 FRONT

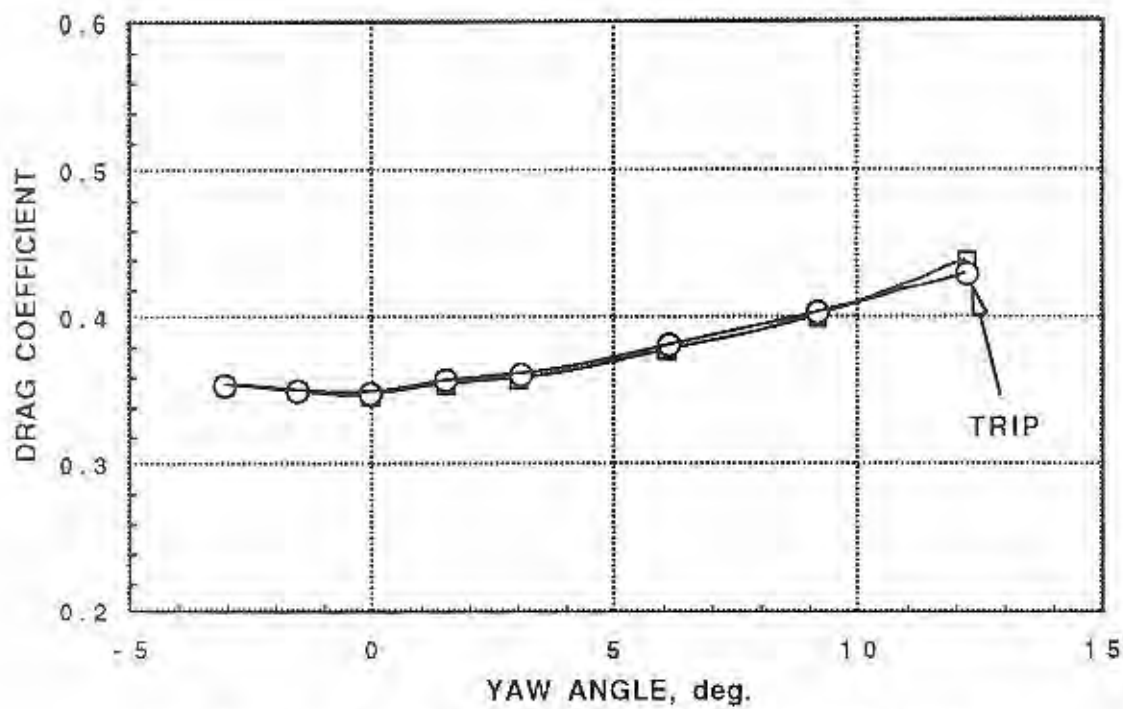


FIG. 9c: EFFECT OF FLOW TRIP - SMOOTH CJ3 FRONT

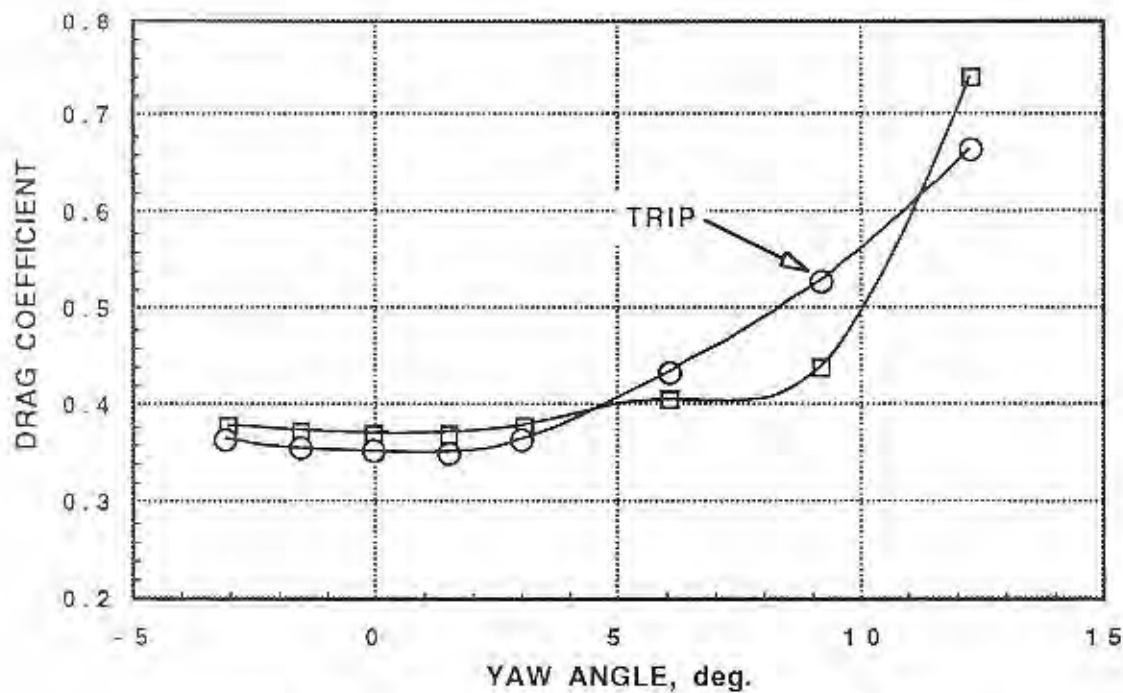


FIG. 9d: EFFECT OF FLOW TRIP - PREVOST FRONT

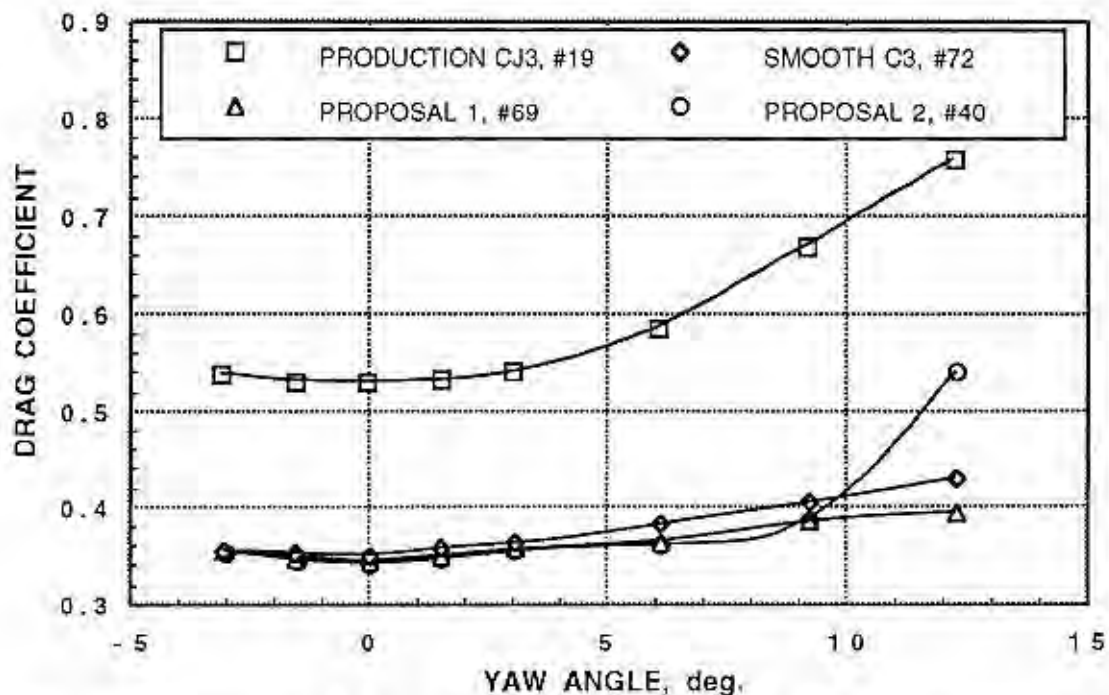


FIG. 10: COMPARISON OF FRONT END SHAPES - PRODUCTION CJ3 AND ALTERNATE PROPOSALS

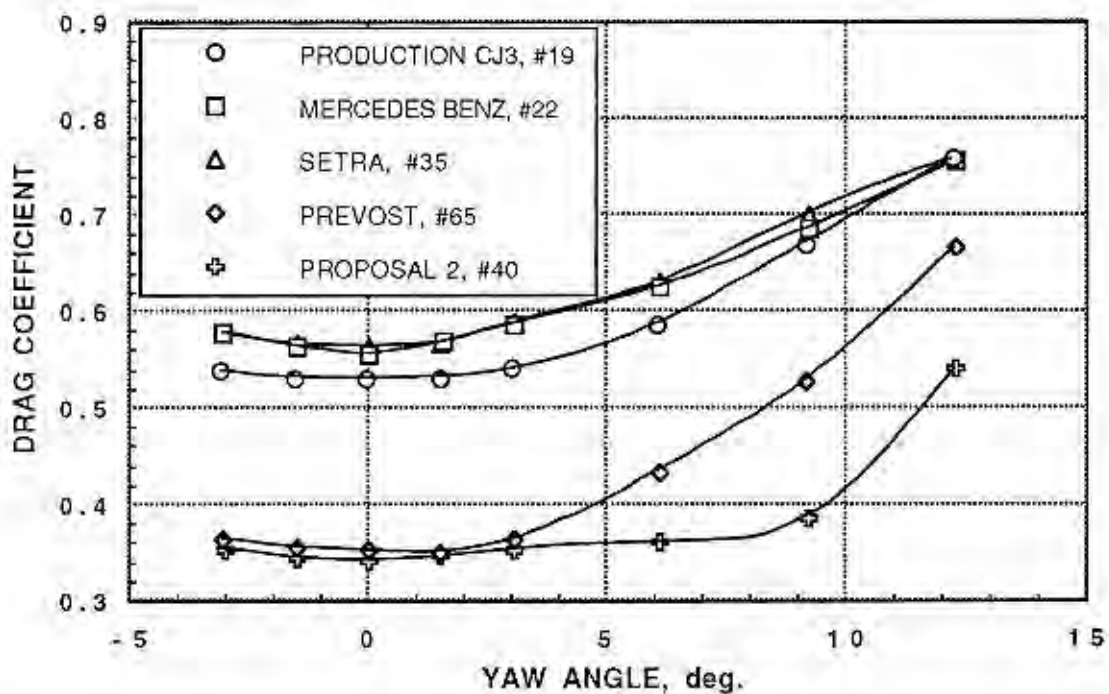


FIG. 11: COMPARISON OF FRONT END SHAPES - PRODUCTION CJ3, PROPOSAL 2, AND COMPETITORS

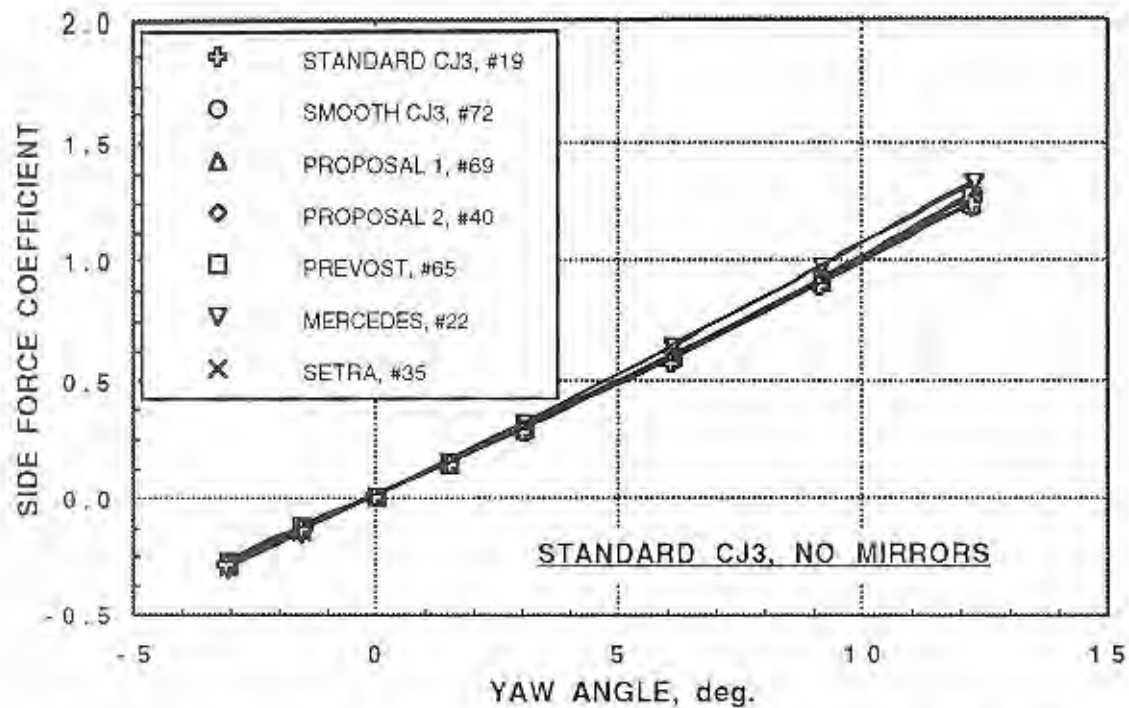


FIG. 12a: COMPARISON OF SIDE FORCE FOR THE VARIOUS FRONTS

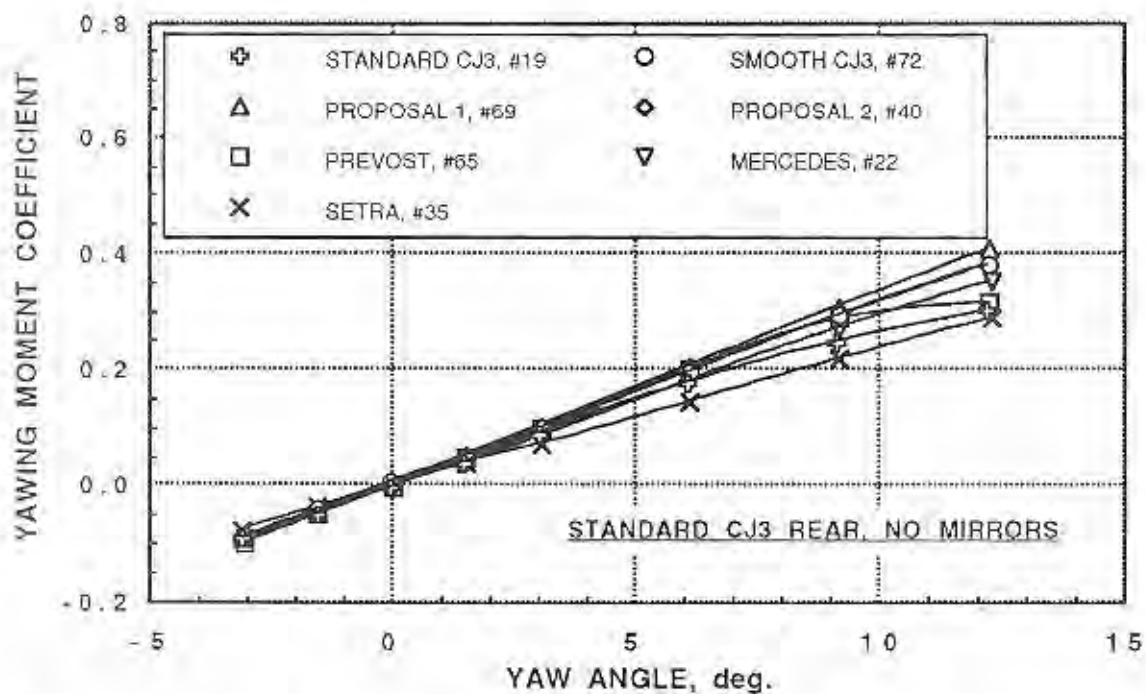


FIG. 12b: COMPARISON OF YAWING MOMENT FOR THE VARIOUS FRONTS

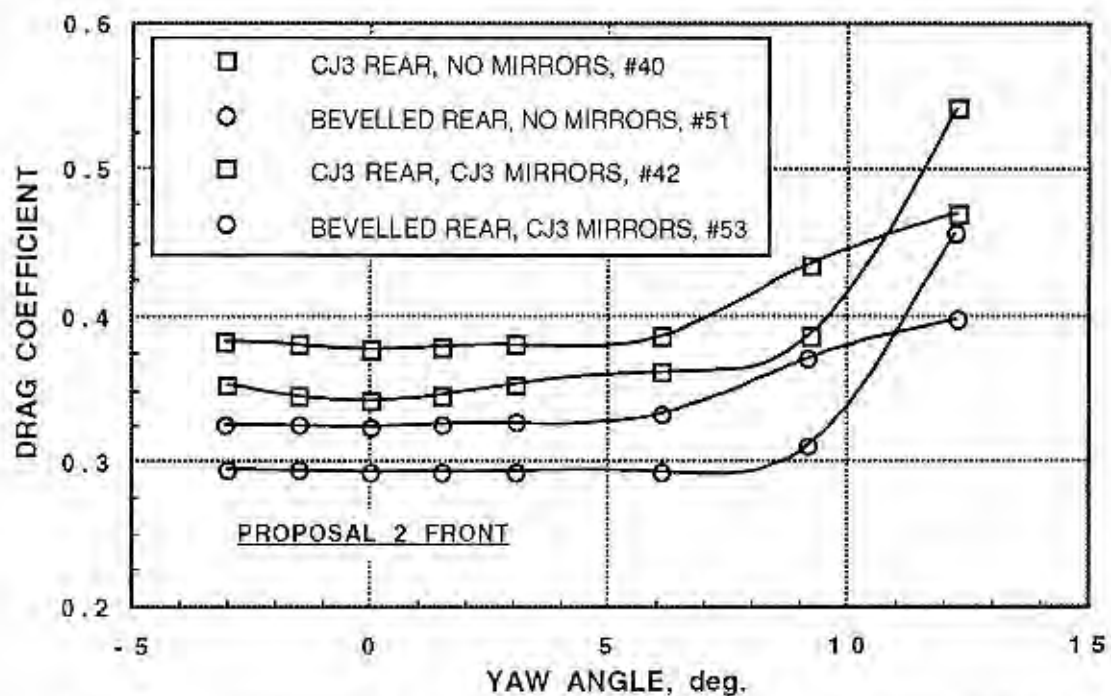


FIG. 13: COMPARISON OF BEVELLED AND STANDARD REAR ENDS WITH AND WITHOUT MIRRORS

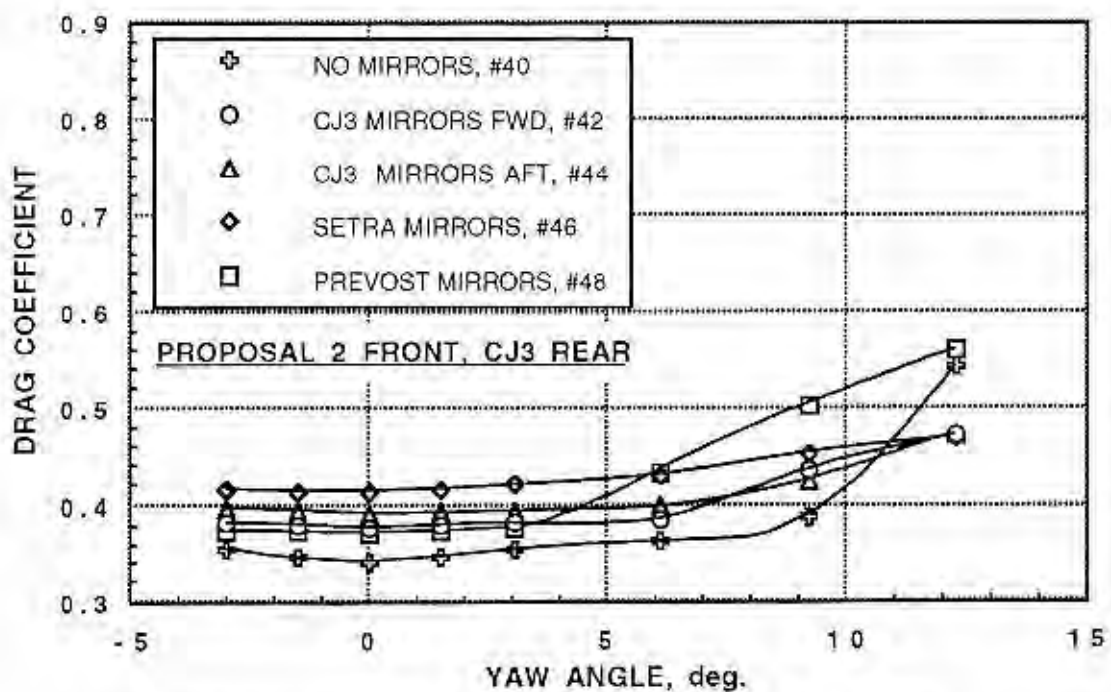


FIG. 14: EFFECT OF MIRROR TYPE AND LOCATION

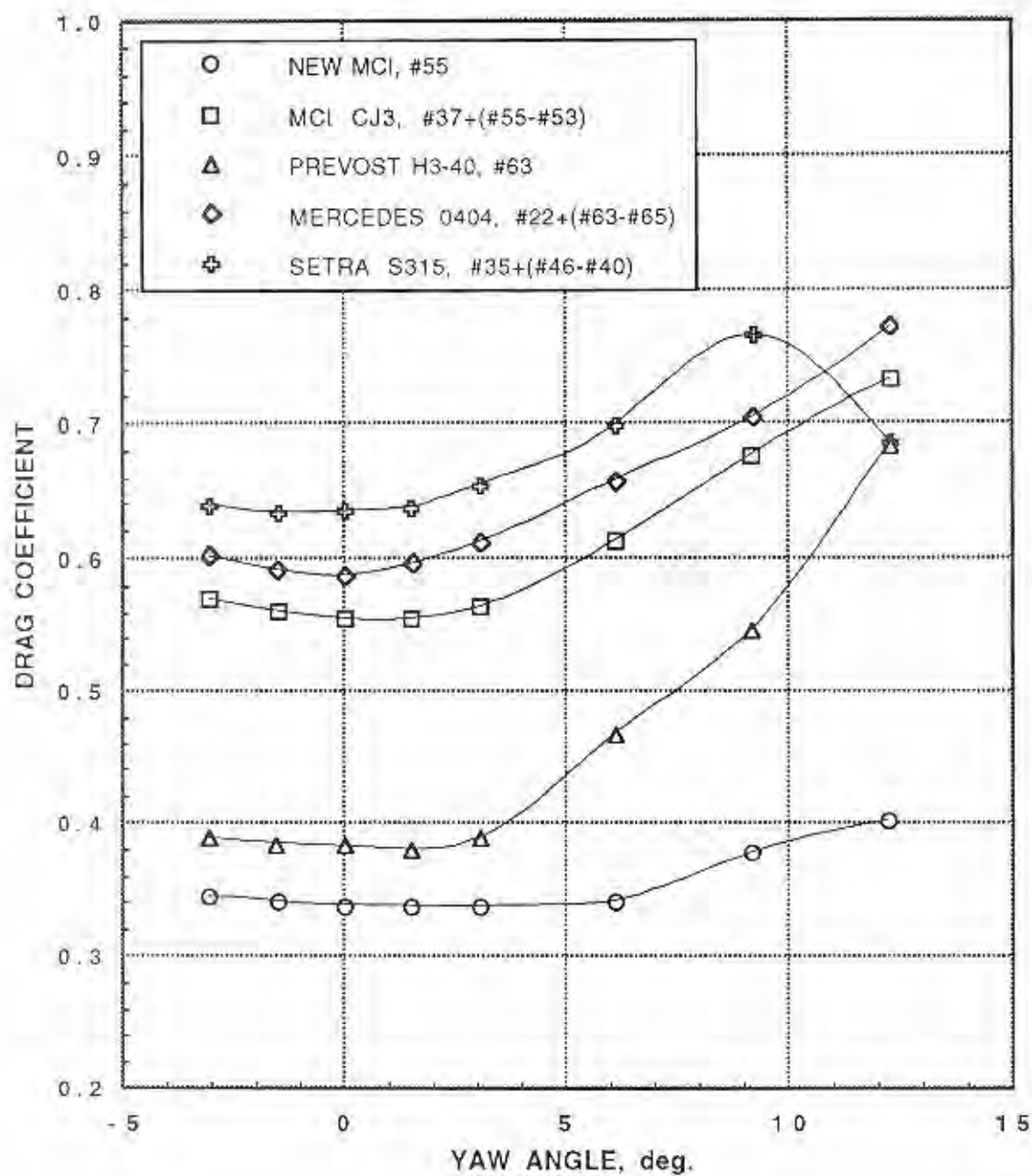


FIG. 15: DRAG COMPARISON OF MAIN CONFIGURATIONS WITH MIRRORS

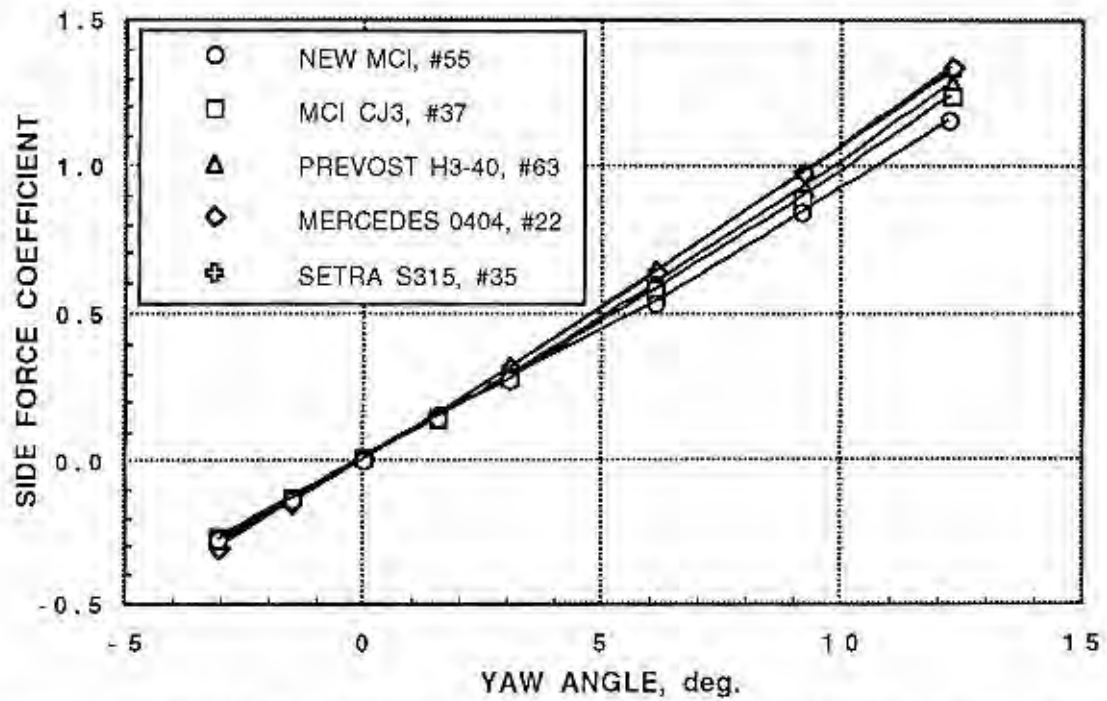


FIG. 16a: SIDE FORCE COMPARISON OF MAIN CONFIGURATIONS WITH MIRRORS

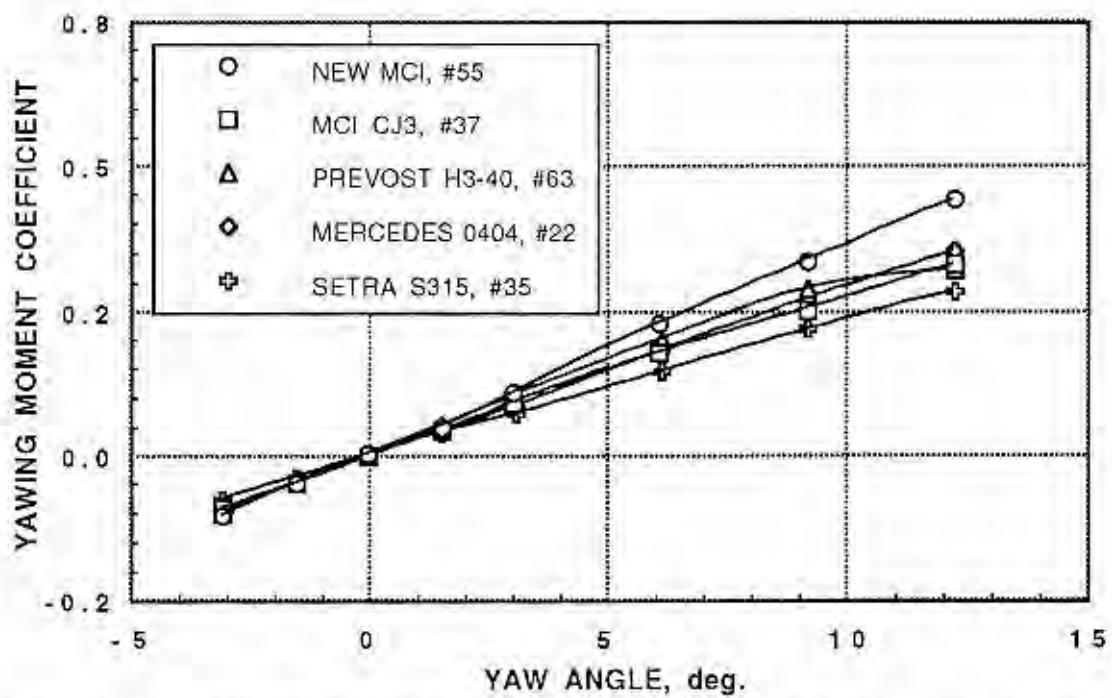


FIG. 16b: YAWING MOMENT COMPARISON OF MAIN CONFIGURATIONS WITH MIRRORS

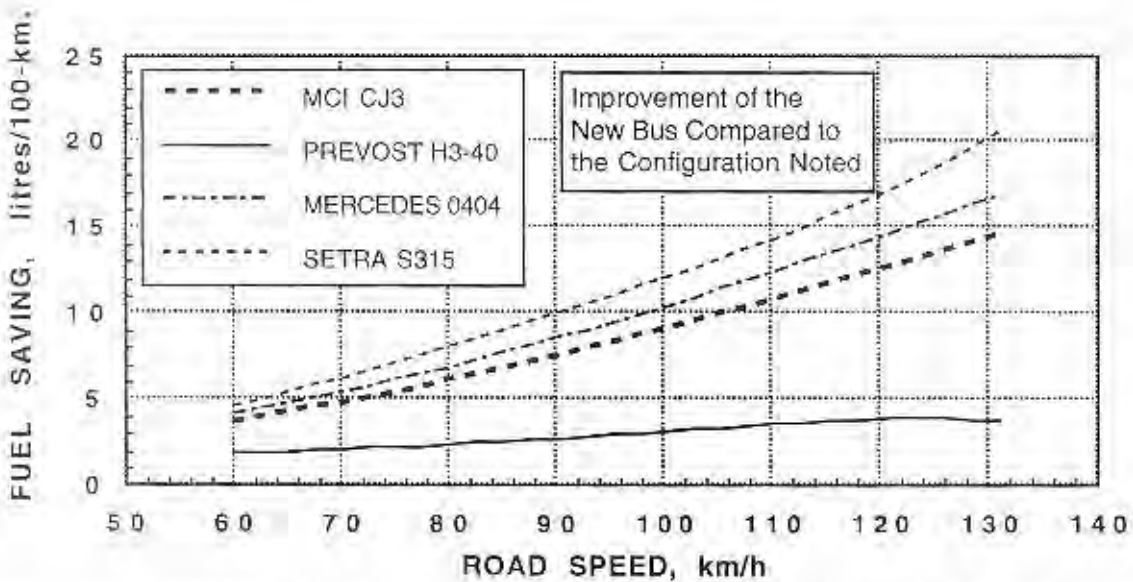
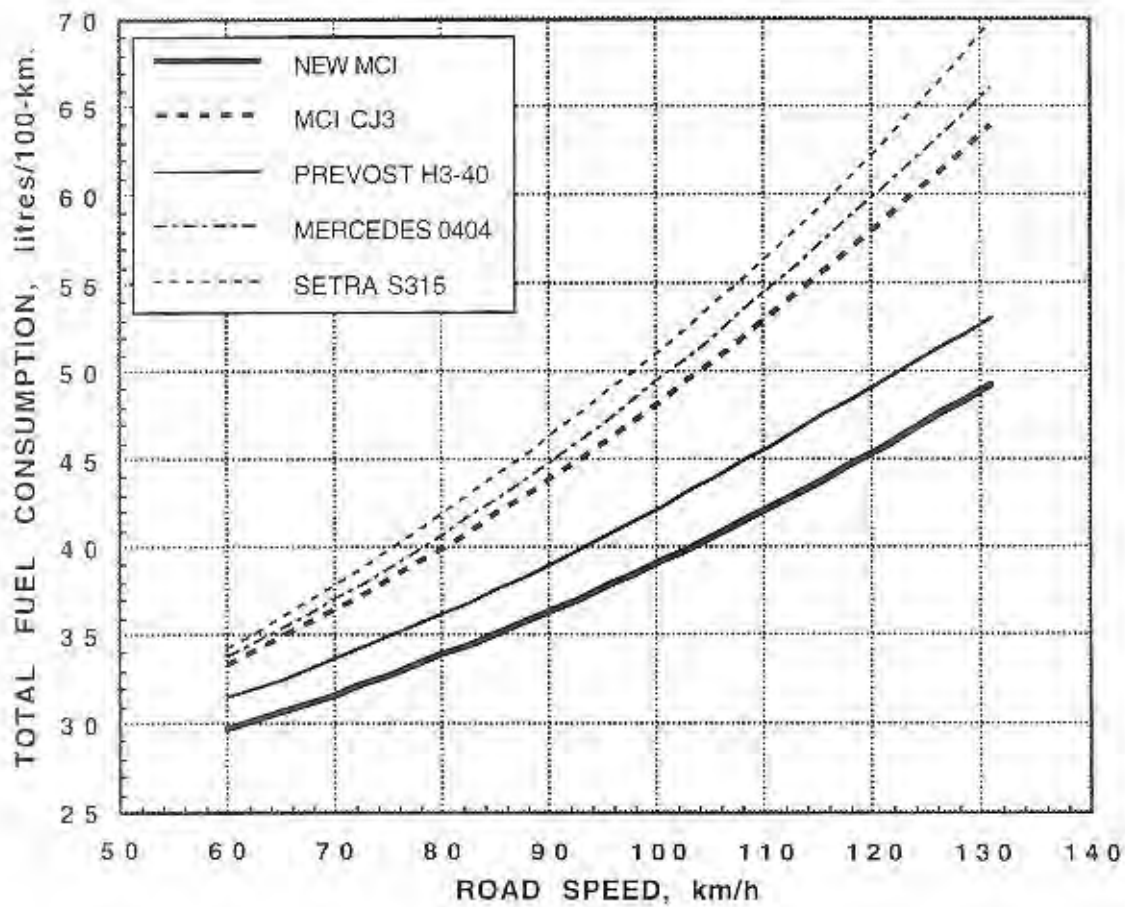


FIG. 17: SUMMARY OF THE PREDICTED FUEL CONSUMPTIONS OF THE MAIN CONFIGURATIONS AND THE SAVINGS PROVIDED BY THE NEW BUS

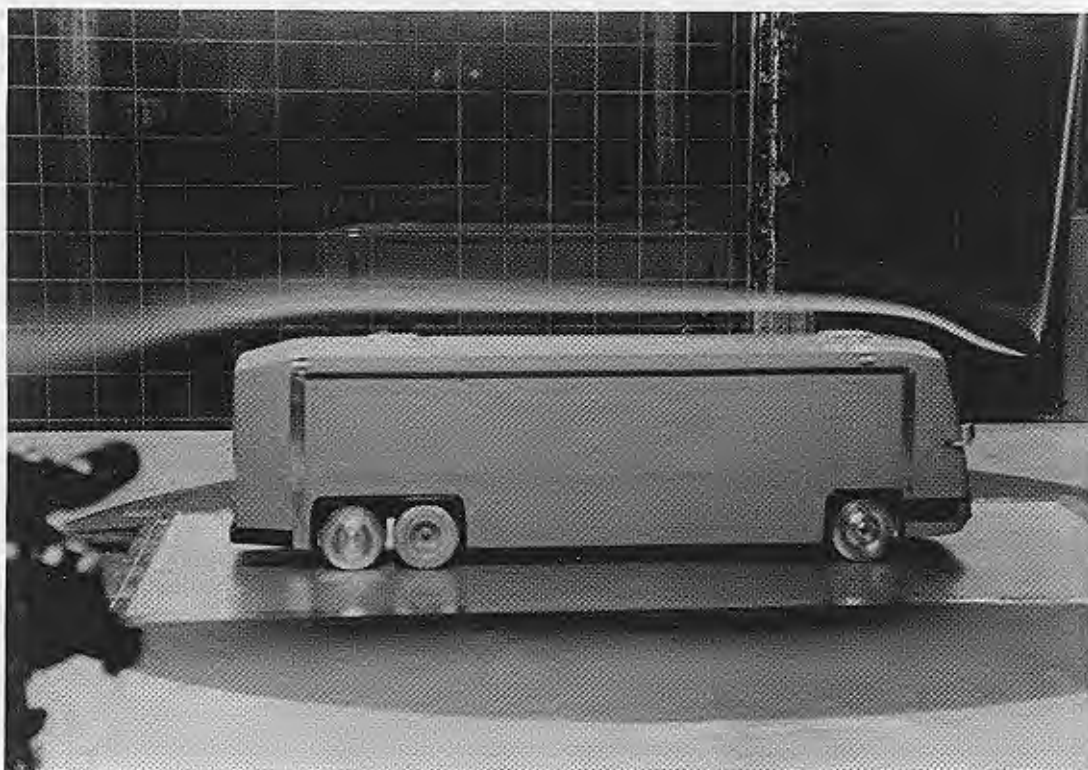


FIG. 18a: OVERALL FLOW FIELD

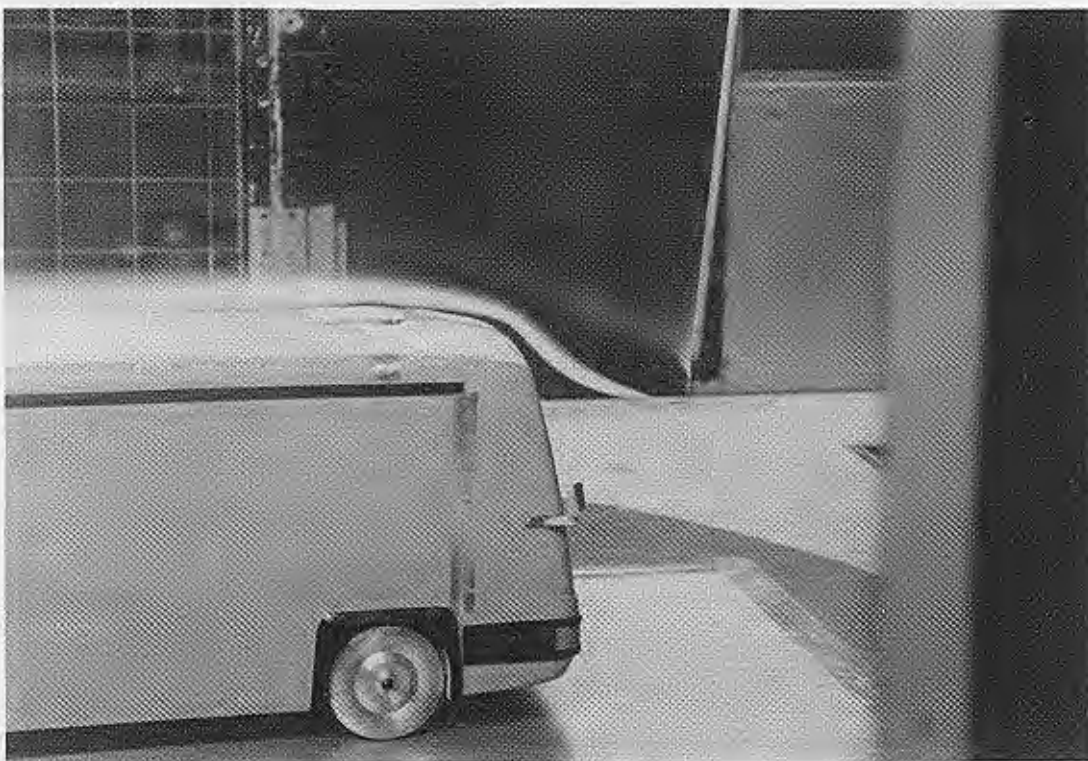


FIG. 18b: LEADING EDGE FLOW

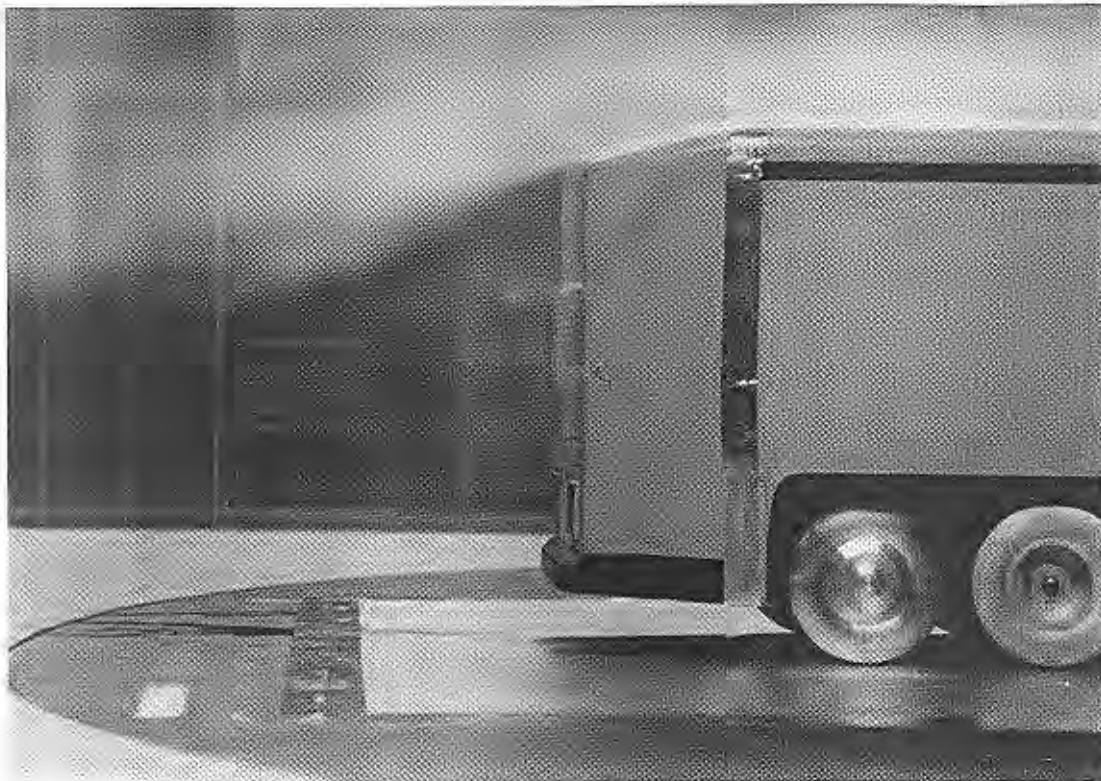


FIG. 18c: ATTACHED REAR BEVEL FLOW

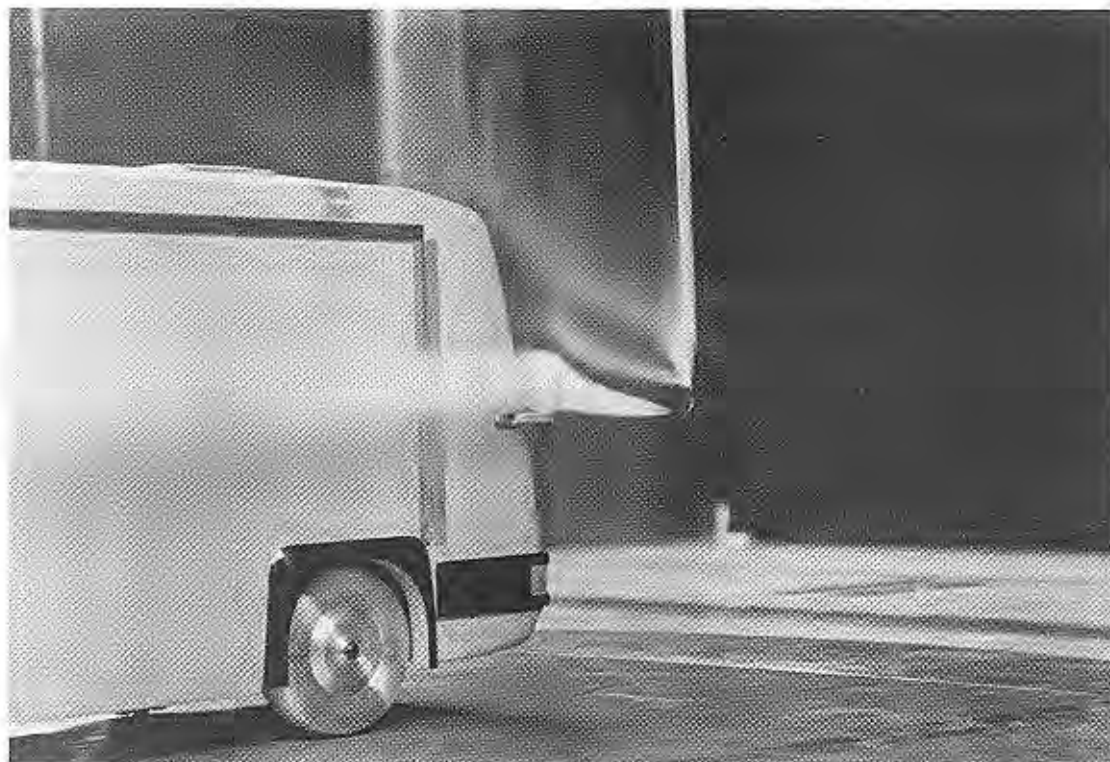


FIG. 18d: MIRROR WAKE

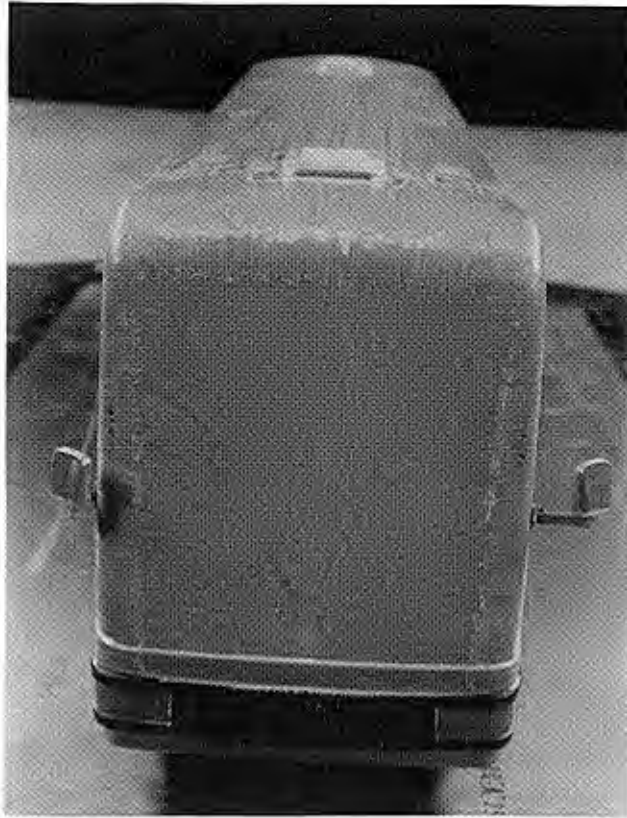


FIG. 19a: FRONT-FACE FLOW SHOWING
STAGNATION POINT AT LOWER CENTRE



FIG. 19b: MIRROR-INDUCED FLOW



FIG. 19c: CLOSE-UP OF MIRROR-INDUCED FLOW



FIG. 19d: BASE FLOW

APPENDIX 1: RUN LOG

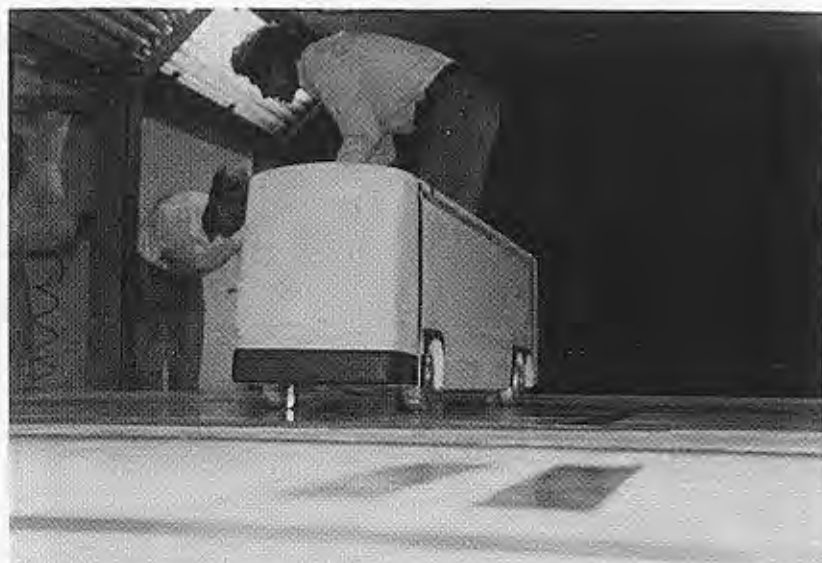
<u>RUN</u>	<u>TYPE</u>	<u>FRONT</u>	<u>REAR</u>	<u>TRIP</u>	<u>HATCH</u>	<u>RAIL</u>	<u>MIRROR</u>	<u>MISC</u>	<u>C_D(88)</u>	<u>PHOTO</u>
13	YAW	SMOOTH CJ3	STANDARD CJ3	NO	NONE	NONE	NONE	NONE	0.443	P1
14	Re									
16	YAW				STD	STD			0.443	P2
18	Re	STANDARD CJ3								P3
19	YAW								0.674	
21	Re	MERCEDES								P4
22	YAW								0.708	
25	Re	PROPOSAL 1								P5
26	YAW								0.435	
28	Re	PROPOSAL 2								P6
29	YAW								0.435	
31	Re	PREVOST								P7
32	YAW								0.472	
34	Re	SETRA								P8
35	YAW								0.717	
37	YAW	STANDARD CJ3					CJ3 FWD		0.689	P9
39	Re	PROPOSAL 2		YES			NONE			P10
40	YAW								0.434	
42							CJ3 FWD		0.479	P11
44							CJ3 AFT		0.498	P12

Wrong appendix

RUN	TYPE	FRONT	REAR	TRIP	HATCH	RAIL	MIRROR	MISC	C _D (88)	PHOTO
46	YAW	PROPOSAL 2	STANDARD CJ3	YES	STD	STD	SETRA		0.524	P13
48							PREVOST		0.472	P14
50	Re		BEVELLED				NONE			P15
51	YAW								0.370	
53							CJ3 FWD		0.411	P11
55							CJ3, RIGHT FWD, LEFT AFT		0.428	P16
57								SKIRTS	0.421	P17
58								AIR DAM	0.467	P18
59								TIRE FAIRING	0.436	P19
60								VORTEX GEN.	0.434	P20
61						MOD		NONE	0.429	P21
63	YAW	PREVOST	STANDARD CJ3	YES	STD	STD	PREVOST		0.488	P22
65		PREVOST					NONE		0.449	P23
66	Re									
68		PROPOSAL 1								P24
69	YAW								0.439	
72		SMOOTH CJ3							0.444	P25

APPENDIX 2: PHOTOGRAPHIC LOG

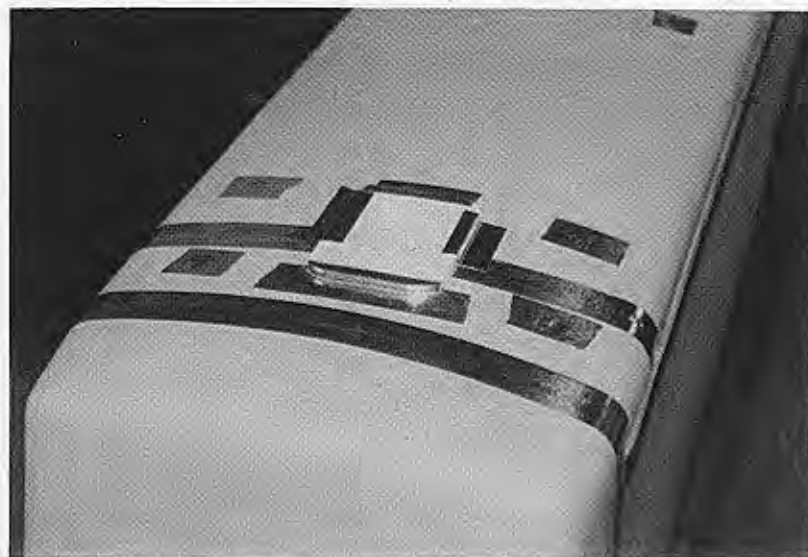
P1	MCI Smooth CJ3 Front and Standard CJ3 Rear
P2	MCI Standard Hatch and Drip Rail
P3	MCI Standard CJ3 Front
P4	Mercedes 0404 Front
P5	MCI Proposal 1 Front
P6	MCI Proposal 2 Front
P7	Prevost H3-40 Front
P8	Setra S315 Front
P9	Standard CJ3 Front with Standard CJ3 Mirrors
P10	MCI Proposal 2 Front with Flow Trip
P11	Proposal 2 Front with Standard CJ3 Mirrors Forward
P12	Proposal 2 Front with Standard CJ3 Mirrors Aft
P13	Proposal 2 Front with Setra Mirrors
P14	Proposal 2 Front with Prevost Mirrors
P15	Rear End with 15° Bevels on Top and Sides
P16	Proposal 2 Front with Standard CJ3 Mirrors Forward and Aft
P17	Proposal 2 Front and Wheel Skirts
P18	Proposal 2 Front with Air Dam
P19	Proposal 2 Front with Tire Fairings
P20	Vortex Generators Immediately Upstream of Bevelled Rear
P21	Modified Drip Rail
P22	Prevost H3=40 Front with Prevost Mirrors
P23	Prevost H3=40 Front with Flow Trip
P24	Proposal 1 Front with Flow Trip
P25	Smooth CJ3 Front with Flow Trip



P1a: MCI SMOOTH CJ3 FRONT



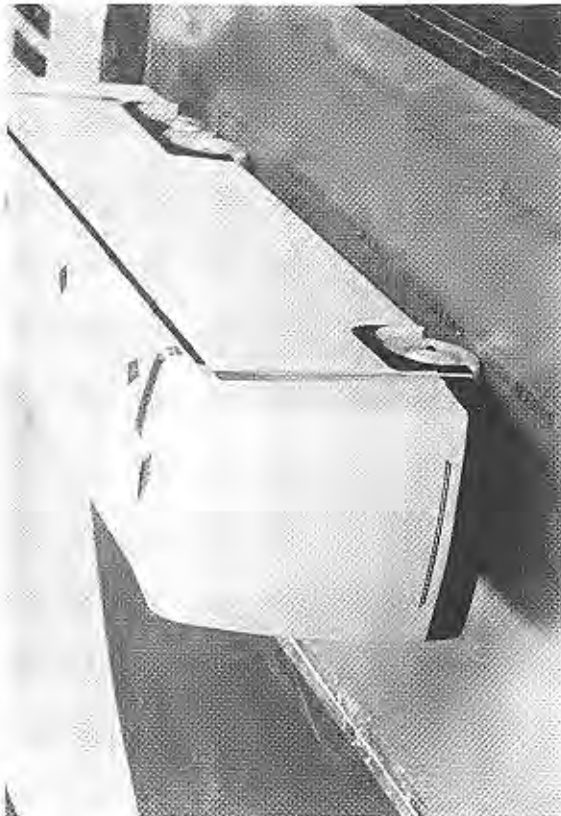
P1b: MCI STANDARD CJ3 REAR



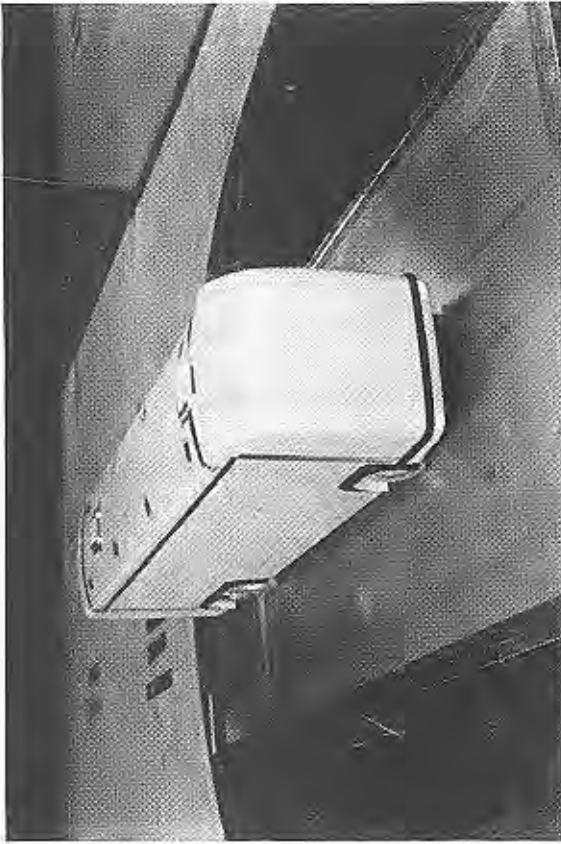
P2: MCI STANDARD HATCH & DRIP RAIL



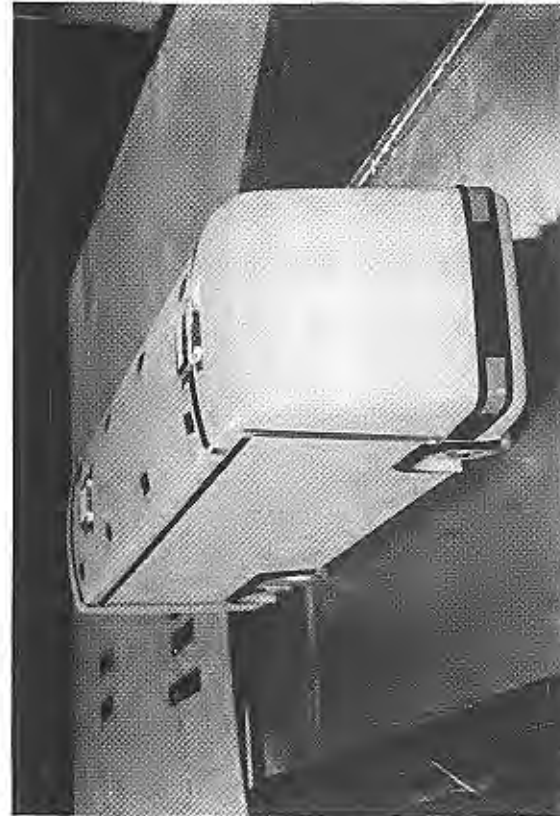
P3: MCI STANDARD CJ3 FRONT



P4: MERCEDES 0404 FRONT



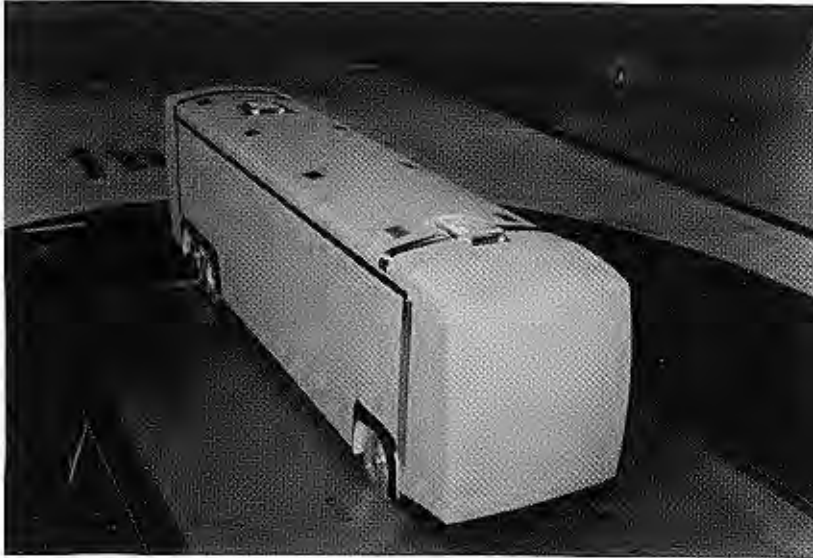
P5: MCI PROPOSAL 1 FRONT



P6: MCI PROPOSAL 2 FRONT



P7: PREVOST H3-40 FRONT



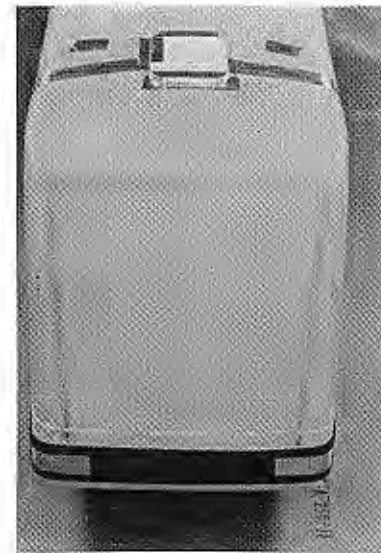
P8: SETRA S315 FRONT



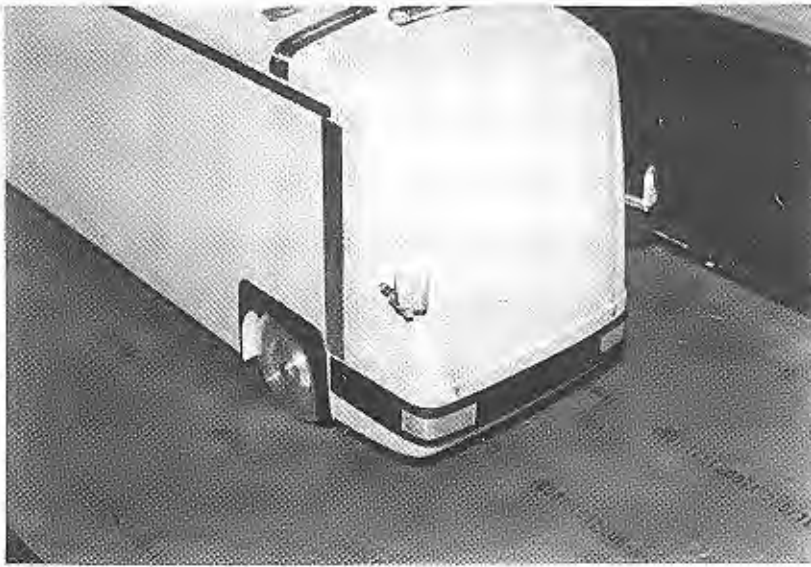
**P9a: MCI STANDARD CJ3 FRONT WITH
STANDARD CJ3 MIRRORS FORWARD**



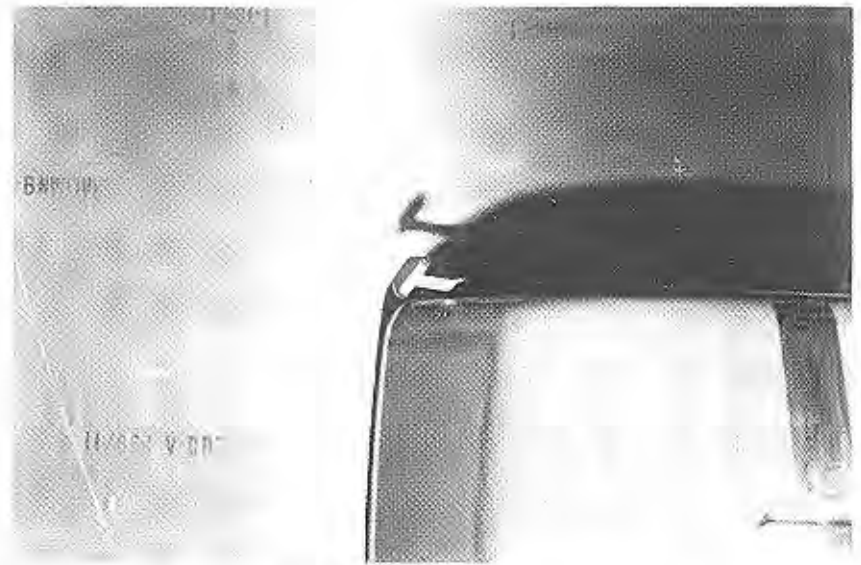
**P9b: MCI STANDARD CJ3 FRONT WITH
STANDARD CJ3 MIRRORS FORWARD**



P10: MCI PROPOSAL 2 FRONT WITH TRIP



P11a: MCI PROPOSAL 2 FRONT WITH
STANDARD CJ3 MIRRORS FORWARD



P11b: MCI PROPOSAL 2 FRONT WITH
STANDARD CJ3 MIRROR FORWARD



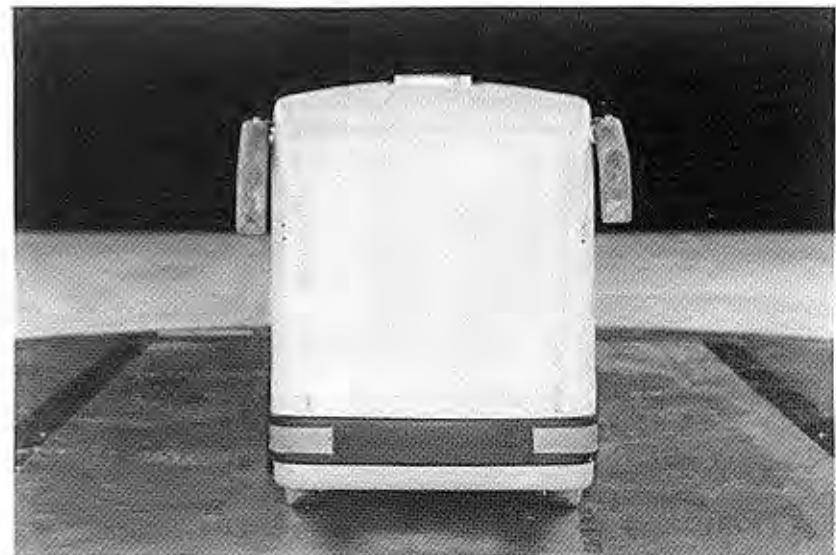
P12a: MCI PROPOSAL 2 FRONT WITH
STANDARD CJ3 MIRRORS AFT



P12b: MCI PROPOSAL 2 FRONT WITH
STANDARD CJ3 MIRROR AFT



**P13a: MCI PROPOSAL 2 FRONT WITH
SETRA MIRRORS**



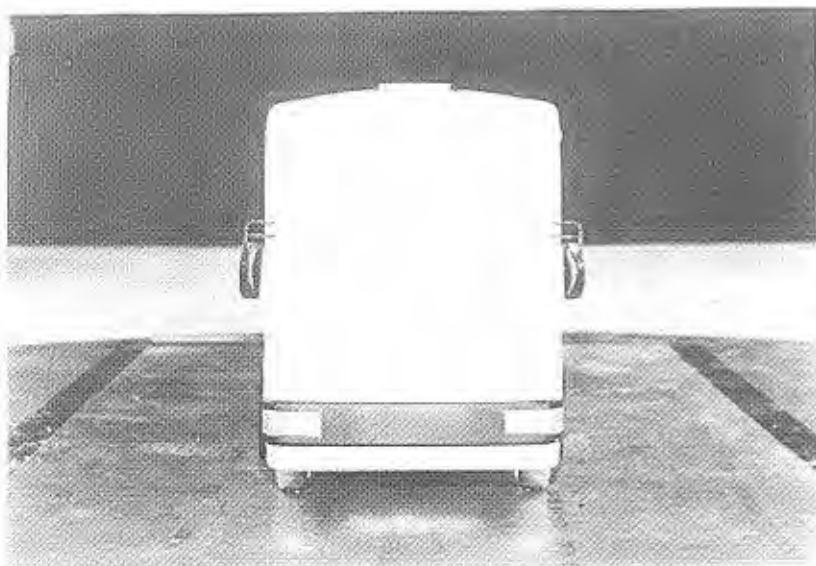
**P13b: MCI PROPOSAL 2 FRONT WITH
SETRA MIRRORS**



**P13c: MCI PROPOSAL 2 FRONT WITH
SETRA MIRRORS**



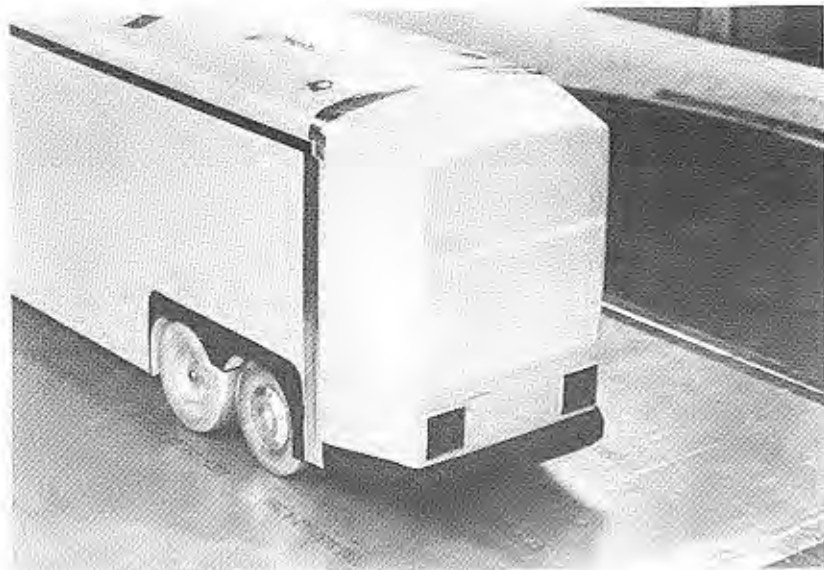
**P14a: MCI PROPOSAL 2 FRONT WITH
PREVOST MIRRORS**



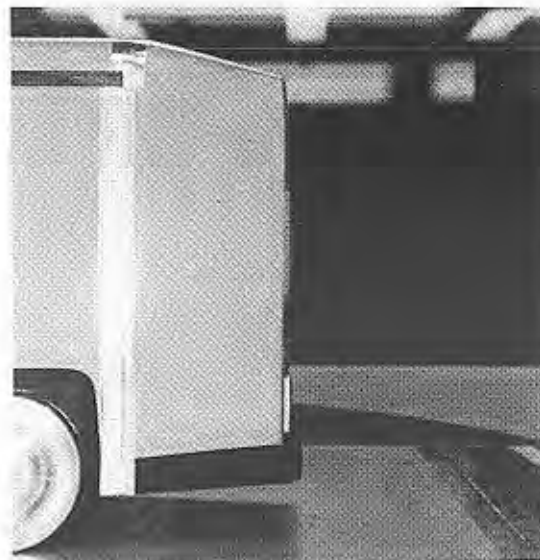
P14b: MCI PROPOSAL 2 FRONT WITH
PREVOST MIRROR



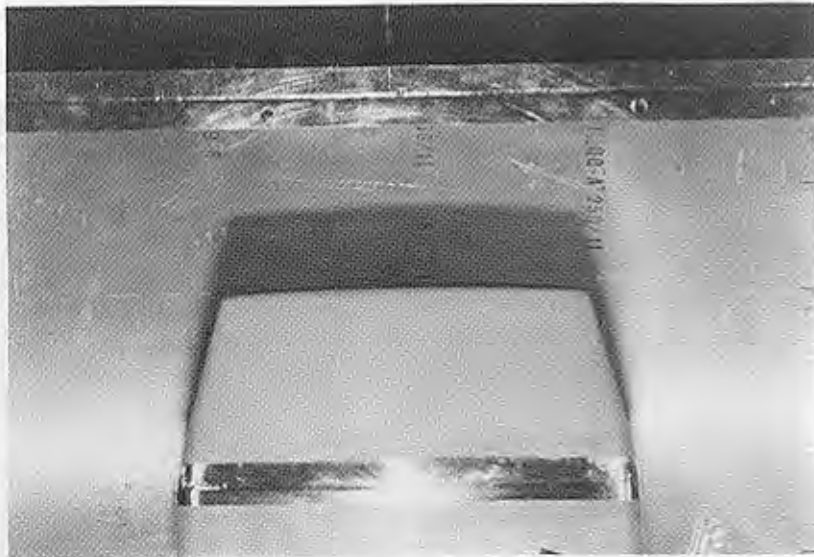
P14c: MCI PROPOSAL 2 FRONT WITH
PREVOST MIRROR



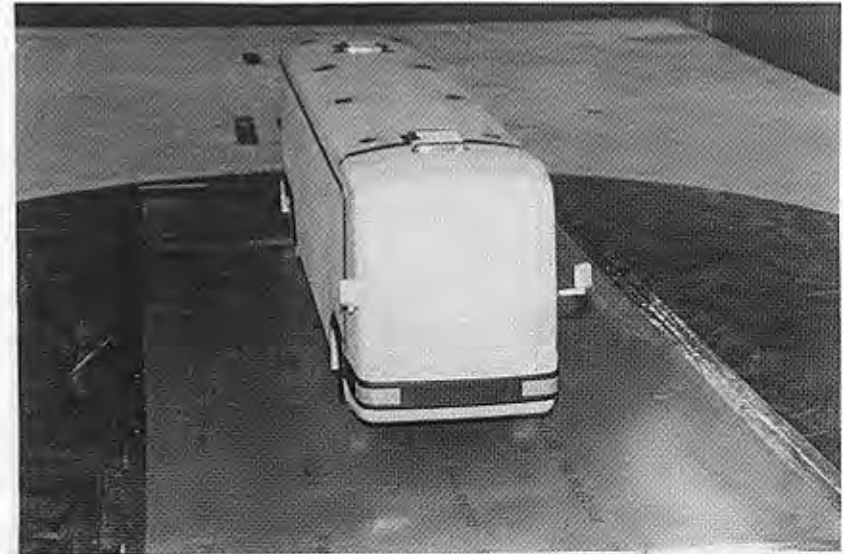
P15a: REAR END WITH 15° BEVELS
ON TOP AND SIDE EDGES



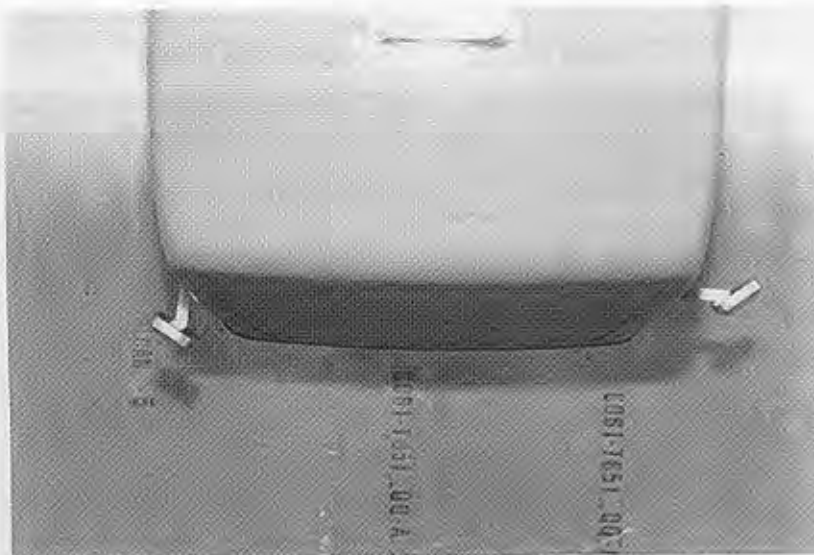
P15b: REAR END WITH 15° BEVEL
ON TOP EDGE



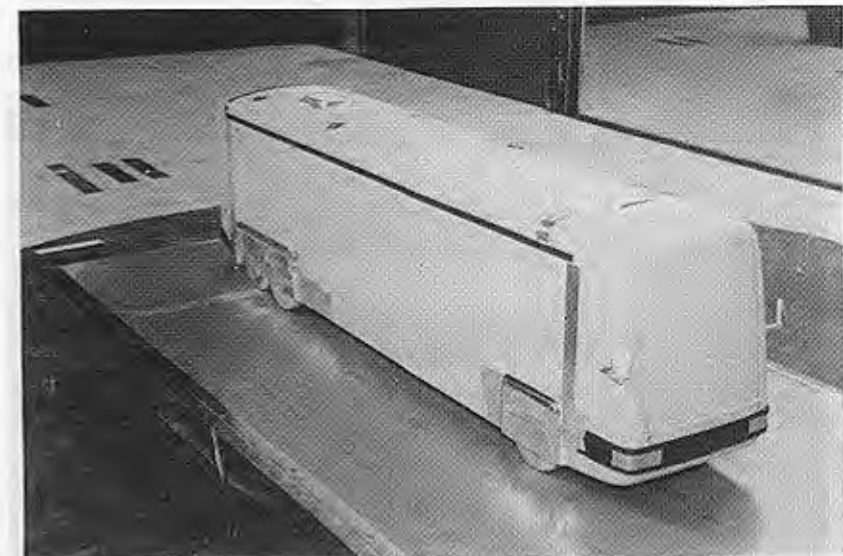
**P15c: REAR END WITH 15° BEVELS
ON SIDE EDGES**



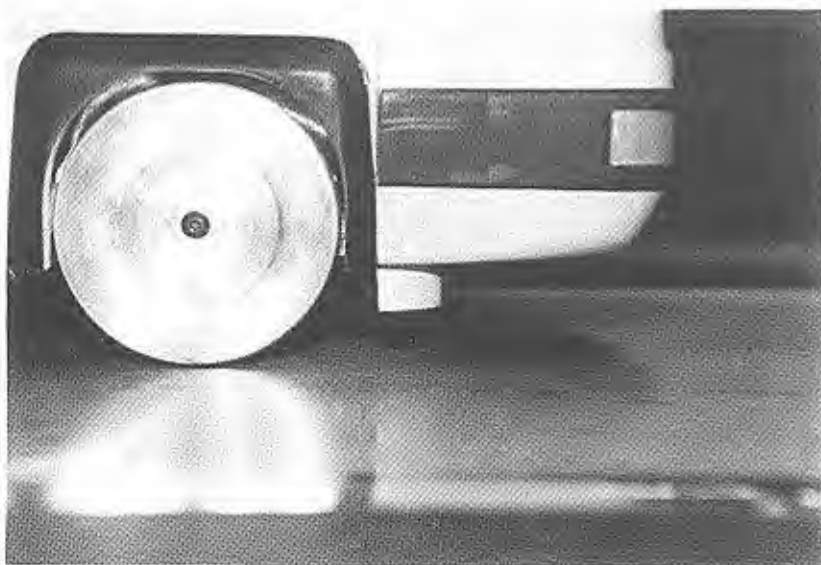
**P16a: MCI PROPOSAL 2 FRONT WITH STANDARD
CJ3 MIRRORS FORWARD AND AFT**



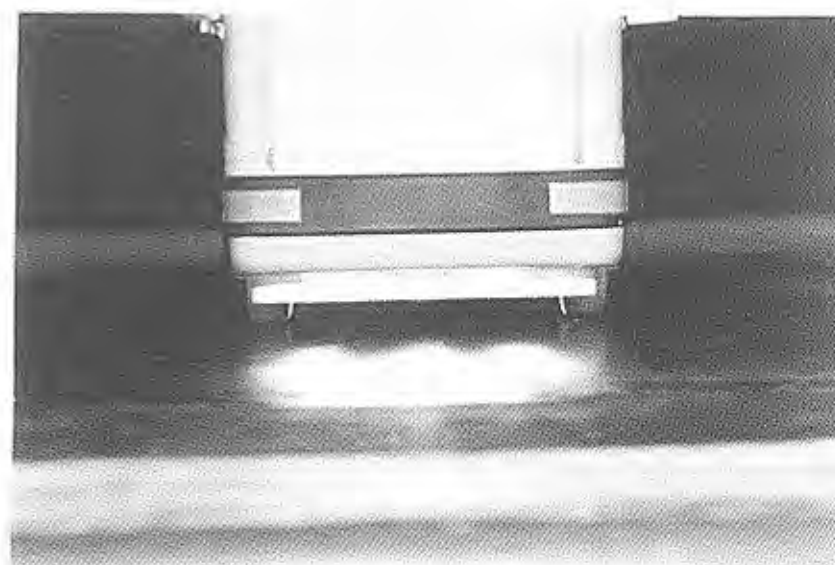
**P16b: MCI PROPOSAL 2 FRONT WITH STANDARD
CJ3 MIRRORS FORWARD AND AFT**



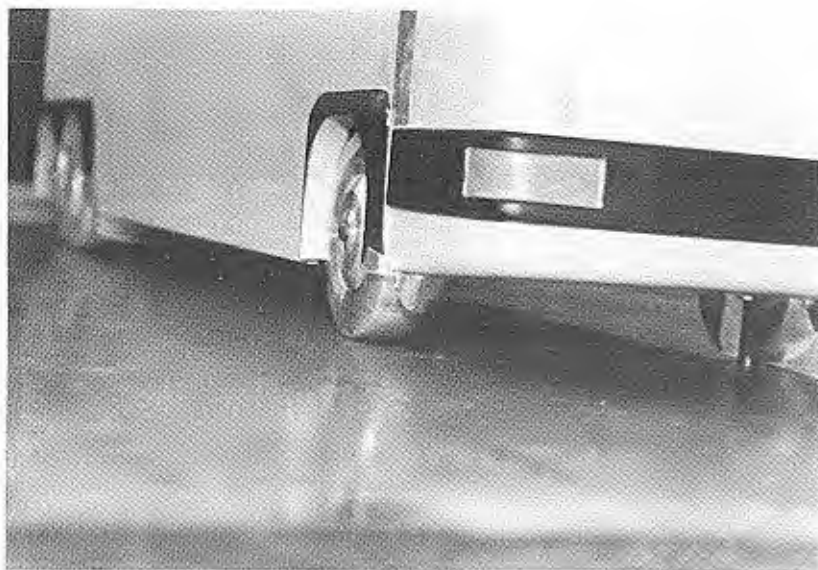
**P17: MCI PROPOSAL 2 FRONT AND
WHEEL SKIRTS**



P18a: MCI PROPOSAL 2 FRONT WITH
AIR DAM



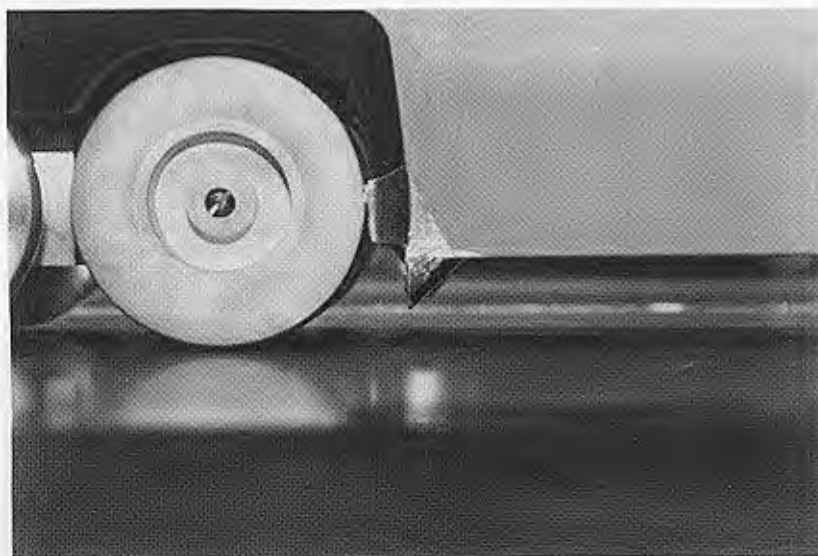
P18b: MCI PROPOSAL 2 FRONT WITH
AIR DAM



P19a: MCI PROPOSAL 2 FRONT WITH
FRONT-TIRE FAIRING



P19b: MCI PROPOSAL 2 FRONT WITH
REAR-TIRE FAIRING



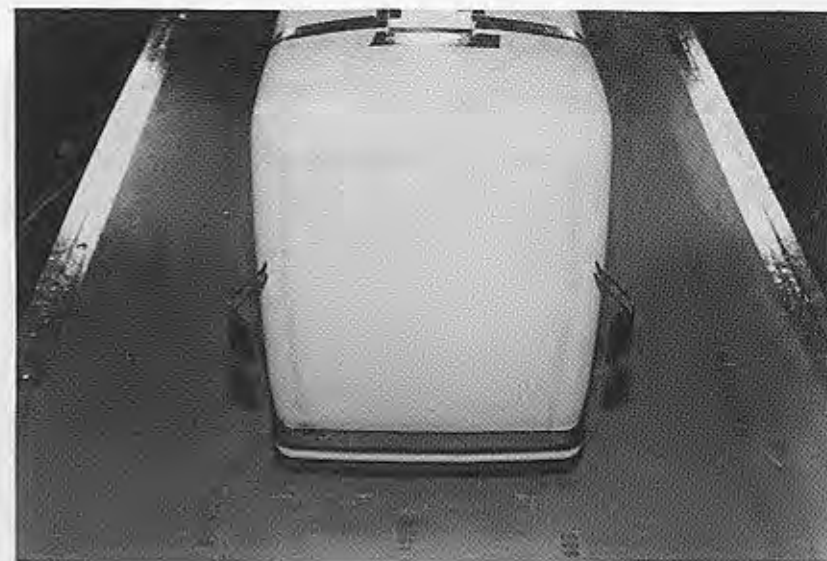
P19c: REAR-TIRE FAIRING



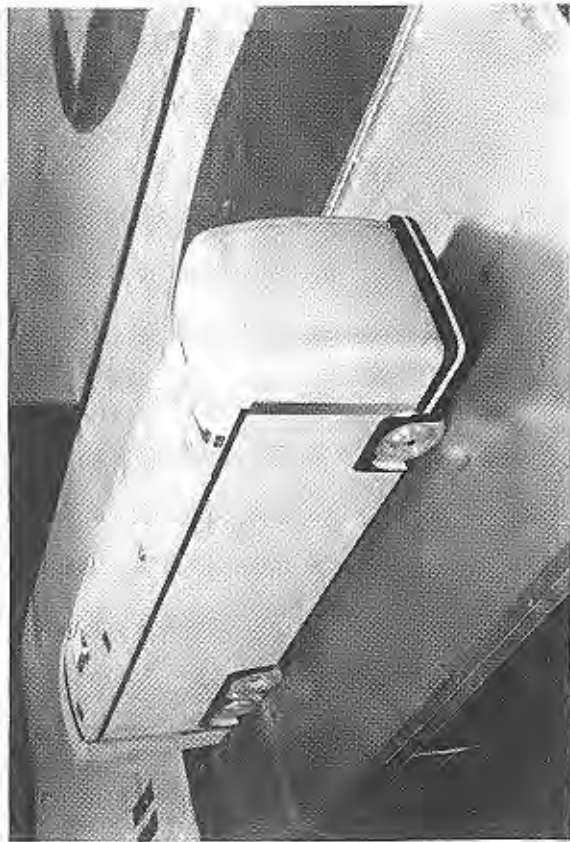
P20: VORTEX GENERATORS IMMEDIATELY
UPSTREAM OF BEVELLED REAR



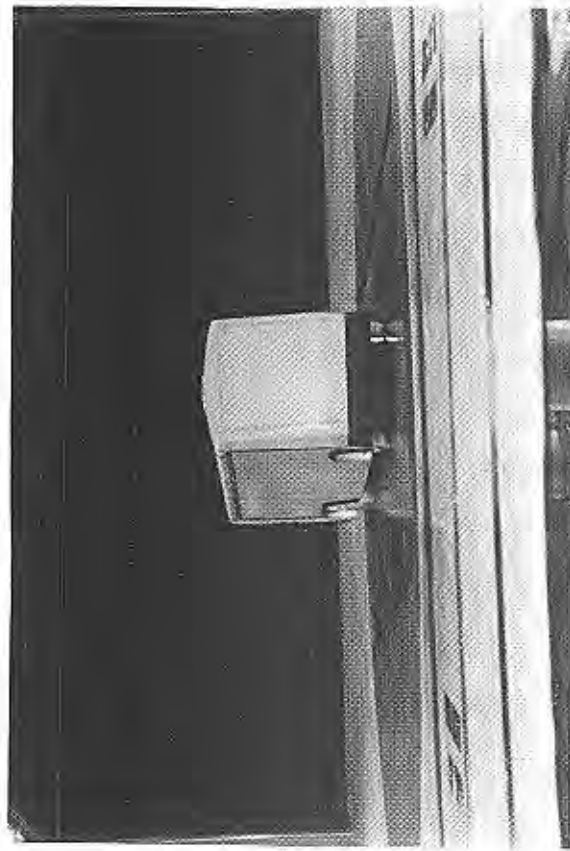
P21: MODIFIED DRIP RAIL



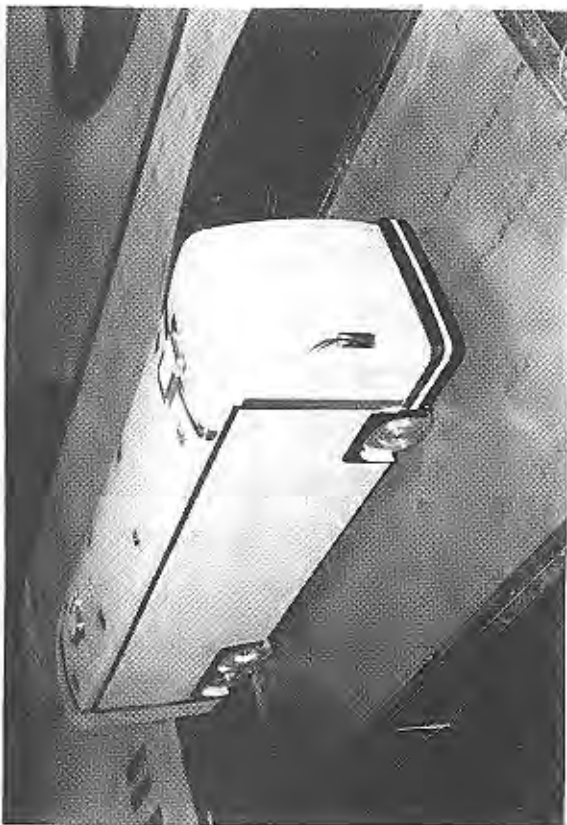
P22a: PREVOST H3-40 FRONT WITH
PREVOST MIRRORS



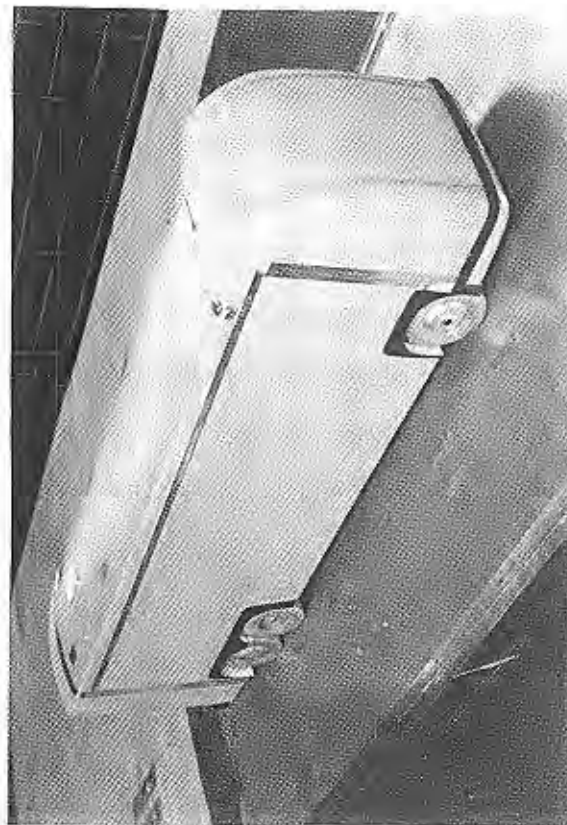
P23: PREVOST H3-40 FRONT WITH TRIP



P25: MCI SMOOTH CJ3 FRONT WITH TRIP



P22b: PREVOST H3-40 FRONT WITH
PREVOST MIRRORS



P24: MCI PROPOSAL 1 FRONT WITH TRIP

APPENDIX 3: DATA TABULATION

The following notation is used in the tabulations:

Rept/Tare/Run = Test number/Run no. for wind-off balance zero readings/Run no.
QC = reference dynamic pressure corrected for wall effects
Re = Reynolds number
PT = point number
VEL = test wind speed based on QC
CL = lift coefficient
CD = drag coefficient
CY = side force coefficient
CM = pitching moment coefficient
CN = yawing moment coefficient
CR = rolling moment coefficient

BUS TEST

Rept/Tare/Run 0607/012/013

C3 SMOOTH FRONT, C3 STANDARD REAR

ATM PRESS= 101.2 KPA TEMP= 24.08 C Density= 1.186 Kg/m3
 Ref length=0.7225 m Ref Area= 0.08358 m2 GC= 3.50 Kpa
 Re= 1.3566 Million

PT	VEL (m/s)	YAW (deg)	CL	CD	CY	CM	CN	CR
01	81.1	-2.95	-0.0156	0.3527	-0.2570	0.0421	-0.0924	-0.0597
02	81.3	-1.44	-0.0376	0.3473	-0.1139	0.0487	-0.0456	-0.0286
03	81.0	0.08	-0.0506	0.3481	0.0213	0.0509	0.0027	0.0044
04	81.3	1.60	-0.0447	0.3507	0.1578	0.0447	0.0507	0.0316
05	81.2	3.15	-0.0894	0.3561	0.3030	0.0316	0.0990	0.0654
06	81.1	6.21	0.0916	0.3801	0.6043	0.0273	0.1947	0.1333
07	80.4	9.27	0.2219	0.4037	0.9167	0.0316	0.2921	0.2055
08	78.8	12.35	0.4223	0.4496	1.2581	0.0256	0.3876	0.2854

Bus speed(mi/h)

35.00
45.00
55.00
65.00
75.00

Wind Averaged CD

0.410
0.387
0.376
0.369
0.363

BUS TEST

Rept/Tare/Run 0607/012/014

C3 SMOOTH FRONT, C3 STANDARD REAR

ATM PRESS= 101.2 KPA TEMP= 22.34 C Density= 1.193 Kg/m3
 Ref length=0.7225 m Ref Area= 0.08358 m2 GC= 0.58 Kpa
 Re= 0.5250 Million

PT	VEL (m/s)	YAW (deg)	CL	CD	CY	CM	CN	CR
01	31.1	-0.03	-0.0877	0.4856	-0.0131	0.1040	-0.0123	-0.0107
02	37.2	-0.03	-0.0834	0.4526	0.0009	0.0941	-0.0036	-0.0024
03	43.2	-0.03	-0.0793	0.4579	0.0027	0.0986	-0.0022	-0.0026
04	49.7	-0.03	-0.0758	0.4517	0.0055	0.0959	-0.0021	-0.0015
05	55.7	-0.03	-0.0703	0.4387	0.0086	0.0857	-0.0014	0.0001
06	62.5	-0.03	-0.0648	0.4331	0.0106	0.0879	-0.0013	0.0008
07	68.5	-0.03	-0.0616	0.4264	0.0115	0.0874	-0.0013	0.0007
08	75.6	-0.03	-0.0552	0.4143	0.0104	0.0862	-0.0015	0.0013
09	80.8	-0.03	-0.0539	0.3477	0.0092	0.0536	-0.0011	0.0013
10	87.2	-0.03	-0.0482	0.3489	0.0051	0.0543	-0.0013	0.0001
11	93.6	-0.03	-0.0419	0.3455	0.0031	0.0543	-0.0022	-0.0002

Bus speed(mi/h)

35.00
45.00
55.00
65.00
75.00

Wind Averaged CD

0.000
0.000
0.000
0.000
0.000

BUS TEST

Rept/Tare/Run 0607/015/016

C3 SMOOTH FRONT, C3 STANDARD REAR

ATM PRESS= 101.1 KPA TEMP= 24.48 C Density= 1.183 Kg/m3
 Ref length=0.7225 m Ref Area= 0.08358 m2 GC= 4.22 Kpa
 Re= 1.4063 Million

PT	VEL (m/s)	YAW (deg)	CL	CD	CY	CM	CN	CR
01	84.5	-3.07	-0.0069	0.3554	-0.2713	0.0415	-0.0951	-0.0645
02	84.4	-1.57	-0.0338	0.3500	-0.1293	0.0501	-0.0480	-0.0339
03	84.7	-0.05	-0.0460	0.3480	0.0089	0.0512	0.0000	-0.0012
04	84.4	1.48	-0.0450	0.3554	0.1502	0.0488	0.0454	0.0305
05	84.5	3.02	-0.0079	0.3588	0.2938	0.0345	0.0957	0.0447
06	84.2	6.07	0.0886	0.3781	0.5925	0.0268	0.1919	0.1345
07	83.4	9.14	0.2223	0.4012	0.9041	0.0272	0.2891	0.2049
08	82.1	12.21	0.4166	0.4401	1.2432	0.0210	0.3841	0.2853

Bus speed(mi/h)

35.00
45.00
55.00
65.00
75.00

Wind Averaged CD

0.409
0.387
0.377
0.371
0.367

BUS TEST

Rept/Tare/Run 0607/017/018

PRODUCTION C3 FRONT, C3 STANDARD REAR

ATM PRESS= 101.1 KPA TEMP= 21.88 C Density= 1.193 Kg/m3
 Ref length=0.7225 m Ref Area= 0.08358 m2 GC= 1.46 Kpa
 Re= 0.8386 Million

PT	VEL (m/s)	YAW (deg)	CL	CD	CY	CM	CN	CR
01	49.5	-0.01	-0.1150	0.5431	0.0136	0.0883	-0.0033	-0.0045
02	55.7	-0.01	-0.1104	0.5449	0.0142	0.0841	-0.0029	-0.0034
03	61.9	-0.01	-0.1044	0.5387	0.0143	0.0817	-0.0029	-0.0024
04	67.8	-0.01	-0.0988	0.5363	0.0152	0.0842	-0.0036	-0.0022
05	74.7	-0.01	-0.0947	0.5364	0.0133	0.0860	-0.0038	-0.0016
06	80.8	-0.01	-0.0885	0.5362	0.0121	0.0852	-0.0043	-0.0015
07	86.8	-0.01	-0.0839	0.5334	0.0094	0.0845	-0.0048	-0.0024
08	92.6	-0.01	-0.0782	0.5273	0.0052	0.0868	-0.0038	-0.0033

Bus speed(mi/h)

35.00
45.00
55.00
65.00
75.00

Wind Averaged CD

0.000
0.000
0.000
0.000
0.000

BUS TEST

Rept/Tare/Run 0607/017/017

PRODUCTION C3 FRONT, C3 STANDARD REAR

ATM PRESS= 101.1 KPA TEMP= 27.09 C Density= 1.173 Kg/m3
 Ref length=0.7225 m Ref Area= 0.09358 m2 GC= 4.18 Kpa
 Re= 1.3947 Million

PT	VEL (m/s)	YAW (deg)	CL	CD	CY	CM	CN	CR
01	84.4	-3.10	-0.0440	0.5380	-0.2758	0.0717	-0.0727	-0.0699
02	84.4	-1.50	-0.0767	0.5306	-0.1331	0.0822	-0.0476	-0.0296
03	84.2	-0.05	-0.0547	0.5304	0.0046	0.0831	-0.0040	-0.0044
04	84.4	1.47	-0.0623	0.5315	0.1442	0.0777	0.0392	0.0276
05	84.0	3.01	-0.0156	0.5410	0.2864	0.0797	0.0902	0.0641
06	83.6	6.06	0.0780	0.5064	0.5618	0.0855	0.1771	0.1308
07	82.9	9.13	0.2239	0.6676	0.8752	0.0953	0.2478	0.2116
08	81.8	12.20	0.4615	0.7581	1.2435	0.0870	0.3019	0.2963

Bus speed(mi/h)

35.00
45.00
55.00
65.00
75.00

Wind Averaged CD

0.662
0.612
0.584
0.567
0.568

BUS TEST

Rept/Tare/Run 0607/020/021

MERCEDES-BENZ FRONT, C3 STANDARD REAR

ATM PRESS= 101.5 KPA TEMP= 21.69 C Density= 1.177 Kg/m3
 Ref length=0.7225 m Ref Area= 0.09358 m2 GC= 1.47 Kpa
 Re= 0.8434 Million

PT	VEL (m/s)	YAW (deg)	CL	CD	CY	CM	CN	CR
01	49.6	-0.02	-0.0500	0.5897	0.0141	0.1467	-0.0005	-0.0035
02	55.0	-0.02	-0.0478	0.5959	0.0137	0.1506	-0.0001	-0.0019
03	61.7	-0.02	-0.0429	0.5862	0.0153	0.1531	0.0006	-0.0018
04	68.0	-0.02	-0.0408	0.5896	0.0158	0.1563	0.0015	-0.0012
05	75.6	-0.02	-0.0369	0.5825	0.0168	0.1508	0.0019	-0.0013
06	80.3	-0.02	-0.0359	0.5773	0.0078	0.1481	-0.0003	-0.0031
07	86.8	-0.02	-0.0316	0.5691	0.0034	0.1448	-0.0022	-0.0051
08	93.0	-0.02	-0.0259	0.5668	-0.0002	0.1461	-0.0030	-0.0059

Bus speed(mi/h)

35.00
45.00
55.00
65.00
75.00

Wind Averaged CD

0.000
0.000
0.000
0.000
0.000

BUS TEST

Rept/Tare/Run 0607/020/022

MERCEDES-BENZ FRONT, C3 STANDARD REAR

ATM PRESS= 101.5 KPA TEMP= 26.74 C Density= 1.178 Kg/m3
 Ref length=0.7225 m Ref Area= 0.09358 m2 GC= 4.16 Kpa
 Re= 1.3870 Million

PT	VEL (m/s)	YAW (deg)	CL	CD	CY	CM	CN	CR
01	84.0	-3.05	0.0139	0.5782	-0.3075	0.1355	-0.0928	-0.0054
02	84.0	-1.53	-0.0172	0.5647	-0.1513	0.1439	-0.0491	-0.0478
03	84.2	-0.01	-0.0250	0.5568	0.0050	0.1437	-0.0009	-0.0059
04	83.9	1.52	-0.0045	0.5684	0.1568	0.1504	0.0391	0.0345
05	84.2	3.06	0.0423	0.5873	0.3170	0.1489	0.0843	0.0788
06	83.6	6.11	0.2094	0.6252	0.6405	0.1554	0.1812	0.1605
07	82.7	9.19	0.4205	0.6952	0.9775	0.1707	0.2707	0.2455
08	81.8	12.26	0.6787	0.7542	1.3393	0.1692	0.3520	0.3370

Bus speed(mi/h)

35.00
45.00
55.00
65.00
75.00

Wind Averaged CD

0.685
0.643
0.620
0.606
0.598

BUS TEST

Rept/Tare/Run 0607/024/025

PROPOSAL #1 FRONT, C3 STANDARD REAR

ATM PRESS= 101.5 KPA TEMP= 23.98 C Density= 1.189 Kg/m3
 Ref length=0.7225 m Ref Area= 0.09358 m2 GC= 1.47 Kpa
 Re= 0.8233 Million

PT	VEL (m/s)	YAW (deg)	CL	CD	CY	CM	CN	CR
01	49.9	-0.02	-0.0691	0.4153	0.0131	0.0929	0.0056	-0.0068
02	56.1	-0.02	-0.0651	0.3512	0.0156	0.0766	0.0033	-0.0036
03	62.5	-0.02	-0.0637	0.3458	0.0146	0.0729	0.0039	-0.0031
04	67.9	-0.02	-0.0616	0.3450	0.0137	0.0700	0.0035	-0.0029
05	76.0	-0.02	-0.0552	0.3447	0.0112	0.0704	0.0029	-0.0024
06	81.2	-0.02	-0.0496	0.3420	0.0081	0.0702	0.0026	-0.0030
07	87.7	-0.02	-0.0443	0.3442	0.0085	0.0732	0.0023	-0.0027
08	94.1	-0.02	-0.0361	0.3404	0.0022	0.0734	0.0002	-0.0036

Bus speed(mi/h)

35.00
45.00
55.00
65.00
75.00

Wind Averaged CD

0.000
0.000
0.000
0.000
0.000

BUS TEST

Rept/Tare/Run 0607/024/026

PROPOSAL #1 FRONT, C3 STANDARD REAR

ATM PRESS= 101.5 KPA TEMP= 29.03 C Density= 1.170 Kg/m3
 Ref length=0.7225 m Ref Area= 0.08358 m2 QC= 4.24 Kpa
 Re= 1.3860 Million

PT	VEL (m/s)	YAW (deg)	CL	CD	CY	CM	CN	CR
01	85.1	-3.04	0.0012	0.3504	-0.2794	0.0593	-0.0932	-0.0675
02	85.1	-1.53	-0.0400	0.3461	-0.1322	0.0725	-0.0484	-0.0367
03	84.9	-0.01	-0.0449	0.3419	0.0072	0.0715	0.0019	-0.0027
04	84.9	1.52	-0.0378	0.3461	0.1544	0.0718	0.0512	0.0277
05	85.0	3.05	0.0107	0.3534	0.3021	0.0650	0.1027	0.0651
06	84.7	6.11	0.1092	0.3592	0.6005	0.0490	0.2064	0.1367
07	84.0	9.18	0.2299	0.3778	0.9144	0.0447	0.3090	0.2111
08	83.6	12.26	0.4024	0.3972	1.2580	0.0316	0.4102	0.2897

Bus speed(mi/h)
 35.00
 45.00
 55.00
 65.00
 75.00

Wind Averaged CD
 0.383
 0.371
 0.363
 0.358
 0.356

BUS TEST

Rept/Tare/Run 0607/027/028

PROPOSAL #2 FRONT, C3 STANDARD REAR

ATM PRESS= 101.2 KPA TEMP= 24.43 C Density= 1.184 Kg/m3
 Ref length=0.7225 m Ref Area= 0.08358 m2 QC= 1.46 Kpa
 Re= 0.8273 Million

PT	VEL (m/s)	YAW (deg)	CL	CD	CY	CM	CN	CR
01	49.6	-0.02	-0.0482	0.4733	0.0146	0.1207	-0.0006	-0.0051
02	55.9	-0.02	-0.0469	0.4655	0.0145	0.1167	-0.0012	-0.0046
03	62.4	-0.02	-0.0431	0.4685	0.0162	0.1193	-0.0011	-0.0033
04	67.2	-0.02	-0.0417	0.4618	0.0153	0.1140	-0.0007	-0.0025
05	75.9	-0.02	-0.0325	0.4492	0.0126	0.1133	0.0006	-0.0017
06	81.2	-0.02	-0.0258	0.4430	0.0123	0.1134	0.0002	-0.0016
07	87.8	-0.02	-0.0189	0.4235	0.0078	0.1111	-0.0014	-0.0027
08	93.9	-0.02	-0.0128	0.4046	0.0078	0.1083	0.0018	-0.0019

Bus speed(mi/h)
 35.00
 45.00
 55.00
 65.00
 75.00

Wind Averaged CD
 0.000
 0.000
 0.000
 0.000
 0.000

BUS TEST

Rept/Tare/Run 0607/027/027

PROPOSAL #2 FRONT, C3 STANDARD REAR

ATM PRESS= 101.3 KPA TEMP= 29.48 C Density= 1.168 Kg/m3
 Ref length=0.7225 m Ref Area= 0.08358 m2 QC= 4.22 Kpa
 Re= 1.3799 Million

PT	VEL (m/s)	YAW (deg)	CL	CD	CY	CM	CN	CR
01	84.9	-3.05	0.0190	0.3543	-0.2836	0.0761	-0.0750	-0.0670
02	84.9	-1.53	-0.0187	0.3467	-0.1346	0.0856	-0.0495	-0.0373
03	84.9	-0.02	-0.0210	0.3423	0.0061	0.0845	-0.0023	-0.0037
04	84.7	1.51	-0.0131	0.3471	0.1533	0.0870	0.0443	0.0291
05	85.1	3.05	0.0287	0.3592	0.3057	0.0784	0.0949	0.0669
06	84.3	6.11	0.1274	0.4833	0.6148	0.0912	0.2065	0.1477
07	84.0	9.18	0.2724	0.5168	0.9300	0.0929	0.2983	0.2212
08	83.1	12.26	0.4498	0.5750	1.2851	0.0818	0.3901	0.3057

Bus speed(mi/h)
 35.00
 45.00
 55.00
 65.00
 75.00

Wind Averaged CD
 0.476
 0.458
 0.436
 0.416
 0.396

BUS TEST

Rept/Tare/Run 0607/030/031

PREVOST FRONT, C3 STANDARD REAR

ATM PRESS= 101.5 KPA TEMP= 25.03 C Density= 1.184 Kg/m3
 Ref length=0.7225 m Ref Area= 0.08358 m2 QC= 1.47 Kpa
 Re= 0.8308 Million

PT	VEL (m/s)	YAW (deg)	CL	CD	CY	CM	CN	CR
01	49.9	-0.01	-0.1222	0.5340	0.0190	0.0700	0.0019	-0.0021
02	55.7	-0.01	-0.1166	0.5234	0.0166	0.0627	0.0003	-0.0022
03	62.0	-0.01	-0.1793	0.4941	0.0144	0.0591	-0.0045	-0.0028
04	66.5	-0.01	-0.1073	0.4721	0.0103	0.0524	-0.0080	-0.0033
05	75.2	-0.01	-0.0918	0.3770	0.0222	0.0314	0.0061	-0.0025
06	81.5	0.00	-0.0853	0.3706	0.0236	0.0307	0.0056	-0.0028
07	88.0	-0.01	-0.0802	0.3709	0.0214	0.0298	0.0047	-0.0025
08	94.2	-1.96	-0.0732	0.3646	0.0032	0.0284	0.0025	-0.0008

Bus speed(mi/h)
 35.00
 45.00
 55.00
 65.00
 75.00

Wind Averaged CD
 0.000
 0.000
 0.000
 0.000
 0.000

BUS TEST

Rept/Tare/Run 0607/030/032

PREVOST FRONT: C3 STANDARD REAR

ATM PRESS= 101.5 KPa TEMP= 27.90 C Density= 1.166 Kg/m3
 Ref length=0.7225 m Ref Area= 0.08358 m2 QC= 4.22 Kpa
 Re= 1.3776 Million

PT	VEL (m/s)	YAW (deg)	CL	CD	CY	CM	CN	CR
01	35.0	-3.04	-0.0495	0.3802	-0.2609	0.0169	-0.0893	-0.0648
02	34.9	-1.32	-0.0741	0.3745	-0.1214	0.0284	-0.0433	-0.0335
03	34.7	-0.01	-0.0813	0.3716	0.0213	0.0313	-0.0051	-0.0016
04	34.7	1.51	-0.0670	0.3721	0.1534	0.0258	0.0522	0.0317
05	34.3	3.06	-0.0387	0.3797	0.2925	0.0192	0.1028	0.0657
06	34.3	6.11	0.0495	0.4001	0.5964	0.0189	0.2016	0.1382
07	34.0	9.18	0.1724	0.4398	0.9091	0.0163	0.2995	0.2115
08	32.3	12.26	0.4902	0.7391	1.3176	0.0613	0.3114	0.3289

Bus speed(mi/h)

35.00
45.00
55.00
65.00
75.00

Wind Averaged CD

0.501
0.417
0.404
0.396
0.390

BUS TEST

Rept/Tare/Run 0607/033/034

SETRA FRONT: C3 STANDARD REAR

ATM PRESS= 101.5 KPa TEMP= 28.46 C Density= 1.164 Kg/m3
 Ref length=0.7225 m Ref Area= 0.08358 m2 QC= 1.48 Kpa
 Re= 0.8310 Million

PT	VEL (m/s)	YAW (deg)	CL	CD	CY	CM	CN	CR
01	50.0	-0.01	-0.0678	0.5713	-0.0105	0.1202	0.0010	-0.0069
02	55.7	-0.01	-0.0701	0.5763	-0.0141	0.1191	0.0022	-0.0045
03	62.2	-0.01	-0.0678	0.5686	-0.0152	0.1157	0.0030	-0.0029
04	65.5	-0.01	-0.0665	0.5679	-0.0151	0.1148	0.0031	-0.0025
05	74.3	-0.01	-0.0583	0.5660	-0.0144	0.1170	0.0021	-0.0018
06	80.5	-0.01	-0.0520	0.5673	-0.0159	0.1198	0.0031	-0.0016
07	87.5	-0.01	-0.0441	0.5638	-0.0104	0.1177	0.0018	-0.0022
08	92.8	-0.01	-0.0386	0.5636	-0.0057	0.1207	0.0007	-0.0029

Bus speed(mi/h)

35.00
45.00
55.00
65.00
75.00

Wind Averaged CD

0.000
0.000
0.000
0.000
0.000

BUS TEST

Rept/Tare/Run 0607/033/035

SETRA FRONT: C3 STANDARD REAR

ATM PRESS= 101.5 KPa TEMP= 27.99 C Density= 1.166 Kg/m3
 Ref length=0.7225 m Ref Area= 0.08358 m2 QC= 4.00 Kpa
 Re= 1.3402 Million

PT	VEL (m/s)	YAW (deg)	CL	CD	CY	CM	CN	CR
01	32.0	-3.08	0.0052	0.5768	-0.2916	0.1087	-0.0753	-0.0742
02	34.0	-1.54	-0.0378	0.5660	-0.1378	0.1171	-0.0378	-0.0399
03	34.6	-0.01	-0.0465	0.5638	0.0081	0.1168	0.0016	-0.0029
04	34.7	1.51	-0.0252	0.5680	0.1605	0.1209	0.0393	0.0344
05	34.4	3.03	0.0199	0.5885	0.3158	0.1116	0.0720	0.0764
06	34.0	6.11	0.1563	0.6301	0.6383	0.1066	0.1448	0.1588
07	33.3	9.19	0.3611	0.7010	0.9757	0.1128	0.2177	0.2463
08	33.3	12.26	0.5973	0.7586	1.3237	0.1091	0.2870	0.3323

Bus speed(mi/h)

35.00
45.00
55.00
65.00
75.00

Wind Averaged CD

0.692
0.631
0.625
0.610
0.601

BUS TEST

Rept/Tare/Run 0607/036/037

PRODUCTION C3 FRONT WITH MIRRORS: C3 STANDARD REAR

ATM PRESS= 101.5 KPa TEMP= 27.76 C Density= 1.174 Kg/m3
 Ref length=0.7225 m Ref Area= 0.08358 m2 QC= 4.18 Kpa
 Re= 1.3939 Million

PT	VEL (m/s)	YAW (deg)	CL	CD	CY	CM	CN	CR
01	34.4	-3.07	-0.0512	0.5507	-0.2719	0.0731	-0.0910	-0.0682
02	34.1	-1.54	-0.0830	0.5451	-0.1341	0.0810	-0.0495	-0.0386
03	33.9	-0.02	-0.0893	0.5421	-0.0079	0.0839	-0.0028	-0.0025
04	33.8	1.51	-0.0676	0.5441	0.1494	0.0774	0.0421	0.0304
05	34.0	3.05	-0.0230	0.5528	0.2874	0.0825	0.0912	0.0650
06	33.8	6.10	0.0768	0.6034	0.5833	0.0921	0.1777	0.1368
07	32.6	9.17	0.2010	0.6492	0.8920	0.0978	0.2538	0.2107
08	32.2	12.24	0.3932	0.7279	1.2387	0.0890	0.3313	0.2927

Bus speed(mi/h)

35.00
45.00
55.00
65.00
75.00

Wind Averaged CD

0.661
0.621
0.596
0.581
0.571

BUS TEST

Rept/Tare/Run: 0607/030/039

PROP 2 FRONT WITH GRIT, C3 STANDARD REAR

ATM PRESS= 101.4 KPA TEMP= 23.51 C Density= 1.190 Kg/m3
 Ref length=0.7225 m Ref Area= 0.08358 m2 GC= 1.49 Kpa
 Re= 0.8399 Million

PT	VEL (m/s)	YAW (deg)	CL	CD	CY	CM	CN	CR
01	50.0	-0.22	-0.0441	0.3566	-0.0054	0.0878	-0.0044	-0.0068
02	56.5	-0.22	-0.0418	0.3529	-0.0049	0.0871	-0.0047	-0.0066
03	61.8	-0.22	-0.0411	0.3474	-0.0047	0.0840	-0.0045	-0.0073
04	68.6	-0.22	-0.0370	0.3472	-0.0048	0.0833	-0.0045	-0.0068
05	75.2	-0.22	-0.0334	0.3469	-0.0066	0.0826	-0.0050	-0.0068
06	81.0	-0.22	-0.0293	0.3428	-0.0087	0.0815	-0.0055	-0.0070
07	87.7	-0.22	-0.0216	0.3445	-0.0097	0.0852	-0.0058	-0.0070
08	94.2	-0.22	-0.0156	0.3414	-0.0144	0.0864	-0.0076	-0.0084

Bus speed(mi/h)
 35.00
 45.00
 55.00
 65.00
 75.00

Wind Averaged CD
 0.000
 0.000
 0.000
 0.000
 0.000

BUS TEST

Rept/Tare/Run: 0607/030/040

PROP 2 FRONT WITH GRIT, C3 STANDARD REAR

ATM PRESS= 101.5 KPA TEMP= 27.81 C Density= 1.173 Kg/m3
 Ref length=0.7225 m Ref Area= 0.08358 m2 GC= 4.20 Kpa
 Re= 1.3862 Million

PT	VEL (m/s)	YAW (deg)	CL	CD	CY	CM	CN	CR
01	84.6	-3.04	0.0194	0.3534	-0.2822	0.0759	-0.0929	-0.0676
02	84.5	-1.53	-0.0190	0.3448	-0.1323	0.0841	-0.0470	-0.0378
03	84.5	-0.01	-0.0217	0.3414	0.0094	0.0864	0.0009	-0.0026
04	84.7	1.51	-0.0126	0.3460	0.1555	0.0904	0.0476	0.0290
05	84.6	3.05	0.0299	0.3537	0.3035	0.0810	0.0971	0.0653
06	84.6	6.11	0.1333	0.3615	0.5994	0.0673	0.1968	0.1362
07	84.0	9.19	0.2601	0.3866	0.9108	0.0620	0.2913	0.2097
08	92.2	12.26	0.4698	0.5420	1.2751	0.0854	0.3817	0.3044

Bus speed(mi/h)
 35.00
 45.00
 55.00
 65.00
 75.00

Wind Averaged CD
 0.422
 0.374
 0.365
 0.359
 0.357

BUS TEST

Rept/Tare/Run: 0607/041/042

PROP 2 FRONT WITH GRIT AND C3 MIRRORS FWD, C3 STANDARD REAR

ATM PRESS= 101.3 KPA TEMP= 27.55 C Density= 1.173 Kg/m3
 Ref length=0.7225 m Ref Area= 0.08358 m2 GC= 4.21 Kpa
 Re= 1.3893 Million

PT	VEL (m/s)	YAW (deg)	CL	CD	CY	CM	CN	CR
01	84.7	-3.08	0.0202	0.3816	-0.2855	0.0850	-0.0948	-0.0691
02	84.6	-1.54	-0.0249	0.3798	-0.1373	0.0943	-0.0468	-0.0386
03	84.5	-0.02	-0.0288	0.3769	0.0047	0.0727	-0.0001	-0.0052
04	84.3	1.51	-0.0197	0.3795	0.1531	0.0952	0.0452	0.0282
05	84.6	3.05	0.0280	0.3804	0.3049	0.0937	0.0958	0.0665
06	84.5	6.11	0.1346	0.3893	0.6003	0.0660	0.1940	0.1361
07	83.3	9.18	0.2585	0.4341	0.9210	0.0690	0.2945	0.2159
08	82.3	12.26	0.4430	0.4698	1.2650	0.0656	0.3899	0.2966

Bus speed(mi/h)
 35.00
 45.00
 55.00
 65.00
 75.00

Wind Averaged CD
 0.434
 0.409
 0.394
 0.387
 0.385

BUS TEST

Rept/Tare/Run: 0607/043/044

PROP 2 FRONT WITH GRIT AND C3 MIRRORS AFT, C3 STANDARD REAR

ATM PRESS= 101.3 KPA TEMP= 27.25 C Density= 1.174 Kg/m3
 Ref length=0.7225 m Ref Area= 0.08358 m2 GC= 4.23 Kpa
 Re= 1.3937 Million

PT	VEL (m/s)	YAW (deg)	CL	CD	CY	CM	CN	CR
01	84.8	-3.08	0.0075	0.3948	-0.2840	0.0830	-0.0923	-0.0683
02	84.5	-1.54	-0.0337	0.3929	-0.1367	0.0915	-0.0468	-0.0387
03	84.4	-0.02	-0.0372	0.3914	0.0107	0.0933	-0.0005	-0.0022
04	84.5	1.51	-0.0283	0.3935	0.1615	0.0928	0.0443	0.0321
05	84.6	3.05	0.0201	0.3938	0.3093	0.0826	0.0944	0.0691
06	84.4	6.11	0.1249	0.3974	0.6058	0.0649	0.1910	0.1392
07	84.1	9.18	0.2517	0.4242	0.9127	0.0618	0.2843	0.2128
08	83.7	12.25	0.4347	0.4717	1.2507	0.0606	0.3608	0.2925

Bus speed(mi/h)
 35.00
 45.00
 55.00
 65.00
 75.00

Wind Averaged CD
 0.438
 0.413
 0.403
 0.400
 0.398

BUS TEST

Rept/Tare/Run 0607/045/046

PROP 2 FRONT WITH GRIT AND CEIRA MIRRORS, C3 STANDARD REAR

ATM PRESS= 101.3 KPA TEMP= 27.48 C Density= 1.173 Kg/m3
 Ref length=0.7225 m Ref Area= 0.08358 m2 GC= 4.25 Kpa
 Rea 1.3937 Million

PT	VEL (m/s)	YAW (deg)	CL	CD	CY	CM	CN	CR
01	85.1	-3.07	0.0244	0.4154	-0.2889	0.1024	-0.0919	-0.0704
02	84.9	-1.54	-0.0102	0.4124	-0.1322	0.1111	-0.0429	-0.0371
03	84.6	-0.02	-0.0117	0.4125	0.0129	0.1126	0.0059	-0.0021
04	84.6	1.51	-0.0042	0.4154	0.1635	0.1129	0.0510	0.0334
05	84.7	3.05	0.0354	0.4196	0.3164	0.1032	0.1053	0.0721
06	84.4	6.11	0.1215	0.4296	0.6169	0.0874	0.2095	0.1442
07	83.6	9.18	0.2316	0.4521	0.9288	0.0762	0.3123	0.2189
08	83.8	12.24	0.3927	0.4680	1.2653	0.0521	0.4127	0.2963

Bus speed(mi/h)

35.00
45.00
55.00
65.00
75.00

Wind Averaged CD

0.457
0.443
0.434
0.428
0.425

BUS TEST

Rept/Tare/Run 0607/047/048

PROP 2 FRONT WITH GRIT AND PREVOST MIRRORS, C3 STANDARD REAR

ATM PRESS= 101.3 KPA TEMP= 27.08 C Density= 1.174 Kg/m3
 Ref length=0.7225 m Ref Area= 0.08358 m2 GC= 4.26 Kpa
 Rea 1.3983 Million

PT	VEL (m/s)	YAW (deg)	CL	CD	CY	CM	CN	CR
01	85.2	-3.07	0.0227	0.3745	-0.2845	0.0881	-0.0952	-0.0671
02	84.8	-1.54	-0.0240	0.3727	-0.1366	0.0953	-0.0476	-0.0393
03	84.7	-0.01	-0.0279	0.3712	0.0127	0.0959	0.0018	-0.0037
04	84.2	1.51	-0.0176	0.3732	0.1576	0.0969	0.0473	0.0292
05	84.9	3.05	0.0314	0.3763	0.3021	0.0853	0.0991	0.0659
06	84.1	6.11	0.1298	0.4330	0.6189	0.0837	0.2080	0.1467
07	83.7	9.18	0.2610	0.5022	0.9359	0.0913	0.2991	0.2259
08	82.8	12.24	0.4550	0.5598	1.2803	0.0892	0.3867	0.3070

Bus speed(mi/h)

35.00
45.00
55.00
65.00
75.00

Wind Averaged CD

0.484
0.446
0.422
0.406
0.397

BUS TEST

Rept/Tare/Run 0607/049/050

PROP 2 FRONT WITH GRIT, REAR 15

ATM PRESS= 101.3 KPA TEMP= 26.02 C Density= 1.179 Kg/m3
 Ref length=0.7225 m Ref Area= 0.08358 m2 GC= 4.60 Kpa
 Rea 0.8607 Million

PT	VEL (m/s)	YAW (deg)	CL	CD	CY	CM	CN	CR
01	52.0	-0.02	0.1551	0.2964	0.0061	-0.0479	0.0068	-0.0043
02	56.4	-0.02	0.1520	0.2989	0.0038	-0.0437	0.0067	-0.0051
03	62.4	-0.02	0.1509	0.2963	0.0042	-0.0456	0.0069	-0.0045
04	67.6	-0.02	0.1502	0.2928	0.0044	-0.0499	0.0070	-0.0039
05	75.6	-0.02	0.1519	0.2919	0.0017	-0.0485	0.0074	-0.0042
06	83.5	-0.02	0.1530	0.2914	0.0003	-0.0455	0.0072	-0.0047
07	88.4	-0.02	0.1561	0.2899	-0.0030	-0.0456	0.0064	-0.0060
08	94.4	-0.02	0.1590	0.2912	-0.0100	-0.0454	0.0056	-0.0070

Bus speed(mi/h)

35.00
45.00
55.00
65.00
75.00

Wind Averaged CD

0.000
0.000
0.000
0.000
0.000

BUS TEST

Rept/Tare/Run 0607/049/051

PROP 2 FRONT WITH GRIT, REAR 15

ATM PRESS= 101.3 KPA TEMP= 29.99 C Density= 1.163 Kg/m3
 Ref length=0.7225 m Ref Area= 0.08358 m2 GC= 4.28 Kpa
 Rea 1.3862 Million

PT	VEL (m/s)	YAW (deg)	CL	CD	CY	CM	CN	CR
01	85.8	-3.04	0.1866	0.2933	-0.2779	-0.0554	-0.0763	-0.0649
02	85.0	-1.54	0.1594	0.2928	-0.1469	-0.0508	-0.0400	-0.0397
03	85.1	-0.02	0.1557	0.2908	-0.0021	-0.0447	0.0056	-0.0055
04	85.4	1.51	0.1655	0.2921	0.1489	-0.0475	0.0534	0.0267
05	85.7	3.05	0.1943	0.2924	0.2812	-0.0541	0.1123	0.0600
06	85.7	6.11	0.3040	0.2924	0.5512	-0.0641	0.2268	0.1248
07	84.6	9.17	0.4335	0.3098	0.8363	-0.0693	0.3342	0.1652
08	83.4	12.23	0.6314	0.4573	1.1499	-0.0478	0.4488	0.2711

Bus speed(mi/h)

35.00
45.00
55.00
65.00
75.00

Wind Averaged CD

0.347
0.305
0.279
0.296
0.295

BUS TEST

Rept/Tare/Run 0607/052/053

PROP 2 FRONT WITH GRIT AND C3 MIRRORS FWD, REAR 15

ATM PRESS= 101.2 KPA TEMP= 28.12 C Density= 1.170 Kg/m3
 Ref length=0.7225 m Ref Area= 0.08358 m2 QC= 4.22 Kpa
 Re= 1.3863 Million

PT	VEL (m/s)	YAW (deg)	CL	CD	CY	CM	CN	CR
01	84.9	-3.08	0.1822	0.3251	-0.2794	-0.0465	-0.0967	-0.0652
02	84.6	-1.54	0.1554	0.3246	-0.1493	-0.0436	-0.0414	-0.0403
03	84.9	-0.02	0.1515	0.3233	-0.0006	-0.0397	0.0070	-0.0043
04	85.0	1.51	0.1648	0.3259	0.1531	-0.0410	0.0537	0.0299
05	85.2	3.05	0.1969	0.3262	0.2813	-0.0472	0.1134	0.0611
06	85.1	6.10	0.3026	0.3326	0.3410	-0.0834	0.2337	0.1216
07	84.5	9.17	0.4270	0.3706	0.8427	-0.0580	0.3427	0.1979
08	83.5	12.24	0.6053	0.3969	1.1543	-0.0583	0.4479	0.2688

Bus speed(mi/h)

35.00
45.00
55.00
65.00
75.00

Wind Averaged CD

0.371
0.351
0.339
0.333
0.331

BUS TEST

Rept/Tare/Run 0607/054/055

PROP 2 FRONT WITH GRIT AND C3 MIRRORS (RIGHT FWD,LEFT AFT), REAR 15

ATM PRESS= 101.2 KPA TEMP= 25.62 C Density= 1.179 Kg/m3
 Ref length=0.7225 m Ref Area= 0.08358 m2 QC= 4.23 Kpa
 Re= 1.4037 Million

PT	VEL (m/s)	YAW (deg)	CL	CD	CY	CM	CN	CR
01	84.7	-3.07	0.1849	0.3443	-0.2747	-0.0398	-0.1044	-0.0653
02	84.7	-1.54	0.1566	0.3410	-0.1419	-0.0380	-0.0476	-0.0380
03	84.5	-0.02	0.1520	0.3366	0.0022	-0.0356	0.0020	-0.0030
04	84.6	1.51	0.1625	0.3371	0.1508	-0.0364	0.0498	0.0294
05	84.9	3.05	0.1966	0.3375	0.2799	-0.0443	0.1086	0.0598
06	84.5	6.10	0.2993	0.3412	0.5390	-0.0479	0.2283	0.1189
07	83.9	9.17	0.4232	0.3769	0.8394	-0.0531	0.3363	0.1914
08	83.5	12.23	0.6051	0.4023	1.1532	-0.0540	0.4418	0.2660

Bus speed(mi/h)

35.00
45.00
55.00
65.00
75.00

Wind Averaged CD

0.379
0.360
0.349
0.343
0.341

BUS TEST

Rept/Tare/Run 0607/056/057

PROP 2 FRONT, GRIT, C3 MIRRORS (RIGHT FWD,LEFT AFT),WHEEL FAIRINGS, REAR 15

ATM PRESS= 101.2 KPA TEMP= 25.63 C Density= 1.180 Kg/m3
 Ref length=0.7225 m Ref Area= 0.08358 m2 QC= 4.23 Kpa
 Re= 1.4041 Million

PT	VEL (m/s)	YAW (deg)	CL	CD	CY	CM	CN	CR
01	84.7	-3.07	0.2065	0.3267	-0.2725	-0.0414	-0.1087	-0.0652
02	84.1	-1.54	0.1849	0.3341	-0.1482	-0.0449	-0.0456	-0.0410
03	84.2	-0.01	0.1761	0.3315	0.0298	-0.0420	-0.0034	-0.0019
04	85.1	1.52	0.1921	0.3291	0.1858	-0.0431	0.0394	0.0348
05	85.0	3.05	0.2097	0.3162	0.2960	-0.0429	0.1039	0.0615
06	84.9	6.10	0.2861	0.3202	0.5555	-0.0342	0.2920	0.1209
07	84.0	9.17	0.4514	0.3504	0.8473	-0.0384	0.3523	0.1897
08	83.8	12.22	0.6489	0.3810	1.1702	-0.0504	0.4593	0.2681

Bus speed(mi/h)

35.00
45.00
55.00
65.00
75.00

Wind Averaged CD

0.357
0.339
0.330
0.325
0.324

BUS TEST

Rept/Tare/Run 0607/056/058

PROP 2 FRONT, GRIT, C3 MIRRORS (RIGHT FWD,LEFT AFT),VERTICAL AIR DAM, REAR 15

ATM PRESS= 101.2 KPA TEMP= 25.64 C Density= 1.180 Kg/m3
 Ref length=0.7225 m Ref Area= 0.08358 m2 QC= 4.18 Kpa
 Re= 1.3943 Million

PT	VEL (m/s)	YAW (deg)	CL	CD	CY	CM	CN	CR
01	84.1	-3.07	0.0969	0.3644	-0.2404	-0.0339	-0.1070	-0.0616
02	84.2	-1.53	0.0887	0.3615	-0.1127	-0.0359	-0.0566	-0.0325
03	84.1	-0.02	0.1026	0.3678	0.0035	-0.0395	-0.0011	-0.0017
04	84.2	1.51	0.1140	0.3665	0.1251	-0.0342	0.0509	0.0241
05	84.3	3.04	0.1343	0.3691	0.2592	-0.0385	0.1075	0.0570
06	84.3	6.09	0.2109	0.3934	0.5215	-0.0524	0.2192	0.1180
07	83.4	9.16	0.3118	0.4340	0.8146	-0.0617	0.3261	0.1841
08	82.0	12.22	0.4418	0.4598	1.1431	-0.0708	0.4165	0.2607

Bus speed(mi/h)

35.00
45.00
55.00
65.00
75.00

Wind Averaged CD

0.430
0.408
0.393
0.384
0.380

BUS TEST

Rept/Tare/Run 0607/056/059

PROP 2 FRONT, GRIT, C3 MIRRORS (RIGHT FWD, LEFT AFT), FWD TIRE FAIRINGS, REAR 15

ATM PRESS= 101.3 KPA TEMP= 26.42 C Density= 1.177 Kg/m3
 Ref length=0.7225 m Ref Area= 0.08358 m2 QC= 4.32 Kpa
 Re= 1.4120 Million

PT	VEL (m/s)	YAW (deg)	CL	CD	CY	CM	CN	CR
01	85.4	-3.05	0.1667	0.3495	-0.2912	-0.0327	-0.0758	-0.0706
02	85.3	-1.55	0.1547	0.3589	-0.1736	-0.0364	-0.0351	-0.0460
03	85.2	-0.02	0.1316	0.3426	0.0075	-0.0319	-0.0008	-0.0022
04	85.3	1.52	0.1604	0.3544	0.1901	-0.0342	0.0327	0.0387
05	85.4	3.05	0.1664	0.3476	0.3115	-0.0357	0.0940	0.0692
06	85.4	6.10	0.2770	0.3389	0.5449	-0.0307	0.2261	0.1212
07	84.7	9.17	0.4325	0.3777	0.8365	-0.0382	0.3414	0.1921
08	83.6	12.23	0.6302	0.4100	1.1493	-0.0492	0.4456	0.2665

Bus speed(mi/h)

35.00
45.00
55.00
65.00
75.00

Wind Averaged CD

0.384
0.364
0.353
0.348
0.349

BUS TEST

Rept/Tare/Run 0607/056/061

PROP 2 FRONT, GRIT, C3 MIRRORS (RIGHT FWD, LEFT AFT), MOD DRIP RAILS, REAR 15

ATM PRESS= 101.2 KPA TEMP= 26.31 C Density= 1.177 Kg/m3
 Ref length=0.7225 m Ref Area= 0.08358 m2 QC= 4.32 Kpa
 Re= 1.4143 Million

PT	VEL (m/s)	YAW (deg)	CL	CD	CY	CM	CN	CR
01	85.7	-3.09	0.1747	0.3492	-0.2936	-0.0462	-0.1020	-0.0718
02	85.2	-1.55	0.1450	0.3440	-0.1547	-0.0431	-0.0477	-0.0410
03	85.1	-0.02	0.1363	0.3378	-0.0010	-0.0397	0.0017	-0.0038
04	85.1	1.51	0.1461	0.3374	0.1525	-0.0399	0.0506	0.0311
05	85.3	3.05	0.1823	0.3411	0.2993	-0.0472	0.1077	0.0685
06	85.4	6.11	0.2843	0.3430	0.6038	-0.0551	0.2236	0.1434
07	84.4	9.19	0.3739	0.3767	0.9670	-0.0640	0.3321	0.2454
08	83.1	12.27	0.5530	0.3902	1.3627	-0.0734	0.4419	0.3549

Bus speed(mi/h)

35.00
45.00
55.00
65.00
75.00

Wind Averaged CD

0.377
0.361
0.351
0.345
0.344

BUS TEST

Rept/Tare/Run 0607/056/060

PROP 2 FRONT, GRIT, C3 MIRRORS (RIGHT FWD, LEFT AFT), REAR VORTS, GEN- REAR 15

ATM PRESS= 101.2 KPA TEMP= 26.22 C Density= 1.177 Kg/m3
 Ref length=0.7225 m Ref Area= 0.08358 m2 QC= 4.31 Kpa
 Re= 1.4134 Million

PT	VEL (m/s)	YAW (deg)	CL	CD	CY	CM	CN	CR
01	85.4	-3.05	0.1711	0.3514	-0.2743	-0.0469	-0.1025	-0.0647
02	85.2	-1.54	0.1486	0.3507	-0.1524	-0.0400	-0.0440	-0.0399
03	85.1	-0.02	0.1405	0.3414	-0.0001	-0.0387	0.0034	-0.0031
04	85.1	1.51	0.1507	0.3407	0.1457	-0.0389	0.0515	0.0282
05	85.3	3.05	0.1855	0.3435	0.2791	-0.0449	0.1086	0.0599
06	85.3	6.10	0.2925	0.3457	0.5358	-0.0519	0.2305	0.1174
07	84.8	9.17	0.3501	0.3810	0.8358	-0.0554	0.3391	0.1914
08	83.5	12.23	0.6001	0.4058	1.1495	-0.0568	0.4451	0.2450

Bus speed(mi/h)

35.00
45.00
55.00
65.00
75.00

Wind Averaged CD

0.384
0.365
0.354
0.348
0.346

BUS TEST

Rept/Tare/Run 0607/062/063

PREVOST FRONT, GRIT, PREVOST MIRRORS, STD DRIP RAILS, STD REAR

ATM PRESS= 101.2 KPA TEMP= 26.52 C Density= 1.176 Kg/m3
 Ref length=0.7225 m Ref Area= 0.08358 m2 QC= 4.29 Kpa
 Re= 1.4079 Million

PT	VEL (m/s)	YAW (deg)	CL	CD	CY	CM	CN	CR
01	85.4	-3.07	-0.0520	0.3880	-0.2750	0.0193	-0.1006	-0.0690
02	85.3	-1.55	-0.0793	0.3830	-0.1305	0.0287	-0.0501	-0.0388
03	85.3	-0.02	-0.0904	0.3837	0.0135	0.0314	0.0012	-0.0036
04	85.2	1.51	-0.0694	0.3793	0.1521	0.0272	0.0510	0.0274
05	85.1	3.05	-0.0410	0.3885	0.2927	0.0158	0.1023	0.0638
06	84.8	6.11	-0.0459	0.4666	0.6021	0.0323	0.2005	0.1409
07	83.4	9.18	0.1694	0.5467	0.9277	0.0429	0.2894	0.2208
08	81.4	12.24	0.4097	0.6826	1.2856	0.0376	0.3228	0.3103

Bus speed(mi/h)

35.00
45.00
55.00
65.00
75.00

Wind Averaged CD

0.537
0.476
0.447
0.428
0.415

BUS TEST

Rept/Tare/Run 0607/064/065

PREVDST FRONT, CRIT, STD DRIP RAILS, STD REAR

ATH PRESS= 101.2 KPA TEMP= 23.26 C Density= 1.189 Kg/m3
 Ref length=0.7225 m Ref Area= 0.08358 m2 GC= 4.27 Kpa
 Re= 1.4247 Million

PT	VEL (m/s)	YAW (deg)	CL	CD	CY	CM	CN	CR
01	84.8	-3.07	-0.0533	0.3641	-0.2675	0.0151	-0.0784	-0.0656
02	84.7	-1.53	-0.0778	0.3556	-0.1237	0.0180	-0.0515	-0.0358
03	84.5	-0.02	-0.0869	0.3529	0.0124	0.0201	-0.0014	-0.0024
04	84.6	1.51	-0.0677	0.3510	0.1522	0.0161	0.0500	0.0284
05	84.7	3.05	-0.0414	0.3643	0.2967	0.0100	0.1004	0.0653
06	84.2	6.11	0.0415	0.4346	0.6006	0.0211	0.2003	0.1397
07	82.8	9.18	0.1751	0.5290	0.9231	0.0367	0.2867	0.2183
08	80.8	12.24	0.4110	0.6654	1.2960	0.0260	0.3163	0.3084

Bus speed(mi/h)

35.00
45.00
55.00
65.00
75.00

Wind Averaged CD

0.513
0.450
0.418
0.399
0.386

BUS TEST

Rept/Tare/Run 0607/064/066

PREVDST FRONT, CRIT, STD DRIP RAILS, STD REAR

ATH PRESS= 101.2 KPA TEMP= 24.05 C Density= 1.185 Kg/m3
 Ref length=0.7225 m Ref Area= 0.08358 m2 GC= 1.46 Kpa
 Re= 0.8312 Million

PT	VEL (m/s)	YAW (deg)	CL	CD	CY	CM	CN	CR
01	49.7	-0.03	-0.1197	0.4146	0.0109	0.0357	-0.0087	-0.0055
02	56.9	-0.03	-0.1043	0.3656	0.0214	0.0260	-0.0010	-0.0006
03	63.0	-0.03	-0.1003	0.3573	0.0224	0.0197	-0.0008	-0.0007
04	68.1	-0.03	-0.0966	0.3550	0.0226	0.0205	-0.0001	0.0001
05	76.6	-0.03	-0.0712	0.3502	0.0167	0.0213	-0.0003	-0.0015
06	82.7	-0.03	-0.0579	0.3505	0.0126	0.0200	-0.0014	-0.0020
07	88.6	-0.03	-0.0841	0.3544	0.0122	0.0221	-0.0017	-0.0026
08	94.3	-0.03	-0.0788	0.3517	0.0089	0.0219	-0.0026	-0.0019

Bus speed(mi/h)

35.00
45.00
55.00
65.00
75.00

Wind Averaged CD

0.000
0.000
0.000
0.000
0.000

BUS TEST

Rept/Tare/Run 0607/067/068

PROP #1 FRONT, CRIT, STD DRIP RAILS, C3 STD REAR

ATH PRESS= 101.5 KPA TEMP= 22.26 C Density= 1.196 Kg/m3
 Ref length=0.7225 m Ref Area= 0.08358 m2 GC= 1.48 Kpa
 Re= 0.8420 Million

PT	VEL (m/s)	YAW (deg)	CL	CD	CY	CM	CN	CR
01	49.7	-0.02	-0.0712	0.3573	0.0153	0.0802	0.0035	-0.0063
02	55.9	-0.02	-0.0714	0.3541	0.0164	0.0759	0.0037	-0.0037
03	62.2	-0.02	-0.0683	0.3485	0.0179	0.0720	0.0048	-0.0030
04	68.5	-0.02	-0.0640	0.3490	0.0176	0.0701	0.0053	-0.0030
05	76.6	-0.02	-0.0587	0.3473	0.0139	0.0694	0.0048	-0.0025
06	80.8	-0.02	-0.0549	0.3451	0.0139	0.0693	0.0045	-0.0027
07	87.5	-0.02	-0.0503	0.3467	0.0098	0.0724	0.0033	-0.0032
08	94.4	-0.02	-0.0451	0.3437	0.0073	0.0730	0.0024	-0.0037

Bus speed(mi/h)

35.00
45.00
55.00
65.00
75.00

Wind Averaged CD

0.000
0.000
0.000
0.000
0.000

BUS TEST

Rept/Tare/Run 0607/067/069

PROP #1 FRONT, CRIT, STD DRIP RAILS, C3 STD REAR

ATH PRESS= 101.5 KPA TEMP= 27.37 C Density= 1.176 Kg/m3
 Ref length=0.7225 m Ref Area= 0.08358 m2 GC= 4.24 Kpa
 Re= 1.3966 Million

PT	VEL (m/s)	YAW (deg)	CL	CD	CY	CM	CN	CR
01	84.9	-3.08	-0.0125	0.3541	-0.2810	0.0618	-0.0932	-0.0694
02	84.9	-1.55	-0.0462	0.3478	-0.1316	0.0699	-0.0464	-0.0379
03	84.9	-0.02	-0.0508	0.3431	0.0106	0.0707	0.0039	-0.0039
04	84.7	1.51	-0.0446	0.3496	0.1541	0.0718	0.0527	0.0278
05	84.7	3.05	0.0020	0.3563	0.3039	0.0640	0.1039	0.0657
06	84.6	6.11	0.1017	0.3645	0.5955	0.0510	0.2066	0.1350
07	83.8	9.18	0.2274	0.3844	0.9115	0.0502	0.3079	0.2103
08	82.5	12.25	0.4086	0.3942	1.2508	0.0376	0.4074	0.2893

Bus speed(mi/h)

35.00
45.00
55.00
65.00
75.00

Wind Averaged CD

0.389
0.376
0.367
0.362
0.360

BUS TEST

Rept/Tare/Run 0607/070/071

C3 SMOOTH FRONT, GRIT, STD DRIP RAILS, C3 STD REAR

ATM PRESS= 101.5 KPa TEMP= 23.07 C Density= 1.193 Kg/m3
 Ref length=0.7225 m Ref Area= 0.08358 m2 GC= 1.50 Kpa
 Rev= 0.8446 Million

PT	VEL (m/s)	YAW (deg)	CL	CD	CY	CM	CN	CR
01	30.1	-0.02	-0.0729	0.2672	0.0176	0.0477	0.0061	-0.0047
02	33.4	-0.02	-0.0737	0.3617	0.0182	0.0424	0.0059	-0.0031
03	42.3	-0.02	-0.0727	0.3548	0.0207	0.0414	0.0070	-0.0022
04	46.3	-0.02	-0.0707	0.3555	0.0197	0.0428	0.0066	-0.0022
05	75.2	-0.02	-0.0670	0.3536	0.0160	0.0456	0.0054	-0.0026
06	80.9	-0.02	-0.0645	0.3492	0.0144	0.0464	0.0055	-0.0034
07	87.5	-0.02	-0.0613	0.3508	0.0098	0.0487	0.0039	-0.0043
08	94.3	-0.02	-0.0555	0.3474	0.0058	0.0491	0.0043	-0.0041

Bus speed(mi/h)

Wind Averaged CD

35.00
45.00
55.00
65.00
75.00

0.000
0.000
0.000
0.000
0.000

BUS TEST

Rept/Tare/Run 0607/070/072

C3 SMOOTH FRONT, GRIT, STD DRIP RAILS, C3 STD REAR

ATM PRESS= 101.5 KPa TEMP= 28.09 C Density= 1.173 Kg/m3
 Ref length=0.7225 m Ref Area= 0.08358 m2 GC= 4.23 Kpa
 Rev= 1.3901 Million

PT	VEL (m/s)	YAW (deg)	CL	CD	CY	CM	CN	CR
01	84.9	-3.07	-0.0260	0.3543	-0.2675	0.0380	-0.0886	-0.0668
02	84.9	-1.55	-0.0510	0.3500	-0.1266	0.0451	-0.0422	-0.0385
03	84.7	-0.03	-0.0613	0.3491	0.0097	0.0482	0.0052	-0.0044
04	85.0	1.50	-0.0584	0.3576	0.1469	0.0477	0.0496	0.0265
05	85.3	3.05	-0.0832	0.3623	0.2918	0.0328	0.0997	0.0626
06	84.5	6.11	0.0724	0.3817	0.5931	0.0251	0.1961	0.1339
07	84.2	9.18	0.2040	0.4040	0.9082	0.0311	0.2935	0.2064
08	83.5	12.24	0.3892	0.4298	1.2358	0.0254	0.3825	0.2848

Bus speed(mi/h)

Wind Averaged CD

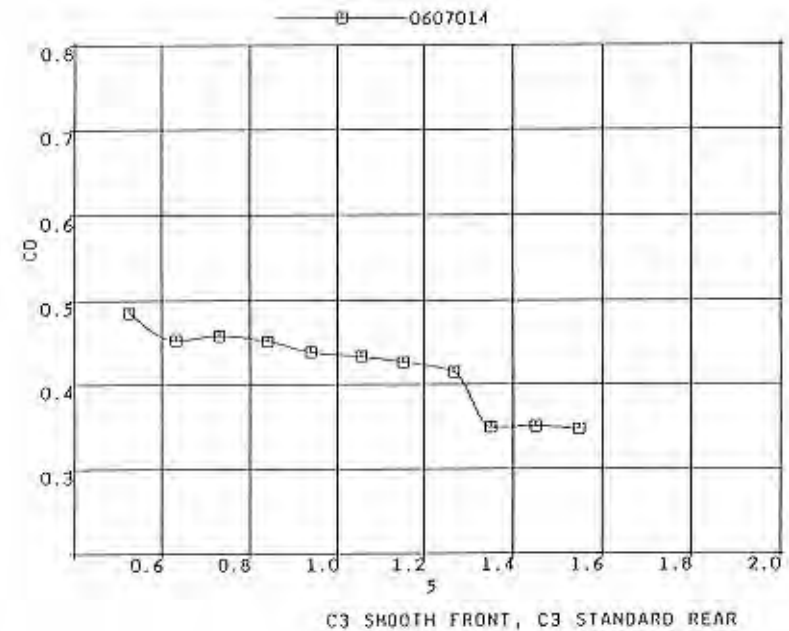
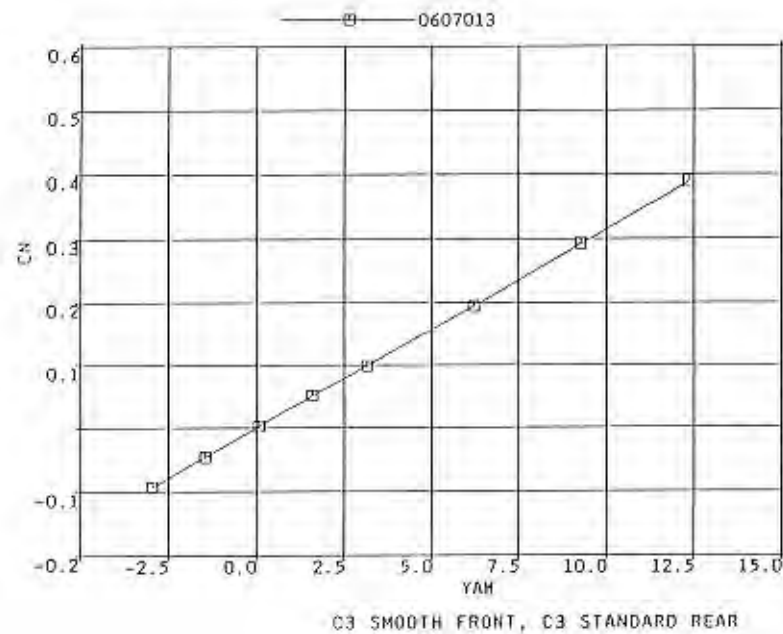
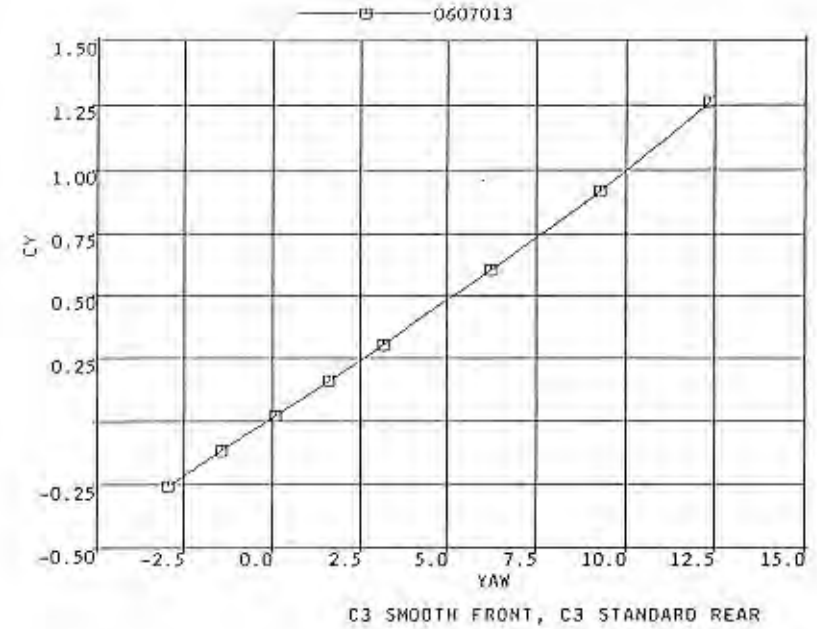
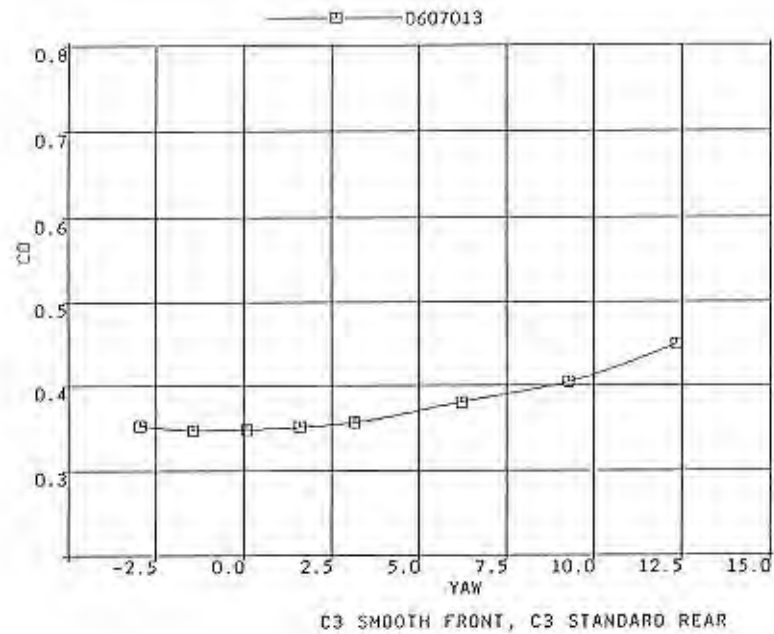
35.00
45.00
55.00
65.00
75.00

0.408
0.390
0.380
0.374
0.370

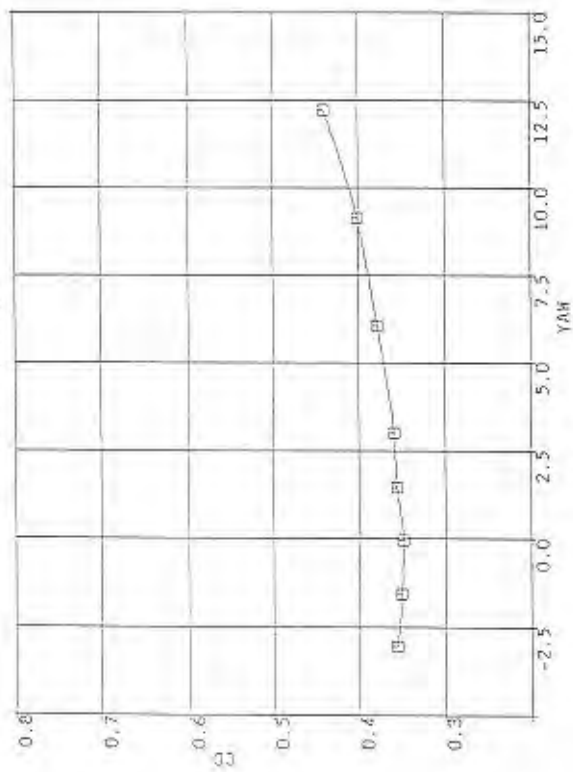
APPENDIX 4: DATA PLOTS

The following plots are presented in the order performed. Each yaw run is summarized by plots of drag coefficient, side force coefficient, and yawing moment coefficient, all versus yaw angle. The run designations are coded in the set of 7 numbers at the top of each plot and they are interpreted as a first group of four digits for the test number followed by three digits for the run number. Thus:

060702 = Test 607, Run 26

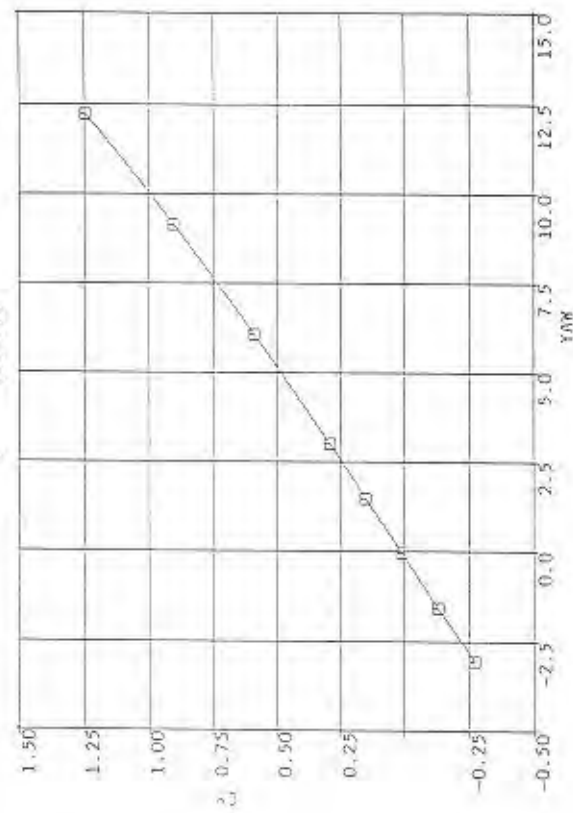


0607016



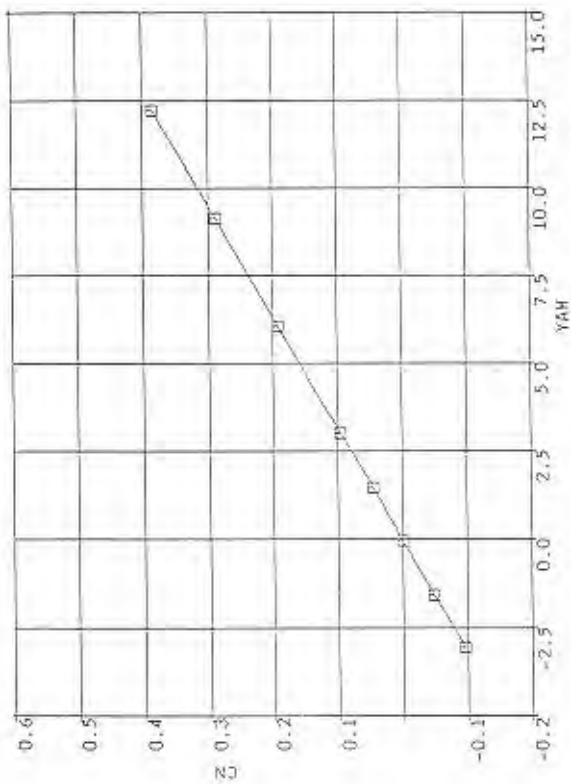
C3 SMOOTH FRONT, C3 STANDARD REAR

0607016



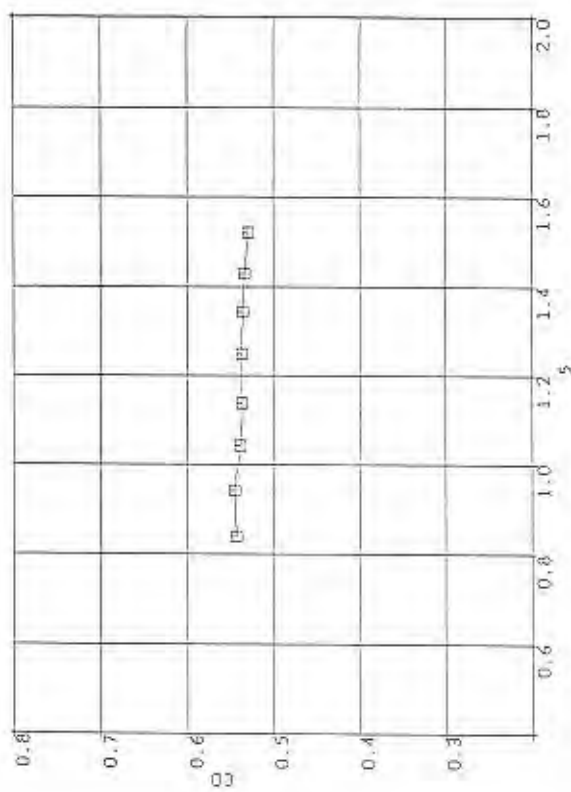
C3 SMOOTH FRONT, C3 STANDARD REAR

0607016

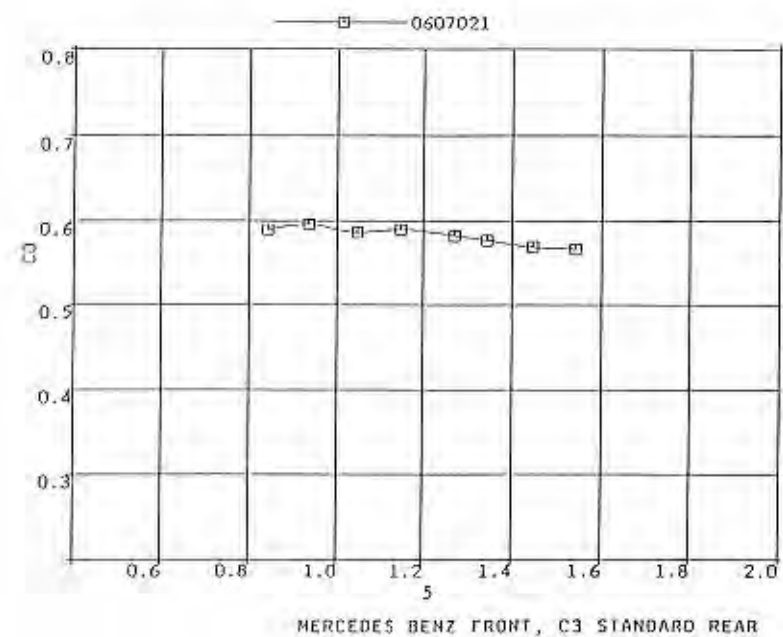
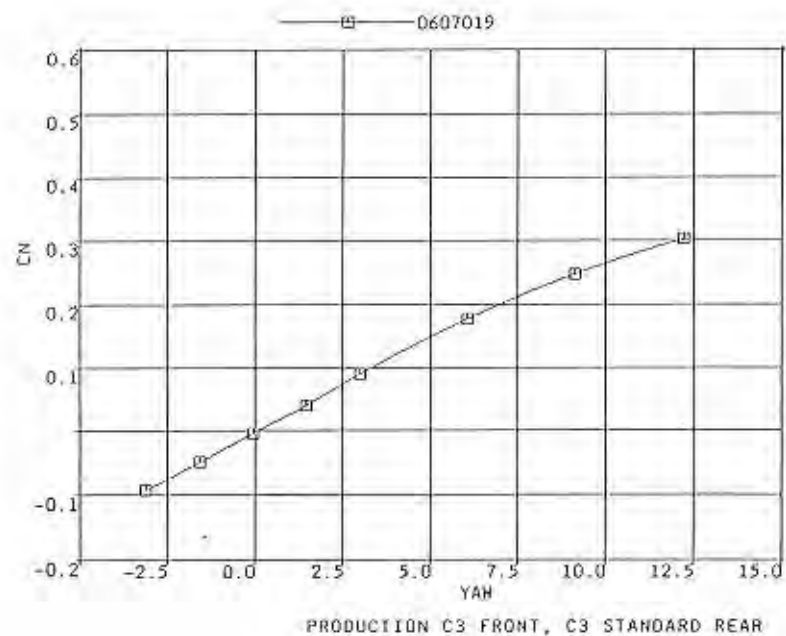
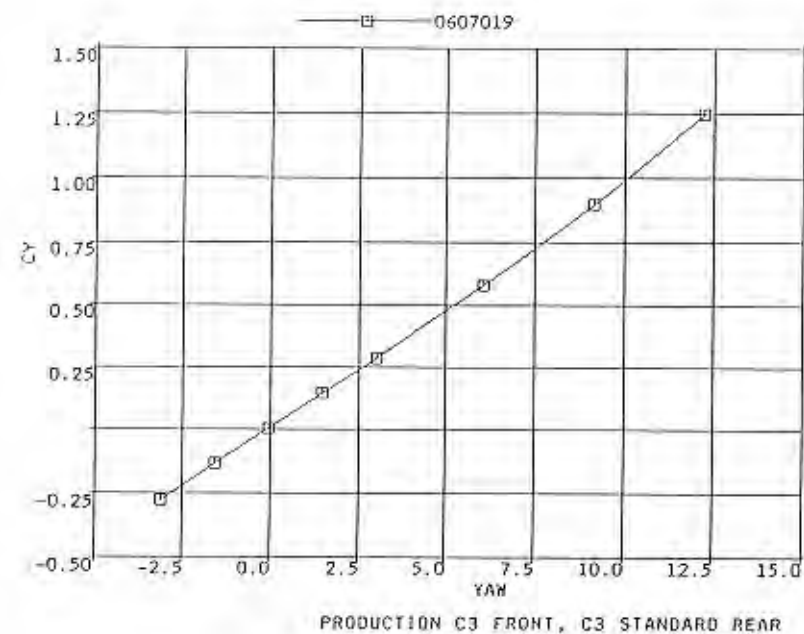
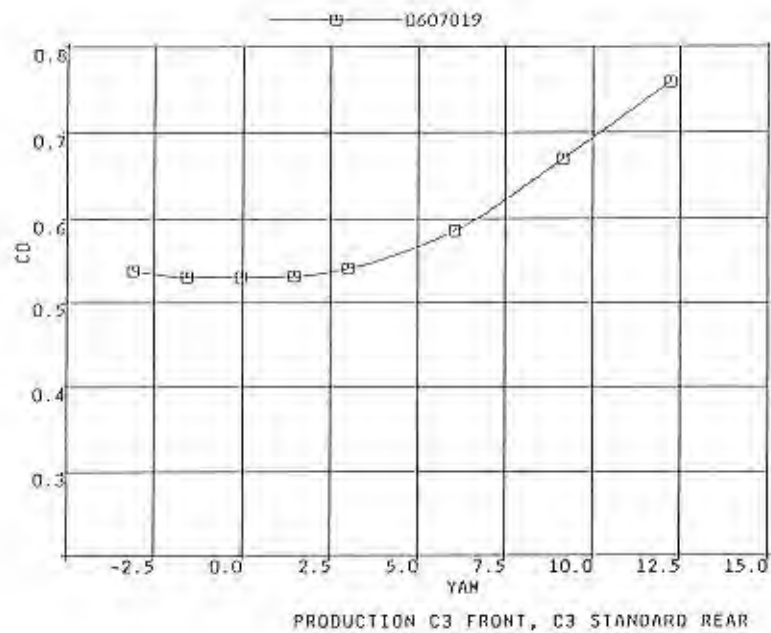


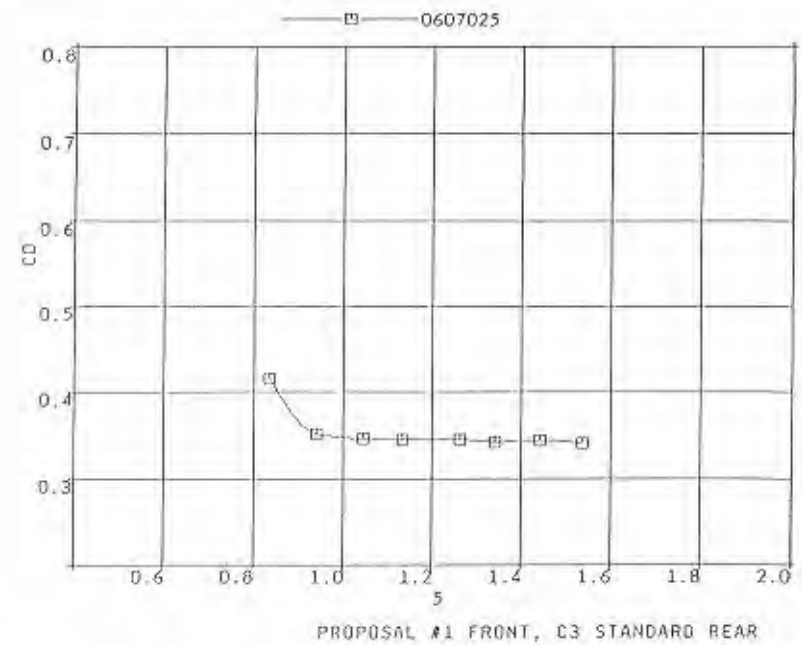
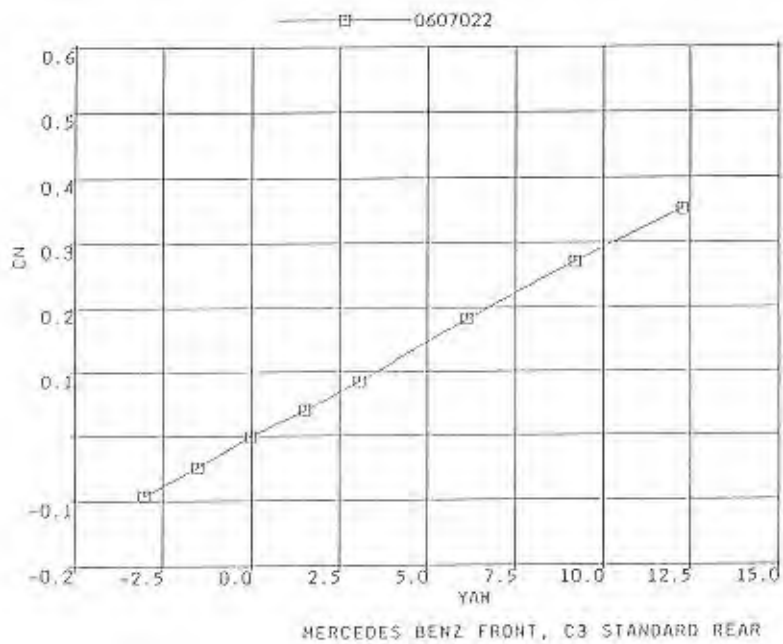
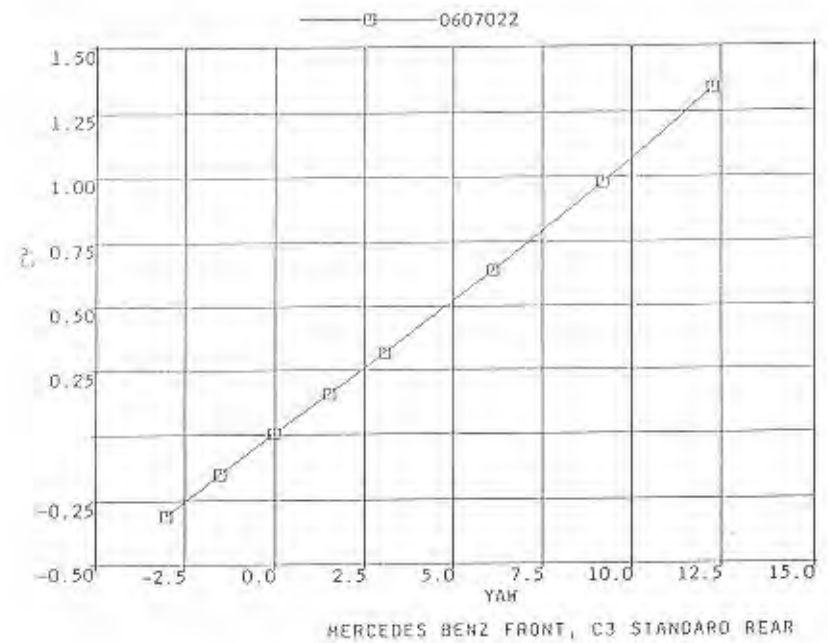
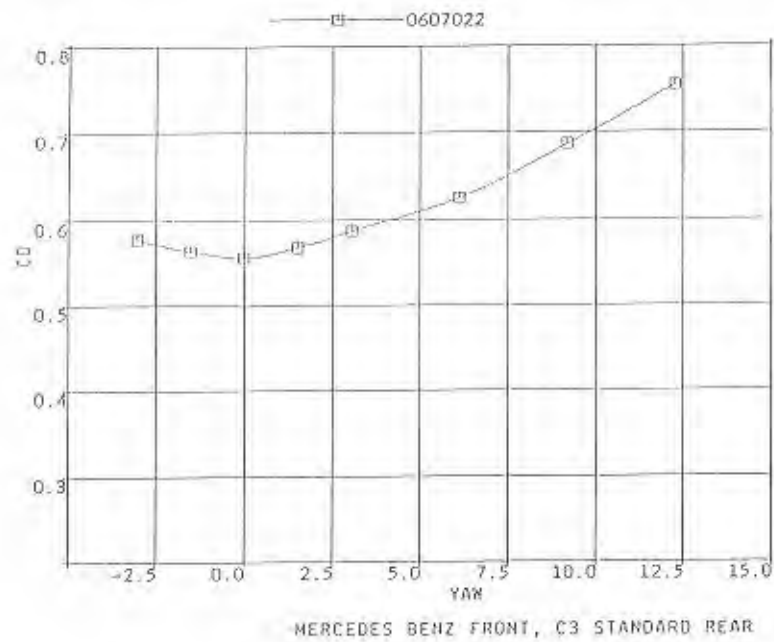
C3 SMOOTH FRONT, C3 STANDARD REAR

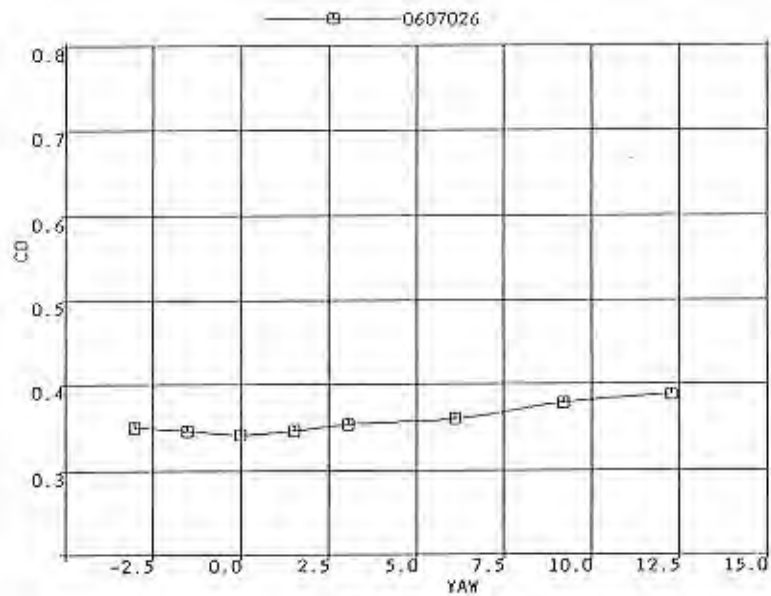
0607018



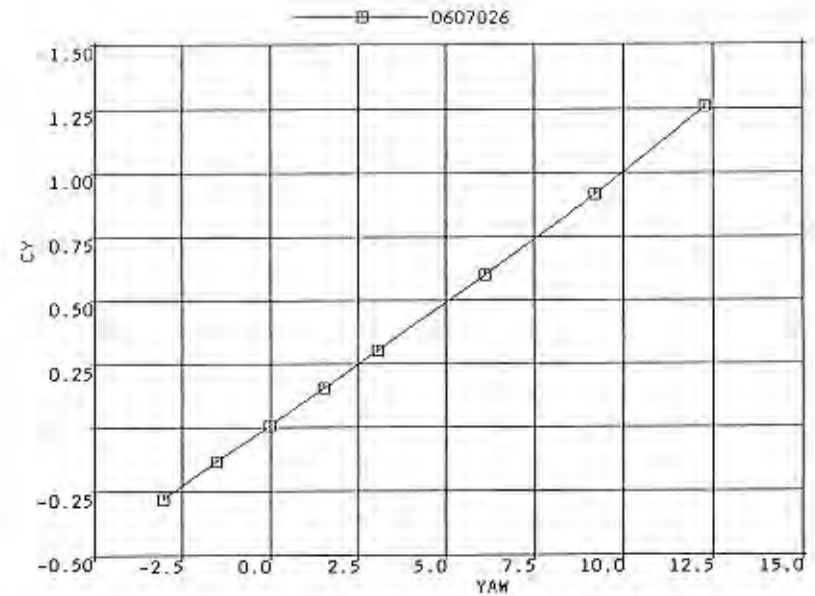
PRODUCTION C3 FRONT, C3 STANDARD REAR



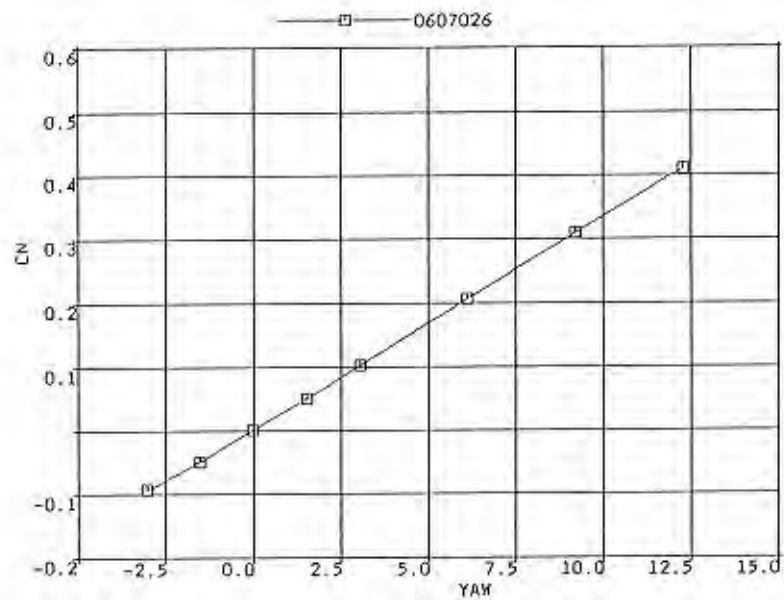




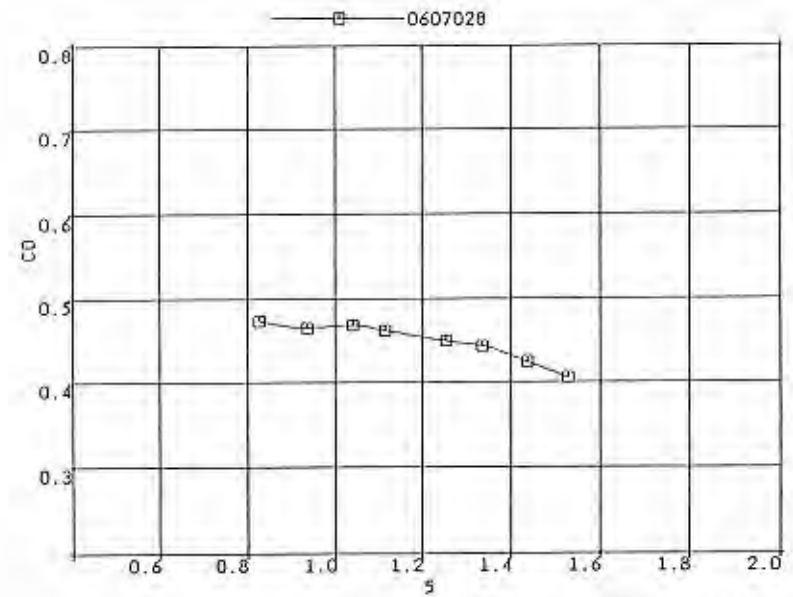
PROPOSAL #1 FRONT, C3 STANDARD REAR



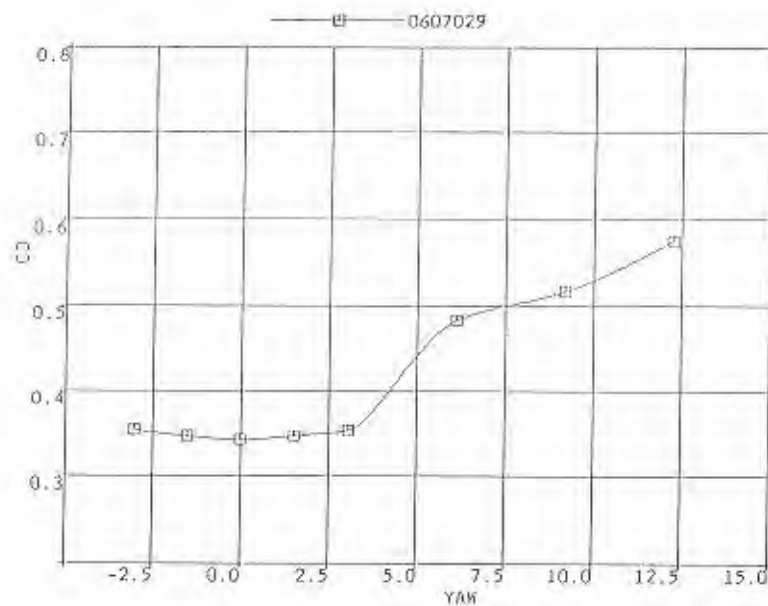
PROPOSAL #1 FRONT, C3 STANDARD REAR



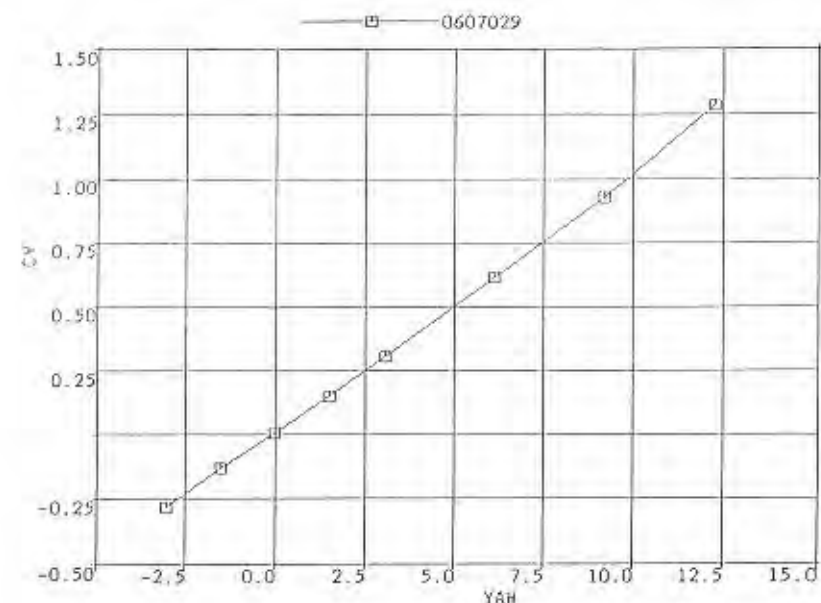
PROPOSAL #1 FRONT, C3 STANDARD REAR



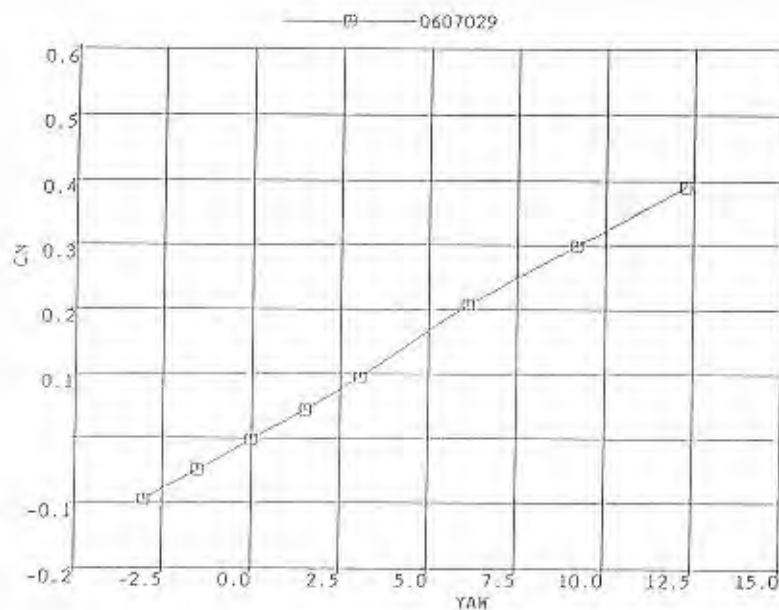
PROPOSAL #2 FRONT, C3 STANDARD REAR



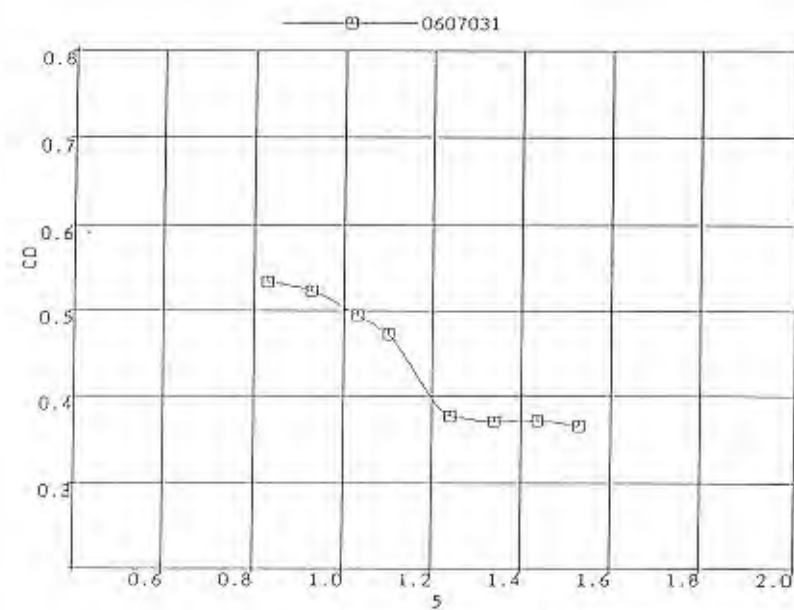
PROPOSAL #2 FRONT, C3 STANDARD REAR



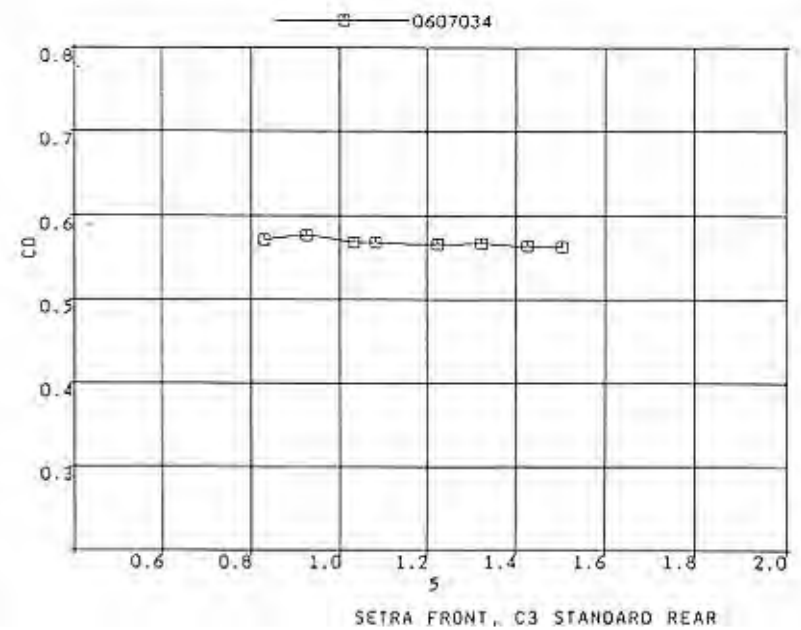
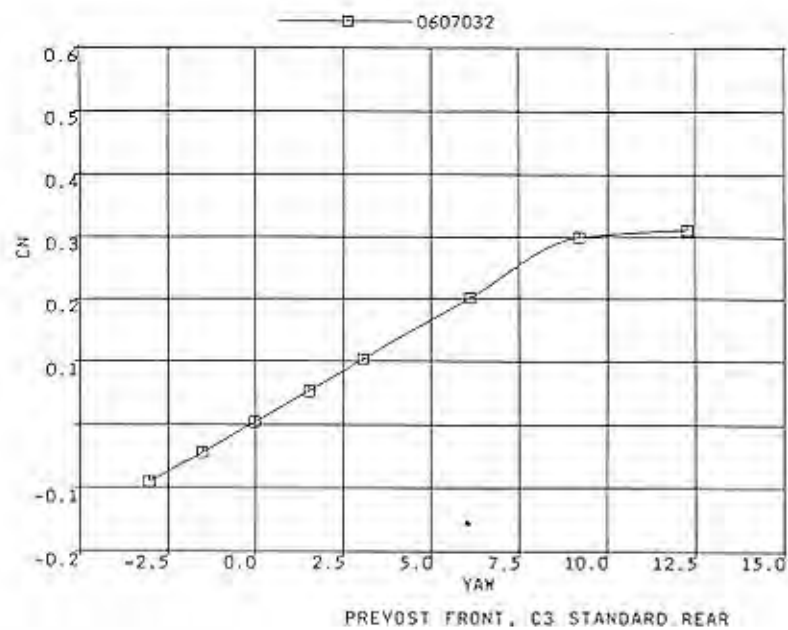
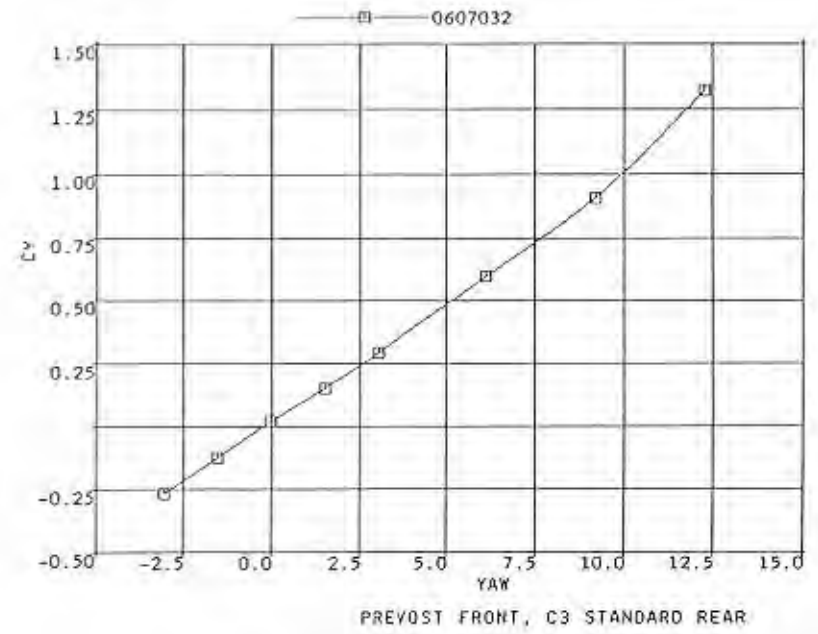
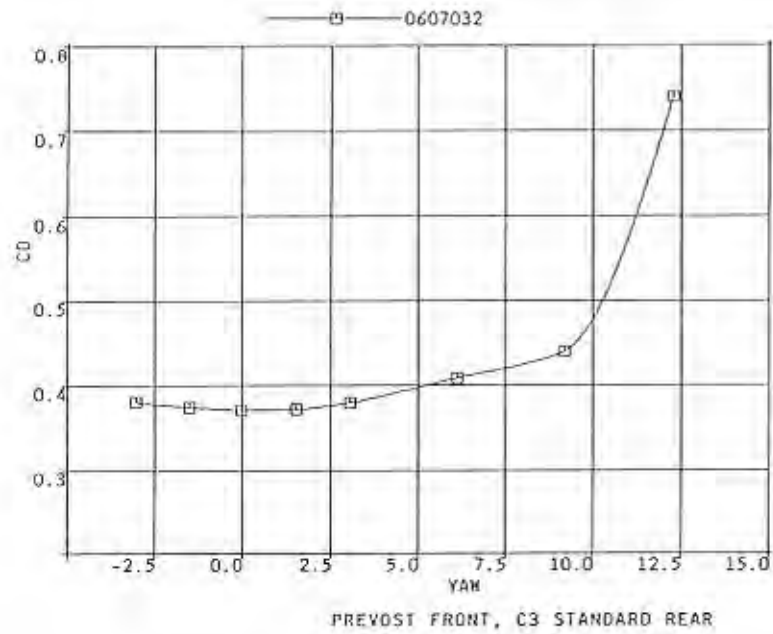
PROPOSAL #2 FRONT, C3 STANDARD REAR

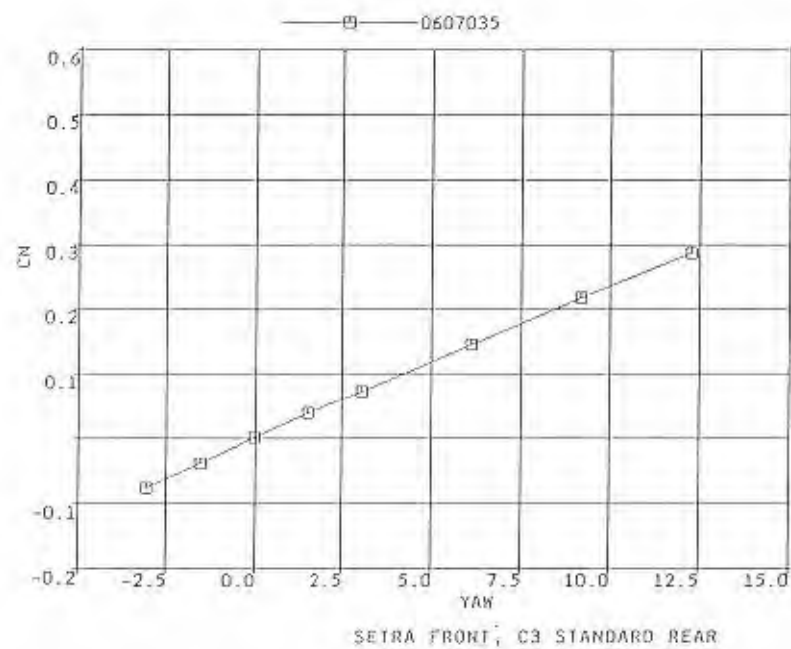
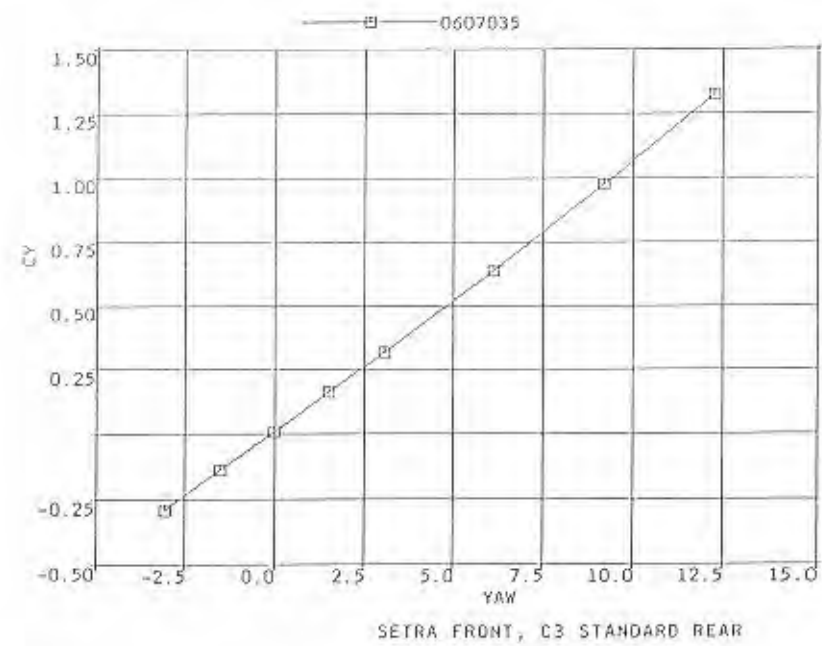
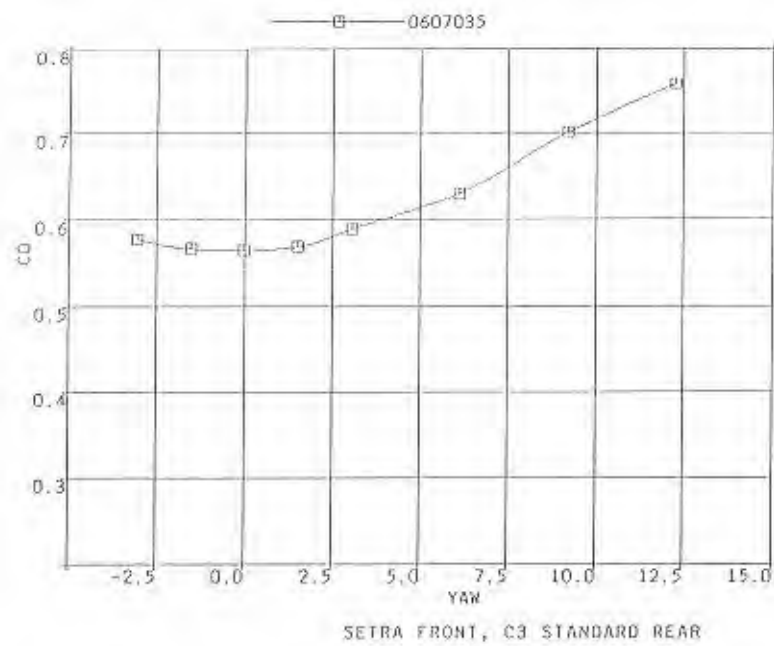


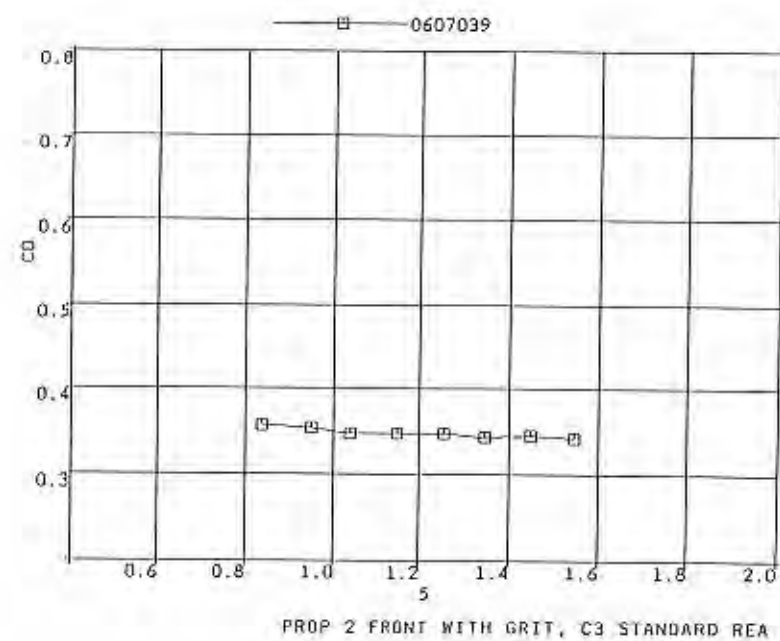
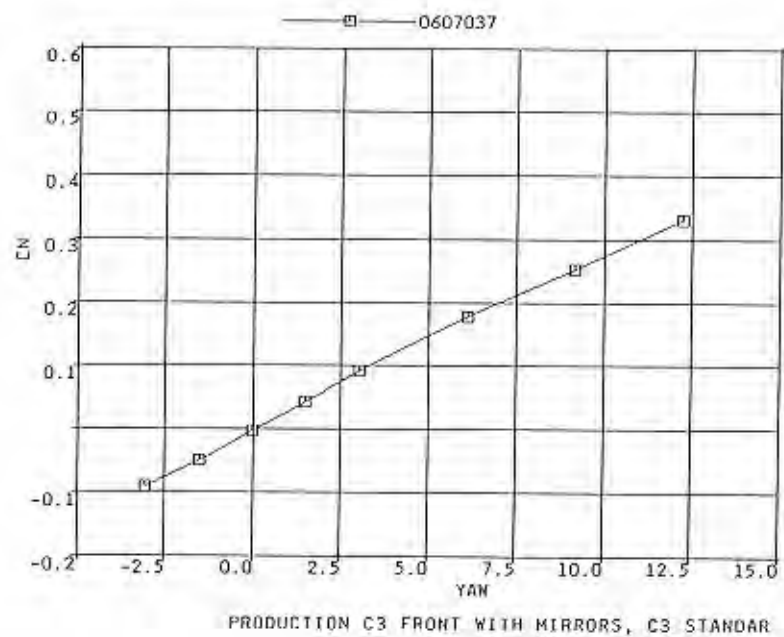
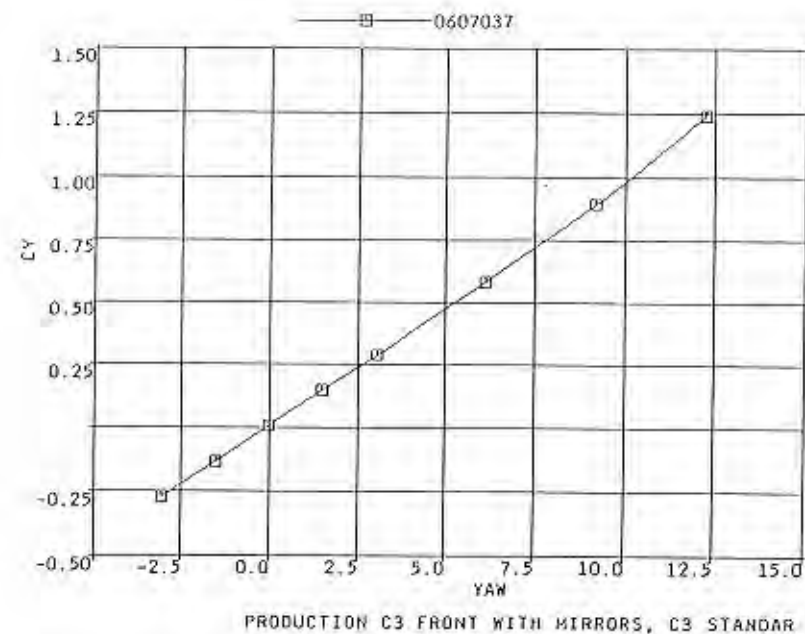
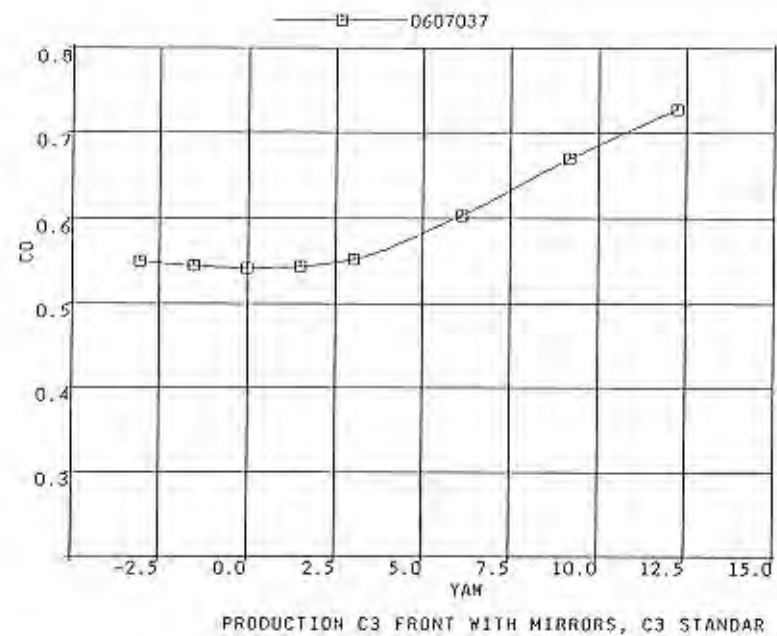
PROPOSAL #2 FRONT, C3 STANDARD REAR

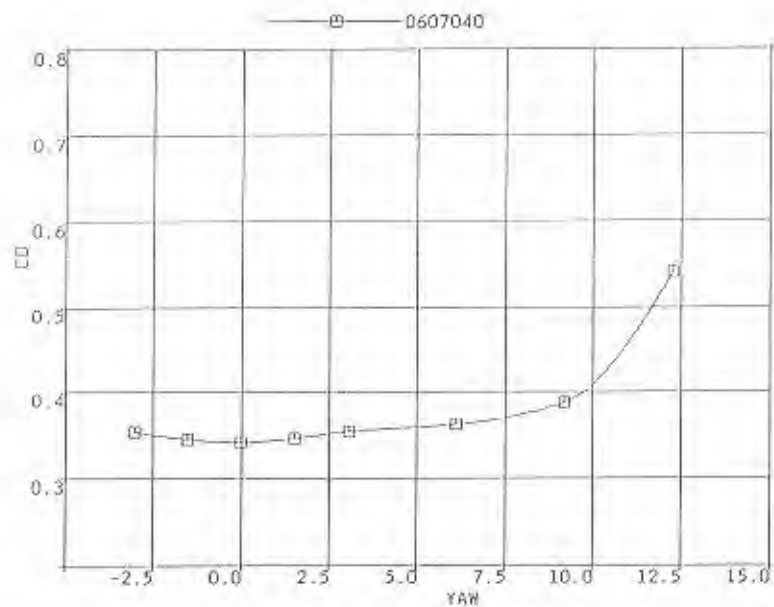


PREVOST FRONT, C3 STANDARD REAR

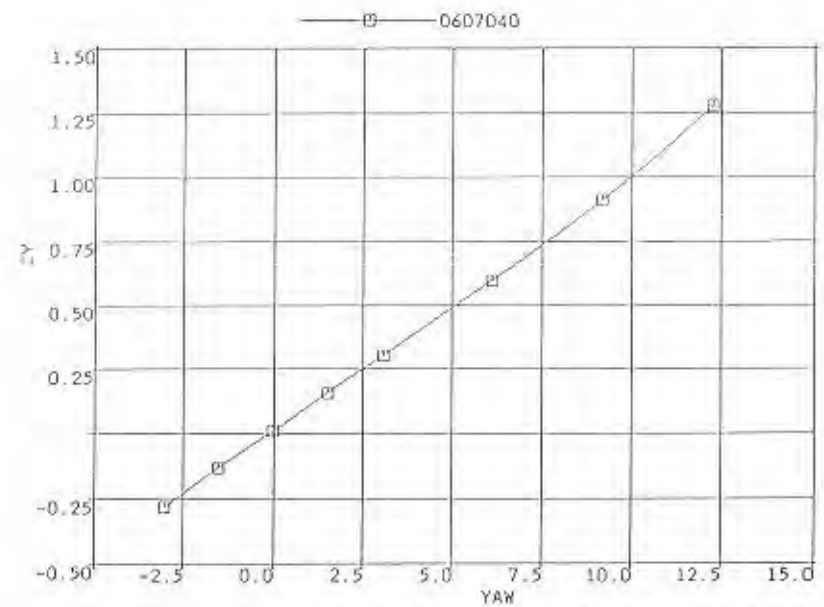




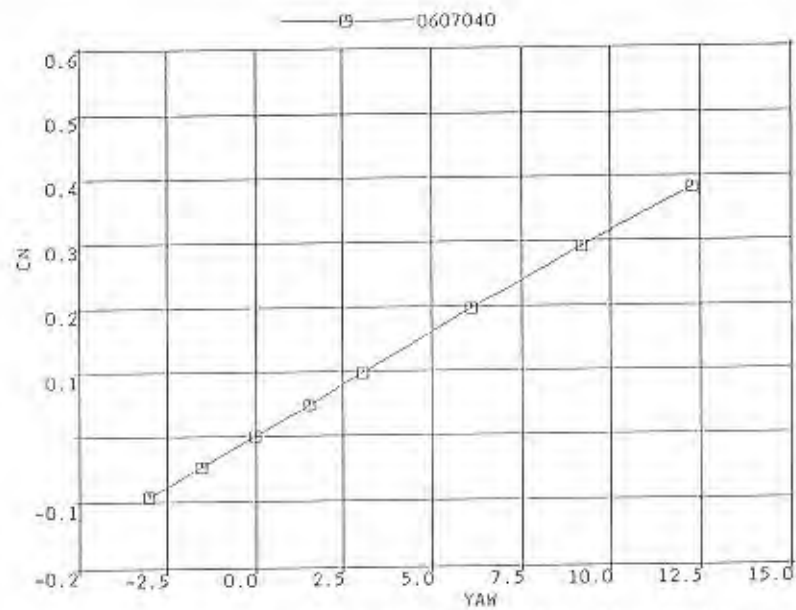




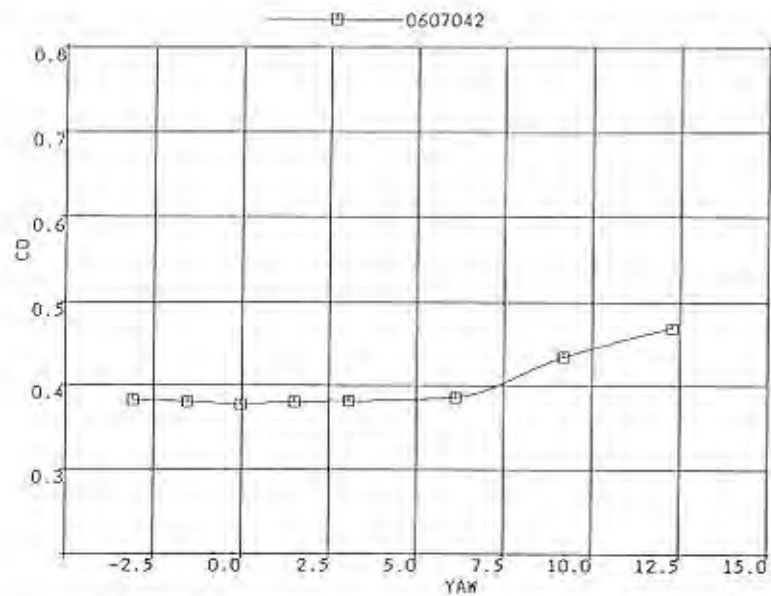
PROP 2 FRONT WITH GRIT, C3 STANDARD REA



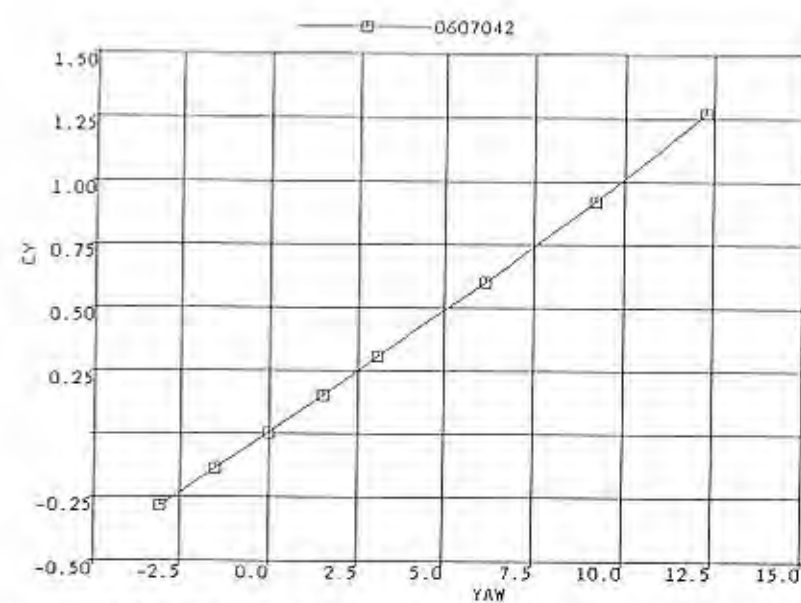
PROP 2 FRONT WITH GRIT, C3 STANDARD REA



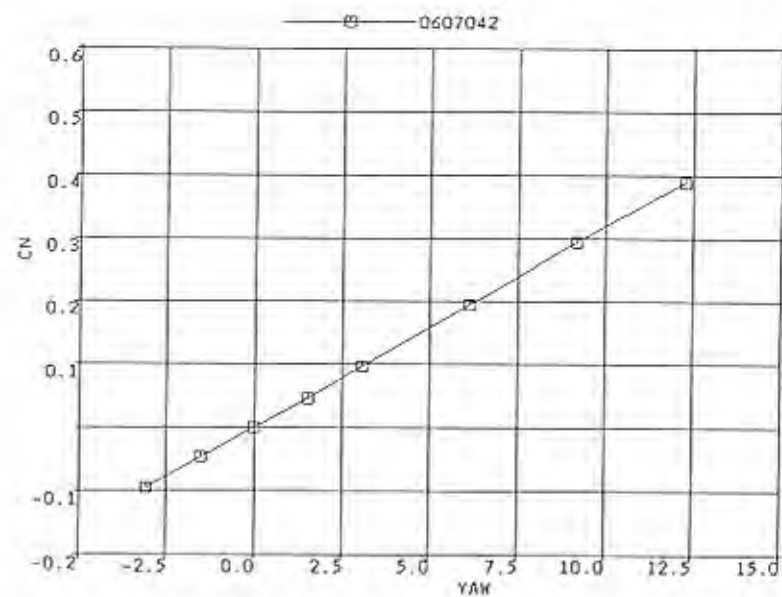
PROP 2 FRONT WITH GRIT, C3 STANDARD REA



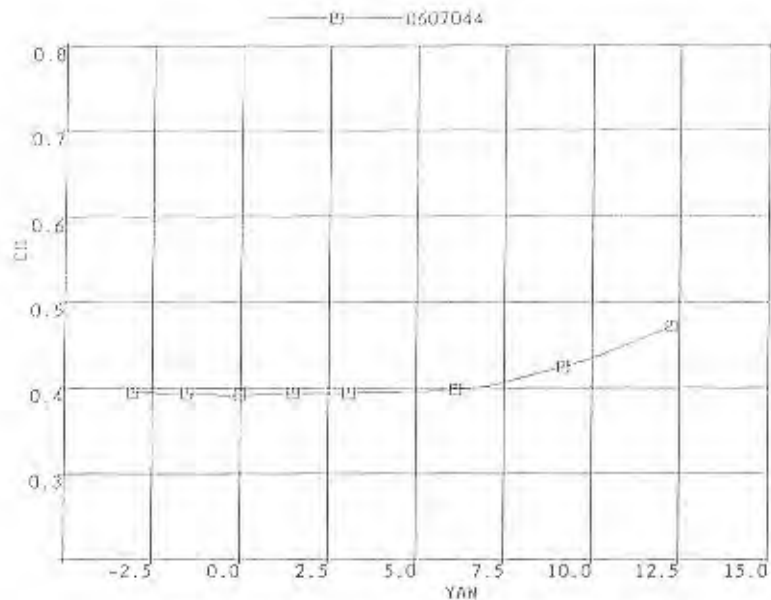
PROP 2 FRONT WITH GRIT AND C3 MIRRORS FWD, C3 STANDARD REA



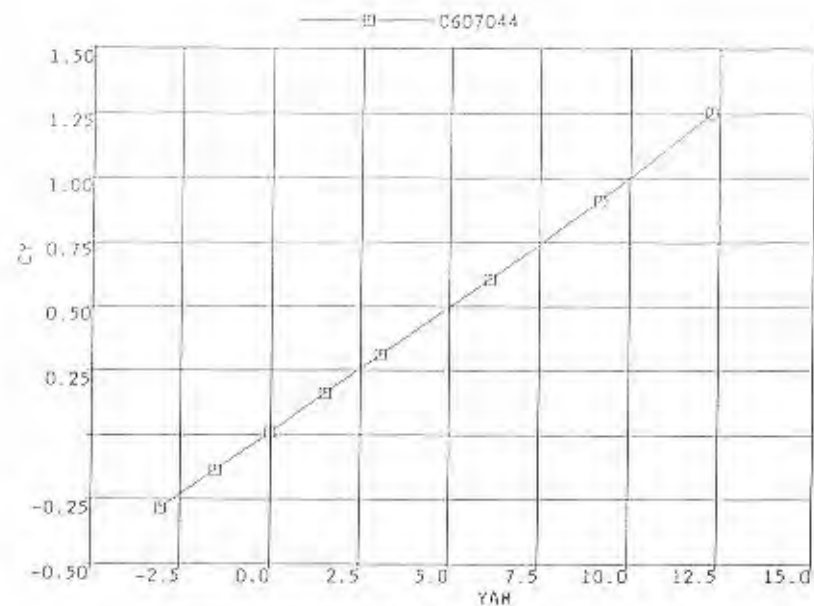
PROP 2 FRONT WITH GRIT AND C3 MIRRORS FWD, C3 STANDARD REA



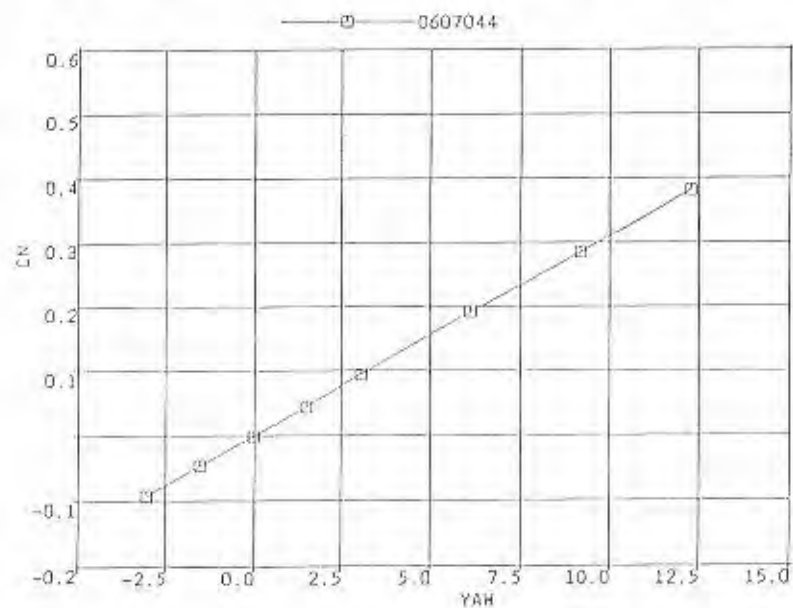
PROP 2 FRONT WITH GRIT AND C3 MIRRORS FWD, C3 STANDARD REA



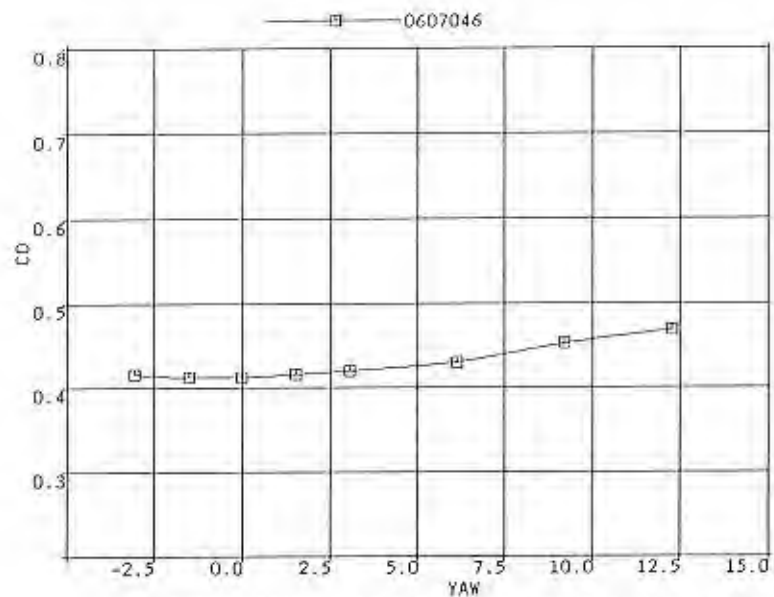
PROP 2 FRONT WITH GRIT AND C3 MIRRORS AFT, C3 STA



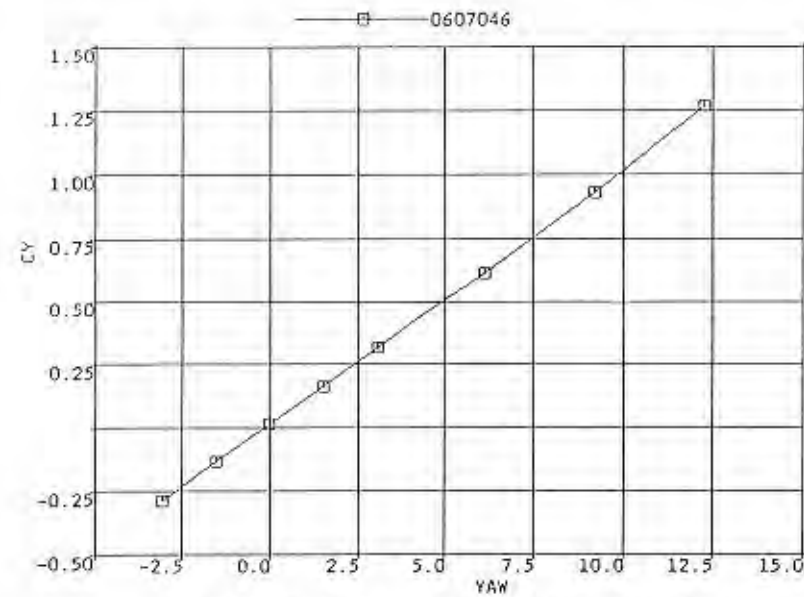
PROP 2 FRONT WITH GRIT AND C3 MIRRORS AFT, C3 STA



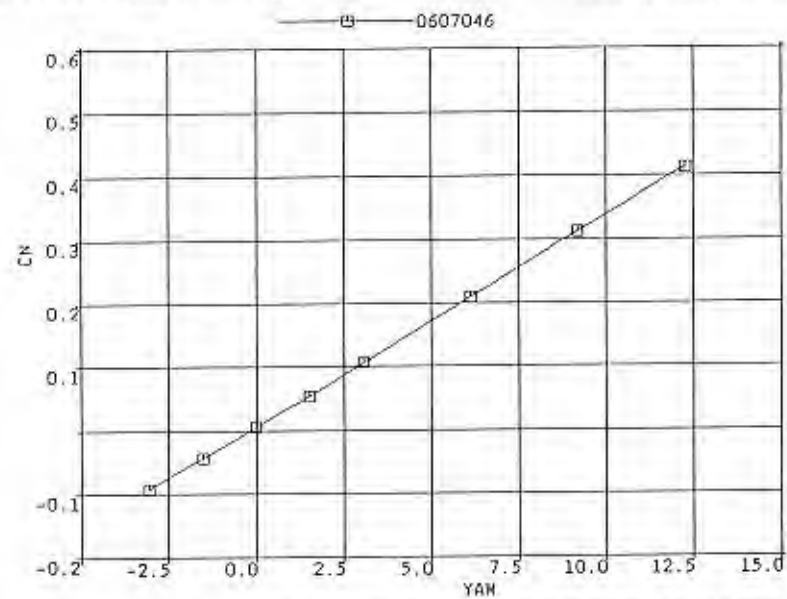
PROP 2 FRONT WITH GRIT AND C3 MIRRORS AFT, C3 STA



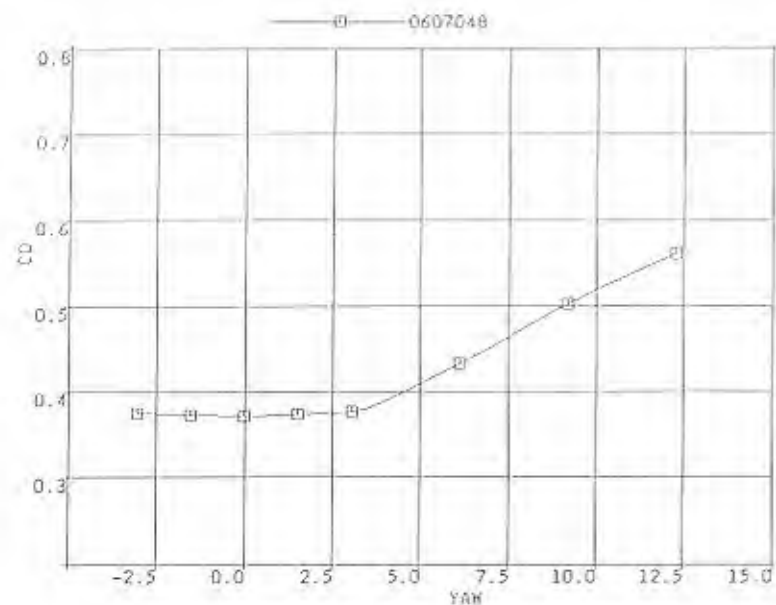
PROP 2 FRONT WITH GRIT AND CETRA MIRRORS, C3 STA



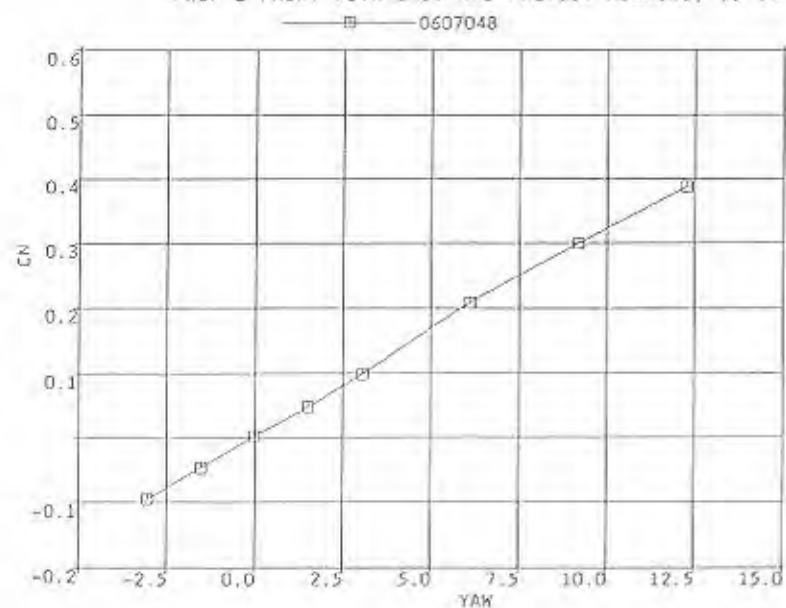
PROP 2 FRONT WITH GRIT AND CETRA MIRRORS, C3 STA



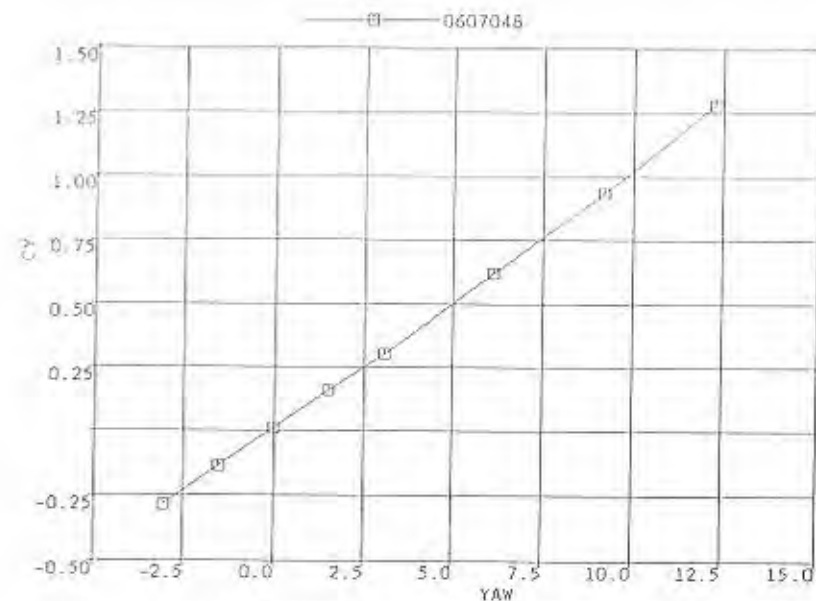
PROP 2 FRONT WITH GRIT AND CETRA MIRRORS, C3 STA



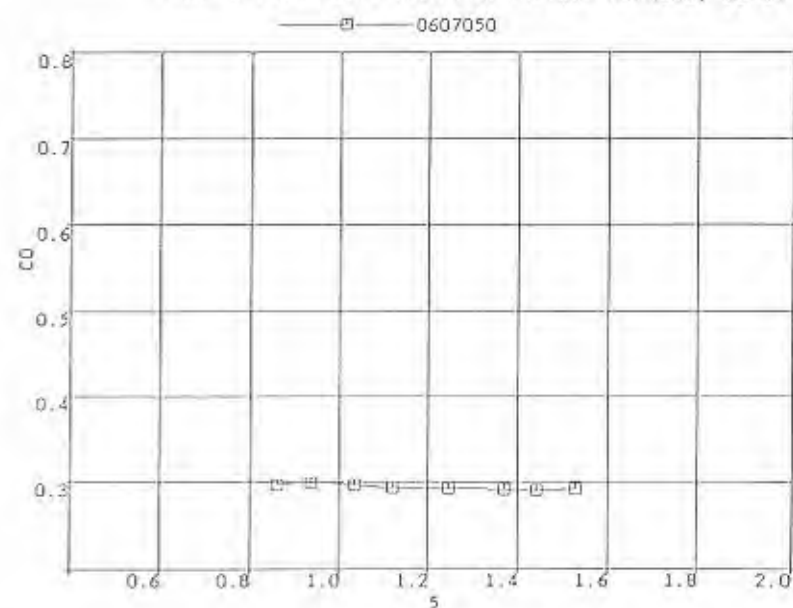
PROP 2 FRONT WITH GRIT AND PREVOST MIRRORS, C3 ST



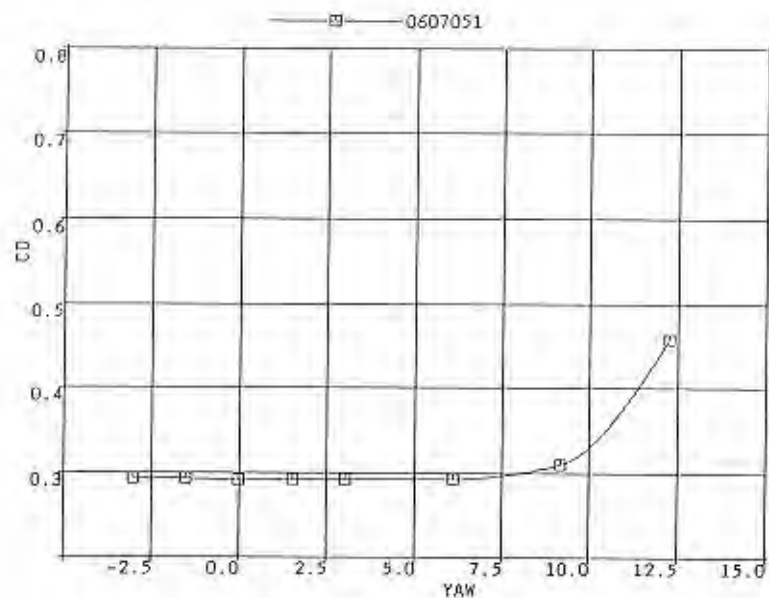
PROP 2 FRONT WITH GRIT AND PREVOST MIRRORS, C3 ST



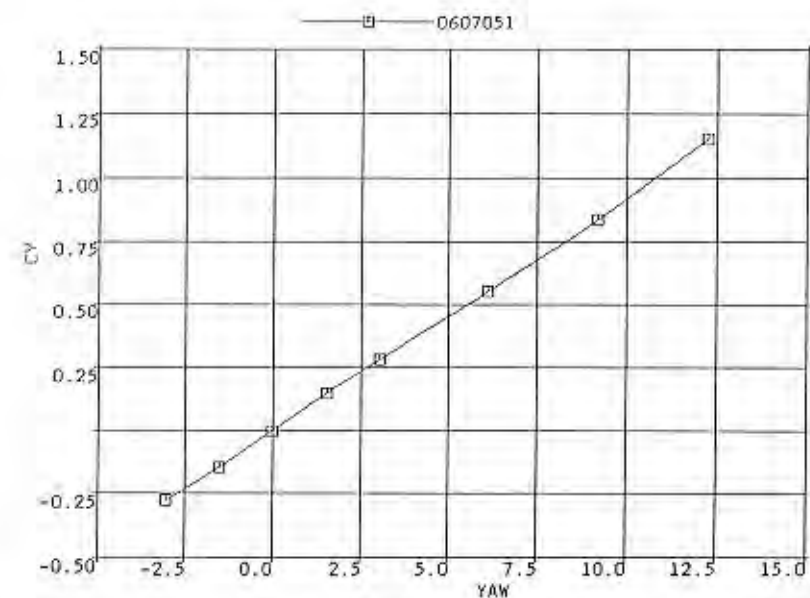
PROP 2 FRONT WITH GRIT AND PREVOST MIRRORS, C3 ST



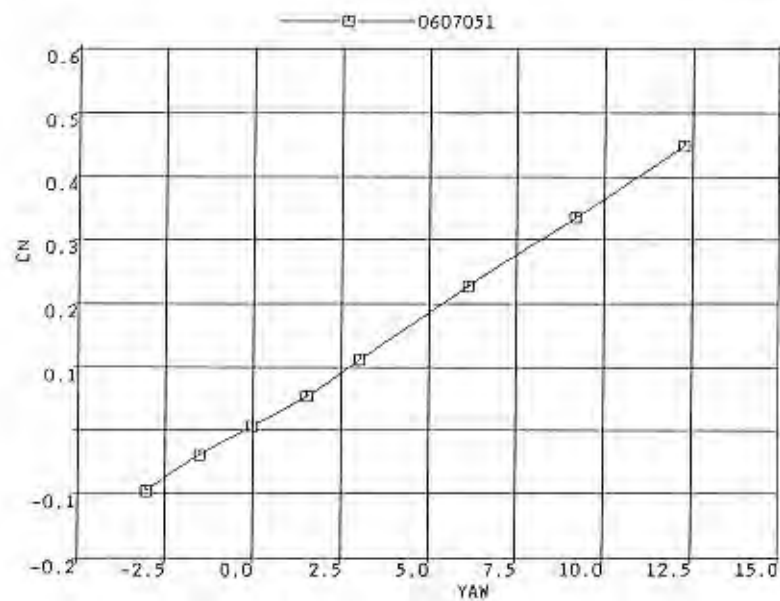
PROP 2 FRONT WITH GRIT, REAR 15



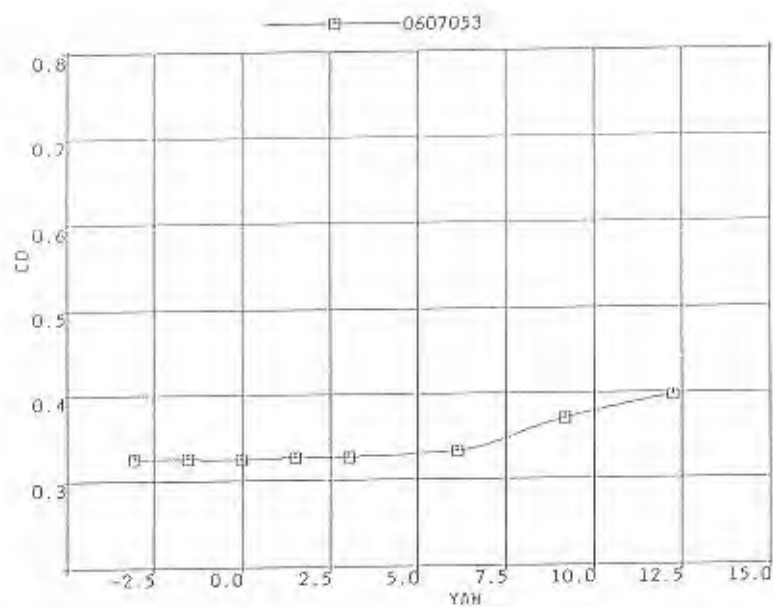
PROP 2 FRONT WITH GRIT, REAR 15



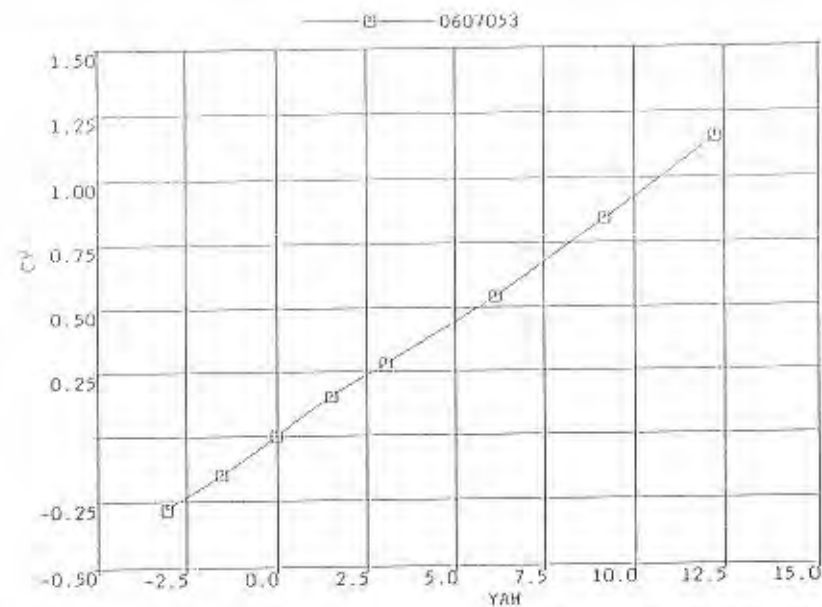
PROP 2 FRONT WITH GRIT, REAR 15



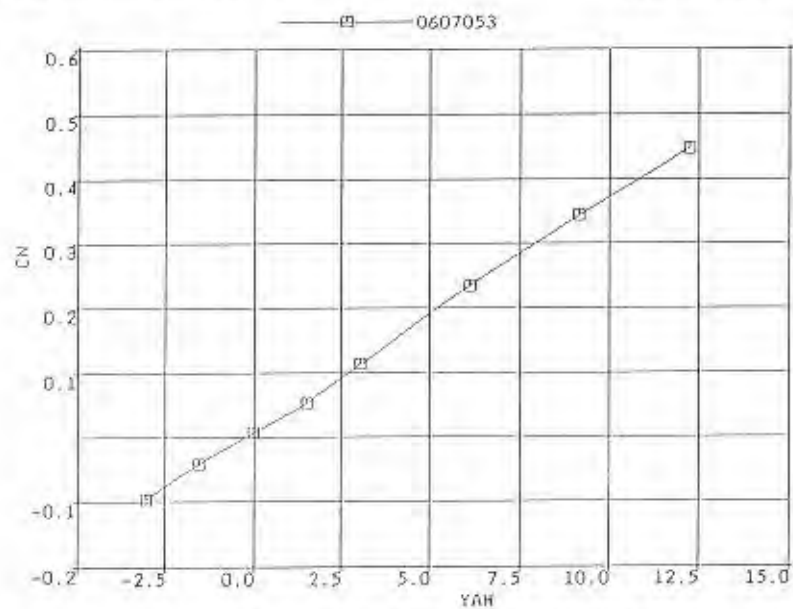
PROP 2 FRONT WITH GRIT, REAR 15



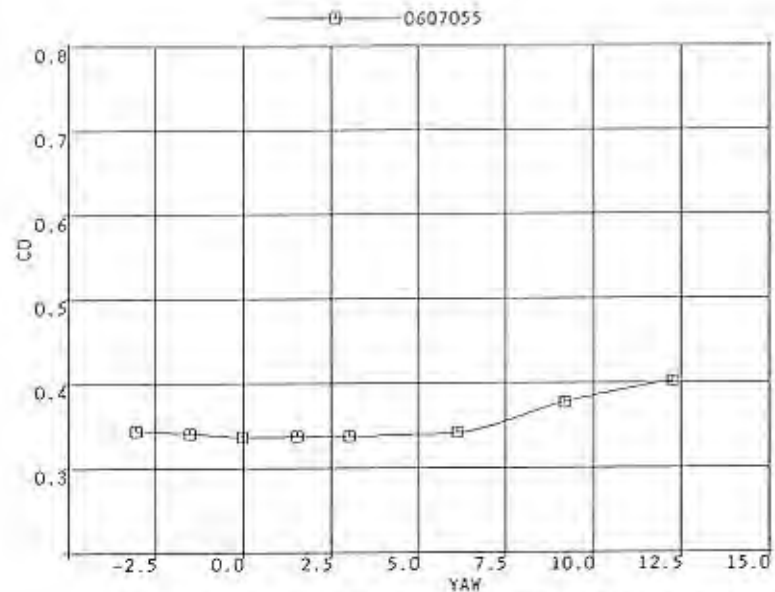
PROP 2 FRONT WITH GRIT AND C3 MIRRORS FWD, R



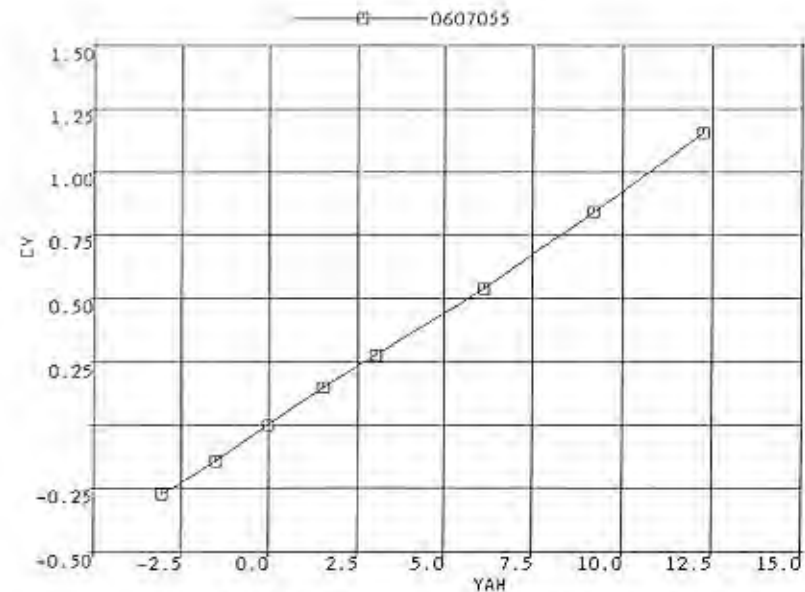
PROP 2 FRONT WITH GRIT AND C3 MIRRORS FWD, R



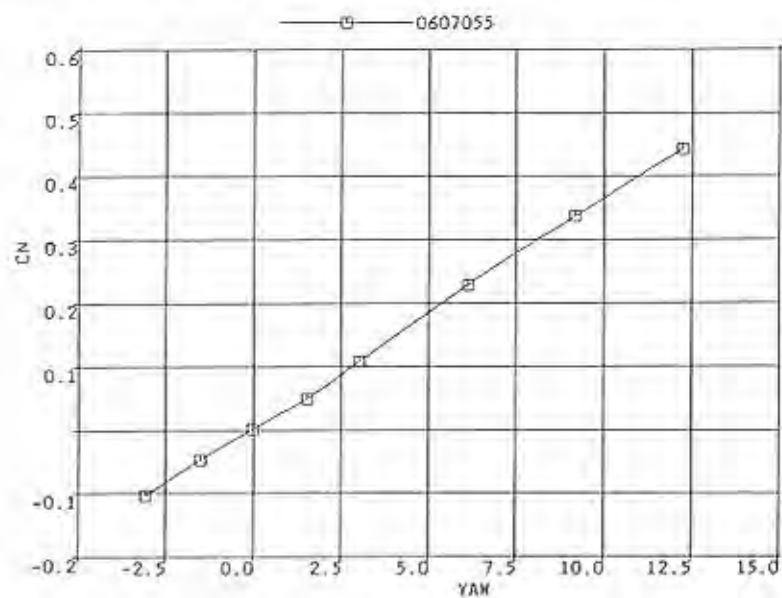
PROP 2 FRONT WITH GRIT AND C3 MIRRORS FWD, R



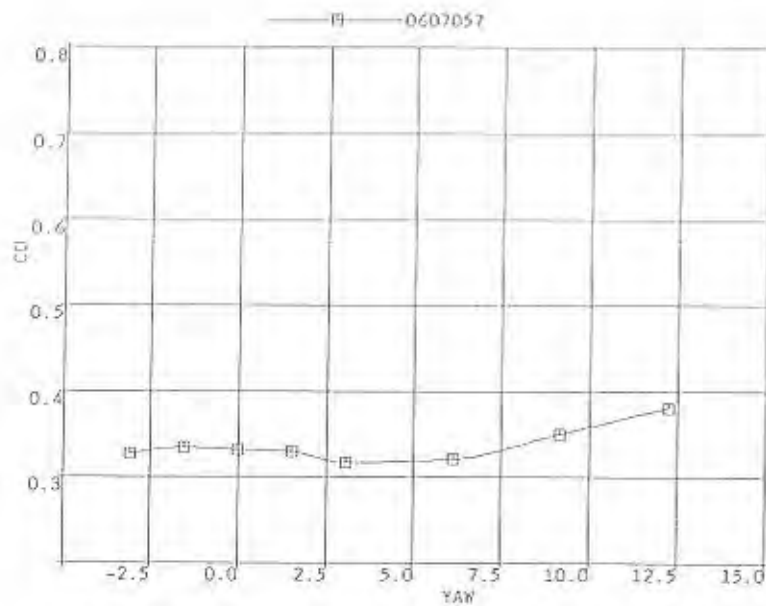
PROP 2 FRONT WITH GRIT AND C3 MIRRORS (RIGHT FWD,LEFT



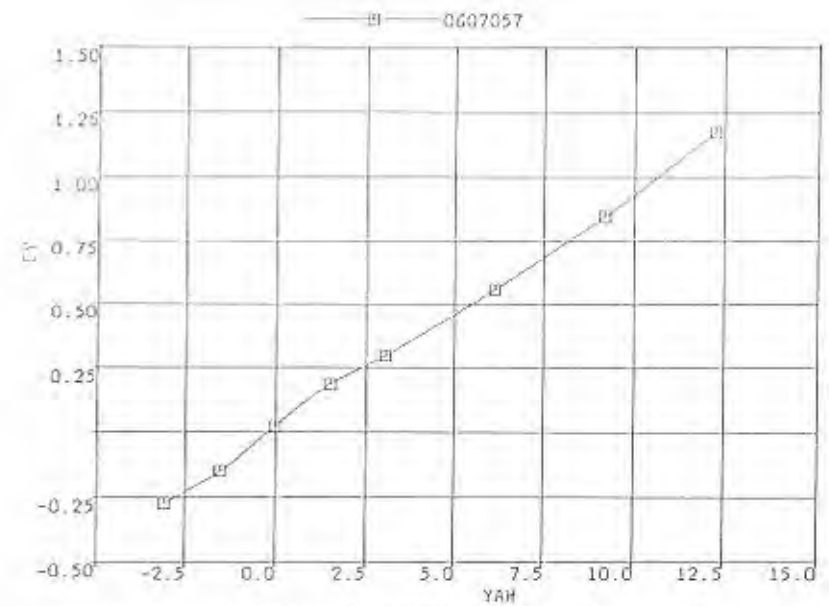
PROP 2 FRONT WITH GRIT AND C3 MIRRORS (RIGHT FWD,LEFT



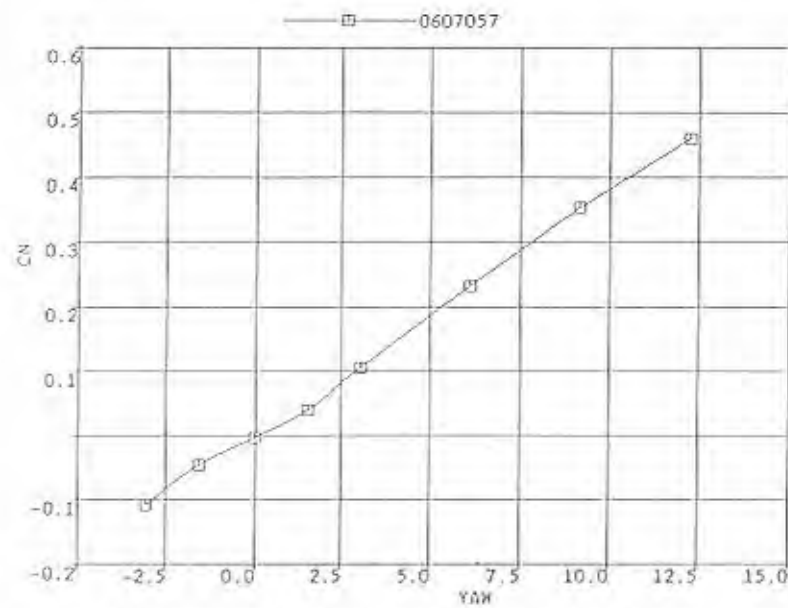
PROP 2 FRONT WITH GRIT AND C3 MIRRORS (RIGHT FWD,LEFT



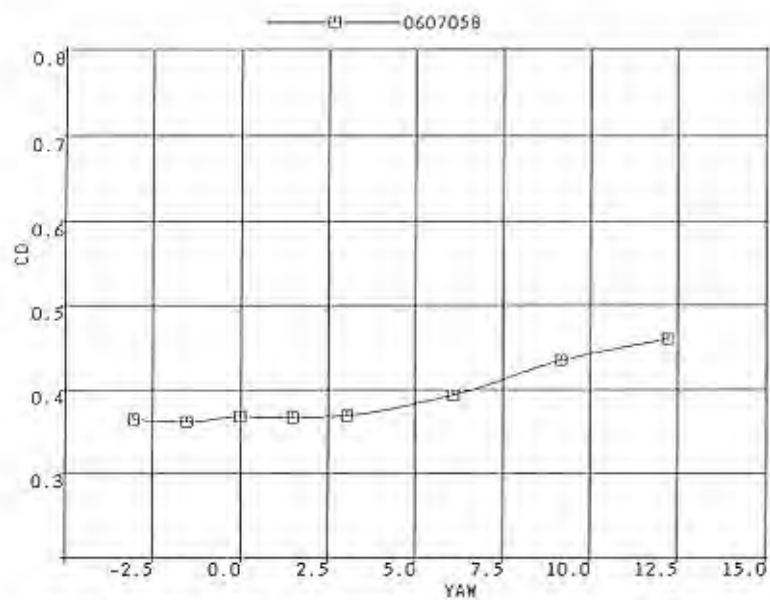
PROP 2 FRONT, GRIT, C3 MIRRORS (RIGHT FWD, LEFT AFT), WHEEL



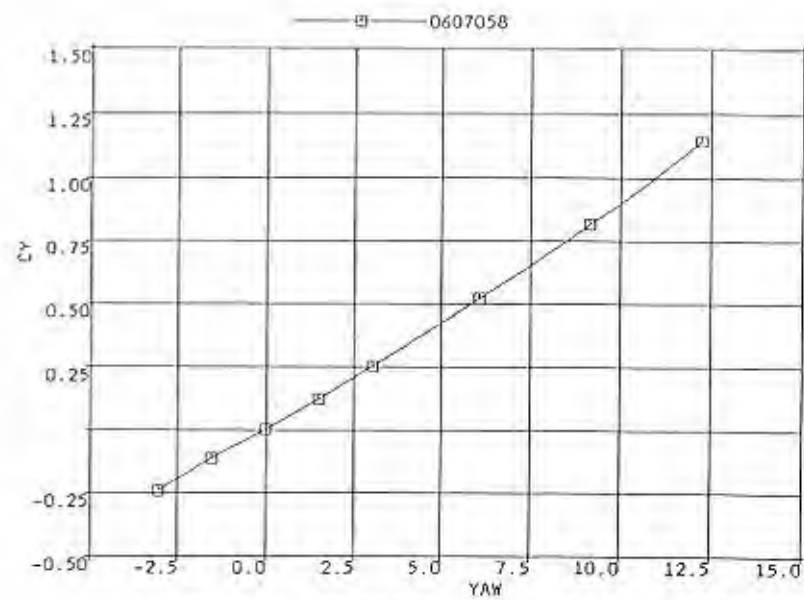
PROP 2 FRONT, GRIT, C3 MIRRORS (RIGHT FWD, LEFT AFT), WHEEL



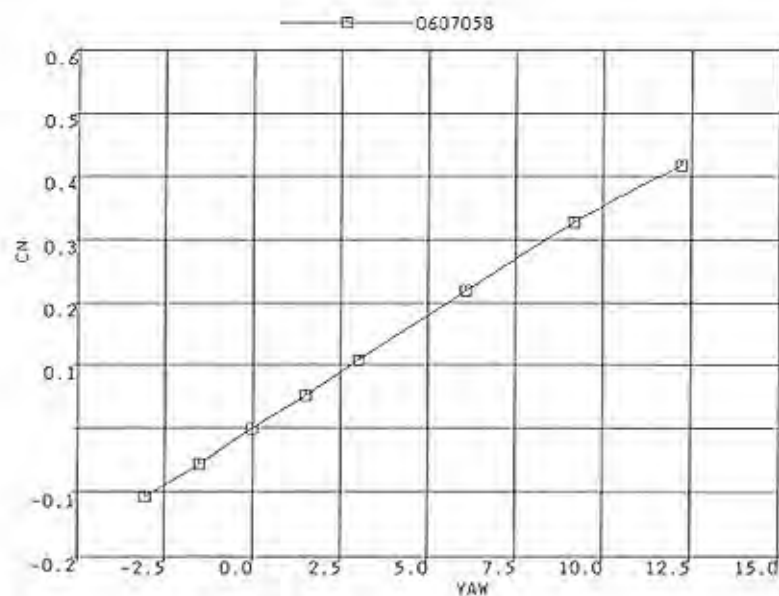
PROP 2 FRONT, GRIT, C3 MIRRORS (RIGHT FWD, LEFT AFT), WHEEL



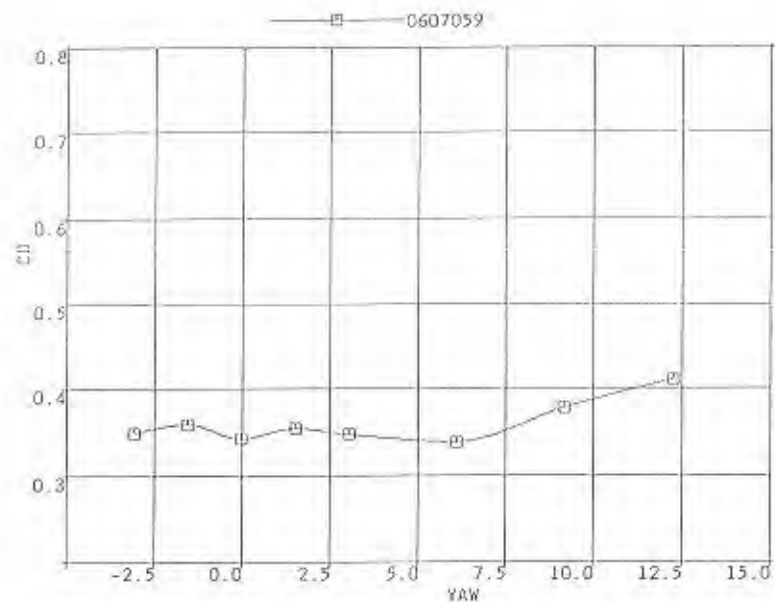
PROP 2 FRONT, GRIT, C3 MIRRORS (RIGHT FWD,LEFT AFT),VERTIC



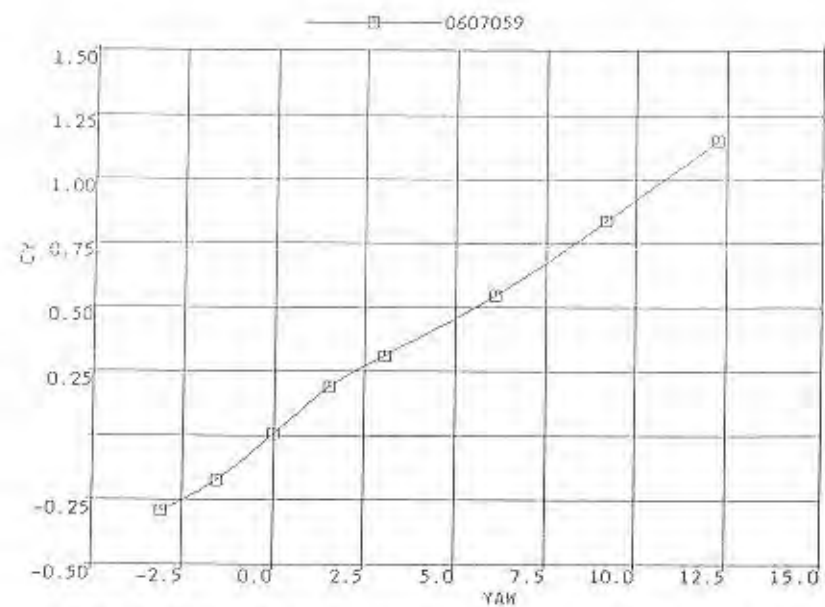
PROP 2 FRONT, GRIT, C3 MIRRORS (RIGHT FWD,LEFT AFT),VERTIC



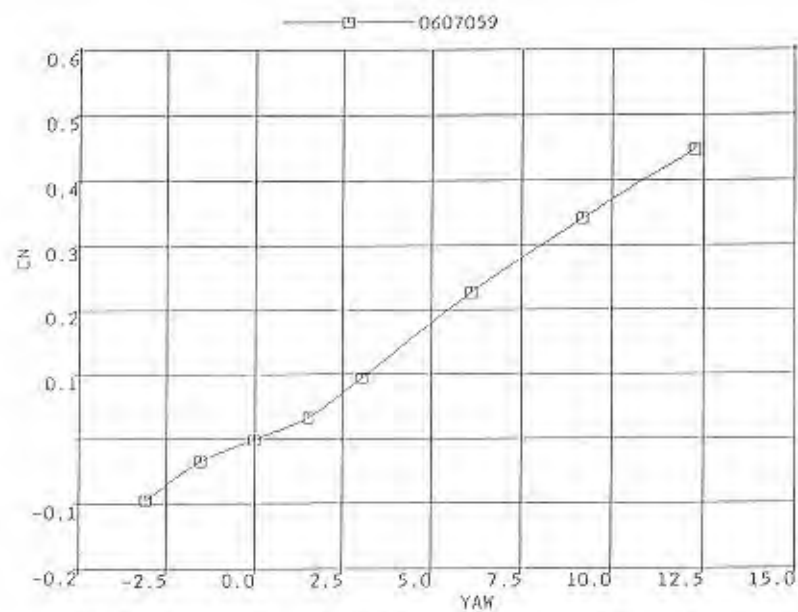
PROP 2 FRONT, GRIT, C3 MIRRORS (RIGHT FWD,LEFT AFT),VERTIC



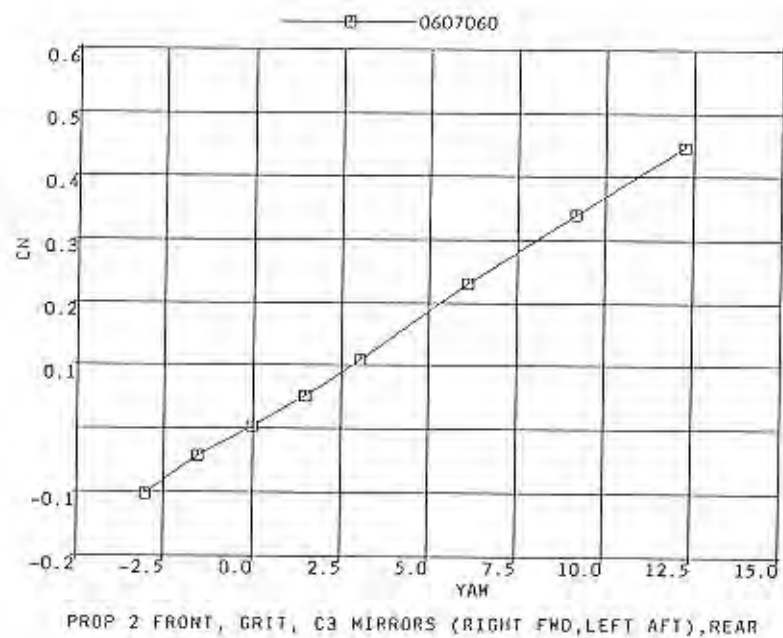
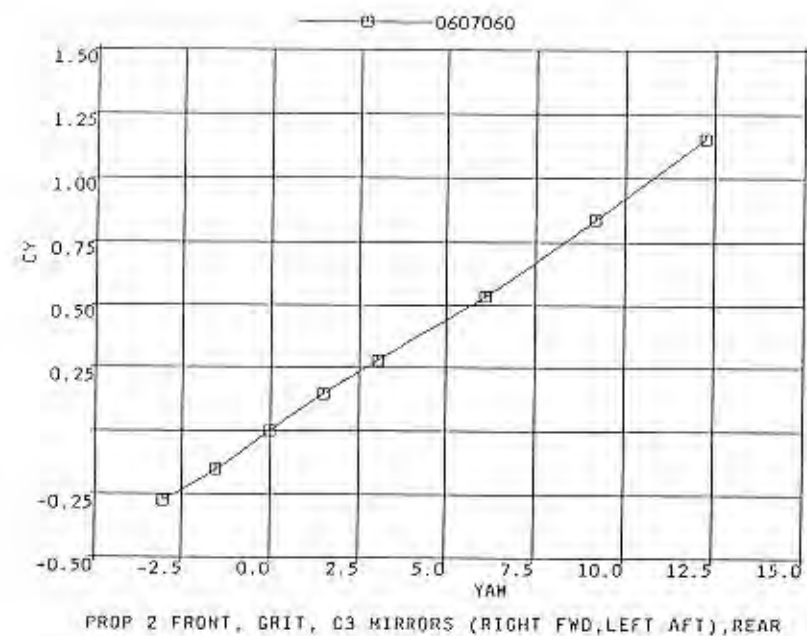
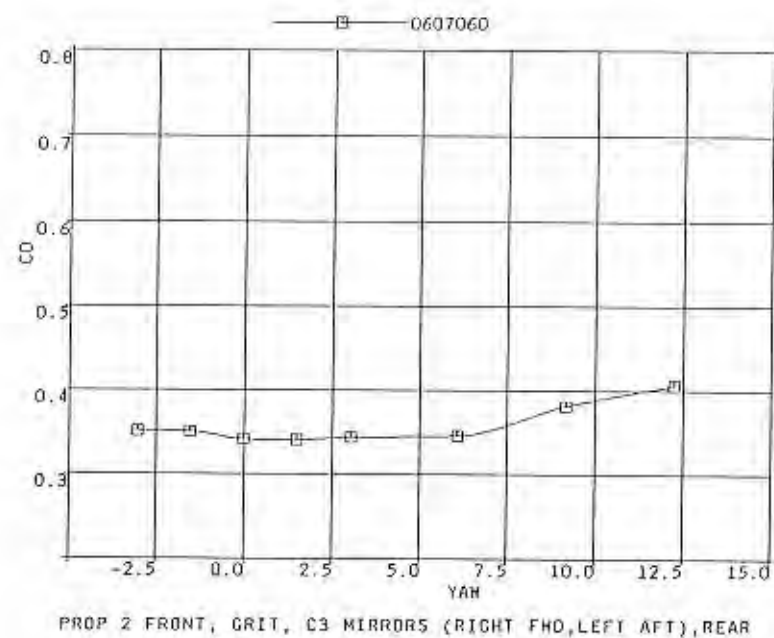
PROP 2 FRONT, GRIT, C3 MIRRORS (RIGHT FWD,LEFT AFT),FWD TI

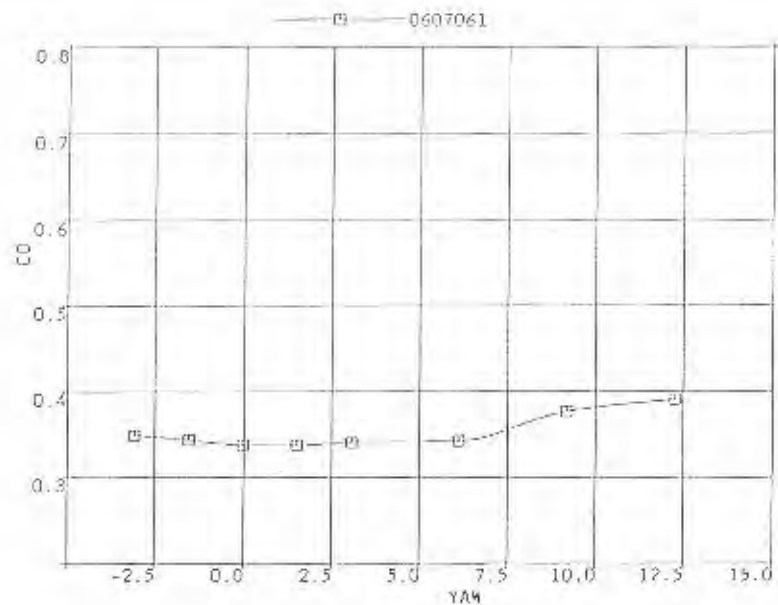


PROP 2 FRONT, GRIT, C3 MIRRORS (RIGHT FWD,LEFT AFT),FWD TI

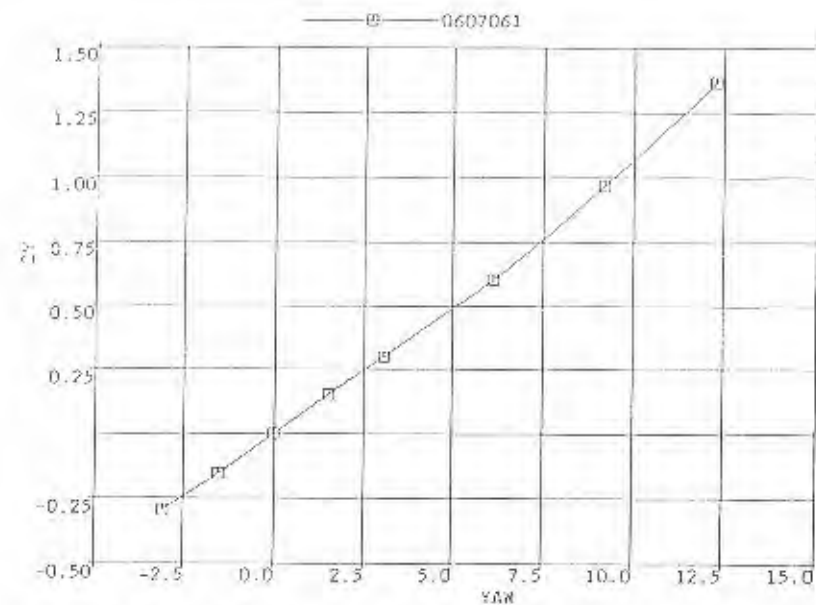


PROP 2 FRONT, GRIT, C3 MIRRORS (RIGHT FWD,LEFT AFT),FWD TI

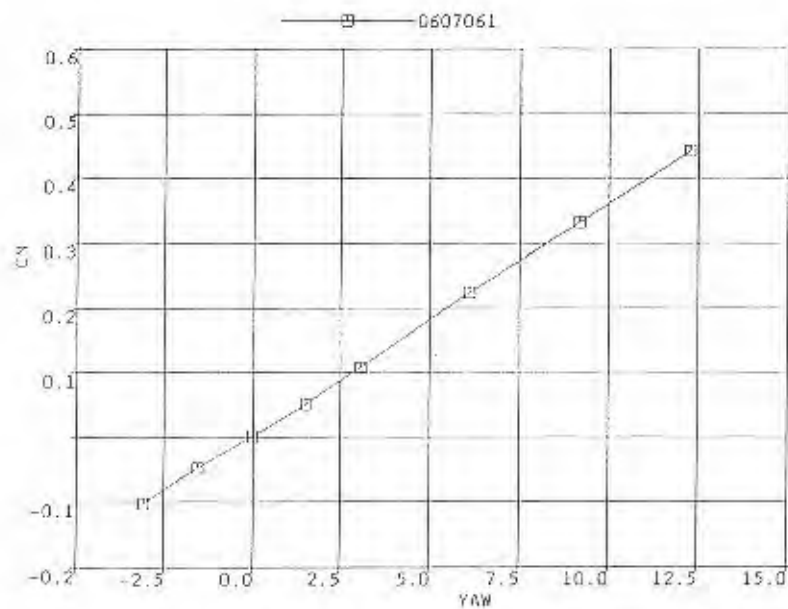




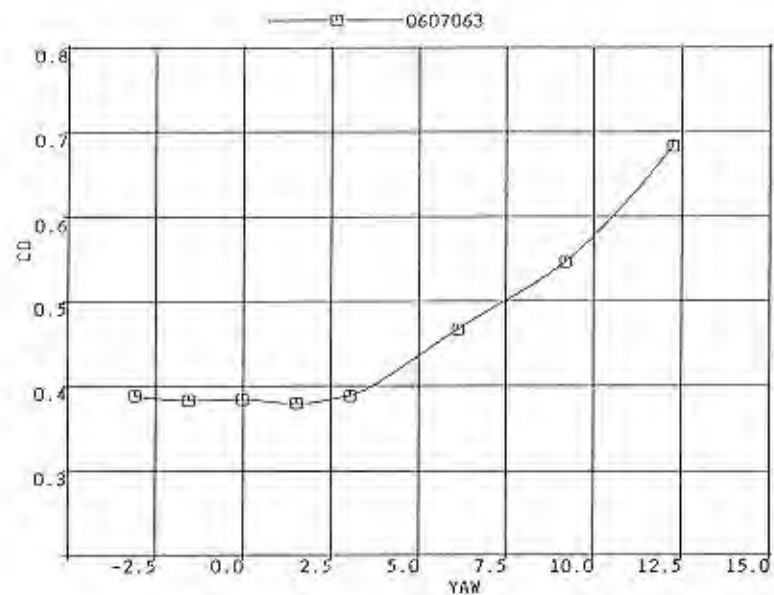
PROP 2 FRONT, GRIT, C3 MIRRORS(RIGHT FWD,LEFT AFT),MOD 0



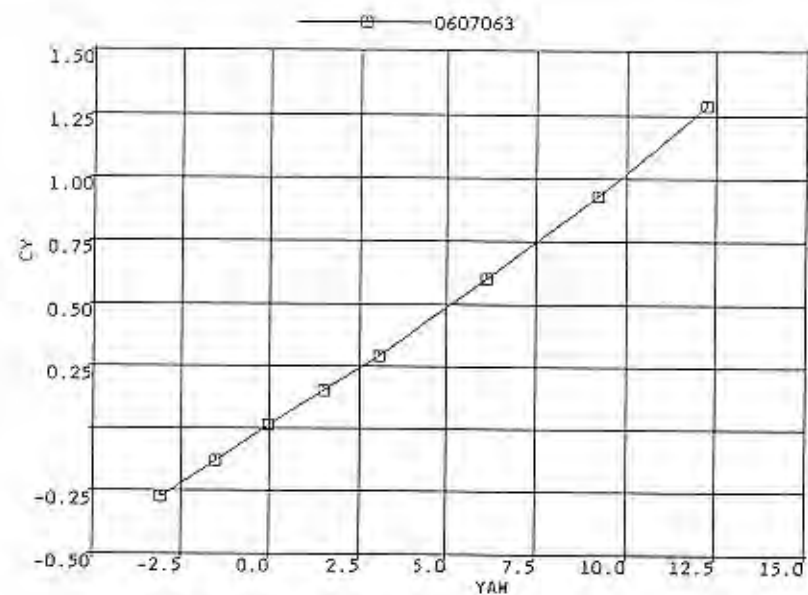
PROP 2 FRONT, GRIT, C3 MIRRORS(RIGHT FWD,LEFT AFT),MOD 0



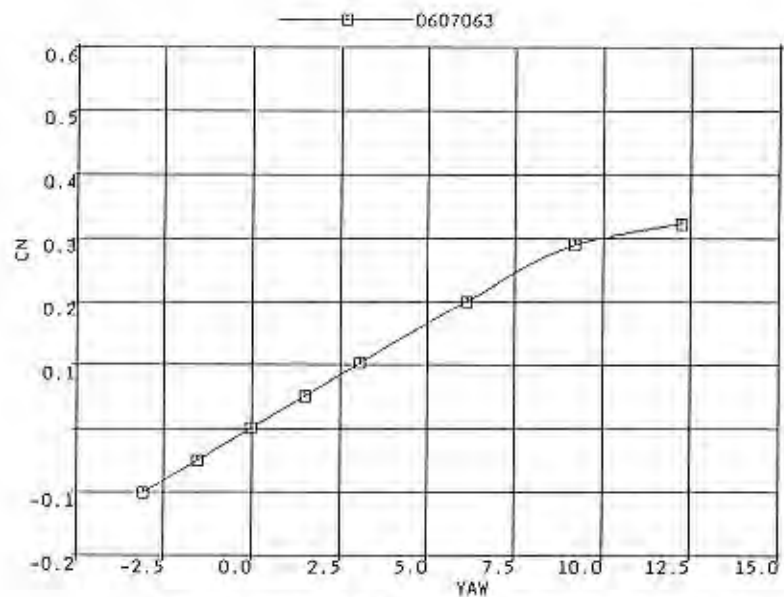
PROP 2 FRONT, GRIT, C3 MIRRORS(RIGHT FWD,LEFT AFT),MOD 0



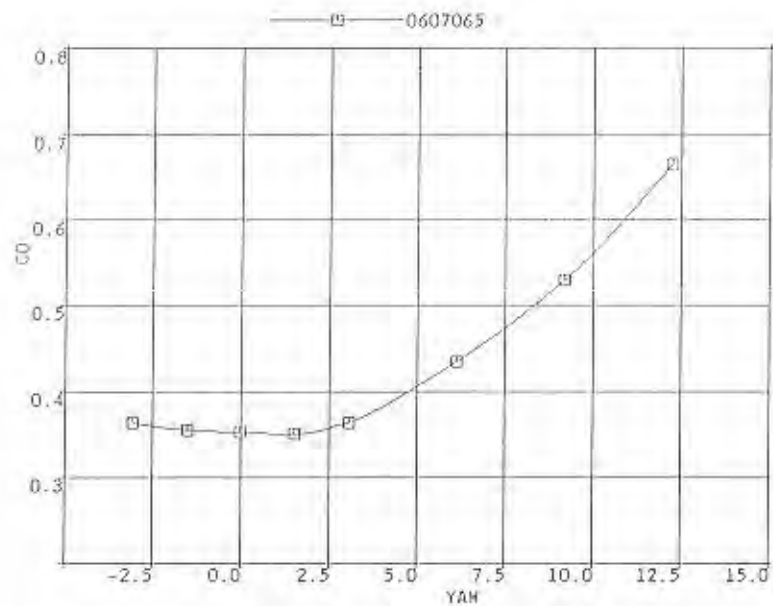
PREVOST FRONT, GRIT, PREVOST MIRRORS,STD DRIP RAIL



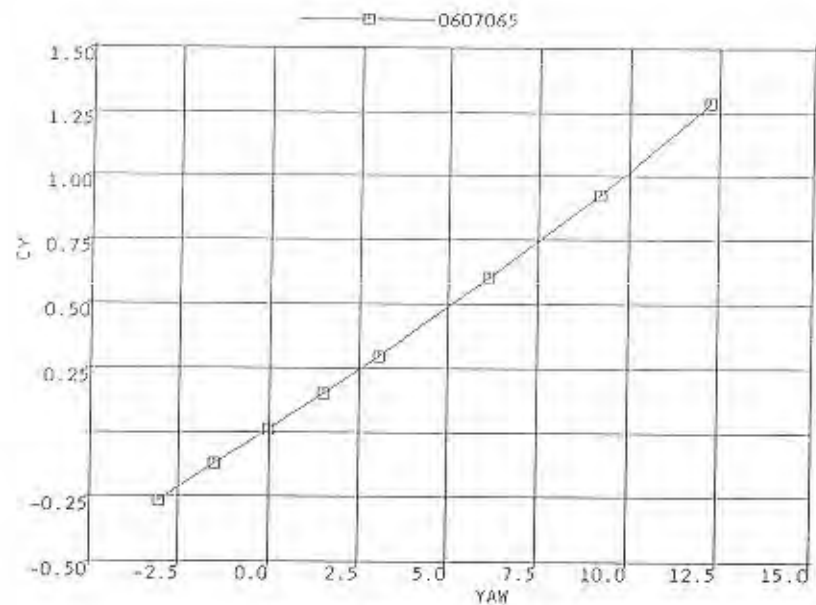
PREVOST FRONT, GRIT, PREVOST MIRRORS,STD DRIP RAIL



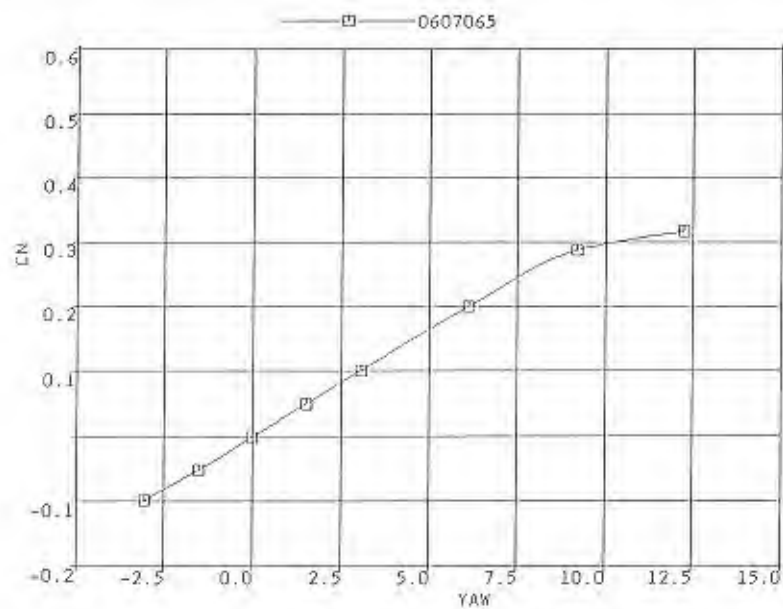
PREVOST FRONT, GRIT, PREVOST MIRRORS,STD DRIP RAIL



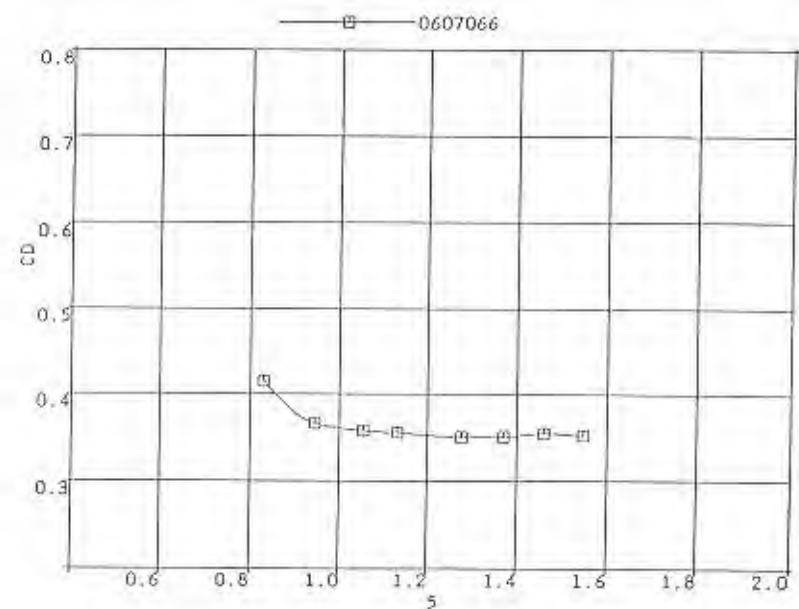
PREVOST FRONT, GRIT, STD DRIP RAILS, STD R



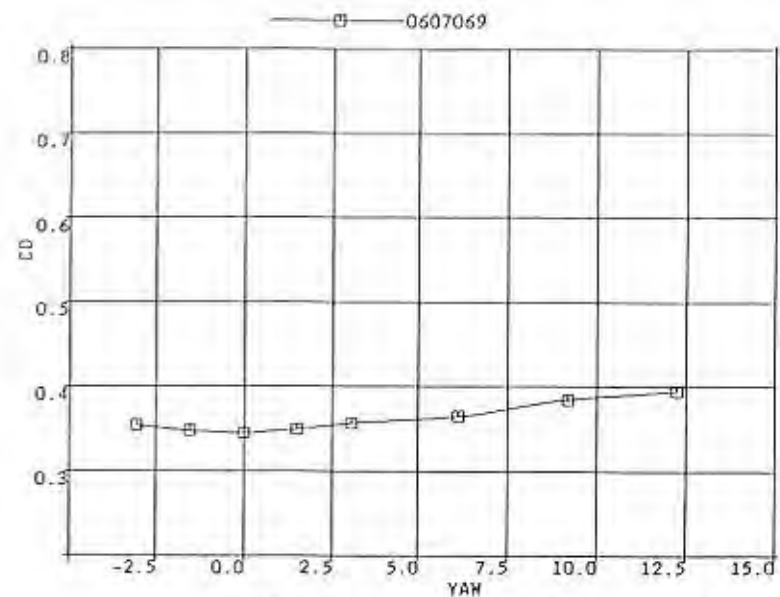
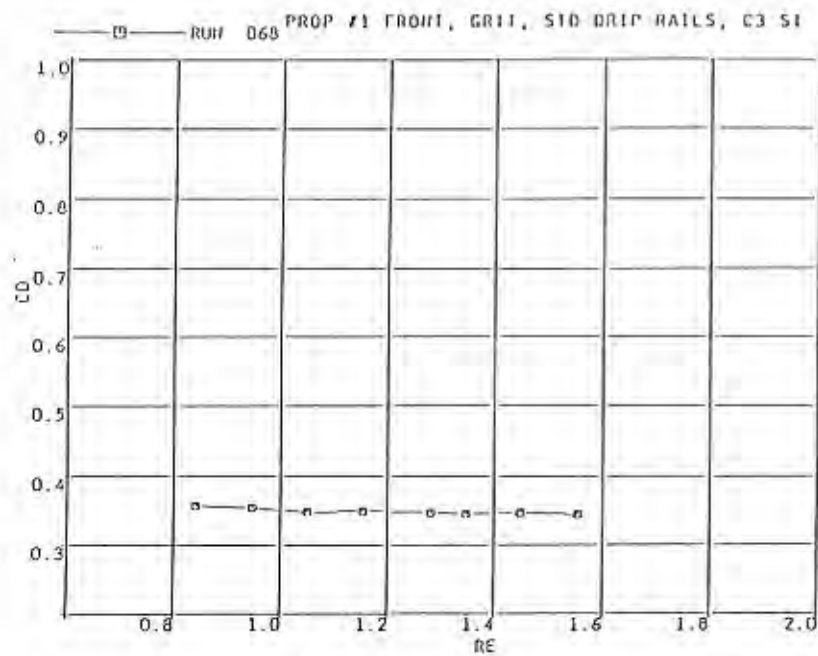
PREVOST FRONT, GRIT, STD DRIP RAILS, STD R



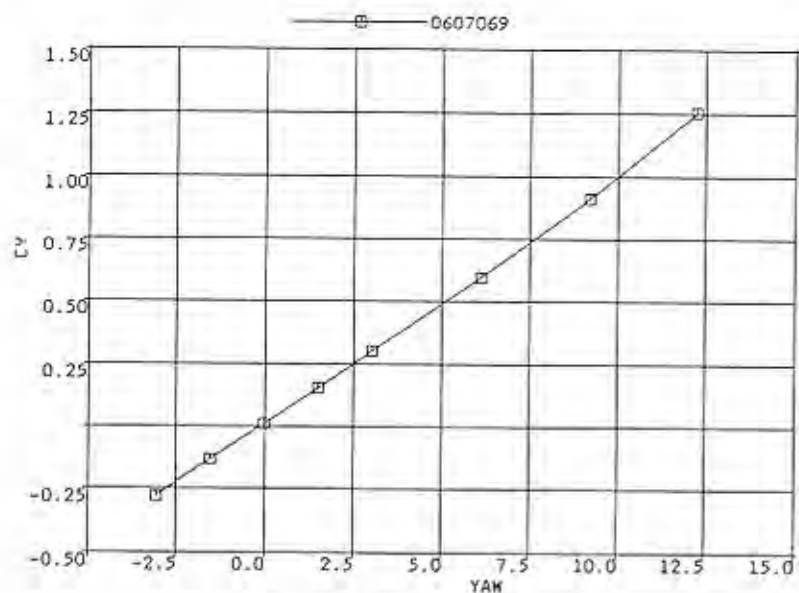
PREVOST FRONT, GRIT, STD DRIP RAILS, STD R



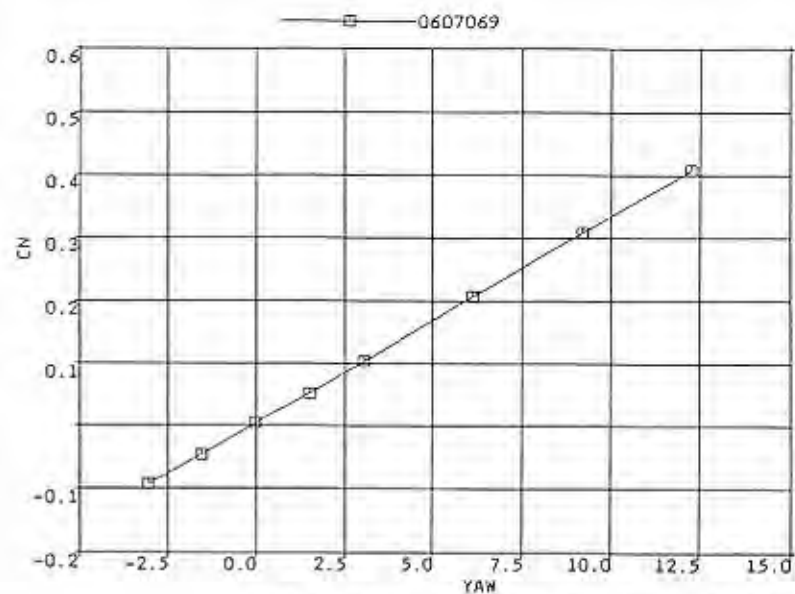
PREVOST FRONT, GRIT, STD DRIP RAILS, STD R



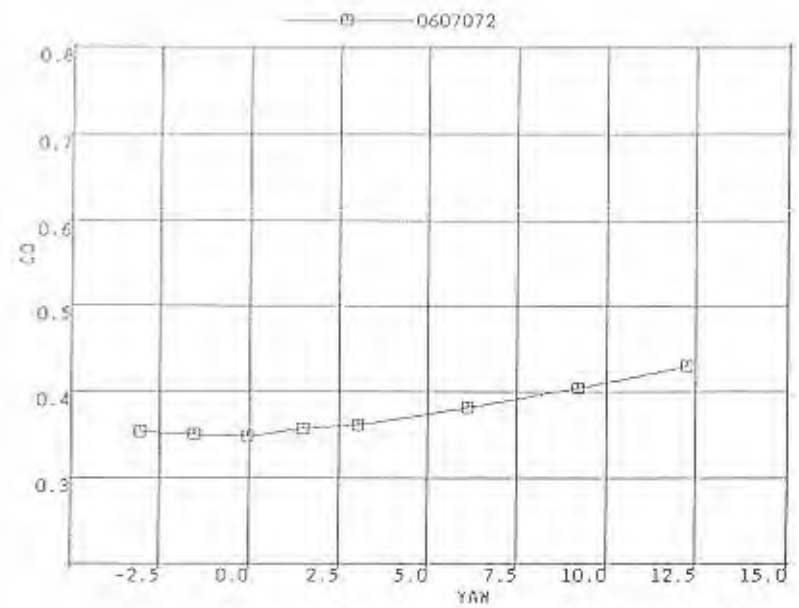
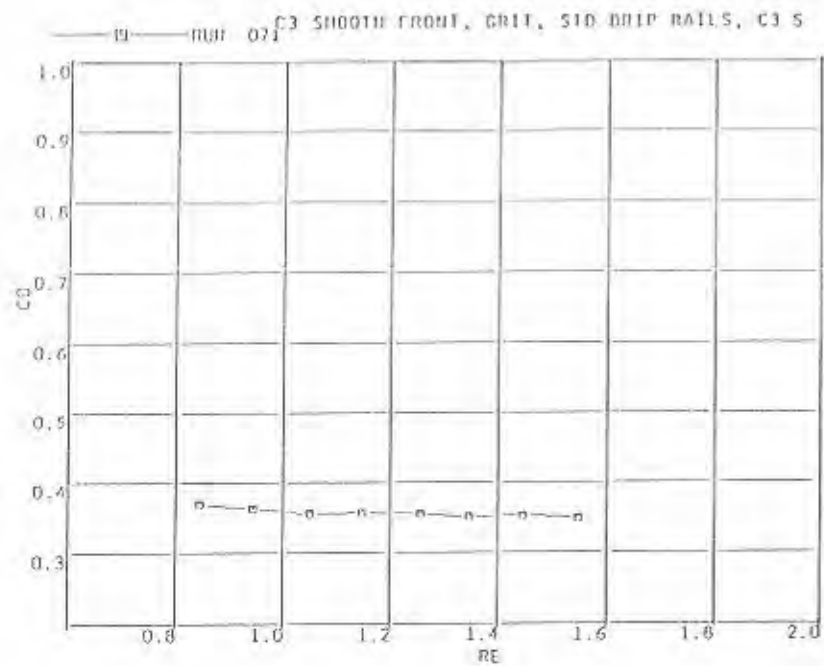
PROP #1 FRONT, GRIT, STD DRIP RAILS, C3 STD



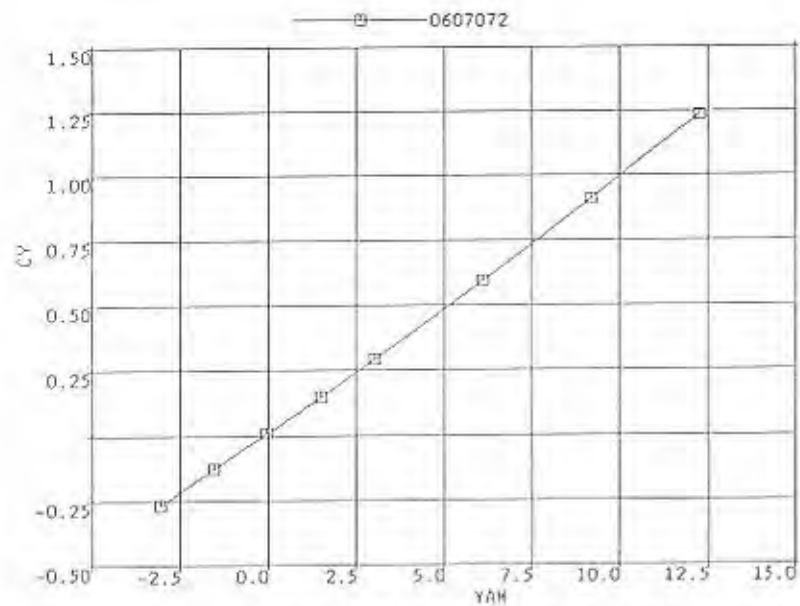
PROP #1 FRONT, GRIT, STD DRIP RAILS, C3 STD



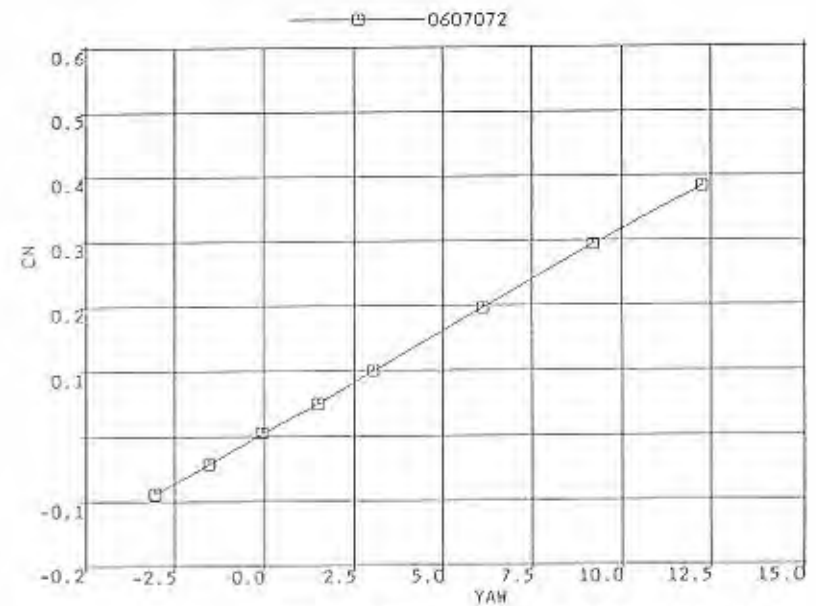
PROP #1 FRONT, GRIT, STD DRIP RAILS, C3 STD



C3 SMOOTH FRONT, GRIT, STD DRIP RAILS, C3 ST



C3 SMOOTH FRONT, GRIT, STD DRIP RAILS, C3 ST



C3 SMOOTH FRONT, GRIT, STD DRIP RAILS, C3 ST



RR #2

000099



RR #3

000100



RR #4

000101



RR #5

000102

Aerodynamic Effects to a Bicycle Caused by a Passing Vehicle

COPYRIGHT 1981
SOCIETY OF AUTOMOTIVE
ENGINEERS, INC.

Yoshikazu Kato, Tetsuo Iwasa,
Mitsuo Matsuda and Yoshihiro Miyai
Dept. of Transportation Engineering
Faculty of Engineering
Osaka Industrial Univ. (Japan)

ABSTRACT

There are many reasons why a bicycle is caused to wobble by a passing vehicle, for example, human engineering factors, riding techniques, the conditions of the road, aerodynamic effects, etc.

In this report, aerodynamic effects to a bicycle by a passing vehicle have been investigated experimentally and theoretically. Experiments were made by driving the 1/6-scale vehicle model with a catapult arrangement near the 1/6-scale bicycle model which was at rest.

Aerodynamic forces acting on the bicycle model were measured with the aerodynamic balance mounted under the bicycle and the flow patterns around the bicycle caused by the vehicle were examined using visualization techniques.

To compare with the experimental results, numerical calculations were carried out on the passing motion of two bodies in an ideal fluid.

IN JAPAN, TRAFFIC CASUALTIES INVOLVING VEHICLES are decreasing every year, but there are many casualties even now. The use of bicycles and small sized motorcycles have been increasing rapidly since the first oil crisis in 1970, and therefore accidents between these bicycles and automobiles have become a social problem.

In this paper, aerodynamic effects to a bicycle caused by a passing vehicle on a narrow road have been investigated. This study includes two kinds of experiments, and a fundamental analysis. One experiment was to measure force acting on the bicycle model, the other was to observe the flow around a bicycle model or a circular cylinder symbolizing a bicycle using visualization techniques. The fundamental analysis was carried out using the method of image doublets and the finite element method. It was very difficult to analyze numerically this problem in actual fluid, so that we studied the problem using two circular cylinders in ideal fluid.

EXPERIMENT

EXPERIMENTAL APPARATUS - When a vehicle passed near a bicycle the experimental apparatus which was developed in order to investigate aerodynamic effects is shown in Fig.1.

This apparatus consists of a track, a carriage and a catapult. The track was 36 meters

long by 0.11 meters wide. On this track, the vehicle (1/6-scale model) or the cylinder symbolizing a vehicle mounted on a carriage was catapulted using an elastic shock cord. After the carriage had passed through the test section, it was decelerated by a braking assembly.



Fig.1-Overall system layout

MEASUREMENT OF AERODYNAMIC FORCE ACTING ON BICYCLE MODEL - When a vehicle passes near a bicycle at velocity V , aerodynamic force F acts on the bicycle. This force F varies in value at every moment with the advancing of the vehicle.

Fig.2 shows the coordinate system.

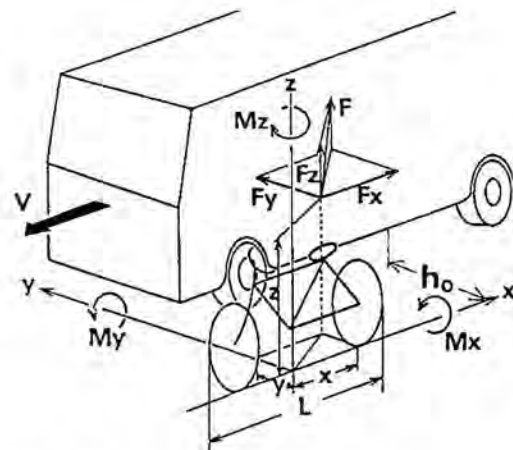


Fig.2-Coordinate system

The origin of coordinates is chosen as the middle point on the ground between the front and rear wheel of the bicycle. The components of

aerodynamic force F were measured by an aerodynamic balance mounted under the 1/6-scale bicycle model. The components of force F are F_x , F_y and F_z in x -, y - and z -direction, respectively. In this experiment, only the component F_y was measured because it appeared that the bicycle was caused to wobble by it. Aerodynamic coefficient C_y of F_y is given as following,

$$C_y = F_y / \frac{1}{2} \rho V^2 S \quad (1)$$

where ρ is density of fluid, and S is the projected area of the bicycle and the rider on x - z plane. Fig.3 and Fig.4 show the 1/6-scale model used in the experiment.

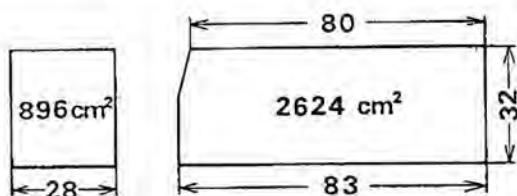


Fig.3- 1/6-scale vehicle model

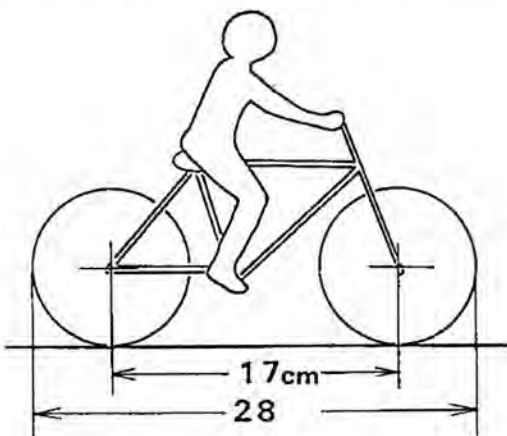


Fig.4- 1/6-scale bicycle model

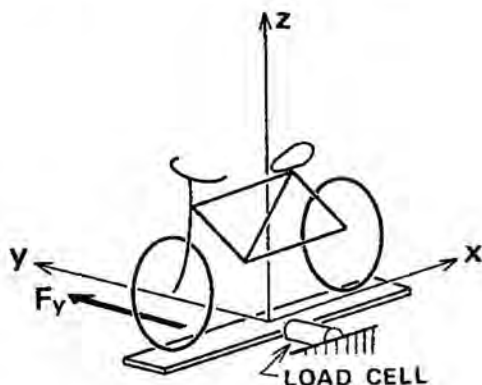


Fig.5-Skeleton of aerodynamic balance system

The skeleton of the aerodynamic balance is shown in Fig.5.

Fig.6 shows a sample of the data obtained by measuring force F_y ,

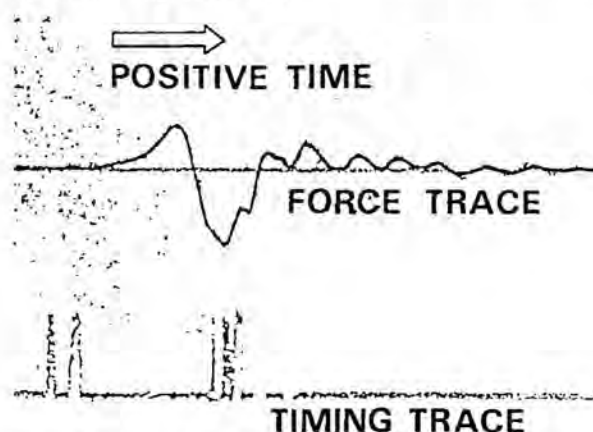


Fig.6-Force F_y , and timing trace

The first peak of force F_y occurs just as the front of the vehicle is even with the rear wheel of the bicycle and the negative value indicates that the force is in a direction away from the vehicle. The second peak occurs when the vehicle is approximately even with front of the bicycle, and the positive value tends to pull the bicycle toward the vehicle.

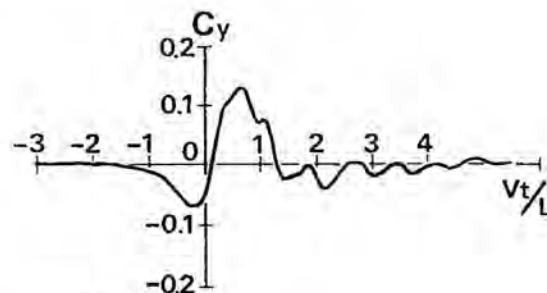


Fig.7- C_y variation

The instant when the front of vehicle is even with the center of the bicycle is chosen as the origin of time ($t=0$), and L is the overall length of the bicycle.

Fig.8 shows the Reynolds number effect on the force coefficient. Where h_0 is the distance between the bicycle and the vehicle, and Reynolds number Re is as following,

$$Re = V\ell/\nu \quad (2)$$

V =velocity of vehicle
 ℓ =overall length of vehicle
 ν =kinematic viscosity.

As seen from Fig.8, the Reynolds number effect on force coefficient C_y was small except $h_0=60\text{mm}$, for $Re=1.5 \times 10^5 \sim 3.5 \times 10^5$.

Fig.9 shows the relation of the second peak value of aerodynamic coefficient C_y to distance, h_0 . The change in the second peak value of C_y is nearly linear with distance h_0 .

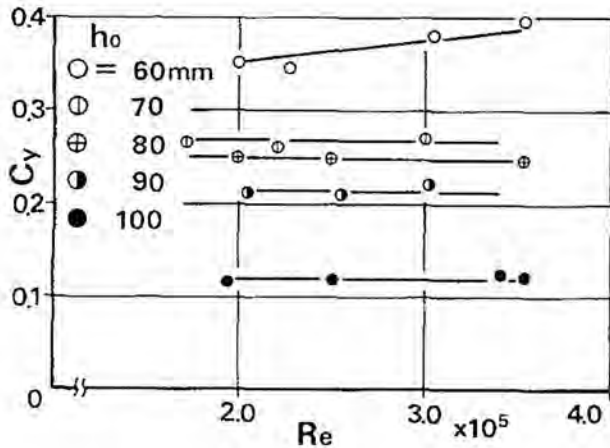


Fig.8 - Reynolds number effect on second peak value of C_y .

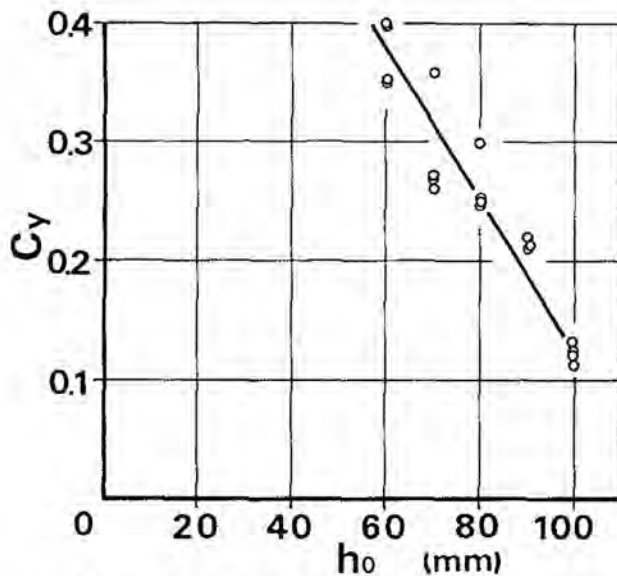


Fig.9 - Second peak value of C_y

OBSERVATION OF THE FLOW USING THE VISUALIZATION TECHNIQUE - Fig.10 shows the arrangement of the apparatus to observe the flow around the two cylinders. A moving large cylinder passed by a stationary small cylinder from right to left. A slender pipe was stuck in any position around the small cylinder. Smoke produced by combustion of yellow phosphor was pushed out through this pipe, as soon as the large cylinder approached it. This experiment was carried out many times at each position of the pipe to observe the flow patterns using a V.T.R. Fig.11 shows the flow patterns around the small cylinder. In Fig.11, the instant when the center of the moving large cylinder is even with the center of the stationary small cylinder is chosen as the origin of time ($t=0$) and $2b$ is the diameter of the small circular cylinder.

The overall flow turns clock-wise around the small cylinder and the smoke direction at

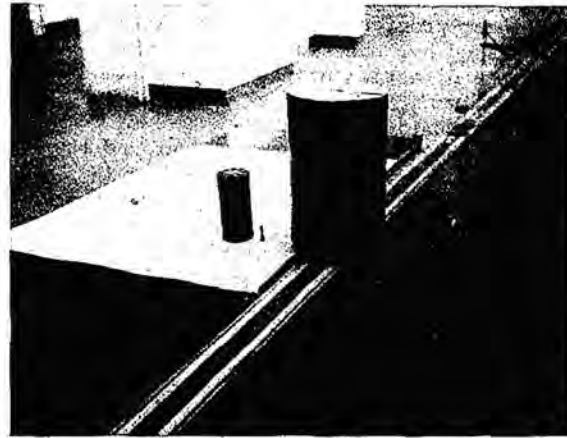


Fig.10 - Arrangement of two cylinder

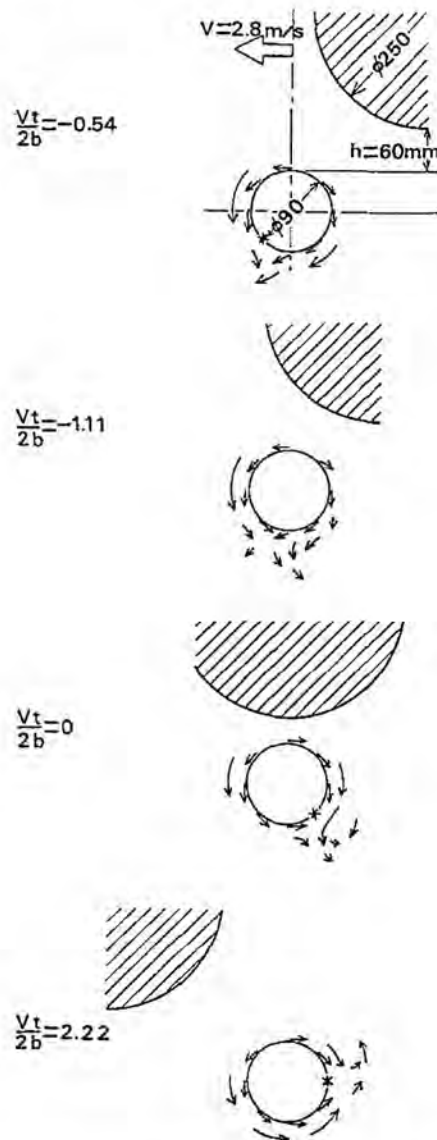


Fig.11 - Flow pattern around the stationary small cylinder

each position change as the passing of the large cylinder progresses. After the large cylinder passed by, the smoke direction is pulled in the direction of the large cylinder. And the positions marked with an asterisk (*) seem to be stagnation points.

Fig.12 shows the flow patterns around the bicycle. The experiment was carried out in much the same way as that of Fig.10. The origin of time ($t=0$) is chosen as the point when the front of the vehicle is even with the center of the bicycle and L is the overall length of the bicycle.

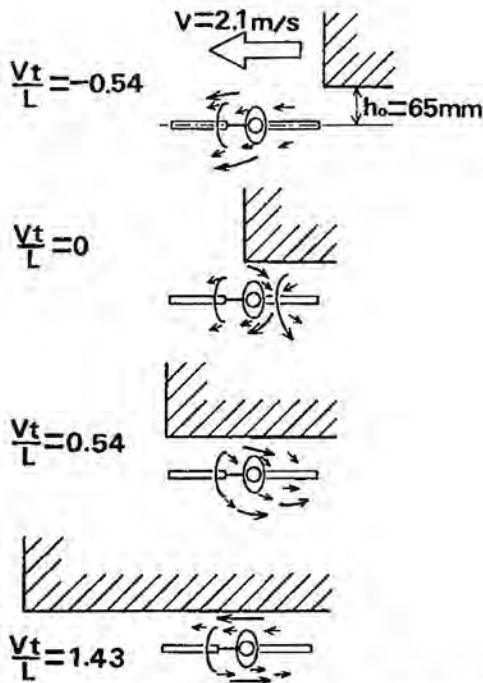


Fig.12 - Flow patterns around the bicycle

Smoke are pushed out as the vehicle approaches (see Fig.12-a). When the middle of the vehicle come to the center of the bicycle, the smoke between the vehicle and the bicycle is parallel to the direction of progress. The smoke on the far side of the bicycle is moving in the opposite direction (see Fig.12-d). The direction of the smoke changes rapidly, during a minute time in which the front of the vehicle passed by the center of bicycle and then when the middle of the vehicle passed by it (see Fig.12-b,c).

NUMERICAL ANALYSIS

METHOD OF IMAGE DOUBLETS - Consider the case where circular cylinder A (of radius a) pass by circular cylinder B (of radius b) with velocity V parallel to the x -axis in ideal fluid at rest. The instant when the two cylinder come closest is chosen as the origin of time ($t=0$) and the middle point of cylinder A and B at $t=0$ is taken as the origin of the coordinate system. Let $2k$ be the closest distance between

the center of cylinder at $t=0$. Fig.13 shows the coordinate system

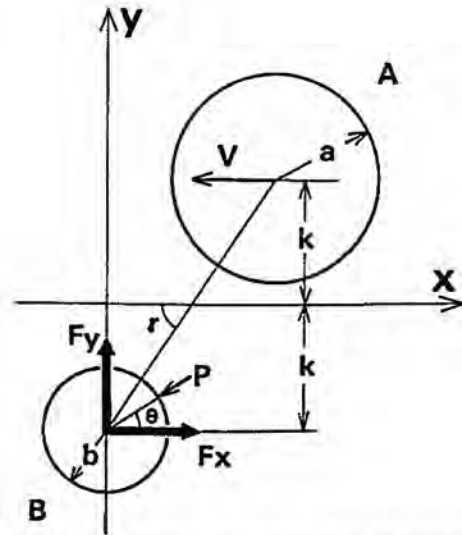


Fig.13 - Notation diagram for passing motion of two circular cylinders in an ideal fluid

The velocity potential around the two cylinders in ideal fluid is determined using the method of image doublets. Consequently, the expression for the velocity potential to the fifth approximation is as following,

$$\phi = \phi_1 + \phi_2 + \phi_3 + \phi_4 + \phi_5 + \dots \quad (3)$$

$$\phi_1 = \frac{Va^2(x-x_1)}{(x-x_1)^2 + (y-y_1)^2} \quad (4)$$

$$x_1 = -Vt, \quad y_1 = k, \quad \xi_1 = 0, \quad \eta_1 = -k.$$

$$\phi_2 = -\frac{Va^2b^2}{(x_1-\xi_1)^2 + (y_1-\eta_1)^2} \times \frac{(x-\xi_2)\cos 2\gamma + (y-\eta_2)\sin 2\gamma}{(x-\xi_2)^2 + (y-\eta_2)^2}$$

$$x_2 = -Vt + Vt\delta', \quad y_2 = k - 2k\delta',$$

$$\xi_2 = -Vt\delta', \quad \eta_2 = -k + 2k\delta',$$

$$\delta' = b^2/(V^2t^2 + 4k^2), \quad \delta'' = a^2/(V^2t^2 + 4k^2),$$

$$\gamma = \tan^{-1}(-2k/Vt). \quad (5)$$

$$\phi_3 = \frac{Va^4b^2}{[(x_1-\xi_1)^2 + (y_1-\eta_1)^2][(x_1-\xi_2)^2 + (y_1-\eta_2)^2]}$$

$$\times \frac{(x-x_3)}{(x-x_3)^2 + (y-y_3)^2},$$

$$x_3 = -Vt + \frac{\delta''}{1-\delta'}Vt, \quad y_3 = k - \frac{2k\delta''}{1-\delta'},$$

$$\xi_3 = -\frac{\delta''}{1-\delta'}Vt, \quad \eta_3 = -k + \frac{2k\delta''}{1-\delta'}. \quad (6)$$

$$\phi_4 = -\frac{Va^4b^4}{[(x_1-\xi_1)^2 + (y_1-\eta_1)^2][(x_1-\xi_2)^2 + (y_1-\eta_2)^2]}$$

$$\times [(\xi_1-x_3)^2 + (\eta_1-y_3)^2]$$

$$\times \frac{(x-\xi_4)\cos 2\gamma + (y-\eta_4)\sin 2\gamma}{(x-\xi_4)^2 + (y-\eta_4)^2},$$

$$x_4 = -Vt + \frac{(1-\delta')\delta''}{1-2\delta'}Vt,$$

$$y_4 = k \left\{ 1 - \frac{2(1-\delta')\delta''}{1-2\delta'} \right\},$$

$$\xi_4 = -\frac{(1-\delta')\delta''}{1-2\delta'}Vt,$$

$$\eta_4 = k \left\{ -1 + 2\delta' \frac{(1-\delta')}{1-2\delta'} \right\} \quad (7)$$

$$\phi_s = \frac{Va^2b^4}{[(x_1-\xi_1)^2 + (y_1-\eta_1)^2][(x_1-\eta_2)^2 + (y_1-\eta_2)^2]} \times [(\xi_1-x_3)^2 + (\eta_1-y_3)^2] \times \frac{1}{(x_1-\xi_4)^2 + (y_1-\eta_4)^2} \times \frac{(x-\xi_s)}{(x-\xi_s)^2 + (y-\eta_s)^2} \quad (8)$$

$$\begin{aligned} x_s &= -Vt + \frac{(1-2\delta')\delta'}{(1-3\delta'+\delta'^2)} Vt, \\ y_s &= k \left\{ 1 - 2 \frac{(1-2\delta')\delta'}{(1-3\delta'+\delta'^2)} \right\}, \\ \xi_s &= -\frac{(1-2\delta')\delta'}{(1-3\delta'+\delta'^2)} Vt, \\ \eta_s &= k \left\{ -1 + 2 \frac{(1-2\delta')\delta'}{(1-3\delta'+\delta'^2)} \right\}. \end{aligned} \quad (9)$$

The x- and y-components of velocity are given as

$$\begin{aligned} u &= u_1 + u_2 + u_3 + u_4 + u_5 + \dots, \\ v &= v_1 + v_2 + v_3 + v_4 + v_5 + \dots, \end{aligned} \quad (10)$$

where the resultant velocity is obtained as $q = \sqrt{u^2 + v^2}$ (11)

and the pressure coefficient on cylinder B is obtained from the generalized Bernoulli's equation,

$$C_p = \frac{P - P_0}{\frac{1}{2}\rho V^2} = -\frac{\partial \phi}{\partial t} / \frac{1}{2}V^2 - \frac{q^2}{V^2} \quad (12)$$

where,

P=pressure on cylinder B

P₀=pressure at infinity

ρ=density of fluid,

Force component F_x, F_y acting on cylinder B is given as follows:

$$\begin{aligned} F_x &= -\oint_B P b \cos \theta d\theta, \\ F_y &= -\oint_B P b \sin \theta d\theta. \end{aligned} \quad (13)$$

Furthermore, F_x, F_y are given by the following expression:

$$\begin{aligned} F_x &= C_x \rho V^2 S / 2, \\ F_y &= C_y \rho V^2 S / 2 \end{aligned} \quad (14)$$

Where S is the cross section area of cylinder B and C_x, C_y are the force coefficients in the x- and y-direction, respectively. Let S=2b.l, and therefore

$$\begin{aligned} C_x &= -\frac{1}{l} \oint_B C_p \cos \theta d\theta, \\ C_y &= -\frac{1}{l} \oint_B C_p \sin \theta d\theta \end{aligned} \quad (15)$$

To rewrite the equations in dimensionless form, we define dimensionless quantities,

$$\begin{aligned} \frac{K}{b} &= m, \quad \frac{a}{b} = n, \quad \frac{Vt}{2b} = S \\ 2m-n-1 &= h, \end{aligned} \quad (16)$$

and any point (x,y) on cylinder B are expressed in the dimensionless form

$$\frac{x}{b} = \cos \theta, \quad \frac{y}{b} = \sin \theta. \quad (17)$$

Example - Numerical calculations were carried out for the following cases:

$$n=1, 2, 3, 4, 5$$

$$m=2.75, 3.0, 4.0, 4.5, 5.0$$

The pressure distribution on the stationary cylinder B for n=4.0, m=3.5 are shown in Fig.14.

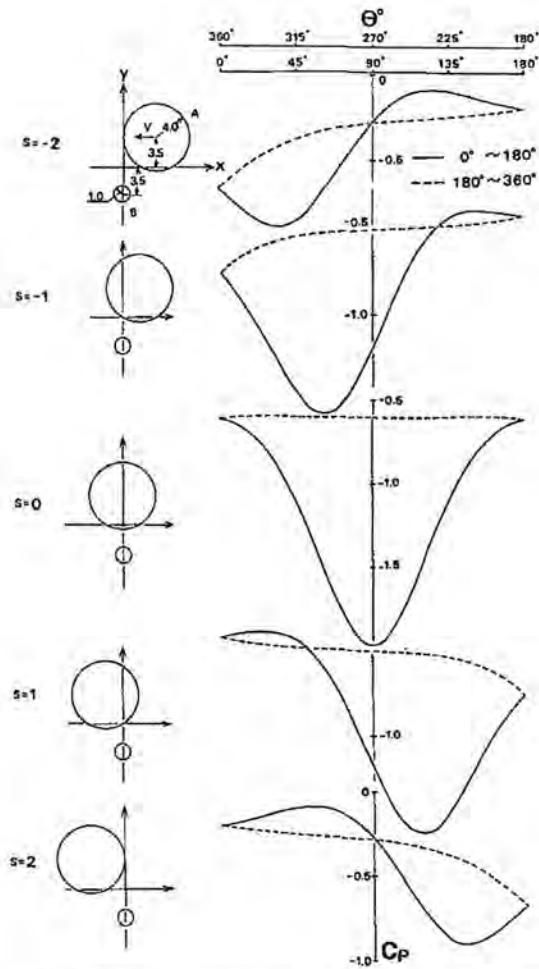


Fig.14 - Pressure distribution on cylinder B for n=4.0, m=3.5

The time history of force coefficients acting on cylinder B for n=4.0, m=3.5 are indicated in Fig.15.

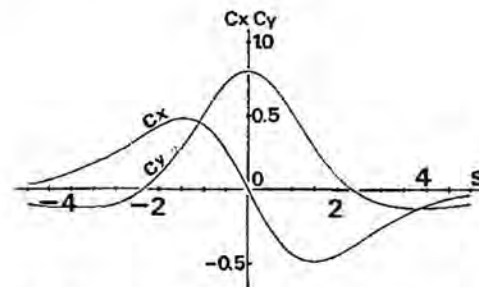


Fig.15 - Force coefficients variation for n=4.0, m=3.5

Fig.16 and Fig.17 show the time history of the force coefficients in the x- and y-direction acting on cylinder B for $n=4.0$ in the case of $m=2.75, 3.0, 4.5, 5.0$, respectively. Fig.18 shows the relationship between the maximum positive value of force coefficient C_y to h . Where h is the dimensionless distance between two circular cylinders.

The negative value of force coefficient C_y occurs up to approximately $s=Vt/2b=-2$ and the negative value indicates that the force is in a direction away from cylinder A. The positive value of C_y is at a maximum when the two cylinders come closest and the positive value force tends to pull the cylinder B toward the cylinder A. The maximum positive force increases markedly with the decreasing in distance between cylinder B and cylinder A.

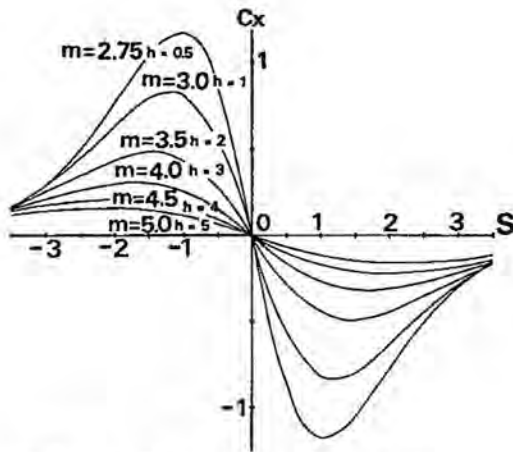


Fig.16 - C_x variation for $n=4.0$

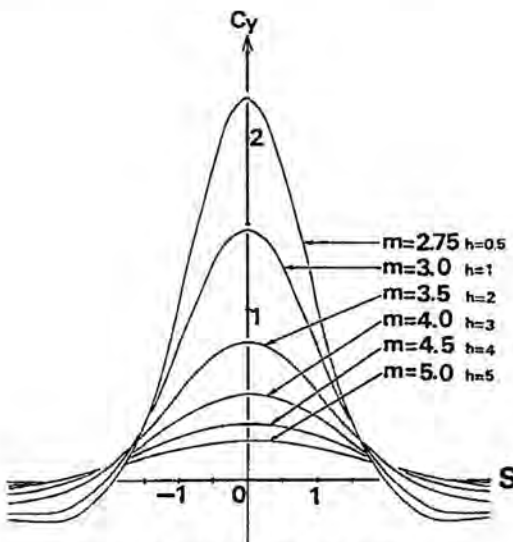


Fig.17 - C_y variation for $n=4.0$

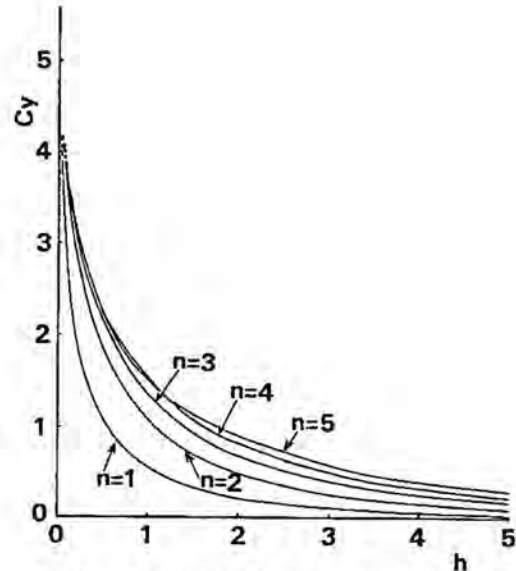


Fig.18 - Relationship between C_y to h for various n

FINITE ELEMENT METHOD - Potential flow to two circular cylinders is obtained by finding the solution to Laplace's equation

$$\frac{\partial^2 \psi}{\partial x^2} + \frac{\partial^2 \psi}{\partial y^2} = 0, \quad (18)$$

subject to boundary conditions

$$\left. \begin{aligned} \frac{d\psi}{dn} &= q \text{ on moving cylinder} \\ \frac{d\psi}{dn} &= 0 \text{ on stationary cylinder,} \end{aligned} \right\} \quad (19)$$

where ψ is the stream function, and $\frac{d\psi}{dn}$ is normal velocity to the surface of the moving cylinder. The x- and y-components of velocity are given as

$$\left. \begin{aligned} u &= -\frac{\partial \psi}{\partial y} \\ v &= \frac{\partial \psi}{\partial x}, \end{aligned} \right\} \quad (20)$$

The variational solution to this problem is the function ψ which minimizes the functional

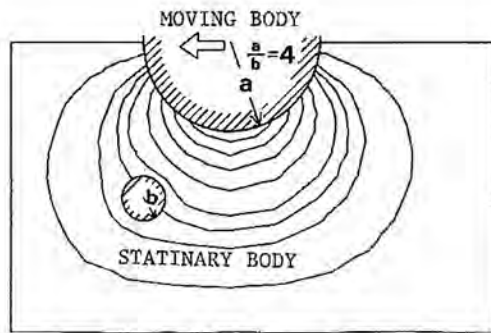
$$x = \int_D \frac{1}{2} \left[\left(\frac{\partial \psi}{\partial x} \right)^2 + \left(\frac{\partial \psi}{\partial y} \right)^2 \right] dD - \int_S q \psi dS, \quad (21)$$

Where D is a domain and S is the boundary of D . The region $D+S$ is divided into triangular elements. Let there be m nodal point in the entire region of $D+S$. From the minimization of the functional is derived the following matrix equation

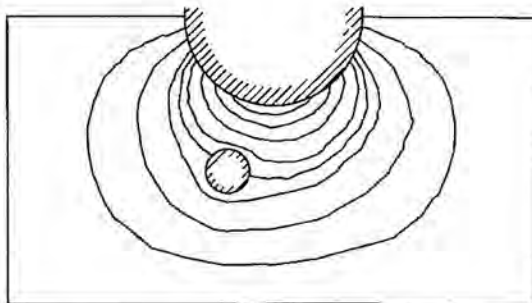
$$[K]\{\psi\} = \{F\}, \quad (22)$$

Where $[K]$ is the global stiffness matrix whose elements are functions of the nodal coordinates, $\{\psi\}$ is the $(m \times 1)$ column matrix whose elements are unknown $\psi_1, \psi_2, \dots, \psi_m$, $\{F\}$ is the global force vector which is determined by the prescribed boundary conditions.

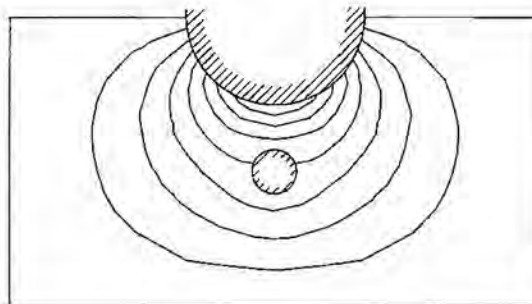
In Fig.19 are shown the streamlines which were obtained from velocity potential calculated using the finite element method proposed by G.de Vries and D.H.Norrie.



(a)



(b)



(c)

Fig.19 - Streamline pattern around two circular cylinders

The extension of the method to arbitrary bodies is under investigation.

CONCLUSIONS

From the results obtained from experiments and numerical calculations, the following conclusions were obtained:

1. The force acting on stationary body (bicycle) in a direction away from the moving body (vehicle) occurs for the first time as the passing begins.
2. The force which pulls the stationary body (bicycle) toward the moving body (vehicle) is at a maximum when the two bodies come closest.
3. The maximum pulling force increases markedly with the decreasing of the distance between the two bodies (bicycle and vehicle).
4. Because effects due to the viscosity are neglected in numerical analysis, the results of the numerical analysis after the instant when the pulling force occurs, do not agree with the experimental results.
5. The research on arbitrary bodies remains to be proved in numerical analysis.

REFERENCES

1. F.N.Beuvals, "Aerodynamic Input to a Parked Vehicle Caused by a Passing Bus," SAE Automotive Engineering Congress, Detroit, Mich, January 12-16, 1970.
2. Y.Kato, T.Iwasa, M.Matsuda and Y.Miyai, "A Simulation of Aerodynamic Effects to a Bicycle Caused by a Passing Vehicle," Bulletin of the Institute for Industrial of Osaka Industrial University, No.3, March, 1980.
3. Mitsutoshi Kawaguchi, "The Flow of a Perfect Fluid around Two Moving Bodies," Journal of the Physical Society of Japan, Vol.19, No.8, August, 1964.
4. L.H.Carpenter, "On the Motion of Two Cylinders in an Ideal Fluid," J.Res. Nat. Bur. Stand, 61, 1958.
5. G.de Vries and D.H.Norrie, "The Application of the Finite Element Technique to Potential Flow Problems: Part I," Mechanical Engineering Report, No.7, University of calgary, August, 1969.
6. G.de Vries and D.H.Norrie, "The Application of the Finite Element Technique to Potential Flow Problem: Part II," Mechanical Engineering Report, No.8, University of Calgary, July, 1969.
7. G.de Vries and D.H.Norrie, "The Application of the Finite Element Technique to Potential Flow Problem: Part III," Mechanical Engineering Report, No.9, University of Calgary, June, 1973.

KEMP, JONES & COULTHARD, LLP
3800 Howard Hughes Parkway
Seventeenth Floor
Las Vegas, Nevada 89169
(702) 385-6000 • Fax (702) 385-6001
kic@kempjones.com

1 WILL KEMP, ESQ. (#1205)
2 ERIC PEPPERMAN, ESQ. (#11679)
3 e.pepperman@kempjones.com
4 KEMP, JONES & COULTHARD, LLP
5 3800 Howard Hughes Parkway, 17th Floor
6 Las Vegas, Nevada 89169
7 Telephone: (702) 385-6000
8 Facsimile: (702) 385-6001
9 -and-
10 CHRISTIANSEN LAW OFFICES
11 PETER S. CHRISTIANSEN, ESQ. (#5254)
12 KENDELEE L. WORKS, ESQ. (#9611)
13 810 South Casino Center Blvd.
14 Las Vegas, Nevada 89101
15 *Attorneys for Plaintiffs*

DISTRICT COURT
CLARK COUNTY, NEVADA

12 KEON KHIABANI and ARIA KHIABANI,
13 minors, by and through their Guardian,
14 MARIE-CLAUDE RIGAUD; SIAMAK
15 BARIN, as Executor of the Estate of Kayvan
16 Khiabani, M.D. (Decedent), the Estate of
17 Kayvan Khiabani, M.D. (Decedent);
18 SIAMAK BARIN, as Executor of the Estate
19 of Katayoun Barin, DDS (Decedent); and the
20 Estate of Katayoun Barin, DDS (Decedent);

21 Plaintiffs,

22 vs.

23 MOTOR COACH INDUSTRIES, INC.,
24 a Delaware corporation; et al.

25 Defendants.
26
27
28

Case No.: A-17-755977-C

Dept. No.: XIV

**PLAINTIFFS' PROPOSED
VERDICT FORM**

1 We, the jury, find as follows on Plaintiffs' different strict liability claims for
2 compensatory damages against MCI:

3
4 1) Is MCI liable for defective design (Right-Side Blind Spot)?

5 Yes _____ No _____
6
7

8 2) Is MCI liable for defective design (Lack of Proximity Sensor)?

9 Yes _____ No _____
10

11
12 3) Is MCI liable for defective design (Lack of Rear-Wheel Protective Barrier)?

13 Yes _____ No _____
14

15
16 4) Is MCI liable for defective design (Aerodynamic Design)?

17 Yes _____ No _____
18

19
20 5) Is MCI liable for failure to warn?

21 Yes _____ No _____
22

23
24 If you answered "Yes" on any of the above liability questions, you must
25 also determine Plaintiffs' claim for punitive damages against MCI:

26 1) Is MCI liable for punitive damages?

27
28 Yes _____ No _____

1 If you answered "Yes" to any of the above liability questions, fill in the
2 amount of compensation that you deem appropriate for each Plaintiff's
3
4 compensatory damages arising from the death of Dr. Kayvan Khiabani:

5 KEON KHIABANI COMPENSATORY DAMAGES

6 Past Grief and Sorrow \$ _____

7
8 Future Grief and Sorrow \$ _____

9 Loss of Probable Support,
10 Companionship, Society, and
11 Comfort \$ _____

12 Pain and Suffering of Dr.
13 Kayvan Khiabani (to be divided
14 Between the heirs) \$ _____

15 Disfigurement to Dr. Kayvan
16 Khiabani (to be divided between
17 the heirs) \$ _____

18 ARIA KHIABANI COMPENSATORY DAMAGES

19
20 Past Grief and Sorrow \$ _____

21 Future Grief and Sorrow \$ _____

22 Loss of Probable Support,
23 Companionship, Society, and
24 Comfort \$ _____

25
26 ///

27 ///

28

KEMP, JONES & COULTHARD, LLP
3800 Howard Hughes Parkway
Seventeenth Floor
Las Vegas, Nevada 89169
(702) 385-6000 • Fax (702) 385-6001
kjc@kempjones.com

1
2
3
4
5
6
7
8
9
10
11
12
13
14
15
16
17
18
19
20
21
22
23
24
25
26
27
28

THE ESTATE OF KATY BARIN, DDS COMPENSATORY DAMAGES

The Grief and Sorrow Suffered by
Katy Prior to Her October 12, 2017,
Death \$ _____

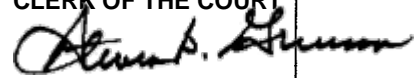
The Loss of Probable Support,
Companionship, Society, Comfort,
and Consortium Suffered by Katy
Prior to Her October 12, 2017, Death \$ _____

THE ESTATE OF KAYVAN KHIABANI, MD COMPENSATORY DAMAGES

Medical and Funeral Expenses \$ _____

DATED this ____ day of March, 2018.

FOREPERSON



1 **ORDR**

2
3 **EIGHTH JUDICIAL DISTRICT COURT**
4 **CLARK COUNTY, NEVADA**

5
6 KEON KHIABANI and ARIA KHIABANI,)
7 minors, by and through their Guardian,)
8 MARIE-CLAUDE RIGAUD; SIAMAK)
9 BARIN, as Executor of the Estate of Kayvan)
10 Khiabani, M.D. (Decedent), the Estate of)
11 Kayvan Khiabani, M.D. (Decedent);)
12 SIAMAK BARIN, as Executor of the Estate)
13 of Katayoun Barin, DDS (Decedent); and)
14 the Estate of Katayoun Barin, DDS)
15 (Decedent);)

11 Plaintiffs,

12 vs.

13 MOTOR COACH INDUSTRIES, INC.,)
14 MICHELANGELO EXPRESS; EDWARD)
15 HUBBARD; BELL SPORTS, INC. d/b/a)
16 GIRO SPORT DESIGN; and SEVENPLUS)
17 BICYCLES, INC. d/b/a PRO CYCLERY)

16 Defendant(s).

CASE NO.: A-17-755977-C
DEPT. NO.: XIV

18 **ORDER**

19 Defendant's objection to Special Master's Order Staying Post-Trial Discovery
20 Including May 2, 2018 Depositions and alternatively Motion for Limited Post-Trial Discovery
21 came on for a hearing before Department XIV of the Eighth Judicial District Court, the
22 Honorable Adriana Escobar presiding, on May 4, 2018. After considering the pleadings and
23 argument of counsel, the Court OVERRULES the objection, and DENIES the alternative
24 motion, according to the following:

25 First, Defendant objects to the decision of the special master staying discovery.
26 Special Master Hale was correct in observing that no post-trial motions had been filed, and
27 this Court had not authorized any post-trial discovery, thus the conclusion that the scheduled

1 deposition should not go forward was correct, regardless of whether Plaintiffs had standing to
2 object on behalf of the deponent. Parties are not allowed to continue discovery beyond the
3 close of discovery, much less after a judgment has been entered, without leave of court.
4 Defendant's objection is therefore OVERRULED.

5 Defendant in the alternative has requested leave to conduct limited post-trial discovery
6 in the form of a subpoena for Dr. Khiabani's employment records. No clear standard is
7 articulated in the NRCP or Nevada case law for determining when post-trial discovery should
8 be allowed. However, Defendant's motion admits that the request for post-trial discovery is
9 intrinsically linked to NRCP 59's allowance for a motion for new trial based upon "newly
10 discovered evidence," and argues that the parties must be allowed to discover any such new
11 evidence. Therefore, the standard for a motion for new trial based on newly discovered
12 evidence is relevant to the Court's determination here of whether post-trial discovery should
13 be allowed. This approach is supported by Defendant's proffered case law on the subject,
14 specifically *In re Wyatt, Inc.*, 168 B.R. 520, 524 (Bankr. D. Conn. 1994).

15 Defendant is not, at this moment, arguing the validity of the verdict based on the
16 evidence presented or the Court's legal rulings, but rather arguing that the jury did not hear
17 vitally relevant evidence that could have resulted in a different verdict. The Court is required
18 to follow the law, and due to the importance of finality in litigation, the law provides very
19 narrow exceptions to the rule that judgments are to be final, and that jury verdicts are to be
20 given great respect. A jury's role as the finder of fact is the cornerstone of our justice system,
21 and thus it is no simple feat to persuade this Court that the jury's verdict was unjust.

22 A new trial based on new evidence is only feasible if the party's "substantial rights"
23 were materially affected due to the discovery of evidence "which the party could not, with
24 reasonable diligence, have discovered and produced at the trial." This requirement implicitly
25 supports the policy of finality of judgments and respect for the value of a jury's time and
26 effort. It bears noting that this trial lasted for six weeks including jury selection, and thus
27 constituted a considerable hardship on the jurors and necessarily required a large amount of

1 resources of the parties and the court system. In reverence for these policy considerations, a
2 court will not discard a jury verdict when the requesting party's own lack of diligence caused
3 the alleged injustice. Similarly, this Court will not allow post-trial discovery to seek out facts
4 which could have, with reasonable diligence, been discovered before trial.

5 The facts Defendant now seeks to discover are surprising and the Court would not
6 expect a reasonably diligent party to specifically ask for this information—in other words, to
7 ask whether Dr. Khiabani had been accused of billing errors, compliance issues, or medicare
8 fraud, or whether Dr. Khiabani had been informed he was going to be terminated. However,
9 under the NRCP 59 standard, the question is not whether Defendant had asked for this
10 specific information that it now seeks, but rather whether Defendant could have uncovered
11 these facts in the course of reasonably diligent discovery. Thus, the issue for the Court would
12 be whether reasonably diligent discovery could have led to disclosure of the sought after
13 information, and whether Defendant failed to conduct this reasonably diligent discovery.

14 It is beyond question that, from the inception of this case, Dr. Khiabani's future
15 income was clearly going to be a material issue for trial. A plaintiff's damages in a wrongful
16 death action are made up of, primarily, emotional damages and damages consisting of lost
17 support from the decedent. The particular facts of this case certainly highlight the importance
18 of lost support as a measure of the Plaintiffs' damages, as the decedent happened to be an
19 extremely well-paid individual who still had numerous years ahead of him before retirement.
20 Thus, the Plaintiffs' damages depended largely on the estimation of Dr. Khiabani's lost
21 income after his death. Indeed, the parties spent considerable effort obtaining expert opinions
22 on how long Dr. Khiabani would have likely provided monetary support to his family, what
23 his economic situation would have been in future years, and what portion of his income would
24 have been available to his family.

25 Knowing that Dr. Khiabani's current and future economic well-being would be a vital
26 aspect for litigation, it would be reasonably diligent to pursue discovery of every fact that
27 would enable the parties to accurately predict what the Plaintiffs' actual loss of support would

1 be. This would include, at least, seeking to determine the specific terms of Dr. Khiabani's
2 employment contract, how long the contract was going to remain in effect had Dr. Khiabani
3 not passed away, whether the contract would have been renewed, and whether this salary or
4 benefits would be likely to change over the remainder of his foreseeable employment.
5 Further, any inquiry into these basic facts sought from Dr. Khiabani's employer could have,
6 and most certainly would have, produced either the very information Defendant now seeks, or
7 a more general response that would be sufficient to spur the Defendant to investigate the
8 issue, such as a response that Dr. Khiabani's contract would not have been renewed.¹

9 However, Defendant here evidently did not pursue any discovery on this topic. The
10 sole discovery request Defendant cites to as evidence of due diligence² is interrogatory
11 number 17 to Dr. Barin, which requests the reasons Dr. Khiabani's employment was
12 terminated by any former employers over the last ten years. Defendant's motion
13 acknowledges that Plaintiffs may not have known about the information which has been
14 recently reported on, and moreover the interrogatory is only incidentally related to this
15 information—it does not show an effort to obtain information relating to the details or extent
16 of Dr. Khiabani's future employment. Dr. Barin was not likely to know the details of the
17 internal audit, nor even that Dr. Khiabani was told the day before he died that he was being
18 terminated, and no discovery will ever be able to confirm Dr. Barin's knowledge due to her
19 untimely death. Regardless, this single interrogatory does not constitute diligence into this
20 area, as there was evidently no discovery propounded to Dr. Khiabani's employer, who would
21

22 ¹ The other possible outcome would be an untruthful response from the employer, which the Court addresses
23 below.

24 ² Although not included in the motion, Defendant's counsel mentioned at the hearing that a subpoena was sent to
25 the Board of Medical Examiners, presumably in the pursuit of any information pertaining to medical malpractice
26 allegations against Dr. Khiabani. The Board would not have any information on Dr. Khiabani's employment
27 status or any awareness of the issues presented by the media because that information was beyond the scope of
the Board's involvement with the daily life of a physician and moreover, as the Defendant asserts, was held in
confidence by the employer. Further, the very emails Defendant relies on in this motion show that the
individuals who were aware of the alleged misdeeds by Dr. Khiabani had not informed the Board. Because a
subpoena to the Board is not an effort to discover the details of Dr. Khiabani's future employment, this effort
does not change the Court's analysis of reasonable diligence here.

1 be the only party likely to have relevant information on Dr. Khiabani's future employment.
2 Additionally, Defendant is now seeking post-judgment discovery on Dr. Khiabani's non-
3 confidential employment records. Even if the information Defendant now seeks would have
4 been considered confidential at the time and Dr. Khiabani's employer would have thus
5 resisted disclosing this information, the fact remains that Defendant did not attempt to get the
6 information. Further, confidentiality concerns could have been addressed by motions to
7 compel and/or stipulated protective orders. To argue that this information could not have
8 been discovered even with reasonable diligence requires an assumption that the employer
9 would not have given the requested information and that the Court could not have provided
10 relief to the Defendant in such a case.

11 While the above is sufficient for the Court to find a lack of diligence, the conclusion is
12 supported by the fact that Plaintiffs provided to Defendant an authorization to obtain Dr.
13 Khiabani's employment records on July 26, 2017, but evidently Defendant never followed
14 through on actually requesting the very information that it now seeks to obtain. Moreover,
15 Defendant evidently has no explanation for why this information was not actually sought after
16 the authorization was given.


17 If the Court were to allow this post-trial discovery, the sole scenario in which the
18 Court may be persuaded to grant a new trial based on the "new" information Defendant now
19 seeks would be if the Defendant had asked Dr. Khiabani's employer for information on his
20 employment records, and had received untruthful responses. In such a case, reasonable
21 diligence would not require any additional pursuit of the subject. However, Defendant has
22 made no allegation that it asked Dr. Khiabani's employer anything, that Plaintiffs were aware
23 of the confidential information that has now been revealed, nor any allegation (much less
24 evidence) that any party withheld information in response to such a discovery request.
25 Without at least some evidence of such deceit, the Court will not permit Defendant to now
26 seek information that it should have asked for during discovery. *See, e.g. Jones v. Illinois*
27

1 *Central Railroad Co.*, 617 F.3d 843 (6th Cir. 2010) (holding that a district court may require a
2 party to show some evidence of the deceit which the party seeks post-trial discovery to prove).

3 Finally, the Court disagrees with Defendant's insinuation that its discovery efforts
4 were diligent in light of the expedited discovery schedule in this case. Defendant was
5 represented by a veritable army of gifted and seasoned attorneys, including several attorneys
6 admitted to practice on a pro hac vice basis, and Defendant was able to complete extensive
7 discovery on every other aspect of the case. There is no explanation for why such a strong
8 legal team did not try to discern an accurate picture of Dr. Khiabani's future income, which
9 was a critical factual issue in this case, even when the Defendant hired economists specifically
10 to try to predict Dr. Khiabani's economic future.

11 The Court does not disagree that, without the requested discovery, Defendant would
12 have a much harder time justifying a new trial based only on the information presented in the
13 media reports. Further, Plaintiffs do not dispute that the new information would at least be
14 relevant to the case. However, even were this discovery allowed, the Court would not grant a
15 motion for new trial based on "newly discovered evidence," because Defendant could have,
16 with reasonable diligence, unearthed this evidence during the pendency of discovery.
17 Therefore, the Court DENIES Defendant's request for post-trial discovery. Further, the
18 subpoena issued by the Defendant for the custodian of records of NSHE is QUASHED.

19
20 DATED this 23rd day of May, 2018.

21
22 
23 _____
24 ADRIANA ESCOBAR
25 DISTRICT JUDGE
26
27

CERTIFICATE OF SERVICE

I hereby certify that on or about the date signed, a copy of this Order was electronically served to all registered parties in the Eighth Judicial District Court Electronic Filing Program and/or placed in the attorney's folder maintained by the Clerk of the Court and/or transmitted via facsimile and/or mailed, postage prepaid, by United States mail to the proper parties as follows:

D. Lee Roberts, Jr., Esq.
Howard J. Russell, Esq.
David A. Dial, Esq.
Marisa Rodriguez, Esq.
WEINBERG WHEELER
HUDGINS GUNN & DIAL LLC
Facsimile: (702) 938-3864
Email: lroberts@wwhgd.com
hrussell@wwhgd.com
ddial@wwhgd.com
mrodriguez@wwhgd.com

AND:

Darrell L. Barger, Esq.
Michael G. Terry, Esq.
John C. Dacus, Esq.
Brian Rawson, Esq.
HARTLINE DACUS BARGER
DREYER LLP
Email: dbarger@hdbdlaw.com
mterry@hdbdlaw.com
jdacus@hdbdlaw.com
brawson@hdbdlaw.com
Attorneys for Defendant Motor Coach Industries, Inc.

Will Kemp, Esq.
Eric Pepperman, Esq.
KEMP JONES & COUTHARD LLP
Email: e.pepperman@kempjones.com

AND:

Peter S. Christiansen, Esq.
Kendele L. Works, Esq.
CHRISTIANSEN LAW OFFICES
Email: pete@christiansenlaw.com
kworks@christiansenlaw.com
Attorneys for Plaintiff

Keith Gibson, Esq.
James C. Ughetta, Esq.
LITTLETON JOYCE UGHETTA PARK &
KELLY LLP
Email: Keith.Gibson@littletonjoyce.com
James.Ughetta@LittletonJoyce.com
*Attorneys for Defendant Bell Sports, Inc.
d/b/a Giro Sport Design*

Michael E. Stoberski, Esq.
Joslyn Shapiro, Esq.
OLSON CANNON GORMLEY ANGULO &
STOBERSKI
Email: mstoberski@ocgas.com
jshapiro@ocgas.com

AND:

C. Scott Toomey, Esq.
LITTLETON JOYCE UGHETTA PARK &
KELLY LLP
Email: Scott.Toomey@littletonjoyce.com
*Attorneys for Defendant Bell Sports, Inc. d/b/a
Giro Sport Design*

Eric O. Freeman, Esq.
SELMAN BREITMAN LLP
Email: efreeman@selmanlaw.com
*Attorney for Defendants Michelangelo Leasing
Inc. d/b/a Ryan's Express & Edward Hubbard*

Michael J. Nunez, Esq.
MURCHISON & CUMMING, LLP
Email: mnuez@murchisonlaw.com
*Attorney for Defendant SevenPlus Bicycles, Inc.
d/b/a Pro Cyclery*

Paul E. Stephan, Esq.
Jerry C. Popovich, Esq.
William J. Mall, Esq.
SELMAN BREITMAN LLP
Email: pstephan@selmanlaw.com
jpopovich@selmanlaw.com
wmall@selmanlaw.com
*Attorneys for Defendants Michelangelo Leasing
Inc. d/b/a Ryan's Express and Edward Hubbard*

Daniel F. Polsenberg, Esq.
Joel D. Henriod, Esq.
LEWIS ROCA ROTHGERBER CHRISTIE LLP
Email: DPolsenberg@LRRC.com
JHenriod@LRRC.com
Attorneys for Motor Coach Industries, Inc.


Diana D. Powell, Judicial Assistant